EUROPA-UNIVERSITÄT FLENSBURG

Influence of grid support functionalities on the mechanical loads and the energy yield of wind turbines

---

Doctoral thesis
submitted in fulfilment of the requirements
for the degree of doctor of philosophy (Ph.D.)

at the
Department of Energy and Environmental Management

By
Arne Gloe

26th June 2023
Flensburg

Reviewers: Prof. Dr. Torsten Faber
            Prof. Dr. David Schlipf
Supervisor: Prof. Dr. Clemens Jauch

Acknowledgment

Abstract

As the share of inverter connected generation increases in power systems, grid operators worldwide increase their demand for system services by wind turbines. One of these services, grid frequency control, is very challenging for wind turbines, as it requires a change of the active power of the wind turbine. Furthermore, wind turbines are curtailed when the grid capacity is not sufficient to transport the produced power: the so-called feed-in management. Hence, the control of the wind turbines has to cope with the needs of the grid. Thus, the wind turbines are exposed to an additional external excitation in addition to the prevailing wind conditions.

In this thesis, the influence of the providing these services on the wind turbine is analysed. The analysis is based on time domain simulations of the wind turbine. The models were partly developed in this project. Additionally, a focus is laid on analysing data to derive realistic scenarios of the grid signals. As some of these signals were not available, several measurement had to be set up and maintained during the project.

In a research project with the wind turbine manufacturer Suzlon Energy, a controller for providing inertial response continuously was developed. In contrast to the state-of-the-art, the magnitude of the inertial response is scaled with the operating point of the wind turbine in order to provide this service reliably and at the same time to use the full potential of the wind turbine in strong wind conditions. This controller is tested with grid frequency scenarios from Europe and India to identify the consequences for the energy yield and the mechanical loads of the wind turbine. It is shown, that neither the energy yield nor the loads are affected significantly.

During the research project, a grid islanding and eventually a blackout occurred in Flensburg. The local grid operator provided data of the grid situation for the day of the blackout. This data allowed to analyse the cause of the blackout and to develop fictive scenarios how wind turbines could have helped to stabilize the islanded grid. In the analysed scenarios it was shown, that wind turbines equipped with an inertial response and a fast frequency response controller could have stabilized the islanded grid making a blackout less likely. However, the wind turbines were also at risk of running in overspeed, as they had to reduce their power drastically when stabilizing the grid.

As a consequence of the overspeed problems, a feedforward loop for the pitch control was added to the grid frequency support controller. It modifies the pitch angle signal from the feedback controller by a signal depending on the pitch sensitivity and the magnitude of the power change for grid frequency support. The proposed controller achieved to reduce the overspeed significantly.

In addition to the grid frequency support, a controller for continuous feed-in management was developed at the institute. It was tested with a fictive case of a weak grid connection, which was designed based on measurements at the campus in Flensburg. In comparison to the state-of-the-art feed-in management, the controller allowed a higher energy yield of the wind turbine and a better utilization of the grid components. The loads of the wind turbine were only slightly increased. Finally, it is also shown, that feed-in management and inertial response can be provided by a wind turbine at the same time, as the excitations and the wind turbine response are largely decoupled in the frequency domain.

It is concluded that wind turbines can provide system services to a larger extend than today without suffering from unduly harm for its mechanical loads and its energy yield.

Table of content

List of publications

This thesis is based on the work reported in the following publications. First are listed all publications, which are peer-reviewed and are published in a journal. These publications count for the requirements of the Doctoral Degree Regulations of 'Europa-Universität Flensburg'. In addition, I also listed publications, which do not meet one of the two requirements, as they also contain parts of the research conducted during the Ph.D. project. The following table lists the publications, indicates which chapter is based on each publication, and states its contribution to the so-called 'P-Wert'. The full bibliographic information is given below the table.

Number	Title	Chapter	P-Wert
1	Design of a System Substituting Today's Inherent Inertia in the European Continental Synchronous Area	5.1	0.5
2	Continuous provision of synthetic inertia with wind turbines: Implications for the wind turbine and for the grid	5.2	0.4
3	Influence of continuous provision of synthetic inertia on the mechanical loads of a wind turbine	5.3	0.33
4	Grid Support with Wind Turbines: The Case of the 2019 Blackout in Flensburg	5.4	0.5
5	Continuous grid frequency support with variable synthetic inertia and feedforward pitch angle adjustment	5.5	1
6	Increased Wind Energy Yield and Grid Utilisation with Continuous Feed-In Management	6	0.4
7	Simultaneous Inertia Contribution and Optimal Grid Utilization with Wind Turbines	7	0.67
		Total	3.8

Publication 1

H. Thiesen, C. Jauch, and A. Gloe '*Design of a System Substituting Today's Inherent Inertia in the European Continental Synchronous Area*' Energies, vol. 9, no. 8: 582, 2016.

Publication 2

A. Gloe, C. Jauch, B. Craciun, and J. Winkelmann '*Continuous provision of synthetic inertia with wind turbines: implications for the wind turbine and for the grid*', IET Renewable Power Generation, vol. 13, no. 5, pp. 668–675.

Publication 3

A. Gloe, C. Jauch, B. Craciun, A. Zanter, and J. Winkelmann '*Influence of continuous provision of synthetic inertia on the mechanical loads of a wind turbine*' Energies. vol. 22, no. 15: 5185, 2021.

Publication 4

A. Gloe, C. Jauch, and T. Räther '*Grid Support with Wind Turbines: The Case of the 2019 Blackout in Flensburg*', Energies, vol. 14, no. 6: 1697, 2021.

Publication 5

A. Gloe '*Continuous grid frequency support with variable synthetic inertia and feedforward pitch angle adjustment*' in Journal of Physics: Conference Series, vol. 2265, no. 3: 032105, 2022.

Publication 6

C. Jauch, A. Gloe, S. Hippel, and H. Thiesen '*Increased Wind Energy Yield and Grid Utilisation with Continuous Feed-In Management*' Energies, vol. 10, no. 7: 870, 2017.

Publication 7

C. Jauch and A. Gloe '*Simultaneous Inertia Contribution and Optimal Grid Utilization with Wind Turbines*' Energies, vol. 12, no. 15: 3013, 2019.

List of figures

List of tables

List of symbols

Symbol	Description	Unit
Roman letters		
C_t	Cash flow at time t	€
$E_{inertia}$	Energy delivered to the grid for inertial response	Ws
E_{kin}	Kinetic energy	Ws
f_{grid}	Grid frequency	Hz
H	Inertia constant	s
H_{dem}	Demanded inertia constant	s
H_{sys}	System inertia constant	s
H_{var}	Variable inertia constant	s
I_0	Initial investment	€
J	Inertia	kgm²
$J_{drive\ train}$	Drive train inertia	kgm²
J_{gen}	Generator inertia	kgm²
J_{sys}	System inertia	kgm²
k_{damp}	Damping coefficient	Nms/rad
$k_{damp,IR}$	Damping factor for IR	-
k_{DT}	Damping factor for drive train accelerations	-
k_{edge}	Damping factor for edgewise blade accelerations	-
k_{flap}	Damping factor for flapwise blade accelerations	-
k_{spring}	Spring coefficient	Nm/rad
k_{SR}	Dampening term for the self-regulation of the loads	%/rad
$k_{tower,lat}$	Damping factor for lateral tower accelerations	-
$k_{tower,long}$	Damping factor for longitudinal tower accelerations	-
P_{aero}	Aerodynamic power	W
P_{dem}	Demanded power	W
P_{elec}	Electrical power	W
P_{gen}	Generated power	W
P_{gen}	Sum of generated and imported power	W
P_{GS}	Power for grid support	W
$P_{GS,lim}$	Limited power for grid support	W
P_{IR}	Power for inertial response	W
$P_{IR,max}$	Maximum power for inertial response	W
$P_{IR,min}$	Minimum power for inertial response	W
$P_{IR,opt}$	Undamped power for inertial response	W
P_{load}	Consumed power	W
P_{load}	Sum of all consumed, lost and exported power	W
P_{max}	Maximum generator power	W
P_{mech}	Mechanical power	W
P_{opt}	Optimal power setpoint	W
P_{rated}	Rated power	W
P_{ref}	Reference power	W
$P_{setpoint}$	Power setpoint for generator	W

Symbol	Description	Unit
P_{WT}	Power of wind turbine	W
r	Discount rate	%
S_{rated}	Rated apparent power	VA
T_{acc}	Accelerating torque	Nm
T_{aero}	Aerodynamic torque	Nm
$T_{elec,GS}$	Electrical torque for grid support	Nm
$T_{elec,opt}$	Electrical torque for optimal power	Nm
v_{wind}	Wind speed	m/s
Greek letters		
η_{PFC}	Factor for primary frequency control	-
$\eta_{PFC,unl}$	Unlimited factor for primary frequency control	-
θ_{dem}	Setpoint for pitch drive	°
θ_{fb}	Pitch angle setpoint from feedback control	°
θ_{ff}	Pitch angle setpoint from feedforward control	°
θ_{max}	Maximum pitch angle of the WT	°
θ_{min}	Minimum pitch angle of the WT	°
θ_{WT}	Collective pitch angle of the WT	°
φ	Angular displacement	rad
ω	Angular speed	rad/s
ω_{gen}	Angular generator speed	rad/s
$\omega_{gen,meas}$	Measured angular generator speed	rad/s
ω_{grid}	Angular grid frequency	rad/s
ω_{nom}	Angular nominal grid frequency	rad/s
ω_{ref}	Reference speed of generator	rad/s
$\dot{\omega}$	Angular acceleration	rad/s²

List of abbreviations

TSO	Transmission system operator
AC	Alternating current
PFC	Primary frequency control
FFR	Fast frequency response
SI	Synthetic inertia
ENTSO-E	European transmission system operators
ROCOF	Rate of change of frequency
DSO	Distribution system operator
TSO	Transmission system operator
PSD	Power spectral density estimate
ECSA	European Continental Synchronous Area
NPV	Net present value
LCOI	Levelised cost of inertia
NREL 5M	5 MW NREL research WT
OEM	Original equipment manufacturer
FIM	Feed-in management

1 Introduction

Power systems around the world are being decarbonised to help fulfilling the goals of the Paris agreement [1]. In 2021, wind turbines (WTs) with a total power of 91 GW were installed [2]. Today, renewable energy produced by photovoltaic (PV) power plants and WTs not only helps to avoid CO_2 emissions, but is also cheaper than energy from new conventional power plants [2].

PV power plants and modern WTs and are connected via power electronics. They are commonly referred to as inverter-connected generation (ICG). Unlike synchronously connected generators, they do not inherently contribute to the system inertia, which helps to stabilize the grid frequency. Additionally, they are often located in remote areas with relatively weak grid connections [3], [4]. Hence, grid operators in grids with large amounts of ICG face new challenges, which have to be solved [5]. These challenges include ensuring the power system stability even when the power production in the grid is dominated by ICG. In such situations, WTs can no longer only be controlled based on the prevailing wind, but have to take the needs of the grid into account. Especially, when such control leads to changes of the active power of the WT, these grid services can have a strong influence on the WT. Two grid services, which require such a change of the active power, are grid frequency support and feed-in management (FIM).

In this thesis, the implications of providing these services with WTs are analysed. The focus is on grid frequency support with WTs. The thesis aims to answer the following research question:

What implication does the provision of grid support have on the WT, especially on its mechanical loads?

During the research, the above question was broken down into the following sub-questions:

1. In which form should frequency support and FIM be provided in a future power system?
2. What are reasonable scenarios to be considered when evaluating load changes by grid support with WTs?
3. What are the economic consequences of providing grid support with WTs?

The rest of this thesis is structured as follows: the foundations of power system stability and WT dynamics are given in chapter 2. This chapter also contains the literature review. In chapter 3, the used simulation models and relevant measurement systems are briefly introduced. A brief overview of the publications used in this thesis and there relation to one another is given in chapter 4. The publications are presented in detail in chapter 5 (frequency support), chapter 6 (FIM), and chapter 7 (combination of frequency support and FIM). Chapter 8 discusses the results and the limitations of the research. Finally, a conclusion is drawn and an outlook is given in chapter 9.

2   Foundations

In this chapter, the foundations of power system stability and wind turbine dynamics are briefly explained. Furthermore, a literature review on the grid frequency support with WTs is given.

2.1   Power system stability

A major task in alternating current (AC) power systems is to keep the grid frequency stable. The grid frequency is system wide property of the power system. The transmission system operators (TSOs) are usually responsible for its stability. The TSOs define services traded on a market and define requirements for power plants in the so-called grid codes. An example for a market based solution are the control energy services defined by the ENTSO-E [6]. A typical requirement is the frequency range during which generators have to remain connected to the grid [7].

In AC grids, energy is not stored. Hence, power generation (by power plants and imports) and power consumption (by loads, losses and exports) have to be balanced at any time. Occurring imbalances are compensated by the changes of the kinetic energy stored in the rotating masses of directly connected synchronous generators, which are typically used in conventional power plants [8]. The mechanical speed of these generators varies in a small band and defines the grid frequency. During a power imbalance in the grid, an imbalance between the electrical and mechanical power of the generator occurs: the generator speed and therefore also the grid frequency changes. This behaviour of a synchronously connected generator is called inertial response (IR). For a single generator, it can be expressed with help of the equation (1):

$$\frac{\delta \omega_{gen}}{\delta t} = \frac{P_{mech} - P_{elec}}{\omega_{gen} \cdot J_{gen}} \tag{1}$$

Where ω_{gen} is the mechanical speed of the generator, P_{mech} its mechanical power, P_{elec} its electrical power and J_{gen} its mass moment of inertia.

On a system's level, the magnitude of the frequency change at a given power imbalance is determined by the inherent inertia of all synchronously connected rotating masses, the so-called system inertia. It is often expressed in the form of the inertia constant, H_{sys}. 80 % - 90 % of the system inertia is provided by generators, the remaining part by loads, which are run by directly connected synchronous machines [9], [10]. Mathematically, small changes of the angular grid frequency, ω_{grid}, can be described by equation (2):

$$\frac{\delta \omega_{grid}}{\delta t} = \frac{P_{gen} - P_{load}}{\omega_{grid} \cdot J_{sys}} \tag{2}$$

Where P_{gen} is the sum of all generated and imported power, P_{load} the sum of all consumed, lost and exported power, and J_{sys} the system inertia.

If the grid frequency, f_{grid}, deviates significantly from its nominal value, the aforementioned control energy services are activated. These services are typically ordered by the allowed time for their activation, from services reacting within seconds, primary frequency control (PFC), to those with an activation time of several minutes, i.e. tertiary control reserve. This thesis deals with services with an even shorter activation time: the supply of synthetic inertia (SI) and fast frequency response (FFR) with WTs [11]. As these services are not inherently supplied by ICGs, their inverter must be controlled accordingly.

In addition to these generation side services, the grid frequency is also automatically stabilized by the self-regulation of the loads [12]. The power consumption of some loads decrease when the grid frequency drops and thus have a dampening effect on changes of the grid frequency. This dampening effect is in the range of 1 %/Hz – 2 %/Hz and is neither in the short term nor in the long term constant [13]. Its magnitude varies significantly in various publications and is expected to decrease in the future [14]. When larger changes of the grid frequency are possible, a dampening term needs to be added to equation (2) in order to assess the full dynamics of the grid frequency leading to equation (3):

$$\frac{\delta \omega_{grid}}{\delta t} = \frac{P_{gen} - P_{load} + k_{SR} \cdot (\omega_{grid} - \omega_{nom}) \cdot P_{load}}{\omega_{grid} \cdot J_{Sys}} \qquad (3)$$

Where k_{SR} is the dampening term from self-regulation of the loads and ω_{nom} the nominal grid frequency.

The behaviour of the electrical grid during a disturbance is shown in Figure 1. With the chosen parameter ($P_{disturbance}$ = -3 GW, P_{load} = 180 GW, H_{sys} = 3 s, k_{SR} = 1 %/Hz), the grid frequency reaches is nadir (49.3 Hz) approximately 10 s after the disturbance.

Once the grid frequency starts to fall, the self-regulation of the loads reduces the power imbalance. After a short delay, the PFC also ramps up. Both effects reduce the needed IR from the generators, and therefore the change of their mechanical speed and the associated rate of change of frequency (ROCOF).
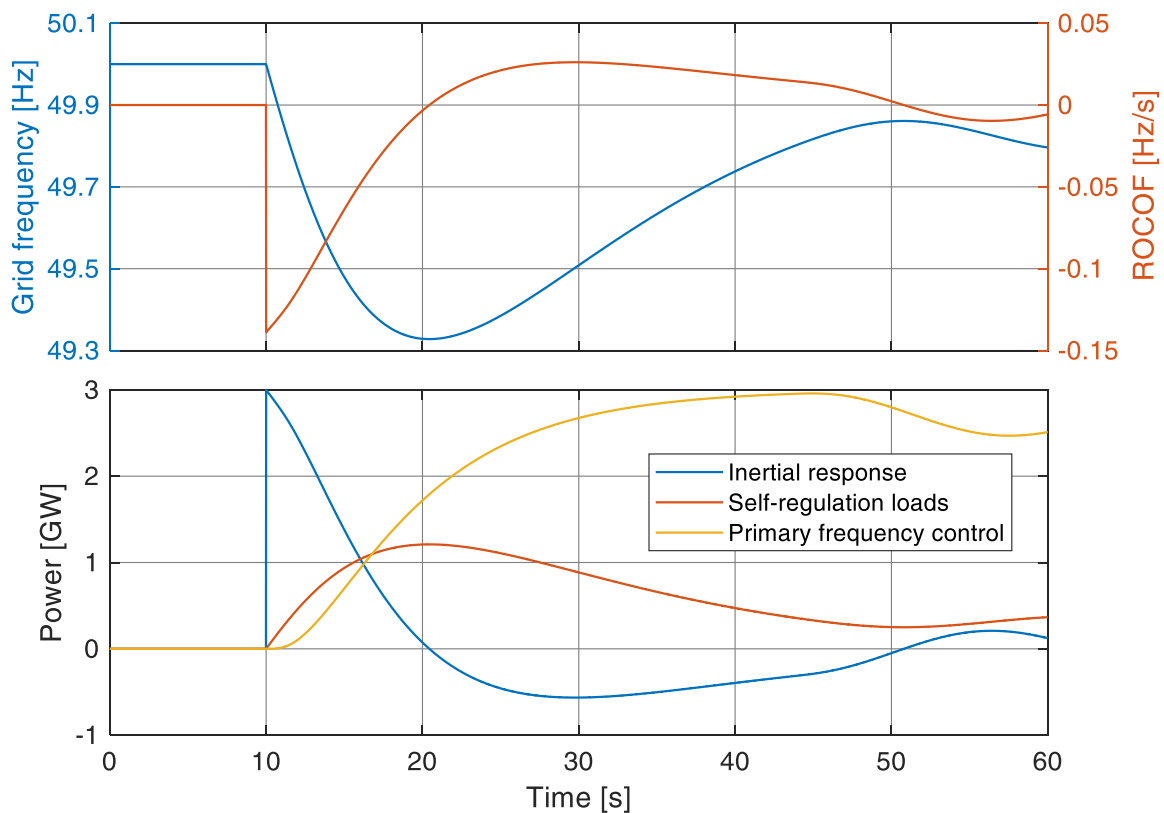
Figure 1 Simplified behaviour of the grid frequency (top, blue), the ROCOF (top, red), the inertial response (bottom, blue), the self-regulation (bottom, red) and the PFC (bottom, yellow) during the ENTSO-E reference case [6].

As argued in publication 1 [15] grid frequency control must fulfil two targets:

1. The grid frequency must be kept within a certain band around the nominal frequency in order to avoid load shedding and shutdowns of generators; in Germany the thresholds are 49.0 and 51.5 Hz respectively [16]. In the case shown in Figure 1 the threshold is achieved as the frequency nadir is reached at 49.3 Hz.

2. The ROCOF must be kept under a certain threshold, e.g. 2 Hz/s, as otherwise ROCOF relay trigger and parts of the power systems are disconnected [7]. As the Central European grid is very large, it can withstand the loss of larger power plants easily. The ENTSO-E reference case assumes the loss of two large nuclear power plants with a total generation of 3 GW. Due to the large size of the power system, this only results in a small power imbalance of 1.67 % of the connected load. Hence, the ROCOF in the Central European grid is even during a serious disturbance as shown in Figure 1 very small.

In addition to the system wide frequency stability issue, local stability issues may arise in an AC power system with high penetration of WTs. As stated above, WTs are often installed in remote location with a weak grid connection [3], [4]. This may cause overloading of single grid components (lines, transformer, etc.), leading to voltage stability issues or thermal overloading of these components. In such cases, the local grid operator secures the stability of the affected grid via FIM, i.e. the power production of WTs and other generators connected to grid are curtailed [17].

2.1.1   Inertial and fast frequency response from renewables

As the share of ICG in the power systems increases, conventional power plants are being replaced and eventually phased out [18], [19]. The resulting decrease of the system inertia is well documented by the TSOs of various synchronous areas, e.g. by the Electric Reliability Council of Texas (ERCOT) [20] or by various European TSOs [18]. This leads to a higher variability of the grid frequency and eventually a failure of the classic frequency stabilisation mechanisms [21], [22]. In order to avoid such situations, TSOs worldwide take different measures to stabilize the grid frequency [5]. Among these measure are the use of synchronous condensers e.g. by Energienet in Danmark [5], the definition of new frequency support services e.g. in the Nordic power system [14], and also stricter requirements for the connection of WTs. Some of the requirements are described in detail in chapter 2.3.1. Here, two of the most common services (SI and FFR) are shortly introduced.

SI requirements can be formulated as the emulation of the IR of a synchronous generator [11], i.e. a power change proportional to the ROCOF. By contrast FFR is a fast version of the well-known PFC, i.e. a power change proportional to the deviation of the grid frequency [11]. Both services can reduce the ROCOF and the frequency nadir shortly after a sudden loss of a generator and thereby buy time for the traditional frequency response to react. This helps to reduce, delay and eventually avoid under-frequency load shedding [23]. As shown in publication 1 [15], it is not economically feasible to provide these services by dedicated storage units providing solely inertia services. However, these services can also be supplied by WTs. In this case, the additional power is typically provided by tapping the kinetic energy stored in the rotation of the WT rotor. The reduced speed leads to a reduction of the aerodynamic efficiency of the WTs and a further decrease of the rotational speed. Therefore, the WTs usually have a period of reduced power production after providing frequency support, the recovery period. The recovery period helps to restore the optimal rotational speed of the WT. During the recovery period, the reduced power infeed may prolong the under frequency event [23], [24]. Thus a coordinated response of different frequency control services is needed [23], which requires a predictable response of the WTs. If the recovery periods of the WTs were to be avoided, the WTs would

have to be curtailed before the frequency event. This is more important for FFR, as a negative frequency deviation lasts longer than a negative ROCOF and thus more energy is drawn from the WT rotor. Despite these problems, frequency support with WTs seems to be one of the cheapest methods to increase the frequency stability in future power systems [25], [26] and is therefore very likely to be demanded by many TSOs.

SI and FFR require an exact measurement of the grid frequency, which is not an easy task. During a disturbance, even the location of the measurement in relation to the location of the disturbance leads to significantly different results [14]. Furthermore, the ideal averaging time of the measurements for different grid services is not clear yet [27], [28].

2.1.2 Feed-in management

Wind power has historically been installed in remote areas with a weak grid connection [3], [4]. This may lead to curtailment of wind power when the construction time of wind turbines is quicker than of the grid infrastructure [5]. Such an effect has led to a strong curtailment of wind energy in Germany [29] and especially in Schleswig-Holstein [30]. In the years 2015 - 2018 between 3,300 GWh and 4,818 GWh wind energy were curtailed [31], which was roughly of 5 % of the produced wind energy in Germany. In addition to the significant costs of several 100 million € [29], this has caused additional 2.1 MT of CO2 emissions in Germany in 2016 [29].

Curtailment of renewables in Germany increased sharply in the years before 2018 [31] but was expected to go down as the grid gets strengthened. However, a recent study claims that even in 2030 curtailment of wind power may be needed to stabilize the grid [32]. Curtailment of renewables is not specific to Germany, but actually occurs worldwide whenever the development of the grid cannot cope with the increase of newly installed renewables [5], [33]. One example is the British power system, where 5.6 % of the metered wind energy was curtailed in 2016 [29].

In addition to the typical time delay between wind power installation and grid expansion, it might also be economically beneficial to allow some level of curtailment [33]. A study by Agora Energiewende [34] claims that 30 % of the grid expansion costs can be saved when 2 % of the available energy production of a PV plant is to be curtailment (and thus increases the generation costs). Similar effects can occur on a larger scale, if cross-border transmission capacities are not expanded. A report of the European transmission system operators (ENTSO-E) from 2020 shows that a reasonable expansion of these transmission capacities can significantly decrease the system costs and reduce CO_2 emissions from the energy sector [35].

Nevertheless, curtailment of wind power might also be needed in certain times of the year when the production of renewables exceeds the load [34] or when previously curtailed WTs are used to provide control power for frequency support [36]. However, this is mainly independent of the local and regional grid utilization and therefore not within the scope of this thesis.

The effect of different FIM strategies on the curtailment of WTs is not easy to assess as it strongly depends on the local and regional grid situation. Especially, the structure of the distribution grids has a strong influence and varies significantly [37]. Larscheid et al. [37] address this problem by creating a high number artificial distribution grids and analysing the effect of different FIM strategies on the curtailment of wind and PV power. The authors show that a FIM based on power flow predictions can drastically decrease the need for curtailment of wind turbines and thus reduces the curtailed energy roughly by a factor of ten. However, curtailment can also be caused the technical and organisational interface between transmission system and distribution system. Such curtailments accounted for

roughly 50 % of the curtailed renewable energy [38]. As the number of the technical bottlenecks is limited, their state might actually be measured and the measurements can be used for a continuous FIM as proposed in publication 6 [39]. Thereby, even less wind energy may be curtailed and CO_2 emissions may be reduced.

Due to the regional importance of FIM in Schleswig-Holstein, this work focuses on improving the state-of-art in Germany in 2016. Feed-in management is typically imposed by the distribution system operators (DSOs). Until today the DSOs curtail WTs in three steps to 60 %, 30 % or 0 % of their rated power [40]. The curtailment signal was valid for ten-minute intervals in 2016 [41]. This has been changed to one-minute intervals today [40].

2.2   Wind turbine dynamics

The components, the structure and the dynamics of different WT types are not discussed here in detail, but can be found in the standard literature on WTs, e.g. Manwell et al. [42], Hau [43], Gasch and Twele [44] or Heier [45].

WTs are exposed to various excitations, mainly caused by the wind, the rotation of the WT and its weight. Excitations cause loads of the WT and its components, which are typically classified as either extreme or fatigue loads [44]. Extreme loads cause the failure of a component after a single or a few occurrences, while fatigue loads stress the components by the a large number of occurrences over the lifetime of a WT. Grid support is an additional source of excitations for the WTs, which might have to be considered in the design of the WTs. Gasch and Twele [44] categorise traditional excitations of WTs by their temporal behaviour. These categories can also be used to categorize excitations caused by grid support.

1. Constant (quasi-static) excitations: examples are gravitational forces of the nacelle and the tower. By contrast, gravitational forces of the blades are an example for a periodic excitation of these components.

2. Periodic excitations: these excitations are very important when looking at possible resonance effects with the eigenfrequencies of the WT. The period of these excitations is usually somehow connected to the rotational speed of the WT. Typical examples are mass or aerodynamic imbalances of the WT rotor, which cause an excitation with a frequency of one time per revolution (1p). Tower blockage effect and vertical wind speed variations occur with a frequency of three times per revolution (3p). Periodic excitations may also be caused by excitations from the grid when the WT supports the grid (e.g. IR during grid frequency oscillations).

3. Stochastic excitations: The most prominent stochastic excitation for WTs is the turbulent wind. These may affect the whole rotor plane but also only parts of the plane. In the latter case, the turbulence also leads to a temporary periodic excitation whenever a blades sweeps through a gusty part of the rotor plane. These turbulence-induced excitations are typically dampened by the rotational sampling and by the aerodynamic damping. The high number of stochastic excitations, which a WT experiences during its lifetime, makes turbulence very important for fatigue loads. A WT supporting the electrical grid continuously as proposed in this thesis, may in addition be excited by stochastic changes of the grid frequency and grid voltage (e.g. caused by (dis-)connection of major consumers). Hence, it is important to analyse the effect of these additional excitations on the lifetime of the WT and its components.

4. Transient excitations: Transient excitations typically occur during the manoeuvres (e.g. emergency stops), disturbances or during extreme situations like drastic changes of the wind

speed or the wind direction. An important transient excitation from the grid side are low-voltage-ride-through events, during which WTs need to be able to withstand a brief (several ms) disruption of the grid voltage. When supporting the grid, drastic changes of the grid frequency (e.g. after a grid islanding) may also cause a transient excitation to the WT.

An example for a mass imbalance in the rotor occurred at the WT (Enercon E30) on the campus in Flensburg. The E30 stopped regularly due to high lateral tower movements, especially in low wind. At these wind speeds, the rotational speed is close to the resonance speed of the tower (27.6 RPM). In a project in collaboration with DNV-GL the E30 and the nearby met mast were equipped with a measurement system [46]. In a conference paper [47], it was shown that periods of high tower accelerations coincided with rotational speeds close to the eigenfrequency of the tower (see Figure 2). The high tower accelerations are also visible in the frequency spectrum of the rotational speed and power of the E30 [47]. Based on the measurements and with help of the simulation model developed in the project, the mass imbalance was estimated to be 53 kgm [46]. Three years later, BerlinWind balanced the E30 after determining the imbalance to 52 kgm [48]: a strong indicator for the accuracy of the used model. The balancing reduced the lateral tower head accelerations by 86 %, when the E30 operates close to the eigenfrequency of the tower according to the report by BerlinWind [48].
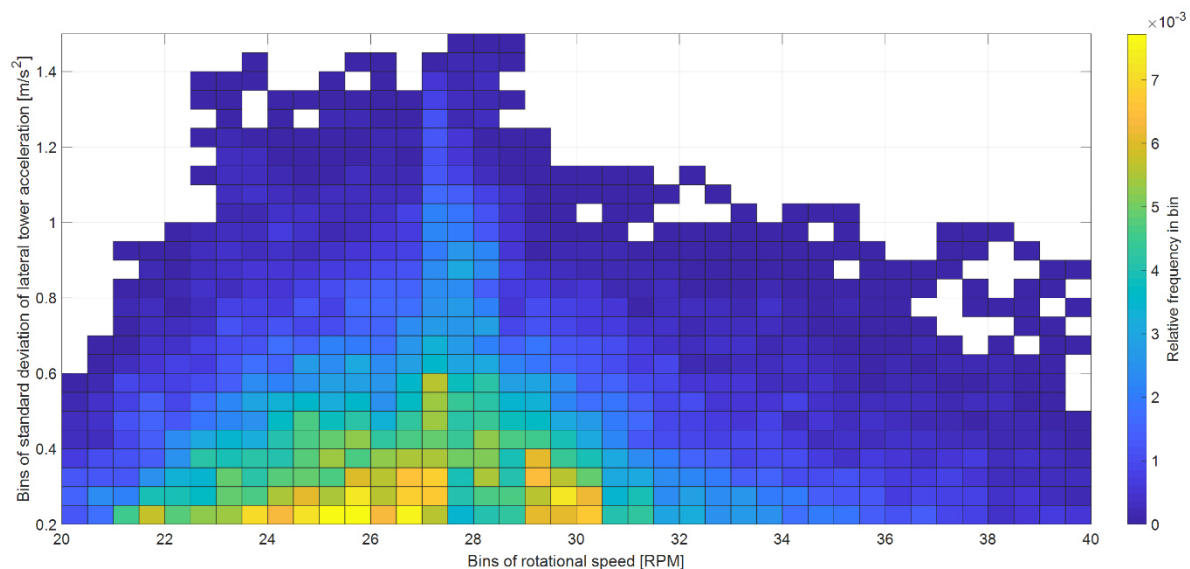
Figure 2 Relative frequency of the standard deviation of tower head accelerations (bin width 0.05 m/s²) vs. rotational speed (bins width 0.5 RPM). The average value of the rotational speed and the standard deviation of the tower acceleration are computed for 2 s periods (appr. one revolution). The first tower eigenfrequency is equal to 27.6 RPM.

The installed measurement equipment allows a comparison of the WT behaviour with and without the mass imbalance. By comparing frequency spectra of the rotational speed, the theoretically described excitations are shown: Figure 3 (a) & (c) show the power spectral density estimates (PSDs) of the rotational speed at two different operating points described by the histograms in Figure 3 (b) & (d) before the rotor was balanced. The PSDs shows the major excitations resulting from the dominant rotational speed (1p, marked with 'A') and its multiples 3p ('C') and 6p ('E'). They also show a very dominant peak at the 1st eigenfrequency of the tower ('B') very likely caused by the mass imbalance of the rotor. In addition, the PSDs also show the assumed eigenfrequency of the mechanical drive train ('G'). However, point 'G' might also be a combined eigenfrequency of the drive train and the blades as it changes slightly with the operating point. In lower part load operation the dominant edgewise eigenfrequency of the blades (see 'D' in Figure 3 (a)) is also visible.

Figure 4 (a) shows the PSD and Figure 4 (b) the corresponding histogram after the rotor is balanced. The operating point is very similar to the one shown in Figure 3 (a). As before the periodic excitations result from the dominant rotational speed (1p, 'A') and its multiples (3p,'C','6p,'E') and have a similar magnitude as in the PSD shown in Figure 3 (a). By contrast, the amplitude of the spectrum at the 1st eigenfrequency of the tower ('B') is approximately 100 times smaller after the rotor is balanced. This shows the positive effect of balancing the rotor not only on the tower but also on the drive train. As before, the eigenfrequencies of the blade ('F') and the drive train ('G') are also prominently visible yet slightly reduced in magnitude.

(a)

(b)

(c)

(d)
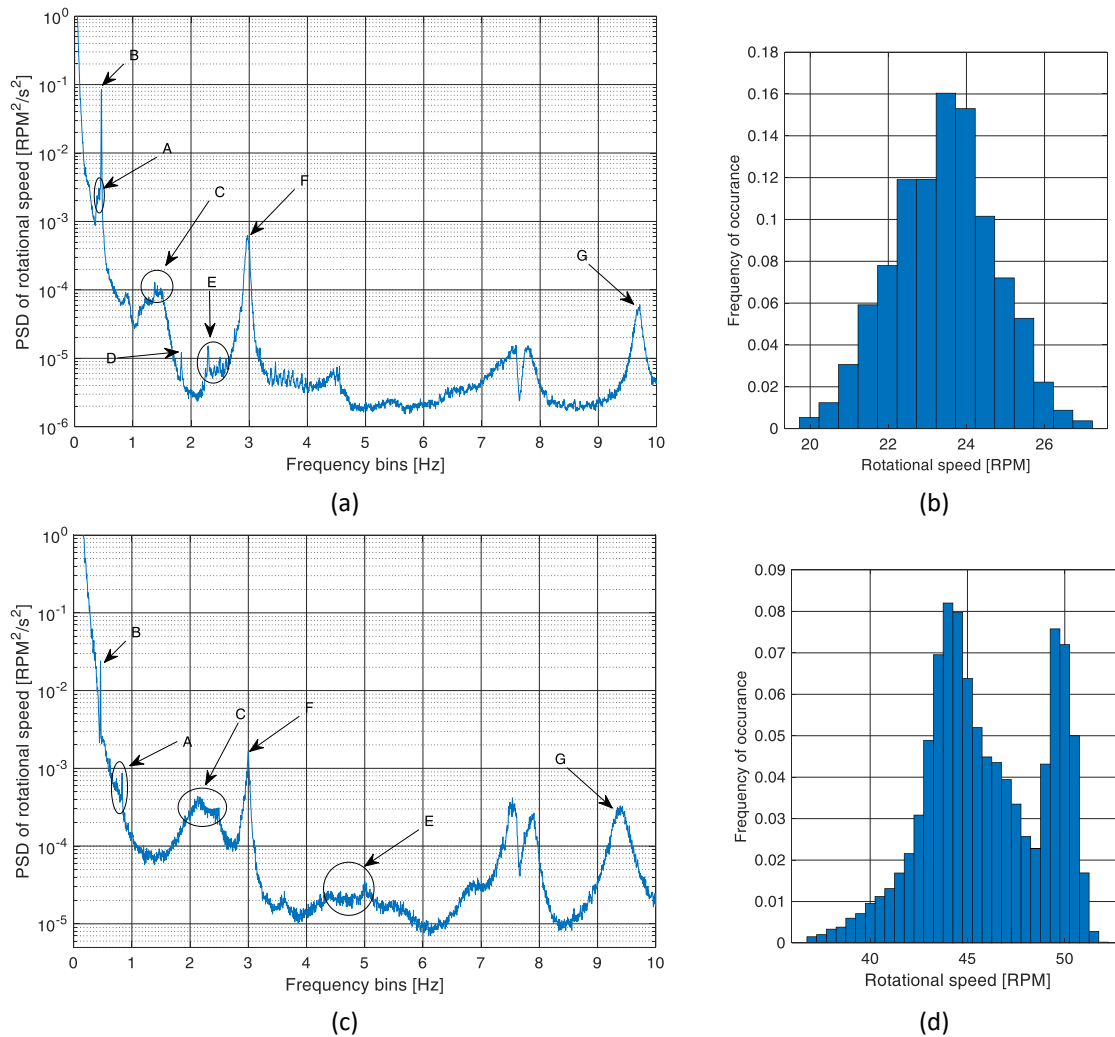
Figure 3 Power spectral density estimates of the rotational speed (a & c) and histograms (b & d) of the rotational speed for two operating points: upper figures close to the 1st eigenfrequency of the tower, lower figures at upper part load and full load. Markers in the frequency spectrum are described in the text. Spectra are calculated for intervals of 262 s and are averaged over 37,000 s (a) and 15,000 s (c).

(a)   (b)
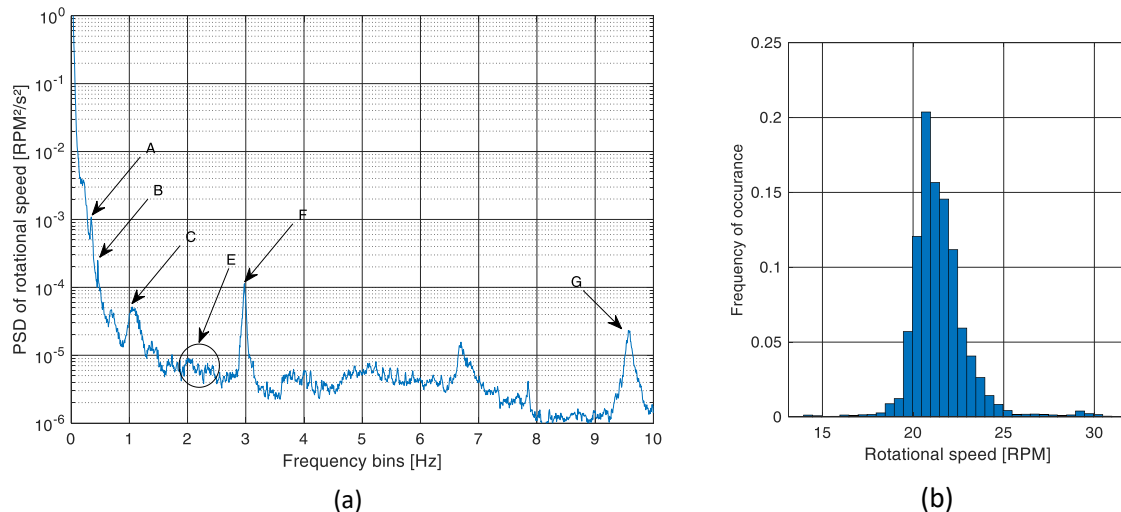
Figure 4 Power spectral density estimate of the rotational speed (a) and histogram (b) of the rotational speed for lower part load after the mass imbalance in the blades has been removed: Markers in the frequency spectrum are described in the text. Spectrum is calculated for intervals of 262 s and averaged over 33,000 s.

2.3   Literature review

The literature review focuses on the requirements for grid frequency support by wind turbines (see chapter 2.3.1), control schemes from original equipment manufacturer (OEMs) and from academia to fulfil these requirements. Furthermore, studies quantifying mechanical loads from grid frequency support are analysed (chapter 2.3.2). In combination, these chapters describe the status-quo for frequency support with WTs. The status-quo for FIM is already described in chapter 2.1.2.

2.3.1   Grid code requirements for frequency support by wind turbines

The requirements for WTs for the connection in electrical grids change constantly. This chapter is based on a review of selected grid codes in 2016 [49] and their updates until 2020. The analysed grid codes are issued by Hydro-Quebec (Quebec, Canada) [50], [51], EirGrid (Ireland) [52], [53], Red Electrica (Spain) [54] and the Central Electrical Authority of India [55]. Furthermore, the results of a working group of National Grid (GB) were considered [56]. These publications were chosen, as these TSOs are known for demanding SI and/or FFR by WTs. The four grids are characterised by a small size with high shares of ICG (Quebec and Ireland), weak grid connections (India) or a large share of ICG with weak connections to the rest of the Central European Synchronous Area (Spain). Hence, all of these grids are likely to experience strong frequency excursions during power imbalances in the grid.

TSOs typically tailor the requirements for the grid connection of WTs to the specific needs in their grid [5]. Hence, in the six analysed documents of grid operators, there is wide variety of frequency support requirements for WTs. The requirements can be sorted in three categories:

1. The WTs have to increase their power output by a predefined value for a specified time once a certain frequency threshold [51], [55] or ROCOF threshold [56] is violated. These requirements can be categorised as special forms of FFR and SI. However, they lack the typical proportionality of the power change to the frequency deviation (droop characteristic) of traditional PFC and the ROCOF proportionality of an IR. In the Quebecois grid, the power output has to be increased by 10 % of the pre-event power output within a second and has to be hold constant for ten seconds. Afterwards, a power reduction during the recovery period is allowed

2. In Ireland, the WTs have to adjust their power output with respect to the frequency deviation with following a droop characteristic defined by the Irish TSO [53]. In addition, the TSO can send power setpoint values directly to the control system of the WT. This requirement can also be characterised as FFR.

3. The WTs have to emulated the IR of a synchronous generator with an inertia constant defined by the TSO [50], [54]. These requirements can be characterised as SI, although they only have to be provided during a limited operating range of the WT, e.g. only if the actual power of the WT exceeds 25 % of rated power.

The requirements of category two and three have the advantage that they are very close to the traditional methods for supporting the grid frequency. Hence, they are not as grid specific as the requirements in category one. Therefore, they allow a more generalized approach to analyse the effect of these grid services on the WTs. By contrast, the requirements of the first category can be tailored best to the specific needs of a grid operator. Therefore, they might perform better than the traditional methods in the specific grids but have to be adopted to the specific grids.

The allowed time for a WT to react to changes of the grid frequency is not well defined. A guideline for measurements of the grid frequency and the calculation of the ROCOF was not available until 2018 [28]. The ENTSO-E publication mentioned up to 1000 ms averaging time for ROCOF measurements during system stability studies. This value seems to be very high compared to another study by the ENTSO-E, which defines allowed reaction time during frequency excursions to less than 100 ms [57]. One of the most challenging situations for a power grid is the frequency stabilization after a severe event [58]. Severe events could be islanding of small parts of the grid (e.g. Flensburg in 2019, publication 5 [59]), larger parts of the grid (e.g. the Iberian peninsula in 2021, [60]) or even splits of extended power systems (e.g. South-eastern Europe in 2021, [61]). Such events can cause large power imbalances up to 40 % of the generated power in an islanded grid [57], which causes very high ROCOFs up to 3 Hz/s [57]. Hence, WT have to provide IR in these situations much faster than the mentioned 1000 ms to keep the grid frequency even within its most extreme stability limits (47.5 Hz - 51.5 Hz). Therefore, the proposed filtering by ENTSO-E is omitted during most of the studies. As this increases the magnitude and variability of the frequency response of the WT, the simulation results can be regarded as a worst case for the WT.

2.3.2 Frequency support methods with wind turbines and resulting mechanical loads

There is a wide variety of publications, addressing the need for frequency support by WTs. In general, the control mechanism mainly follow the requirements of the TSOs. WT manufacturer and sometimes TSOs publish results for grid specific controller, e.g. Enercon [62] and Hydro-Quebec [24] for parts of the Canadian grid. By contrast, academia tries to develop functionalities, which work in various grids e.g. a working group at NREL and University of Colorado [63]–[66]. Early research on IR with WTs was published by Holdsworth et al. in 2004 [67], by Morren et al. in 2006 [68] and by Ramtharan et al. in 2007 [69]. An excellent overview of the development in the field of IR and FFR with WTs in recent years is given by Fernández-Guillamón et al. [19]. The authors sort the publications based on the used control strategies: some adjust the power output proportionally to the ROCOF (i.e. IR) [70]–[74], others to the deviation of the grid frequency (i.e. FFC) [70], [72], [75], [76], and some also on combination of both (typically with two control loops) [70], [74], [77], [78]. From these publications only Hwang et al. [77] also focus on the dynamics of the WT in different operating points. The authors use a similar control approach as this thesis by scaling the frequency response with the operating point of the WT to avoid a high deceleration of the WT.

When WTs need to be curtailed in part load operation, it can be achieved by an increase of the pitch angle [79]–[81] or letting the WT run at super-optimal rotational speed [82]–[85]. For the WT on the campus in Flensburg, Enercon uses a combination of both strategies by alternating the speed setpoint for curtailment below approximately 75 % of rated power [46]. However, the WT will always run at super-optimal speed, which allows stabilising the power output during negative gusts. Theoretically, sub-optimal rotor speed is another option to curtail the WT, but that would require a transient decrease of the electrical power before it could be increased. Hence, this strategy is not suitable for frequency support.

The analysis of structural loads induced by grid services are today typically limited to grid faults, most importantly low-voltage ride through events. Such events lead to high mechanical stress for the drive train of the WT as the electrical torque changes abruptly [86], [87]. Hence, they are considered in the load calculations of WTs. By contrast, there is little research on the consequences of frequency support or FIM. As these services often require a reduction of the active power, Fleming et al. [88] compared different derating strategies, and calculated the effect on the mechanical loads. However, the study did not consider any dynamics during transients, as the WT remains in de-rated operation during the entire simulation time. Wang et al. [89] studied the effect of different IR control methods for two different predefined frequency scenarios at two different wind speeds. The most comprehensive report so far was published by Fischer et al. [90]. They researched the interactions between the supply of various grid services and structural loading of the WT. However, they mainly work with scenarios from the Central European grid, which is very stiff compared to other grids and therefore not very challenging for IR.

3 Simulation models and measurement systems

This chapter briefly introduces the models used for most publications (chapter 3.1 to 3.3) and measurement systems, which were used to develop the scenarios (chapter 3.4).

3.1 Model of the wind turbine

For the main part of this thesis, the so-called 1st eigenmodes simulation model was used to simulate the WTs. It was developed by Clemens Jauch and is documented in detail in a technical report [91]. In this thesis, a brief overview of the most important submodels is given. The model was implemented in Matlab/Simulink by the author and compared to an independent implementation by Clemens Jauch.

The main idea is to model the most important dynamics (i.e. the first eigenmodes) of the main components of a WT (blades, drive train and tower). As shown in the power spectra in Figure 3 and Figure 4 the dynamic of the rotational speed is dominated by the periodic excitations and the eigenmodes of the affected components. Hence, the model allows a reasonable representation of the wind turbine dynamics while saving computational time compared to more detailed models like FAST [92] or FLEX 5 [93] making it a good tool for controller development. The following description of the 1st eigenmodes model is based on the technical report mentioned above [91].

The model of the blades and the drive train is shown in Figure 5. There are eight degrees of freedom: each blade can move in inplane and out-of-plane direction. The aggregated hub mass and the aggregated high-speed-shaft mass can rotate around the main rotation axis of the WT. Each of the blades is divided into two lump masses. The outer masses are located at the centre of gravity of each blade represented by the inertia J_blade_SI_var in Figure 5. The inner masses of the blades and the mass of the hub are combined into one lump mass represented by a combined inertia. The outer and the inner masses are connected via two spring-damper-systems, one in inplane direction and one in out-of-plane direction. The mechanical drive train is represented by a spring-damper-system connecting the hub and blade root inertia with the inertia of the high-speed shaft via an ideal transmission. The high-speed shaft inertia consists mainly of the inertia of rotor of the generator. Hence, the dynamics of the four systems can be expressed by equations similar to (4).

$$J \cdot \dot{\omega} = T_{acc} - k_{damp} \cdot \Delta\omega - k_{spring} \cdot \varphi \qquad (4)$$

Where J is the inertia of the lumped mass, $\dot{\omega}$ is the angular acceleration of the lumped mass, T_{acc} the accelerating torque, k_{damp} the damping coefficient, $\Delta\omega$ the speed difference between the considered mass and the next mass, k_{spring} the spring coefficient, and φ the angular twist between the considered mass and the next mass.
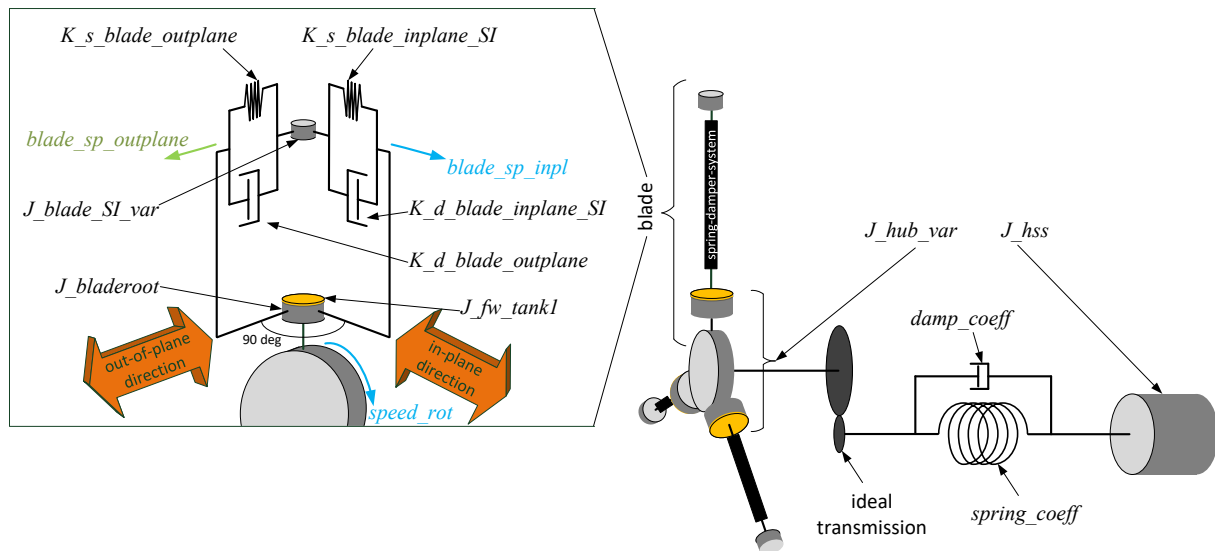
Figure 5 Combined rotor and drive train model of the 1st eigenmodes mode. Figure by Jauch taken from [91].

The aerodynamics in the model are represented by two-dimensional look-up tables of thrust and torque coefficients [91]. The inputs to the look-up tables are the pitch angle and the tip speed ratio. The aerodynamic torque is generated in the outer lumped mass of each blade. By contrast, the thrust force acts partly on the outer lumped mass bending the blade in out-of-plane direction, and partly on hub. Therefore, the latter part of the thrust force bends directly the tower and has no influence on the blades.

The tower is modelled as a single mass at hub height, which is connected to the ground via a system of spring and damper. The tower head mass has two degrees of freedom: it can move in wind direction and perpendicular to it.

The pitch drive is modelled as a PT1 element with a limited slew rate. The input to the pitch drive model is the control signal of the speed controller. Thus, the acceleration of the pitch drive is neglected but the pitch speed is limited.

The generator-converter unit is also modelled as PT1 element modifying the output signal of the power controller. Compared to the model of the pitch drive, it has a much smaller time constant and no limitation to the slew rate. Therefore, power changes can be realized much faster than changes of the pitch angle. The use of PT1 elements for the electrical parts is reasonable, as the electro-magnetic dynamics are much faster than the dynamics of the mechanical components and can therefore be neglected in most situations.

In addition to the work by the author, this thesis also presents some results provided by the industry partner Suzlon Energy. They used the aero-elastic model Flex 5 [93] to calculate load changes and verified the intended controller behaviour of the variable inertia controller.

3.2   Model of the wind turbine control

The WT controller consists of baseline controller for the pitch angle (speed controller) and the generator power (power controller). A simplified block diagram of the modelled control system is depicted in Figure 6.
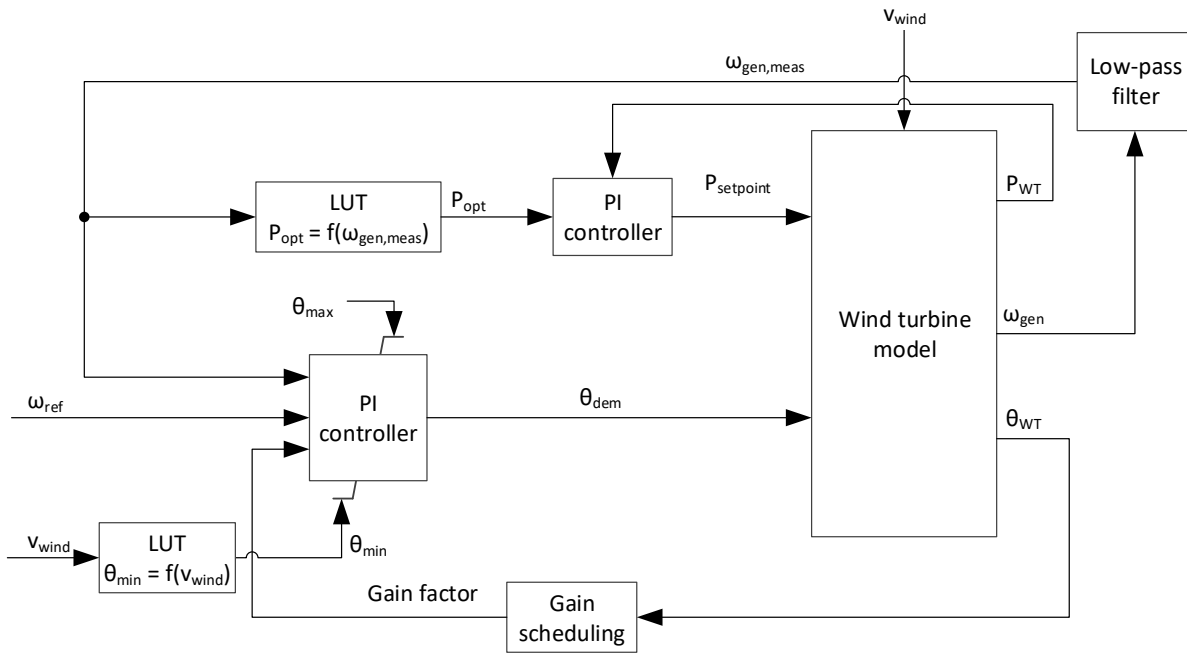
Figure 6 Simplified block diagram of the modelled control system in the 1st eigenmodes model

The speed controller is depicted in the bottom left part of Figure 6. It consists of a PI controller for the pitch angle and a limitation of the output signal. While the maximum pitch angle is constantly 90°, the minimum pitch angle may depend on the actual wind speed and is determined in a look-up table. The inputs to the controller are a typically constant reference speed and the measured generator speed. The measurement of the generator speed is modelled by a PT1 element. The controller gains are scheduled to account for the varying pitch sensitivity in different operating points.

The power controller is depicted in the upper left part of Figure 6. It consists of a look-up table, which chooses the demanded power for the current generator speed, P_{opt}. P_{opt} and the current generator power, P_{WT}, are the inputs to the PI power controller, which determines the power setpoint for the generator converter model. An option for an external power reference is also modelled in the power controller but omitted in Figure 6 for the sake of simplicity. The external power reference can e.g. be used to simulate the effects of a FIM signal from the grid operator. The implementation of the applicable grid support controller into the control system are described in chapter 5 to 7.

3.3   Wind model

The wind model of the 1st eigenmodes model calculates wind speed signals for the three blades separately and an additional signal for the wind at hub height. The model is described in detail in [91]. Here only a brief summary based on [91] is given. The calculation of the wind speed, perceived by the blades, consist of four components:

1. An ambient, turbulent wind speed signal at hub height.
2. Vertical wind shear: The ambient wind at hub height is modified for each blade individually to account for the vertical wind shear in the actual position of the blade (the position of the outer lumped mass as described in chapter 3).
3. The tower blockage: Whenever a blade is close to the tower, the wind speed of the blade is reduced. The speed reduction is faded in and faded out, reaching its maximum when the blade is directly in front of the tower.

4. Interference with tower and blade motion. The wind speed signals calculated in step 1-3 are overlaid with the tower (in wind direction) and blade (out-of-plane) motions.

3.4 Relevant measurement systems and data analysis

One focus of this PhD project is to work with realistic scenarios based on real-world data. Therefore, the most important sources of the used data are summarized in this chapter.

3.4.1 Grid frequency measurements

The effect of the grid frequency support largely depends on the analysed grid frequency scenarios. There are two types of grid frequency scenarios, which were simulated: frequency scenarios derived from measured data in Europe and India as well as a standardised test scenario (i.e. the ENTSO-E reference case [6]).

Within a synchronous area, the grid frequency is almost identical in the whole grid. Its dynamics largely depend on the analysed grid. Hence, geographically smaller grids and grids without strong AC interconnections among itself or to neighbouring grid, are more likely to exhibit strong variations of the grid frequency. This effect is especially strong, when a large amount of ICG (e.g. modern WTs) are connected to the grid and replace generation of conventional power plants. By contrast, the Central European Grid is highly interconnected, stretches almost over the entire continent and has high share of synchronously connected generator in conventional power plants providing much inherent inertia (e.g. nuclear in France, coal in Germany and Poland, hydro in Spain). Hence, its grid frequency varies very little. At the start of the PhD project, there was very little publically shared data of the grid frequency in Europe or in fact anywhere in the world. The available data was not sufficient for simulations of the dynamic response in terms of precision and time resolution. On the upside, the power production in the Central European grid was well documented down to the level of single power plants at any hourly interval [94]. Hence, it was possible to set up a measurement campaign for the grid frequency in the Central European grid [95] and analyse the correlation between load levels, shares of renewable power on the generation and the ROCOF [96]. The idea was to derive a correlation between the generation mix and the ROCOF, which allows estimating the behaviour in more volatile (future) grid. However, the results show a relatively weak correlation between the ROCOF and the share of ICG. One explanation for this effect is that power plants provide their full inertia as long as they are connected to the grid, i.e. independently of their operating point. Hence, the data was not extrapolated to generate scenarios for the grid frequency behaviour in a grid dominated by ICG.

However, Suzlon Energy was able to provide high-quality measurements recorded in one of their Indian wind farms. As the Indian grid is very weak compared to the Central European, the grid frequency data shows much more variability and much higher ROCOFs. Therefore, the data can be used to estimate the effect of IR on the WT in a challenging grid, comparable to the situation in a (future) grid with less inherent inertia. An analysis of the Indian data showed that there are often abrupt changes of the grid frequency, which are called events hereafter. Providing inertial response during these events causes high mechanical loads to some components of the WT [49]. Furthermore, there are extended periods during which the grid frequency oscillates. When these oscillations occur with at specific periods, they may excite WT components to critical oscillations. By contrast, the study also revealed that the normal behaviour of the grid frequency on a typical day did not cause significant harm to the WT. Hence, the data was once more analysed with a focus on the frequency events and periods of grid frequency oscillations. From this analysis, the scenarios used in publication 3 were derived.

In addition, data from a measurement campaign in Ireland was used [97]. As the Irish power system is only connected via HVDC links to other power system, it is a good example for a small grid with occasionally high shares of ICG and thus little inherent inertia.

As a side effect, the measurement campaign in Flensburg revealed market-induced hourly and quarter-hourly regular patterns of the grid frequency. One example is shown in Figure 7: in the morning, the grid frequency regularly exceeds 50 Hz so much, that PFC is activated.
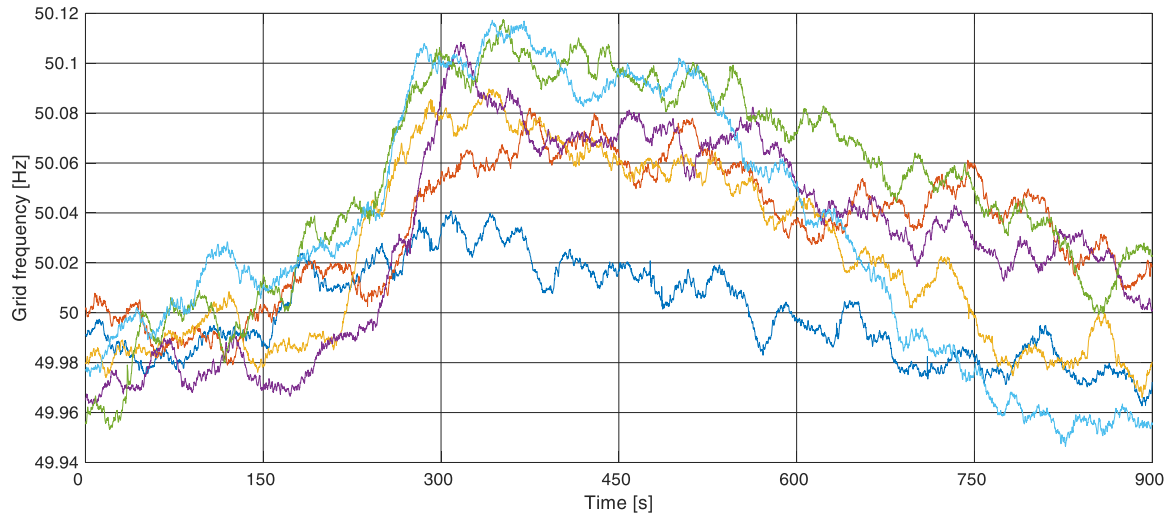
Figure 7 Changes of the grid frequency in Flensburg on the hour, 6 a.m., for various days used in [98]

Such grid frequency patterns occur very regularly and can cause significant deviation of the grid frequency from 50 Hz. Hence, they should be analysed to understand its significance for the supply of IR by WTs. However, an analysis of the data reveals that, these changes occur at small ROCOFs. In a conference paper [98] it was shown, that SI supply during these frequency patters do not cause high power variations and have no significant affect on the energy yield of the WT. Therefore, the regular patterns in Central European grid frequency can be ignored for the further analysis of the controller evaluation.

3.4.2   Wind data

Several publications use data from the met mast on the campus in Flensburg. During a previous research project, the met mast was equipped with three Thies ultra-sonic anemometers, metrological sensors and a new data logger. The measurement system is described in detail in the report of the project [46].

Additionally, data published by the German Weather Service [99] were used in publication 5 [59] due to a downtime of the measurement system on campus caused by maintenance.

3.4.3   Other grid data

For publication 6 [39]and 7 [100], power measurements recorded at the point of common coupling of the campus Flensburg were used. The measurements were read via a Modbus connection from a standard measurement device [101], which has already been installed at the grid connection point. The publications also used power measurements of the E30 recorded with the measurement system described in [46].

For the analysis of the blackout in Flensburg, the Stadtwerke Flensburg provided data from their SCADA system. The data mainly consisted of RMS values for voltage and current at the power station and

important grid nodes as well as frequency measurements at the power station. This data was analysed, aggregated, and combined with frequency measurements at WETI to derive the scenarios for publication 5.

4   Research overview

For this dissertation, research was conducted related to FIM and grid frequency support. While both grid services deal with different aspects of operating an electrical grid, they both lead to changes of the active power of the WT. Hence, the effects on the WT operation are comparable: the control of the WT is partly decoupled from the available power in the wind. Figure 8 lists the peer-reviewed journal papers published during this dissertation project and shows how they are related. The publications are not numbered chronologically but with respect to the researched field. The author is the main author of publication 2 -5. The contribution of each author is documented in the respective publications.

Publication 1, [15], assesses the importance for SI provision in the (future) grid in continental Europe, and quantifies the needed supply of SI. Furthermore, the economic value is estimated by comparing the provision costs with different storage technologies.

Publication 2, [102], introduces the variable H controller as a new concept of providing synthetic inertia with WTs and compares it to a classic approach. The variable H controller seeks to balance the interests of WT manufacturers, WT operators and the grid operators. The general idea is that WTs provide SI continuously depending on their current operating point.

Publication 3, [103], quantifies the effect of providing SI on the mechanical loads of a state-of-the-art WT. It is also written in collaboration with Suzlon Energy and extends the findings of a common research project [49]. This study analysis the effect of grid frequency scenarios carefully derived from high-quality measurements of the Indian grid frequency. It also looks at the effects of using a standard measurement system in comparison to the high quality data.

Publication 4, [59], analyses the capabilities of grid frequency support by WTs in case of grid islanding. The case study is based on measurements conducted during the black out in Flensburg in 2019. In addition to the aforementioned variable H controller, a FFR controller is used to stabilise the grid with help of WTs.

Publication 5, [104], extends the frequency support controller used in publication 4 by a feedforward loop. It is designed to avoid overspeed situations of the WT, which can occur during extreme grid events. The publication analyses the effect of this additional control loop on the accelerations of the most affected WT components and on its energy yield.

Publication 6, [39], introduces continuous FIM and compares it to the classical German FIM strategy in terms of the grid utilization, WT dynamics and its energy yield. The case study is designed based on measurements carried out at the campus in Flensburg and seeks to model a weak grid connection, which commonly occurs in Schleswig-Holstein and other remote areas.

Publication 7, [100], extends publication 6 by simultaneously and continuously providing SI and FIM. Consequently, the case study is extended by a measurement of the grid frequency and the corresponding IR of the WT. In addition to the time-domain simulations of the study case, it interaction of both grid services is also analysed in the frequency domain.

Additionally, Table 1 gives an overview of the models, the controller and the scenarios of the simulations used in the publications 2-6.
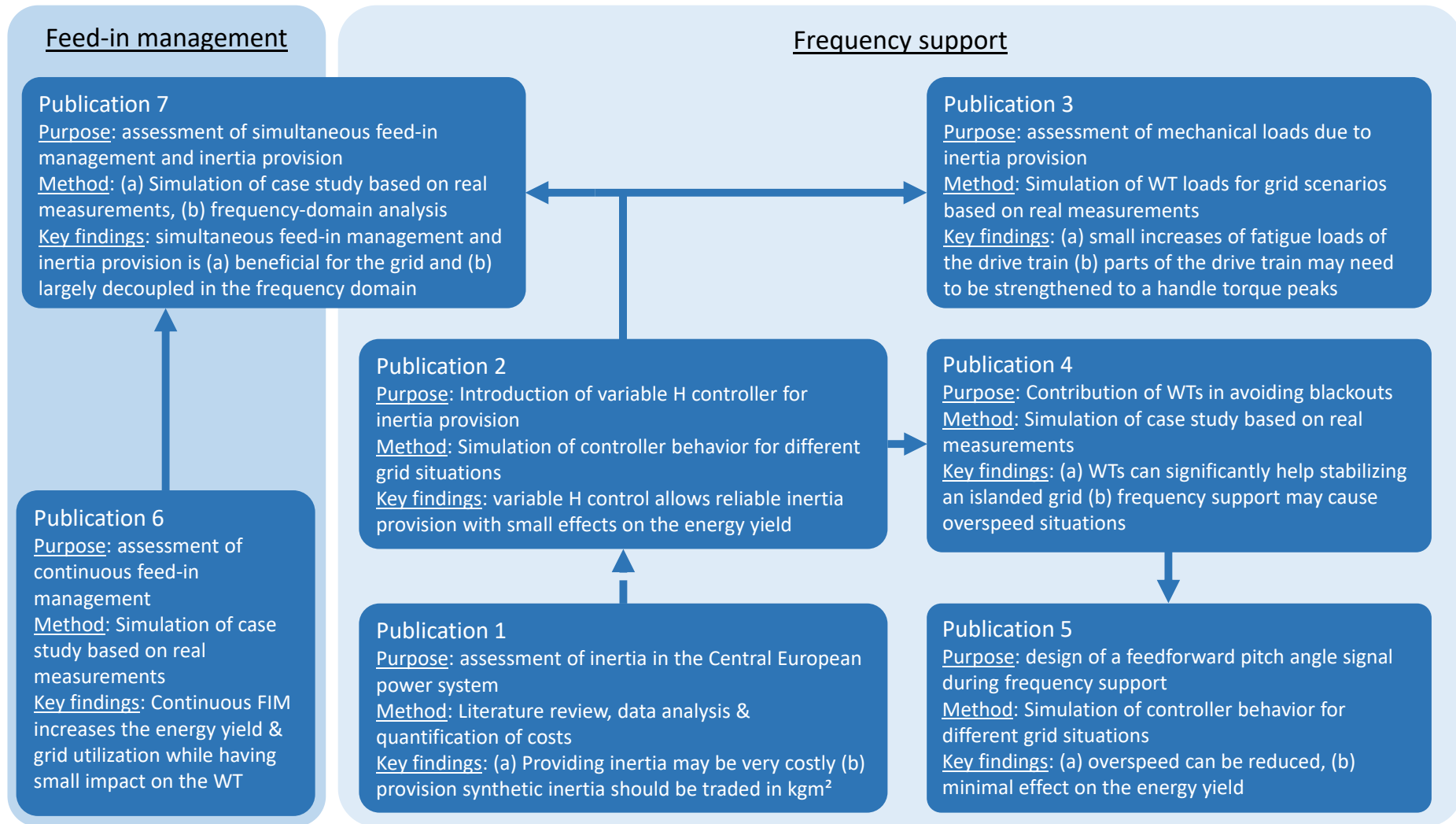
Figure 8 Overview of the peer-reviewed publications used in this dissertation and their relationship

Table 1 Overview of the used models, controller, parameter and scenarios for the peer-reviewed publications with WT simulations

No	Wind turbine & wind model	WT controller	WT parameter	Grid support controller	Database grid scenarios	Wind scenarios
2	1st eigenmodes model	Suzlon state machine	Suzlon DFIG WT 2.x MW	Inertial response	ENTSO-E reference case Measurements Suzlon Measurements WETI	3 wind speeds, 2 turbulence seeds
3	Flex 5	Suzlon state machine	Suzlon DFIG WT 3.x MW	Inertial response	Measurements Suzlon	5 wind speeds, 5 turbulence seeds
4	1st eigenmodes model	Baseline controller	NREL 5M	Inertial response Fast frequency response	Measurements WETI and Stadtwerke Flensburg	time trace based on scaled measurements 10 turbulence seeds
5	1st eigenmodes model	Baseline controller	NREL 5M	Inertial response Fast frequency response Pitch angle adjustment	Measurements WETI and Stadtwerke Flensburg ENTSO-E reference case Measurement Ireland	6 wind speeds, 20 turbulence seeds
6	1st eigenmodes model	Baseline controller	NREL 5M	Feed-in management	Measurements WETI	24 h time trace based on scaled measurement with offsets
7	1st eigenmodes model	Baseline controller	NREL 5M	Inertial response Feed-in management	Measurements WETI	24 h time trace based on scaled measurement with offsets

5   Frequency support with wind turbines

This chapter summarizes the publications 1-5. It describes the models and the controller used in the publications, the simulated scenarios and the results of the studies. Henning Thiesen is the main author for this publication.

5.1   Publication 1

Publication 1 [15] assesses and quantifies the need for SI in the electrical grid covering most of continental Europe, i.e. the European Continental Synchronous Area (ECSA). In the publication, it is shown that the inherent inertia in the power systems tends to decline due to the phase out of conventional power plants and the tendency to connect rotating loads via power electronics. In the publication it is assumed, that the current, proven system of frequency support as outlined in chapter 2.1 should be preserved. In combination with the decline of inherent inertia, this leads to an increasing need for synthetic inertia or a similar service in a future power system. Such a service has to help the grid operator to fulfil both targets of the grid frequency control stated in chapter 2.1. Inherent inertia automatically exchanges power with grid whenever the grid frequency changes. As it is a measure of the kinetic energy, E_{kin}, stored in the directly connected rotating masses, the power can be expressed by the change of the stored energy with respect to time (see equation (5)):

$$P_{inertia} = \frac{\delta E_{kin}}{\delta t} = J_{Sys} \cdot \omega_{grid} \cdot \frac{\delta \omega_{grid}}{\delta t} \qquad (5)$$

The energy provided by inertia over a certain time can then be obtained by integrating equation (5). The power and the energy aspect of inertia help to fulfil the two targets for frequency control outlined in chapter 2.1. Hence, it is reasonable to require a certain inertia rather than a specific power or a specific energy, if inertia is to be emulated. Otherwise, one target of frequency control is neglected.

In the publication, it is argued that inertia provision in a future power system should rather be a tradeable commodity or a payed service than a requirement. Some generation types (e.g. PV power plants) have no inherent energy storage comparable to the rotating rotor of a WT and thus additional storage units or curtailment to provide IR. Hence, unlike today inertia will have a certain value in a future power system. The publication is a first attempt to quantify this value of inertia. For the example of the ECSA, the needed amount of inertia is a future system is quantified to be $3.11 \cdot 10^6$ kgm² by using simulations of the grid frequency during for the ENTSO-E reference incident [6]. This value is combined with the frequency thresholds, for which generators have to remain connected to the grid, to estimate the needed power and energy of a storage system to provide inertia. As inherent inertia provides large amounts of power but only for a very short time, the storage system requires a high rated power (P_{SI} = 12.65 GW) but comparable little energy (E_{SI} = 6.75 MWh).

The cost of the energy storage system are compared for five technologies: three different batteries types (lead-acid, lithium-ion and sodium sulphur), super capacitors and synchronously connected flywheels. Based on a literature review, the costs (e.g. investment costs, operation and maintenance) and the lifetime of the storage system as well as the needed power electronics are estimated. Based on this data, the net present value (NPV) can be calculated for each storage system using equation (6).

$$NPV = I_t + \sum_{t=1}^{T} \frac{C_t}{(1+r)^t} \qquad (6)$$

Where I_t is the initial investment, C_t the cash flow at time t, r the discount rate, and T the assessed period.

The cost per provided unit of inertia is also calculated, by introducing the levelised cost of inertia (LCOI). The calculation follows the approach of calculating the levelised cost of energy. In doing so, the overall costs of the storage systems are allocated to the inertia provision per year over the assessed period.

Table 2 Data and result table for the economic evaluation

		Lead Acid	Li-Ion	Sodium Sulphur	Super Capacitor	Flywheel
Data used for calculation						
Cost Storage (Power)	(€/kW)	175	175	175	15	300
Cost Power Electronics	(€/kW)	155	155	155	270	-
Cost Storage (Capacity)	(€/kWh)	175	550	600	15,000	1,000
Operation & Maintenance	(€/(kW·years))	11.50	9	18	4	4
Life Time	years	10	20	20	12	20
Results						
NPV	(billion €)	11.8	8.82	10.6	8.24	7.19
LCOI	(€/(kg·m²·year))	275	206	247	192	167

Table 2 shows the data used for the economic assessment and the results of the NPV and the LCOI. A flywheel storage system proved to be the cheapest option for inertia provision under the assumptions of the study. However, the annual price of 167.64 €/(kgm²·year) is very high. Therefore, an inertia provision with a storage system dedicated solely for this purpose is not recommended.

The publication is connected to the other publications in the field of frequency support by showing and quantifying the need for and the value of SI in Central Europe. Furthermore, it shows that defining a specific amount of inertia is a reasonable way of the covering the power and the energy aspect of inherent inertia.

5.2   Publication 2

Publication 2 [102] is an extension of a paper originally published at the Wind Integration Workshop in Berlin in 2017 [105]. After the workshop, the authors received an invitation to publish an extended and peer-reviewed version in IET Renewable Power Generation. The purpose and the main contribution of this paper is to introduce the idea of a variable H controller, which is described in detail in chapter 5.2.2.

5.2.1   Simulation model, control system and parameter

The 1st eigenmodes model described in chapter 3 is used for the WT simulation in publication 2. The parameter represent a Suzlon 2.x MW DFIG WT. The Suzlon state machine is used as control system of the WT and linked to the 1st eigenmodes model in Matlab/Simulink. The interface is described in detail in the report of the research project [49]. As drive train and tower dampening is deactivated, the power and speed control is similar to the one used in the 1st eigenmodes model (see Figure 6).

5.2.2   Controller grid support

As stated in chapter 2.3.1 inertial response with WTs is demanded by an increasing number of TSOs. The definition of a specific amount of inertia is a reasonable way of demanding inertial response as shown in chapter 5.1. In order to account for different sizes of the power plants, it is typically expressed as an inertia constant, H. The inertia constant is defined as the theoretical time a power plant can provide its rated (apparent) power, S_{rated}, solely from its rotational kinetic energy at rated speed [8]. It can be calculated using equation (7).

$$H = \frac{E_{kin}}{S_{rated}} = 0.5 \cdot J \; \frac{\omega^2}{S_{rated}} \tag{7}$$

For the sake of simplicity, it can be assumed that $S_{rated} \approx P_{rated}$. Rearranging equation (7) and combining it with equation (3), the power injection from a synchronously connected generator can be expressed with help of the inertia constant. Furthermore, the angular velocity is replaced by the frequency as the term 2π can be removed from the fraction, leading to equation (8).

$$P_{IR} = -2 \cdot H \cdot P_{rated} \; \frac{ROCOF}{f_{grid}} \tag{8}$$

The concept of a fixed inertia constant makes sense for a conventional power plant, as these typically use directly connected, synchronous generators. Such generators operates in a very narrow speed band around rated speed. Even during extreme scenarios, the generator speed varies by less than 5 %. By contrast, variable speed WTs can vary their speed by at least 40 % (doubly fed induction generators, [102]) or even more than 60 % (full converter WTs [46]). Hence, the stored kinetic energy varies with the operating point of the WT. This makes it difficult to supply the same amount of IR over the full operating range. However, when WTs operate in part load operation, they need to provide less IR compared to the operation in full load. As argued in the conference paper [105], the grid needs a specific amount of inertia to be stable. When operating in part load WTs only provide a share of the power production to the grid and therefore only need to provide a share of the needed inertia. Consequently, the concept of a variable H controller for the provision of synthetic inertia with WTs was developed.

The concept of the variable H controller ensures a reliable reaction of the WT during IR, regardless of the operating point. A study conducted for the Australian Electricity Market Operator from 2017 backs this approach by stating that a reliable provision of IR by WTs is more important than mimicking the IR

of a SG exactly [106]. In the same study, WT OEMs state that the capability to provide IR varies 'roughly linearly with the power level'. This is very similar to the general idea of the variable H controller of scaling the inertia constant demanded by the TSO with the available kinetic energy stored in the WT drive train. The available energy is defined by the differences in kinetic energy between the current rotational speed of the generator, ω_{gen}, and the cut-in rotational speed, ω_{cut-in}, at which the WT starts to produce power:

$$\frac{H_{var}}{H_{dem}} = \frac{0.5 \cdot J_{WT} \cdot (\omega_{gen}^2 - \omega_{cut-in}^2)}{0.5 \cdot J_{WT} \cdot (\omega_{rated}^2 - \omega_{cut-in}^2)} \tag{9}$$

Figure 9 shows the effect of the variable H concept on the inertial response of the WT: the WT provides very little inertial response at lower part load operation when there is little kinetic energy stored. By contrast, it has to provide the full inertial response when a lot of kinetic energy is stored. The figure also shows values for rotational speeds above rated speed for the transient operation in overspeed. This logic works as long as the demanded inertia constant in the same range as the (hidden) inertia of the WT. For WTs in the 2-3 MW class inertia constants of 5 s to 6 s have been reported [19]. The tendency to use longer rotor blades for the same power rating (especially on low wind speed sites) [107] should increase the (hidden) inertia of the WT further. Therefore, it is likely that more kinetic energy is available for frequency support in the future.

Today, some grid operators define power thresholds below which the WTs does not have to provide IR at all [51]. When looking at the reliability of the IR, it seems beneficial to scale the response over the full operating range than defining on/off thresholds. Furthermore, the IR is sometimes only activated once a certain ROCOF or grid frequency threshold is violated [51], [56]. This seems to work well in the current situation with only a moderate reduction of the inherent inertia. However, as the power systems strive towards 100 % renewables, inherent inertia will be reduced dramatically. Hence, even small power imbalances in the grid may lead to strong frequency excursions and to frequent violations of such thresholds. In order to reduce any frequency excursions, it is proposed to provide synthetic inertia continuously.
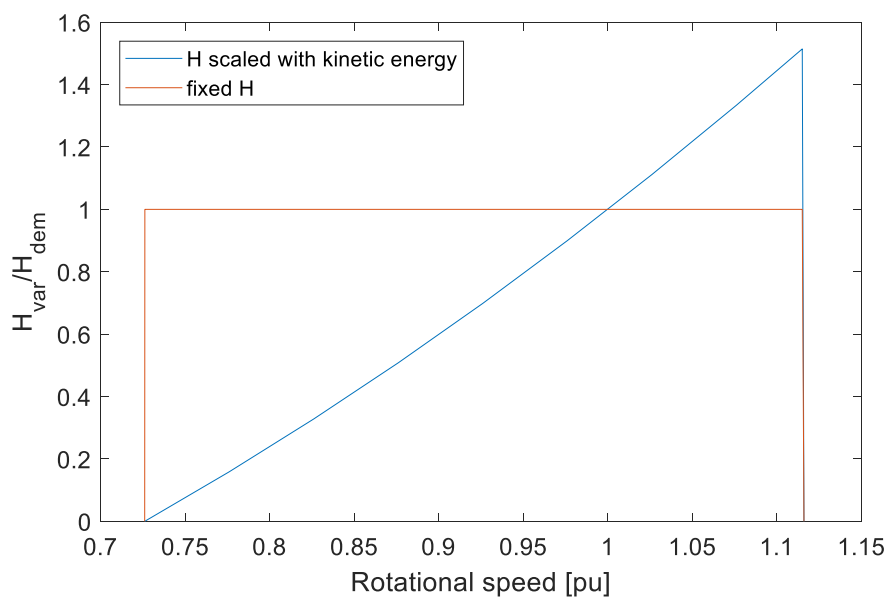
Figure 9 Comparison of the normalised variable and fixed inertia constants, i.e. the strength of the inertial response, for the full operating range of a DFIG WT [102].

The variable H controller is implemented in the power controller of the WT (see Figure 10 and Figure 11). The power for IR, P_{IR}, is added to the output of the power-vs-speed characteristic of the WT, P_{opt}, to create a modified reference value, P_{ref}, for the PI controller. Hence, the WT will leave its optimal operating point for steady-state operation because of the IR. The IR is calculated using equations (8) and (9). Hence, there are three inputs to the calculation: the demanded inertia constant, H_{dem}, specified by the TSO, the grid frequency measured at the WT and the measured generator speed.

As there were concerns, on whether the provision of IR may cause oscillations of WT components, the accelerations of the most important WT components were also used in the control concept. If the accelerations of these components had exceeded a certain threshold, the P_{IR} signal would have been dampened. The outputs of the LUTs in Figure 11 vary between 0 and 1 depending on the RMS value of the corresponding acceleration signals. However, the simulations have shown that these precautions were not necessary. Hence, this part of the controller is omitted in future publications.

Furthermore, the minimum pitch angle table has been extended by also considering the actual generator speed. The idea was to keep a constant angle of attack in part load operation even though the WT leaves its optimal operating point. However, as the simulations have shown that the gain of the energy yield was minimal, the concept was also dropped to reduce the pitch activity of the WT.
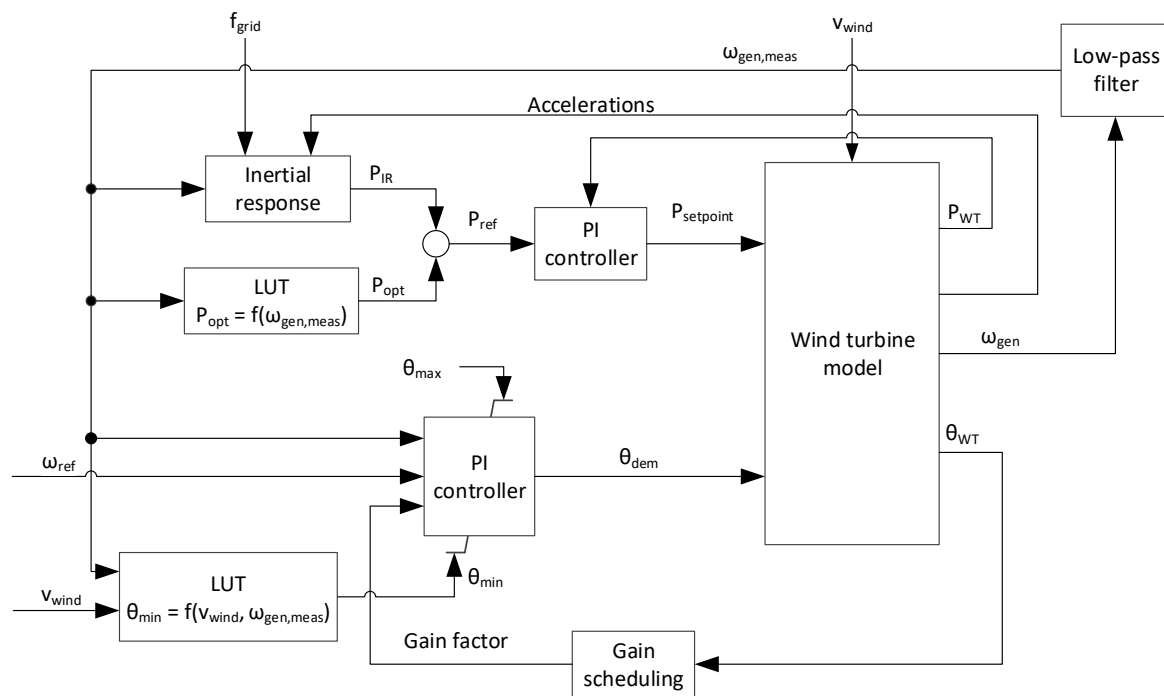
Figure 10 Implementation of the inertial response into the control system of the WT
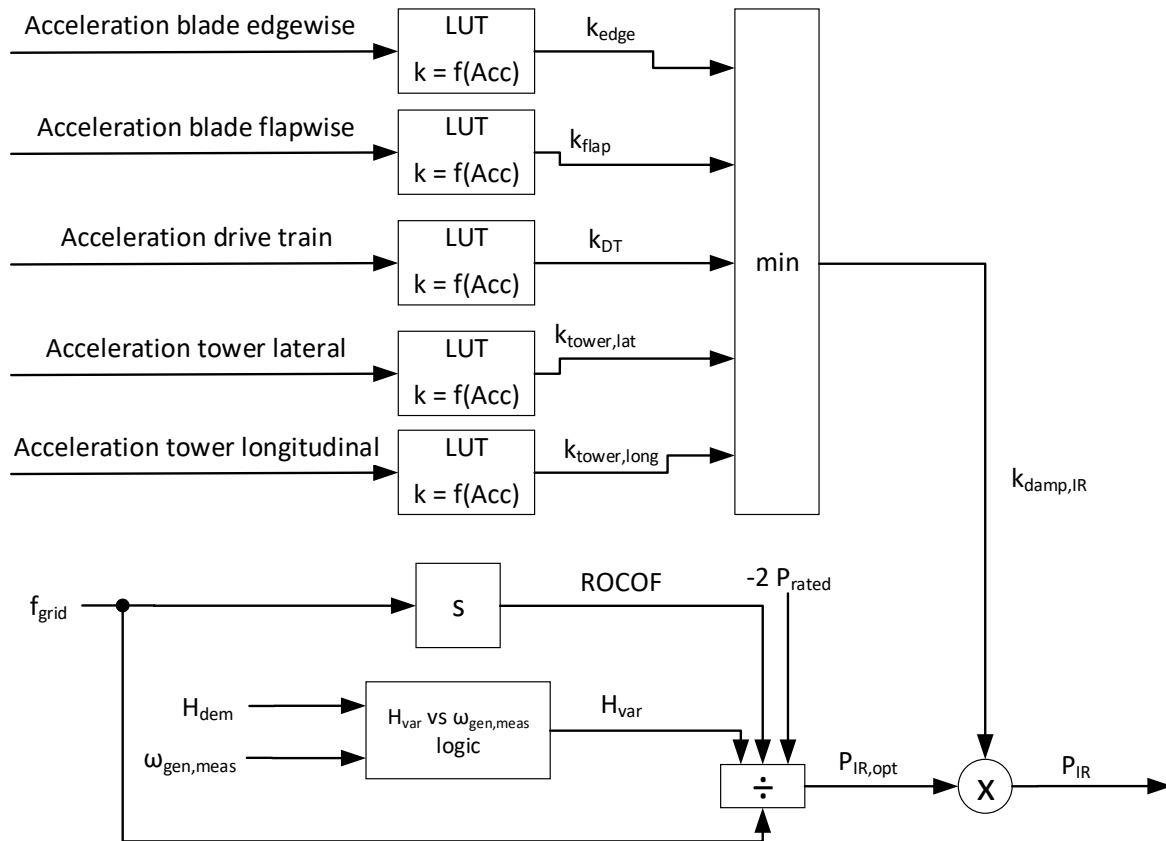
Figure 11 Content of the inertial response block in Figure 10.

5.2.3   Analysed scenarios

All simulations used in the publication compare the behaviour of a WT providing IR with the variable H controller, to one with a fixed H controller (using equation (7)) and to one without IR. The inertia constant demanded by the grid operator, H_{dem}, is set to 6 s, which is a typical value for some conventional power plants [8], [19] and some WTs [19].

In the publication, the behaviour of the WT providing IR is shown for two scenarios of the grid frequency and different wind speed scenarios:

a) The well-known ENTSO-E reference case [6] is used show the general behaviour of the controller. It is shown for three time traces of the wind speed in part load operation, one at lower part load with a low turbulence intensity (TI = 0.08) and two at higher part load; one with a low TI and one with a high TI (0.1 and 0.2). For the latter TI, the time traces of grid frequency and the wind speed have been aligned such that the WT needs to provide additional power at the end of a negative gust.

b) A measurement of the Indian grid frequency as discussed in chapter 3.4 is used to analyse the energy losses in part load operation. To cover the typical variations of the grid frequency during the day, a 24-hour long time trace of the grid frequency is used. The average wind speed during the simulation is constant at 8 m/s and at a low TI (0.1).

5.2.4   Results

The results of the simulation show, that a variable H controller allows the WT to provide SI reliably even during challenging scenarios. A coinciding negative gust may decrease the aerodynamic power, while the WT has to provide additional electrical power for frequency support. Hence, the drive train

is strongly decelerated. Simulations have shown that a WT equipped with a fixed H may drop out of power production when the generator speed falls below the cut-in speed for too long. The exact behaviour of the WT depends on the used state machine. Figure 12 shows the simulation results with the Suzlon controller in lower part load. The WT with the fixed H controller drops out of power production soon after the start of the frequency event (at t = 20 s). Thus, not only the IR is lost, but also the normal power production of the WT. The WT with the variable H controller hardly provides inertia in this situation but remains connected to the grid. As argued above the WT does not have to support the grid strongly in this operating point but it has to remain connected.
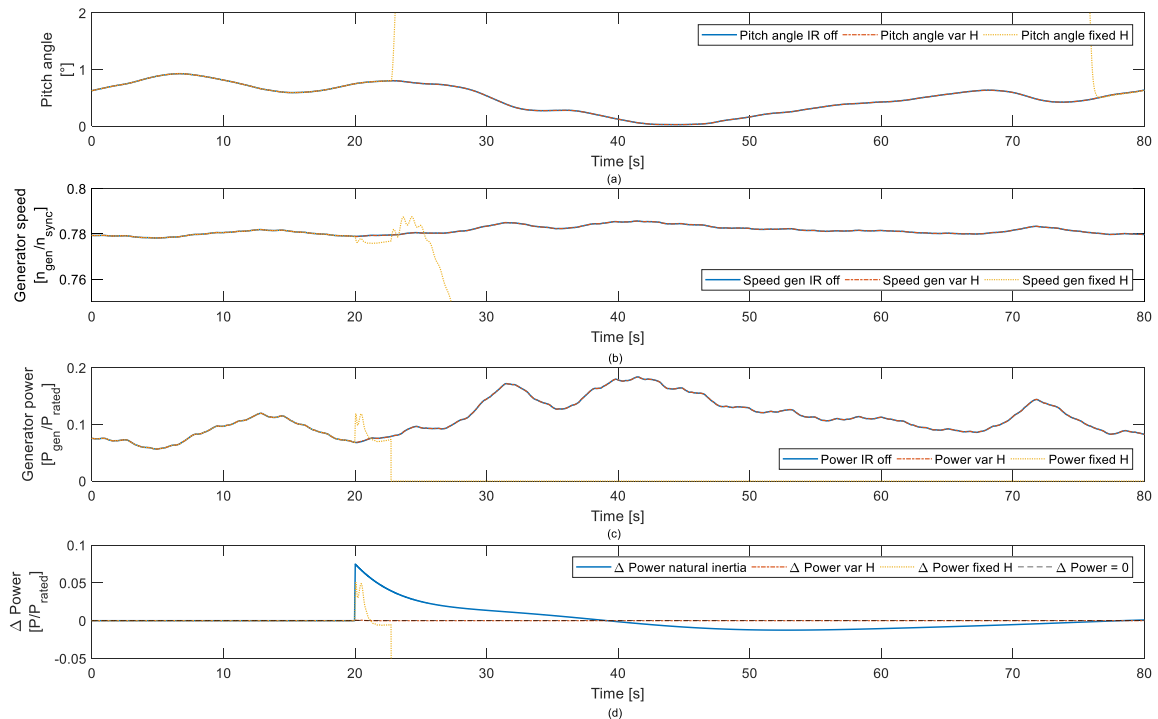
Figure 12 Simulation results for lower part load. Comparison of the pitch angle (a), the generator speed (b), and the generator power (b) for the variable H controller (dash–dotted lines), the fixed H controller (dotted lines), and without providing IR (solid lines). In (d) the power differences are given for the variable H controller (dash–dotted line), fixed H controller (dotted line), and the theoretical value for a synchronous generator with H = 6 s (solid line, according to (7)).

Figure 13 shows the simulation results for the upper part load and low TI scenario. After the frequency event at t = 20 s, the power increase for the fixed H controller is slightly higher than the for the variable H controller (see Figure 13 (c) and (d)). However, the generator speed remains higher for the variable H controller (see Figure 13 (b)) and thus the power deficit in the recovery phase of the generator speed (starting at t ≈ 28 s) is smaller. Hence, both controller provide approximately the same amount of energy within in the first 20 s after the frequency event. This makes the performance of both controllers in terms of grid support is very similar in this operating point.
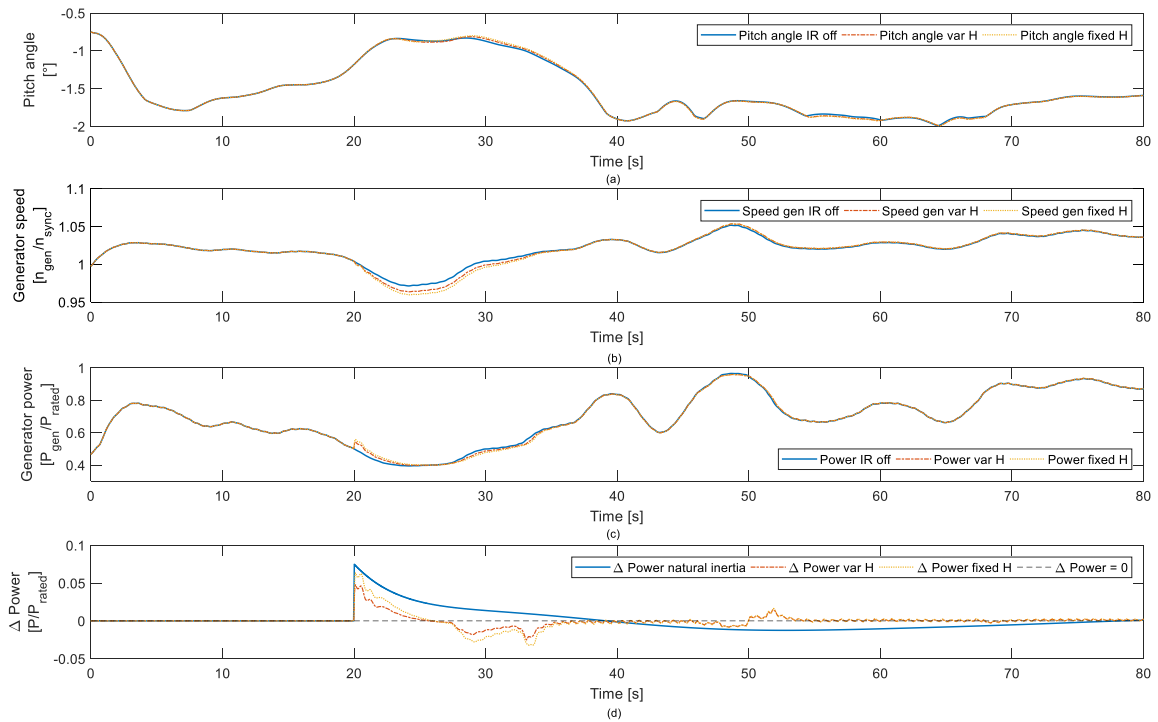
Figure 13 Simulation results for upper part load and low TI. Comparison of the pitch angle (a), the generator speed (b), and the generator power (b) for the variable H controller (dash–dotted lines), the fixed H controller (dotted lines), and without providing IR (solid lines). In (d) the power differences are given for the variable H controller (dash–dotted line), fixed H controller (dotted line), and the theoretical value for a synchronous generator with H = 6 s (solid line, according to (7)).

In addition to the behaviour of the controller during grid events, it also important that the energy yield of the WT does decrease unduly during normal operation. For this purpose, a 24 h simulation as defined in chapter 5.2.3 was chosen. The provision of IR reduces the energy yield of the WT by approximately 0.3 % for both tested controller (see Figure 14 (a)). The losses are relatively small considering that the power adjustments for SI vary between ± 0.1 pu due to the high volatility of the Indian grid frequency.
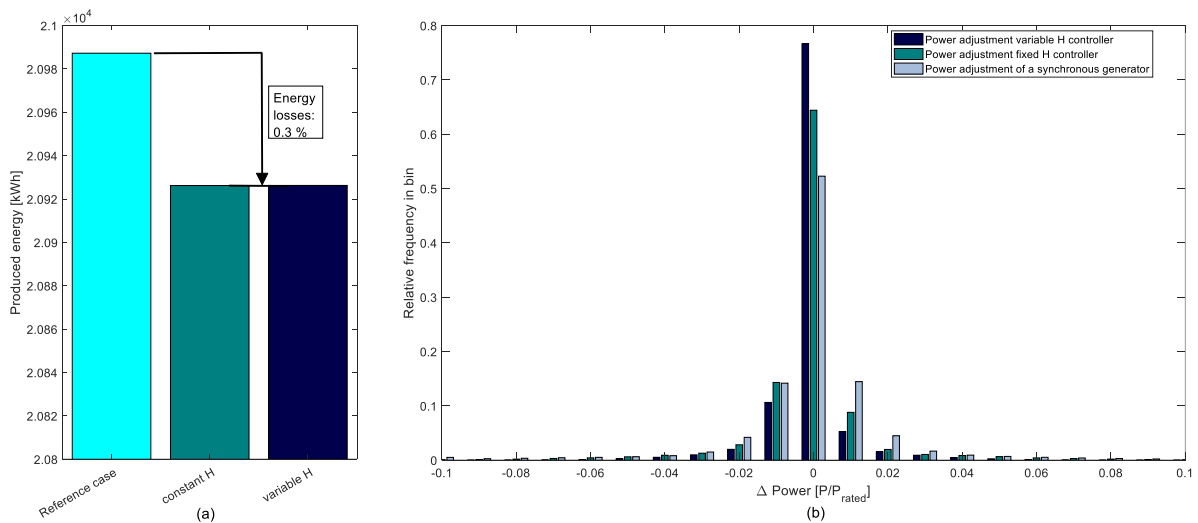
Figure 14 Simulation results for the quantification of the energy losses. (a) Comparison of the energy production in the reference case (no SI), with constant H control, and variable H control, (b) Histogram of the power adjustments for SI of the fixed and variable H controller compared to the theoretical power adjustment of a synchronous generator with H = 6 s.

5.3   Publication 3

Towards the end of the research project of Suzlon Energy and when writing the final report [49], it became clear that the influence on the mechanical load heavily depend on the simulated grid frequency scenarios. Furthermore, there was a significant lack of scientific literature dealing with the effect of grid support on mechanical loads of WTs. Consequently, the Indian grid frequency data was analysed in detail. Detailed scenarios were derived and were tested for a state-of-the-art Suzlon WT (3.x MW). These simulations were supplemented with hardware-in-the-loop tests to look at the effects of the used frequency measurement system in the WT. An overview of the methodology used in publication 3 [103] is depicted in Figure 15.
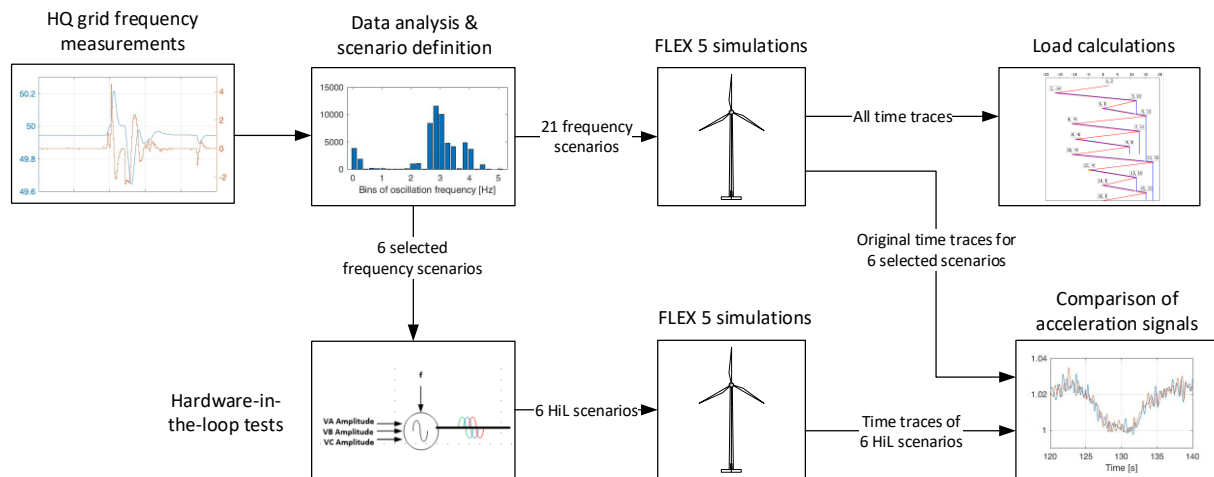
Figure 15 Overview of the methodology used in publication 3.

5.3.1   Simulation model, control system and parameter

All simulations for this publication have been conducted by Suzlon using Flex 5 [93] with a second-order model of the generator-converter unit. The parameter of the simulation model represent a state-of-the-art 3.x MW DFIG WT.

Suzlon's state machine including drive train and tower damper is used for the control. A simplified version is shown in Figure 16, which does not depict the drive train and tower damper. It is extended by the variable H controller as described in chapter 5.3.2. The control system is implemented in Matlab/Simulink and exchanges data with the Flex5 model.

5.3.2   Controller grid support

The basic variable H controller as depicted in Figure 17 is used in this publication. Its implementation in the control system is shown in Figure 16. Compared to the controller introduced in publication 2, some the variable H controller was changed as listed below. These changes are partly requested by the Suzlon and partly the result of the previous research:

1. The magnitude of the IR is limited to ± 30 % of the rated power as TSOs typically define thresholds for its magnitude [51], [56]. The chosen magnitude exceeds these thresholds and also the current capabilities of WTs [106] to consider the possibility of more challenging requirements in the future.
2. The maximum power is limited to 123 % of rated power and the maximum torque to 107 % of rated torque to protect the electrical and the mechanical part of the drive train. These limitations are depicted as a speed depending maximum power in Figure 16.

3. The monitoring of the accelerations of the WT components have been excluded from the controller as they have not critical thresholds in any simulations conducted in the research project with Suzlon [49].

4. The two-dimensional minimum pitch angle table has also been excluded as the minimal gain in energy yield did not justify the increased pitch activity [49].

5. The grid frequency is filtered with a 10 Hz low-pass filter following recommendations by ENTSO-E [28].
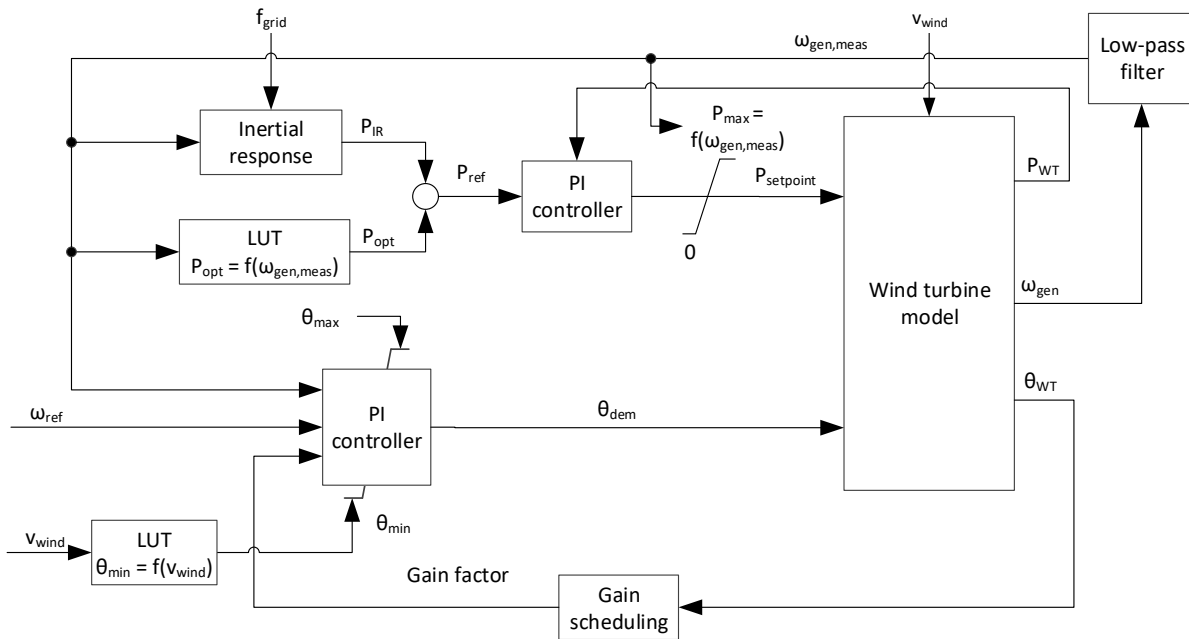
Figure 16 Implementation of the inertial response into the control system of the WT
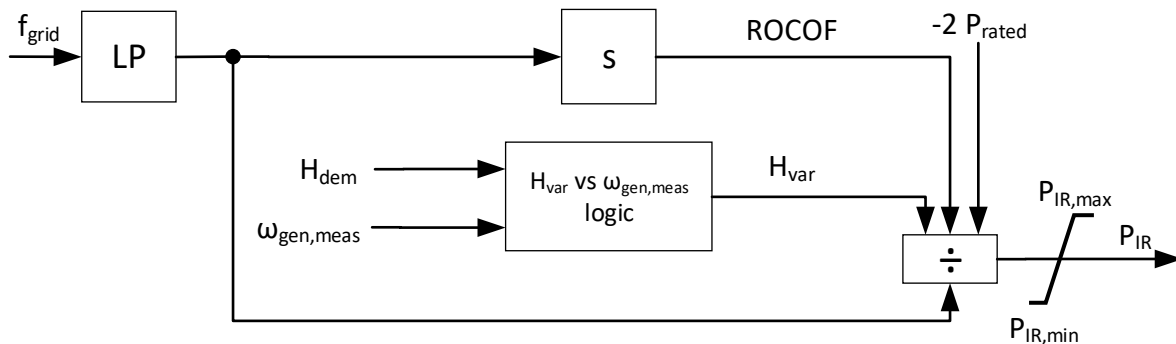
Figure 17 Content of the inertial response block in Figure 16.

5.3.3 Analysed scenarios

The research project with Suzlon has shown that the provision of IR with WTs does not lead to significant changes of the mechanical loads during most of the time [49]. However, grid situations were identified for which the loads of some WT components could be strongly affected:

1. Oscillations of the grid frequency: when the grid frequency oscillates, the power setpoint for IR also oscillates and creates periodic excitations of the WT. Such oscillations can be critical if they occur with a frequency close to the eigenfrequency of a WT component, as it may cause resonance.

2. Abrupt changes of the grid frequency: the measurements revealed some abrupt changes of the Indian grid frequency called frequency events hereafter (see Figure 18). Most of these changes followed a regular pattern, which is likely be caused by the measurement system. However, there were also some irregular frequency events, which are likely to be measured with other measurement systems, too.

In order to quantify the effects of both situations, 21 scenarios of the grid frequency were defined in terms of magnitude and likelihood of occurrence. In addition, 6 of these scenarios were tested on hardware-in-the-loop test bench to analyse the effect of the measurement system on the IR of the WT.
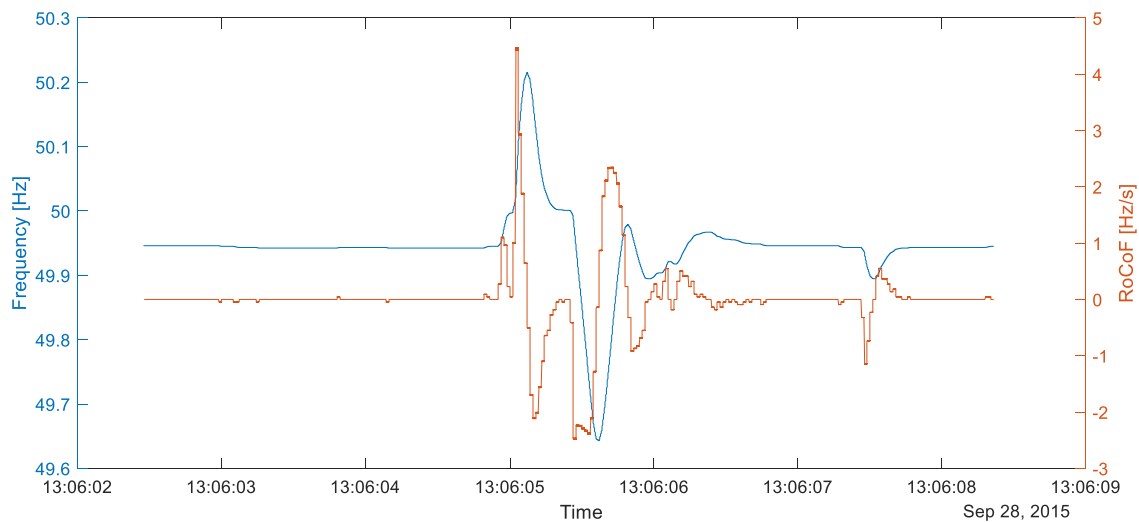
Figure 18 Example for an event of the grid frequency.

The simulated wind speeds allow extrapolating the results to the full operation range. The turbulence intensity is set to 0.17 at 15 m/s. The mechanicals loads at the different wind speeds are weighted based on a Weibull distribution to represent a site with an average wind speed of 7.3 m/s at hub height. This implies that the grid frequency scenarios are assumed to be independent on the prevailing wind conditions.

Two cases for the inertia constant demanded by the grid operator, H_{dem}, are tested: 6 s and 12 s. The results are compared to the behaviour of a WT, which does not supply IR. For the load analysis, 10E7 load cycles are assumed which represent 20 years lifetime of the WT. The load analysis is only carried out for normal operation (design load case 1.2 [108]).

5.3.4 Results

The hardware-in-the-loop tests reveal that the resolution and the measurement frequency of the standard measurement equipment is not high enough to measure the grid frequency accurately in all scenarios. Figure 19 show the differences of the WT reaction to a fast oscillation of the grid frequency (scenario 2 in [103]) depending on the used measurement system (high quality and standard measurement system in blue and red, respectively). Figure 19 (b) shows the differences of the power offset SI, i.e. PIR, caused by the limitations of the standard measurement system. The power offset calculated with the standard measurement system does not follow the expected oscillating pattern, but changes almost arbitrarily between ± 0.19 pu. However, when looking at the generator power (Figure 19 (c)) and the generator speed (Figure 19 (d)), the differences are highly reduced by the reactions of the generator-converter unit and the physical inertia of the drive train. The effect of the

measurement system on the changes of the mechanical loads is estimated by comparing the accelerations of the tower head and the drive train. These components were chosen, as they were most affected by IR provision in the simulations during the research project [49]. The drive train is directly affected through the changing generator torque, and the tower indirectly through the changing aerodynamic thrust. The results of the comparison are listed in Table 3 and are discussed in detail in the publication. The main results are that the drive train is much more affected than the tower and that the standard measurement systems leads to smaller increases of the accelerations than the high quality measurement system for most scenarios.
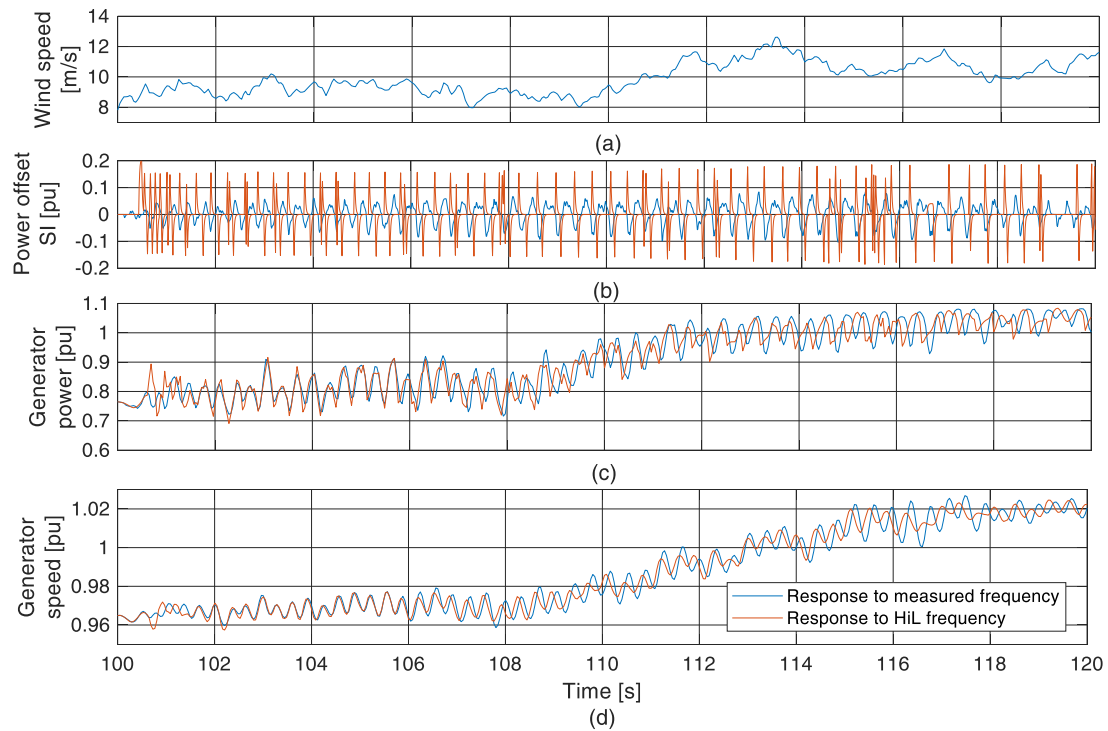
Figure 19 WTG reaction to a fast oscillation of the grid frequency. The figure shows the results for the measured frequency (blue) and the HiL frequency. (a) Wind speed, (b) power offset for SI provision, (c) generator power and (d) generator speed. Time axis of (d) is valid for the above subplots as well.

Table 3 Change of the standard deviation of the analysed acceleration signals for six scenarios. Scenario description is given in the publication.

Scenario number	Tower head acceleration (fore-aft)		Tower head acceleration (side-side)		Drive train acceleration	
	Measured frequency	HiL frequency	Measured frequency	HiL frequency	Measured frequency	HiL frequency
1	-6.7 %	2.9 %	2.9 %	2.7 %	3.5 %	8.8 %
2	3.2 %	0.1 %	1.7 %	0.8 %	133.6 %	86.1 %
4	18.1 %	-0.2 %	6.9 %	0.3 %	204.1 %	57.2 %
7	0.8 %	3.6 %	9.5 %	13.0 %	308.1 %	222.4 %
8	4.9 %	-0.9 %	5.7 %	4.4 %	202.7 %	232.9 %
10	2.5 %	-0.7 %	6.7 %	6.7 %	254.3 %	253.2 %

 In order to calculate the effect of SI provision on the WT, the simulation results of all scenarios defined in chapter 5.3.3 are used. For each sensor in Flex5, the damage equivalent loads (DELs) of the frequency support case are divided by the damage equivalent loads of the reference case without frequency support. These calculations are performed by Suzlon for various Woehler line exponents as these exponents are material depending (e.g. 4 is the relevant coefficient for steel towers while 10 is used for concrete towers). Although a very high H_{dem} is tested, the load increases shown in Table 4 are 0.65 % or smaller for tower and the drive train (indicated by the main bearing). For all other components, the increases were even below 0.1 % . As the changes are below well 1 %, it can be concluded that the components do not have strengthened to account for the additional fatigue loads caused by SI provision. However, the simulations revealed that the WT has problems to provide the full IR when operating in upper part load and full load conditions due to the torque limitation mentioned in chapter 5.3.2. In such wind conditions, it is likely that WTs provide a high share of the power production in the grid. Hence, a reliable SI provision by WTs is especially important and the drive train has to be strengthened to allow a higher torque. For the analysed WT this could be achieved by replacing the coupling between the gearbox and the generator. It also has to be mentioned that the peaks in the generator torque are a direct result of the challenging scenarios of the weak Indian grid and the high value of H_{dem}. Furthermore, the cut-off frequency in the low pass filter of the grid frequency has a very high influence on the magnitude of the torque peaks, as high ROCOFs only occur for a very short time. It might be possible to reduce this effect further by an adequate filter design.

Table 4 Load changes for sensors with an increase of more than 0.1 % caused by the provision of SI.

Sensor name [109]	Sensor description	Woehler coefficient	Load increase, H_{dem} = 6 s	Load increase, H_{dem} = 12 s
MzR1	Main bearing torque	m = 4	0.21 %	0.27 %
MzR1	Main bearing torque	m = 8	0.14 %	0.65 %
Mx	Tower top torsional moment	m = 10	0.12 %	0.12 %
My	Tower bottom fore-aft bending	m = 4	0.24 %	0.20 %
Mz	Tower bottom side-side bending	m = 4	0.17 %	0.17 %

5.4   Publication 4

In addition to the effects on the WT discussed in chapter 5.3, the capability of WTs to support the grid frequency is analysed for the case of a blackout, which occurred in Flensburg in January 2019. The Stadtwerke Flensburg provided measurement data for the day of the blackout and the sequence of events, which first lead to a grid islanding and finally to the blackout. Based on this data, scenarios were developed and simulated how WTs could have helped to avoid the blackout [59].

5.4.1   Simulation model, control system and parameter

The 1st eigenmodes model is used as a simulation model of the WT. The parameter represent the NREL 5M. The model also uses the baseline controller proposed by NREL extended by the grid support functionalities as described in chapter 5.4.2 (also see Figure 20). The wind speed is simulated with the wind model of the 1st eigenmodes model. Depending on the scenarios described in chapter 5.4.3 up to ten independent instances of the WT model are run in parallel. Each instance uses a unique turbulence seed, as the scenarios do not take a distinct spatial distribution of the fictive WTs into account. Due to the available data, the grid model has to be reduced to a power balance within in the islanded grid (single bus bar) and the corresponding change of the grid frequency (using equation (2) and (3)).

5.4.2   Controller grid support

In order to help controlling the islanded grid in Flensburg, WTs do not only have to provide IR but also FFR. For this purpose, a FFR controller was modelled based on the requirements in the Irish grid code [53]. The general idea is that WTs are only allowed to produce a certain amount of the available power during over-frequency situations by calculating a scaling factor, η_{FFR}. The grid operator may also curtail WTs during unstable grid situations, and thus is able to release additional power during under-frequency situations. The frequency support controller with FFR and IR is depicted in Figure 21. The used parameter settings are documented in the publication [59].
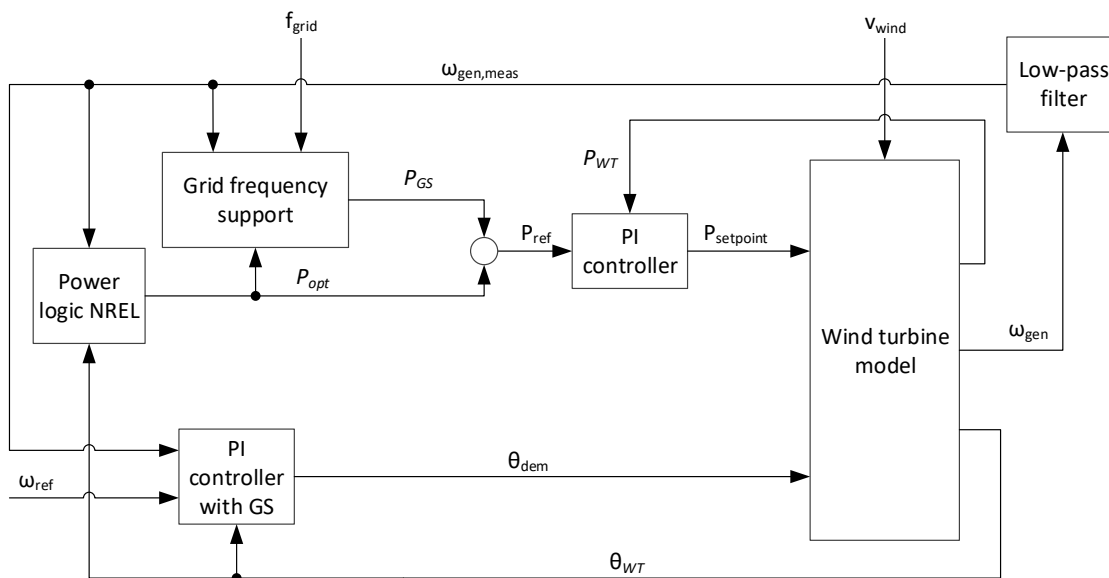
Figure 20 Implementation of the frequency support into the control system of the WT
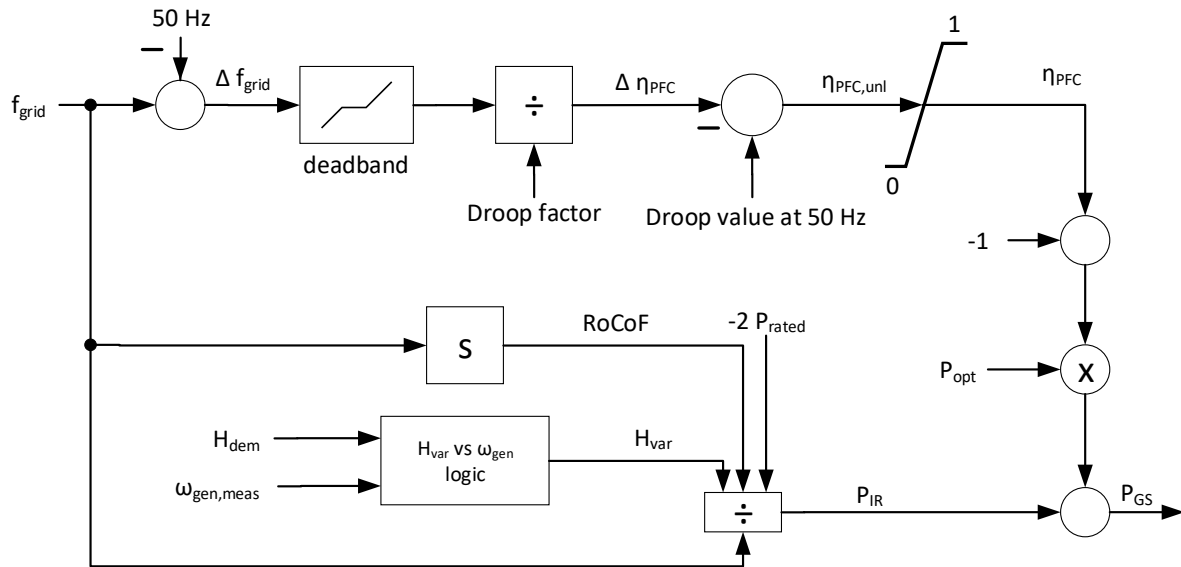
Figure 21 Content of the frequency support block in Figure 20

5.4.3   Analysed scenarios

The simulated scenarios are based on the situation in Flensburg at the day of the blackout. The average wind speed for the simulations is chosen based on data from the German Weather Service recorded at the Flensburg airport [99]. The measured wind speed was scaled to hub height using a logarithmic vertical wind profile. The TI was assumed 0.12 at 13 m/s. The Stadtwerke Flensburg provided a large data set with electrical measurements of the generation, consumption, and the grid frequency (see Figure 22a) on the day of the blackout. This data was supplemented with higher quality frequency measurements recorded at WETI [95] (see Figure 22b).
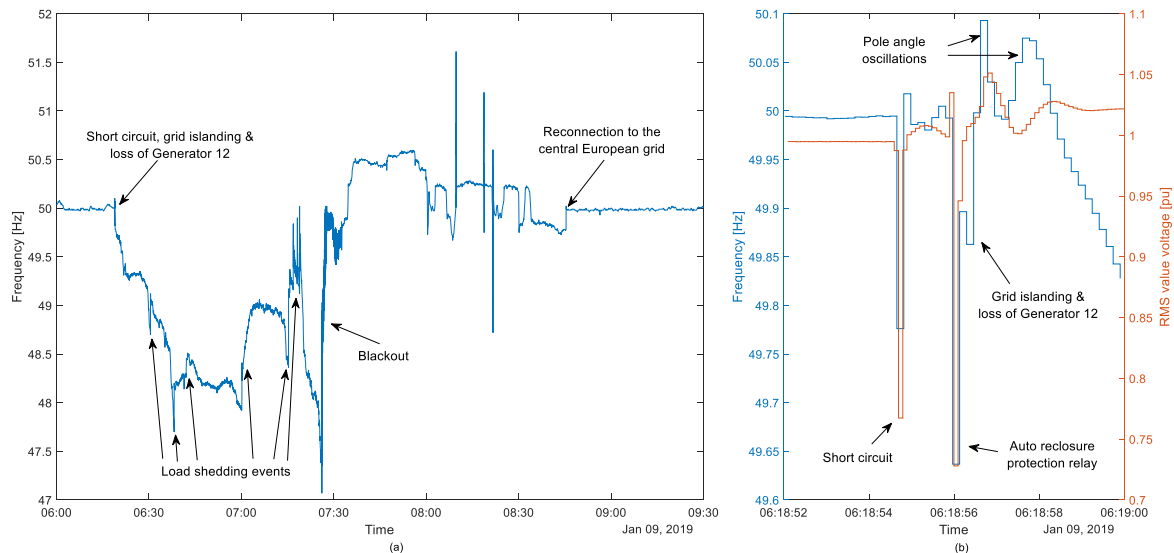
Figure 22 (a) Grid frequency measured at the Flensburg power station on 9 January 2019. (b) Grid frequency and root mean square (RMS) value of the grid voltage measured at WETI during the initial event on 9 January 2019.

From the combination of the data and the frequency measurements, the power imbalances in the islanded grid can be calculated. Immediately after the loss of the export capabilities, the islanded grid experienced a massive power surplus (similarly to the ENTSO-E expectations for a system split [57]) leading to an initial ROCOF of 1.8 Hz/s. Hence, the reaction time to avoid a shutdown of the generator

due to violating the upper frequency limit (51.5 Hz) is approximately 830 ms. Therefore, any filtering of the grid frequency was omitted in the scenarios.

In order to avoid the blackout three scenarios were simulated: avoiding the loss of the gas-fired generator with (I.) WTs providing only IR and (II.) WTs providing IR and FFR. In these two scenarios, the ROCOF has to be reduced quickly to avoid ROCOF relays from triggering and to avoid the grid frequency to rise above 51.5 Hz. In the third scenario, the small power imbalance in the grid immediately after losing the gas-fired generator is balanced with WTs providing IR and FFR. In doing so the frequency in the islanded grid can be stabilised around 50 Hz making a quicker reconnection to the central European grid (minutes instead of hours) much easier. For this scenario, it is assumed that the WTs were curtailed to 90 % of the available power before the event.

5.4.4   Results

The simulations show that WTs need to provide IR and FFR to keep the grid frequency below the allowed upper threshold. Providing IR allows reducing the ROCOF quickly but fails to keep to frequency below 51.5 Hz. When WTs additionally provide FFR, the grid frequency can be stabilised around 50.8 Hz (see Figure 23).
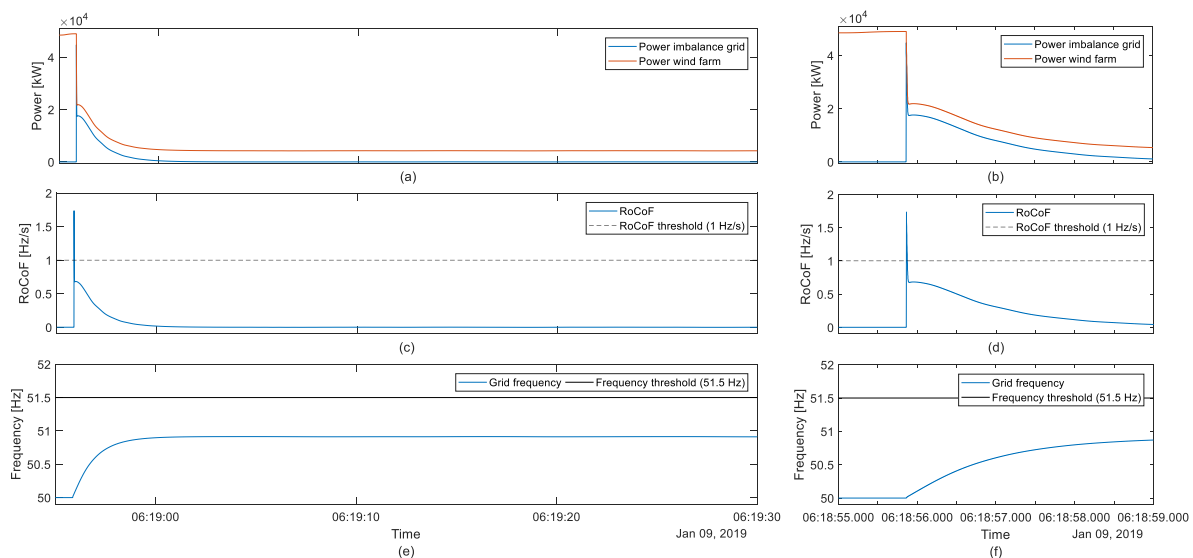
Figure 23 Results of scenario II in publication 4: power imbalance in the islanded grid and power of the simulated wind farm for (a) the full simulation time and (b) a zoom to the time of the event; (c)/(d) ROCOF and ROCOF threshold; (e)/(f) grid frequency and frequency threshold. Time axes of (e,f) are valid for the above subplots as well.

However, due to the massive power imbalance in the islanded grid, the WTs need to reduce their power output (and their electrical torque) almost instantaneously. This leads to a very strong acceleration of the drive train of the WTs, causes oscillations of the drive train, and leads to overspeed situations for most of the simulated WTs (see Figure 24). Obviously, this could be reduced by changing the power setpoint with a limited ramp rate, but then the WTs would shut down due to overfrequency in the electrical grid. However, in scenario II some WTs would likely have shut down due to overspeed, if a full state machine was used instead of the baseline controller. Such unexpected shutdowns contradict the goal of reliably providing IR with WTs. Hence, it is proposed to extend by the used grid support controller a modification of the pitch angle, which is introduced in publication 5. Although, the drive train of the WT is heavily affected by the drastic changes of the torque, it is unlikely to cost much lifetime of the WTs. It is unlikely that a single WT is affected regularly by a system split, which would

make it relevant for the fatigue load calculation. Furthermore, although the torque change is drastic in the shown scenarios, it is smaller and slower than during low-voltage-ride-through, which is a typical extreme burden for the drive train [86], [87].
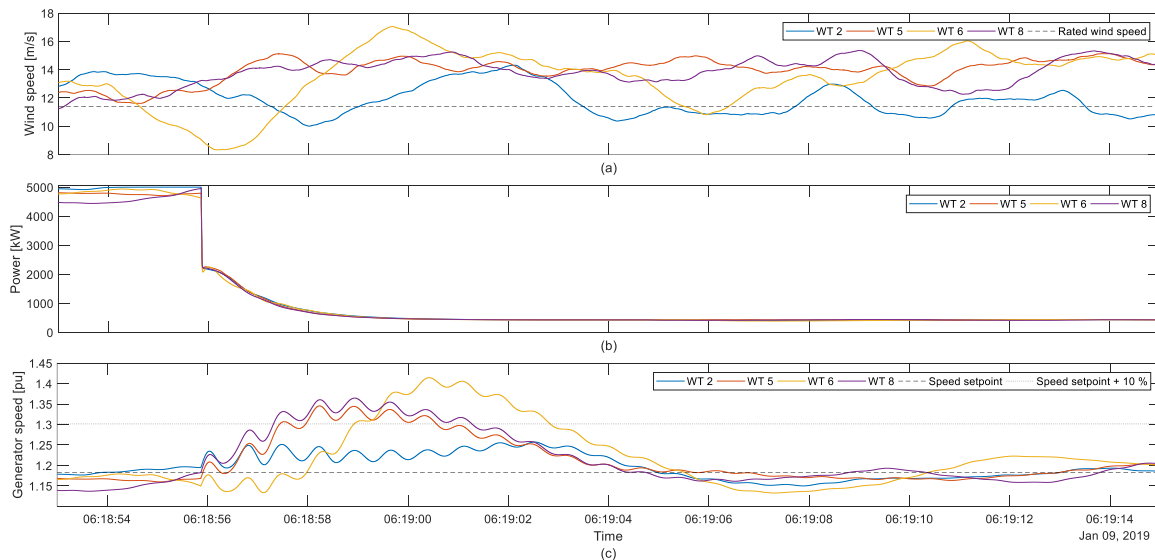
Figure 24 Simulation results of scenario II in publication 4 for four WTs with different turbulence seeds: (a) Wind speed and rated wind speed; (b) Generator power; (c) generator speed, speed setpoint, and overspeed threshold. The time axis of (c) is valid for the above subplots as well.

Figure 25 shows the results for scenario III. As the WTs were curtailed before the grid islanding, they were able to increase their power output and thus allowed to increase the grid frequency to 50 Hz. However, due to variations in the power production of the two WTs (see Figure 25a), the grid frequency regularly left the frequency tolerance band of 50 Hz ± 10 mHz (see Figure 25c). Hence, the reconnection to the Central European grid would have been facilitated but could not be guaranteed.
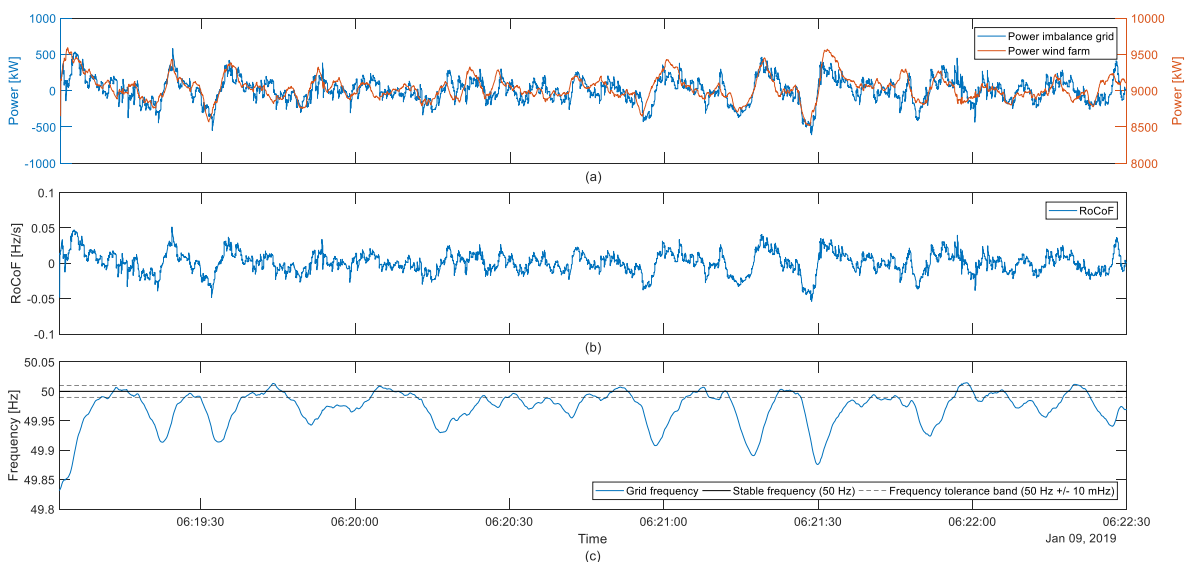
Figure 25 Results of scenario III in publication 4: (a) power imbalance in the islanded grid and power of the simulated wind farm; (b) ROCOF; (c) grid frequency, stable frequency, and frequency tolerance band.

5.5   Publication 5

As shown in publication 4, WTs may shut down unexpectedly due to overspeed. Such an unforeseeable behaviour can be highly problematic for the grid operator, especially when the grid is already in a critical operating point. Unexpected shutdowns of WTs have e.g. contributed to a black in South Australia in 2016 [110]. Hence, it is proposed to alter the pitch angle, if the grid support leads to drastic changes of the power setpoint. As the pitch angle is altered before the rotational speed has increased, it is called feedforward control loop. The proposed addition to the grid support controller is tested with respect to (I.) its capability to avoid overspeed, (II.) its influence on the energy yield and (III.) on the loads. The latter goal is approximated by analysing the accelerations of relevant signals.

5.5.1   Simulation model, control system and parameter

The used simulation model is identical to the one described in chapter 5.4.1, except that only one instance of the WT is simulated and the grid model is omitted. The baseline control system of the NREL 5M is extended as shown in Figure 26. As the WT performance highly depended on the wind during, shortly before and shortly after the grid islanding (see chapter 5.4.4), 20 turbulence seeds are used for each wind speed.

5.5.2   Controller grid support

As stated above, the grid support controller is extended by a so-called feedforward loop directly modifying the demanded pitch angle whenever grid support requires drastic power changes of the WT (see Figure 26). When the power is changed, the electrical torque deviates from its optimal value, $T_{elec,opt}$, by the electrical torque for grid support, $T_{elec,GS}$. The controller seeks to modify the pitch angle such that this deviation is compensated by an identical change of the aerodynamic torque, T_{aero}. If this could be achieved the change of the generator speed would be zero (see equation (10)). The needed change of the pitch angle can be calculated with help of the pitch sensitivity in the current operating point of the WT (see Figure 27) as power and torque are directly connected through the rotational speed of the WT. The feedforward pitch angle, θ_{ff}, is added to the feedback pitch angle, θ_{fb}, calculated by the PI speed controller. However, as the pitch system reacts much slower to setpoint changes than the generator-converter unit, the effect on the speed can only be reduced and not avoided.

$$\frac{\delta\omega_{gen}}{\delta t} = \frac{T_{aero} - (T_{elec,opt} + T_{elec,GS})}{J_{drive\ train}} \tag{10}$$

When the WT needs to provide additional power for grid support and thus the WT runs at suboptimal speed, it may also be beneficial for the aerodynamic efficiency to decrease the minimum pitch angle. As shown in this publication, it is only beneficial down to -1° for the NREL research WT. Therefore, the change of the minimum pitch angle is limited to the range between 0° and -1°.

The power change for grid support, P_{GS}, is calculated in the grid frequency support block in Figure 26. It is almost identical to the controller depicted in Figure 21. The controller is extended by a notch filter removing the 1st torsional eigenfrequency of the drive train as proposed by Guo and Schlipf [111]. The notch filter is applied to the ROCOF and the speed signal used in the variable H calculation. In order to avoid unnecessary pitch manoeuvres, a deadband with three regions is used:

1. For $|P_{GS}| < 0.5\ \% \cdot P_{rated}$ the feedforward loop is deactivated
2. For $|P_{GS}| > 1\ \% \cdot P_{rated}$ the feedforward loop is fully activated
3. For $0.5\ \% \cdot P_{rated} < |P_{GS}| < 1\ \% \cdot P_{rated}$ the feedforward loop is linearly faded in
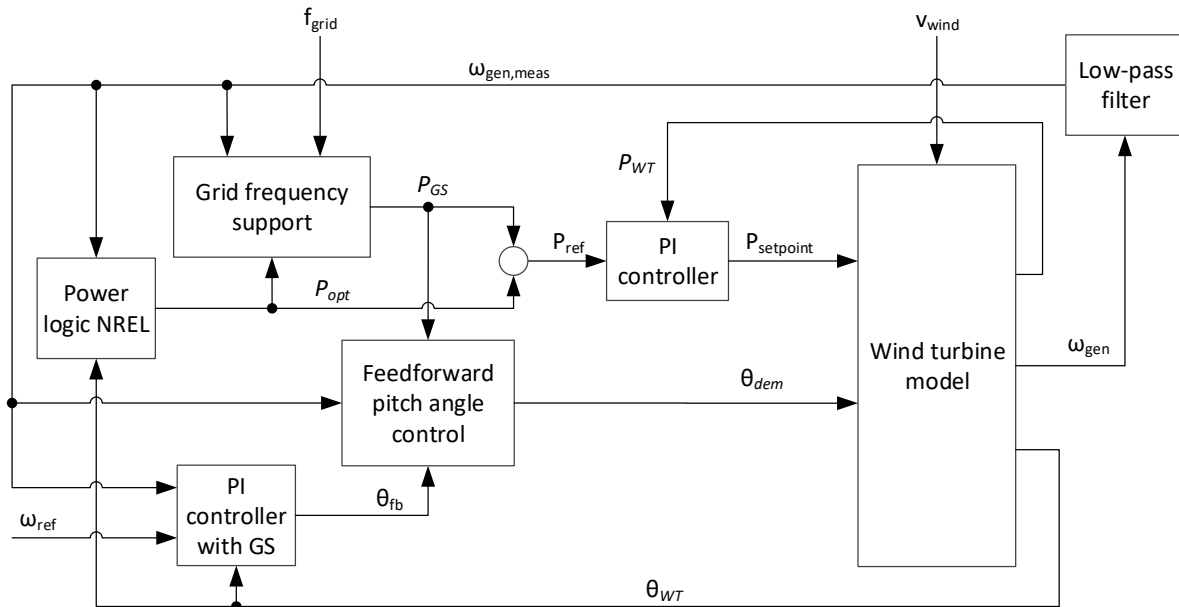
Figure 26 Implementation of the frequency support and the feedforward loop into the control system of the WT
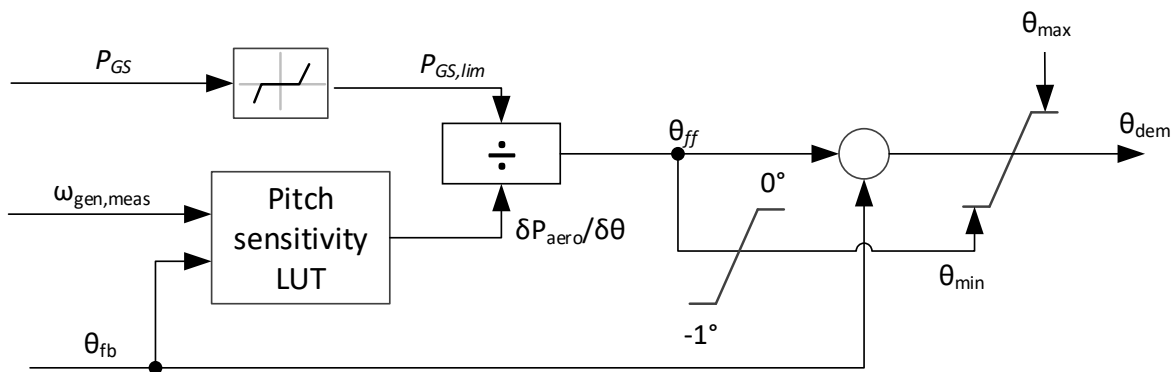
Figure 27 Content of the feedforward pitch angle block in Figure 26.

5.5.3   Analysed scenarios

In the publication, three different scenarios for the grid frequency are used:

a) A time trace of the frequency in Flensburg as simulated for scenario 2 in publication 4: This scenario is used to analyse the capability of the modified controller to avoid overspeed.

b) A time trace of the ENTSO-E reference case simulated with a small system inertia constant (H_{sys} = 3 s): For this scenario only the IR controller is activated, as the provision of FFR would require a curtailment of the WT before the event. This scenario is used to evaluate the effect of the feedforward loop on the aerodynamic efficiency when providing additional power.

c) Two time traces of the Irish grid frequency without abnormities: this scenario tests the controller during normal behaviour of the grid frequency. As the ROCOF oscillates during normal operation around 0 Hz/s, the feedforward loop should hardly be active and therefore should not increase the loads significantly. This scenario is also used to estimate the effect of the feedforward loop on the energy yield.

All scenarios are tested at six wind speeds covering the full operation range of the WT. For scenario a) and b), 20 turbulence seeds are used for each wind speed to show the effect of coinciding frequency

events and gusts on the controller performance. As there is no frequency event in scenario c), it is only tested with two turbulence seeds.

5.5.4   Results

For all discussed scenarios, the WT provides grid frequency support and its behaviour with an activated & deactivated feedforward controller is compared. The results are discussed in detail for scenario a). To show the full variability of the results for different turbulence seeds, the results are presented in boxplots (see Figure 28). A detailed discussion of the results for scenario b) can be found in the publication [104].

In scenario a), the controller's ability to avoid overspeed situations in extreme grid scenarios is tested. When the feedforward loop is deactivated, the generator speed exceeded 110 % of rated speed in 19 % of the simulations. When the loop is activated, the maximum speed during all simulations is 109.3 %. The capability of the controller to reduce the maximum speed is also shown in the top left of Figure 28. The controller is especially effective in part load operation and in the transition between part load and full load operation.

The effect on the loads can be estimated by comparing the pitch rate, and accelerations of the tower and the drive train for an activated and deactivated feedforward loop. Figure 28 shows that the effects of the controller on the WT are strongest in part load operation and in the transition region between part load and full load. In addition to the reduction of the maximum generator speed, the acceleration of the rotor is also reduced in nearly all simulations (see top right of Figure 28). This is achieved by strong increase of the pitch rate (see bottom right of Figure 28), especially when the average wind speed is close to the transition region between part load and full load operation. In this region, the pitch sensitivity is small resulting in high values of θ_{ff}. The high changes of the pitch angle also explain the strong effect on the tower at these wind speeds (see bottom left of Figure 28). Furthermore, the thrust coefficient is also very sensitive to changes of the pitch angle in this region. However, the effect here depends heavily on the used turbulence seed, i.e. the dynamics of the wind speed at the time of the frequency event. While tower head accelerations are increased in many simulations, there are also reductions of the tower accelerations for more than 25 % of the turbulence seeds (indicated by lower end of the blue box in Figure 28). This shows the complex dependency of the thrust on changes of the wind speed and of the pitch angle in this region.
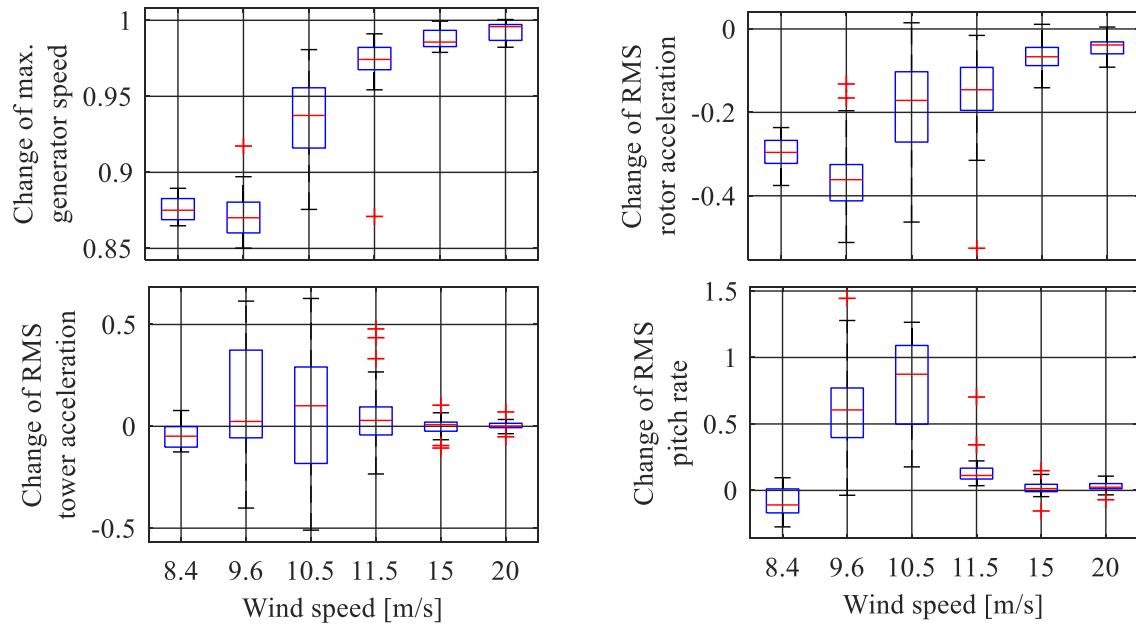
Figure 28 Changes of the maximum generator speed (top left), the rotor acceleration (top right), the fore-aft tower acceleration (bottom left) and the pitch rate (bottom right) when feedforward control is activated for all turbulence seeds in scenario a). Boxplots show the median (red line), upper and lower quartiles (box), typical range (whiskers), and outliners (red crosses).

The results for the ENTSO-E reference case indicate that the feedforward loop should not be used to increase the energy yield during the provision of IR in the simulated grid scenario. The power increase for IR only lasts a few seconds and is small compared to scenario a). Hence, the pitch system is too slow to have a positive effect on the aerodynamic efficiency and the change of the power in the wind regularly outweighs the power increase for IR. In the scenario c) it is shown that the feedforward loop does not lead to additional loads of the relevant components (drive train, tower, pitch system) but to a slightly higher energy yield (0.15 %).

6 Feed-in management with wind turbines

As mentioned above, WTs often need to be curtailed when grids are congested. This leads to economic losses for both the WT operator and the grid operator, who pass the losses on to the customers. Hence, these losses should be minimised. In publication 6 a controller for FIM is proposed, which controls the WT based on measurements of the grid state instead of predictions [39]. The controller and the case study were designed, performed and analysed mainly by Clemens Jauch. The case study is outlined in Figure 29. It is modelled after a typical situation for FIM in Schleswig-Holstein: a new WT is connected to an existing grid creating a bottleneck for the power transmission. Measurements recorded on the campus in Flensburg allow an accurate representation of the local situation. The study is based on previous work in a research project [46] and based on the general idea of continuous FIM [112].
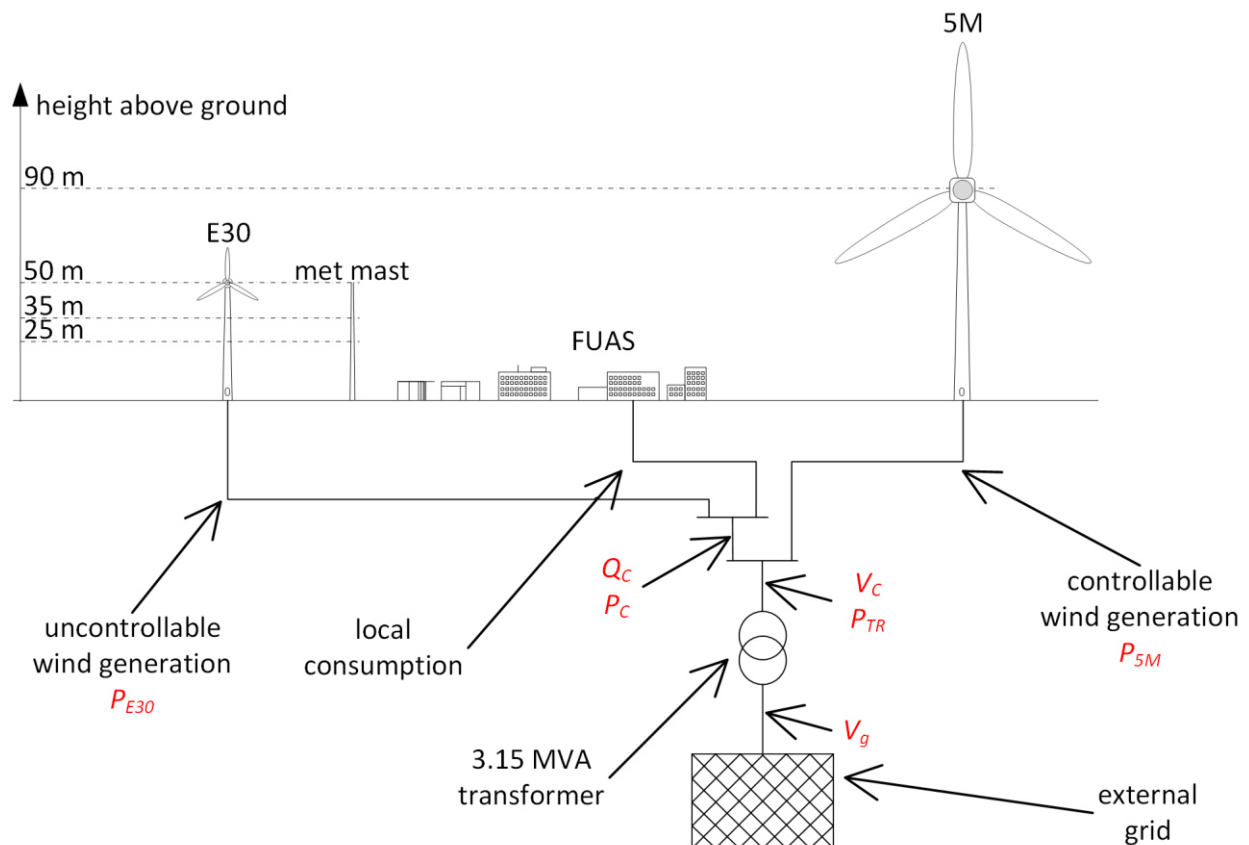
Figure 29 Sketch of the fictitious case study used in publication 5: a NREL 5M is connected to the campus grid in Flensburg via a transformer with smaller capacity. Figure by Jauch taken from [39].

6.1 Simulation model, control system and parameter

The study uses the 1st eigenmodes model of the WT. The parameter represent the NREL 5M. The control system is modelled to represent the baseline controller of the NREL 5M.

The wind model of the 1st eigenmodes model is modified by adding four sinusoidal terms to the wind speed. The eigenfrequencies of four WT components (tower bending, drive train torsion, blades bending edgewise and flapwise) are chosen as frequencies for these sinusoidal terms. By adding these terms, the WT has to withstand the additional excitation from continuous FIM while already being highly excited from the wind. This represents a worst case for continuous FIM [112].

The campus grid is modelled as a single bus bar, which is connected via a transformer to the stiff external grid. The transformer is modelled electrically as an impedance as documented in [46].

Furthermore, the thermal behaviour of the transformer is modelled as a PT1 element. All relevant parameters are listed in publication 6 [39].

6.2 Controller grid support

The FIM controller aims to stabilise the temperature of the congested grid element (here the transformer) and to keep the voltage in the (campus) grid within the allowed threshold. This is achieved by limiting the output of the power vs speed characteristic of the WT (see Figure 30).

The continuous FIM controller consists of two-cascaded PI controller (see Figure 31): the outer loop controls the temperature of the transformer. This controller is slow as the thermal time constant of the transformer is high. Furthermore, the output is limited to keep the voltage within the allowed limits. The inner loop controls the power demanded from the WT by monitoring the power flowing via the transformer.

The conventional FIM controller also limits the output of the power vs speed characteristic of the WT. Following the former state-of-the-art, the limits are updated every 10 minutes. Four limits can be chosen: 100 %, 60 %, 30 % and 0 % of rated power. The value is determined based on the transformer temperature and the grid voltage.

The voltage could also be controlled using the reactive power of the WT. However, this would increase the current flowing via the transformer and thus limiting further the active power, which can be fed into the grid. As the impendence of a grid component is typically much higher than its resistance, reactive power flows have strong influence on the voltage drop across the affected component. Hence, the reactive power control of the WT is used to balance the reactive power within the campus grid.
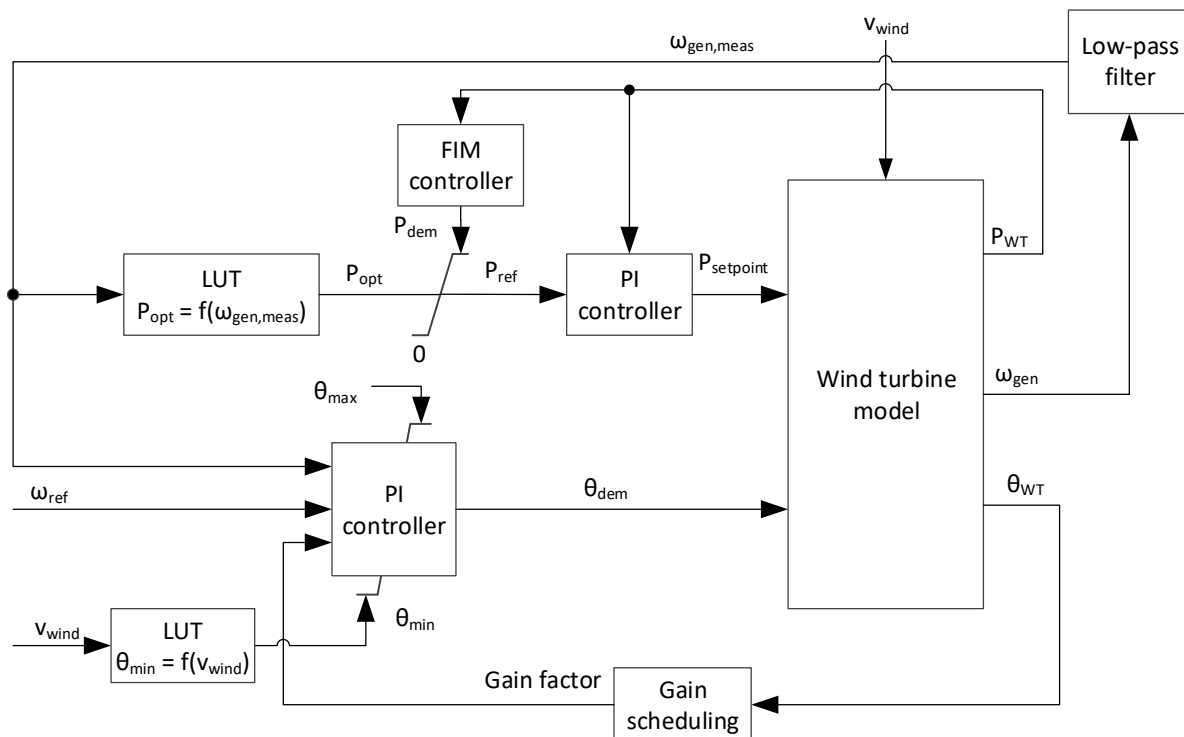
Figure 30 Implementation of the FIM controller into the control system of the WT
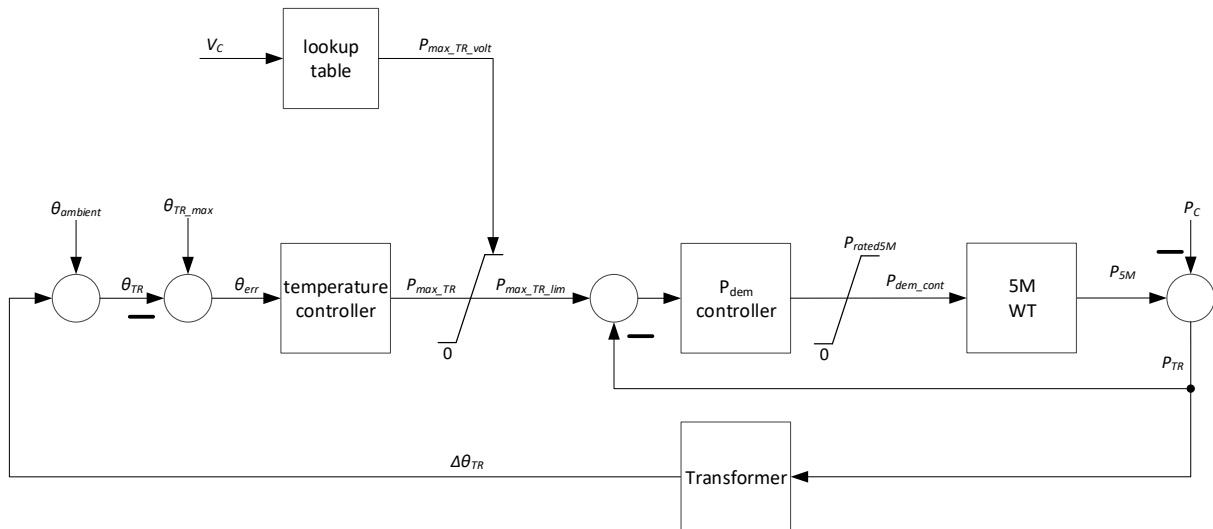
Figure 31 Power demand controller for continuous FIM. Figure by Jauch taken from [39].

6.3   Analysed scenarios

The case study is based on measurements recorded at the campus in Flensburg: the load on the campus and the power of an existing WT were measured on an arbitrary workday during the semester (5th April 2017) using the measurement system described in chapter 3.4. The measurements were used to calculate the residual load (P_C and Q_C in Figure 29). The ambient wind speed was measured in three heights at the local met mast. The recorded data were used to extrapolate the time series to hub height of the NREL 5M. This signal is used as the average wind speed in the simulation. Furthermore, the ambient temperature is used as input signal to the continuous FIM controller (see Figure 31). The measured wind speed at 50 m and the ambient temperature are shown in Figure 32. As the wind speed is very low in the morning and increases significantly around noon, FIM is only necessary in the second half of the day.
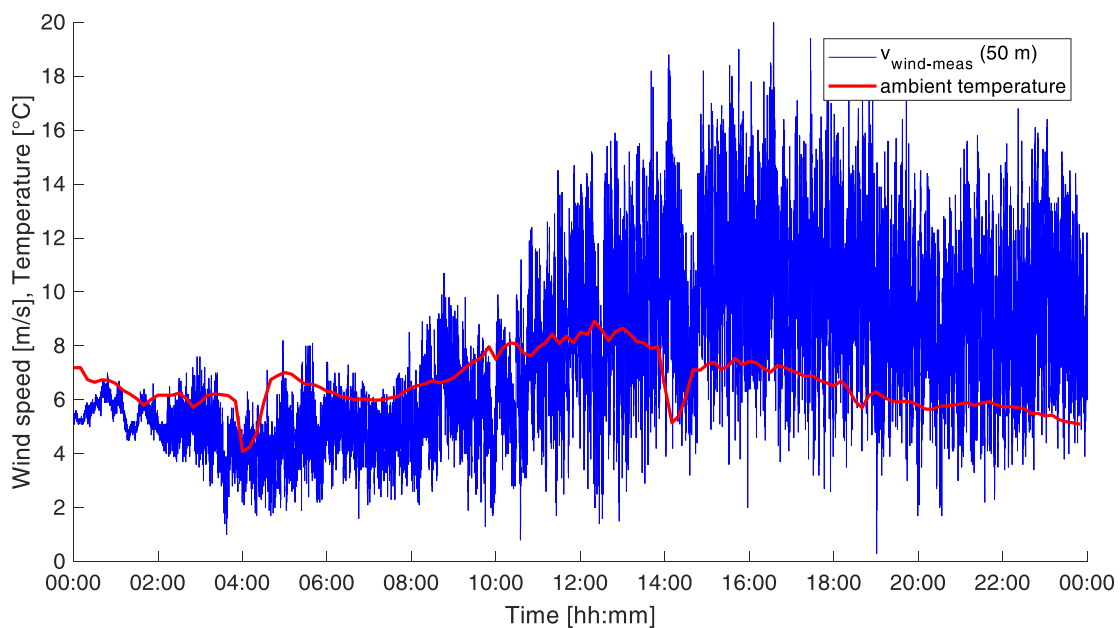
Figure 32 Wind speed at 50 m above ground (hub height of the E30) and temperature on campus measured on 05 April 2017. Figure by Jauch, taken from [39].

6.4   Results

The study compares the effects of the two FIM strategies on the grid and the WT.

The most prominent effect for the grid is the increase of the energy yield of the NREL 5M: with continuous FIM the WT can produce 13.5 % more energy compared to conventional FIM. This goes along with a higher utilisation of the grid assets, in this study represented by the temperature of the transformer: with conventional FIM, the transformer never reaches its target temperature of 50°C and even hardly 45°C. Furthermore, its temperature varies more, which is likely to increase temperature-induced wear and tear of the material. Lastly, the variability of the voltage in the campus grid is reduced when using continuous FIM indicating a higher quality of the delivered power.

The effect on the WT loads is analysed in detail in the publication for the accelerations of the tower top and blade tip in two directions. Continuous FIM causes only small increases for three of these signals. Moderate increases can be observed for the lateral acceleration of the tower top. These accelerations are caused by a modelled mass imbalance: one blade is 100 kg heavier than the other two. Hence, the imbalance is a 1p excitation for the tower. The increase of the accelerations can be explained by the frequent changes of the rotational speed when continuous FIM is used.

The increases of the accelerations of the WT components can also be explained by the chosen scenario. The eigenfrequencies of the NREL 5M, excited by the sinusoidal offsets in the wind speed, are visible in the frequency spectra of the power demand signal, P_{dem}, when continuous FIM is used (blue line in Figure 33 middle). The dynamics in the power system are dominated by the power production of the NREL 5M as shown in its frequency spectra (blue line in Figure 33 bottom). Therefore, the WT components are excited both from the wind and from the power demand signal. The excitation from the grid side would likely be smaller, when a larger power system (e.g. a WF) was simulated, as the variability of the power production in the grid decreases with the number of WTs (e.g. by spatial smoothing and the phase shift of the periodic excitations).
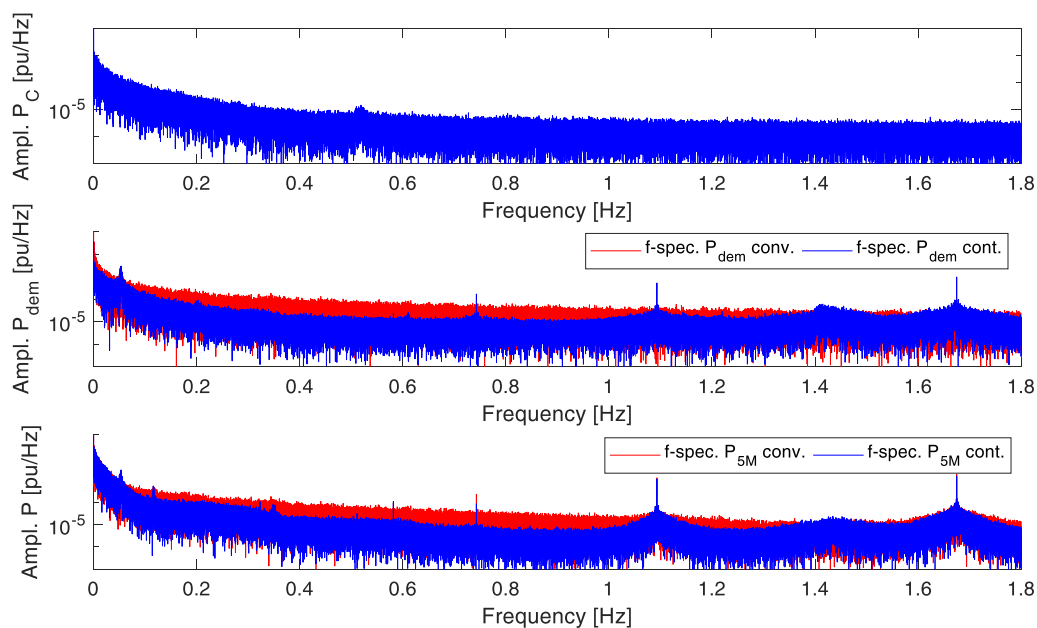
Figure 33 Frequency spectra of the residual load (P_C, top), the power demand signal (P_{dem}, middle) and the power of the NREL 5M (P_{5M}, bottom). Figure by Jauch taken from [39].

The standard deviation of pitch rate of the NREL 5M increases by 24.2 % (1.11 deg/s and 1.38 deg/s) when switching from conventional to continuous FIM. As Figure 34 reveals, it is difficult for the WT to keep a reduced power setpoint in high wind speeds, whether the setpoint is constant or varying slightly. For both controller, the highest pitch rates occur when the power setpoint is changed in a big step.
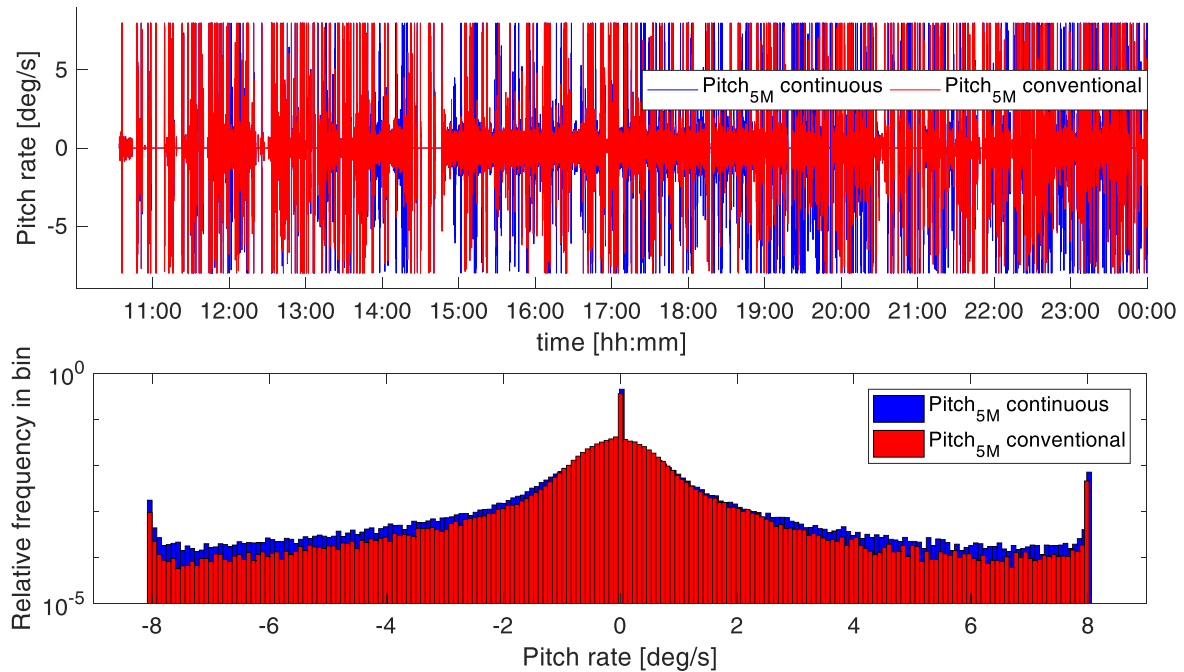
Figure 34 Time traces (top) and relative frequencies (bottom) of the pitch rate for the NREL 5M for continuous (blue) and conventional (red) FIM. Figure by Jauch taken from [39].

As the analysis of the two controller is limited to a case study, the results can only indicate the effect of the controller on the WT. The increased energy yield in a congested grid is a promising result given that only the pitch rate and the lateral accelerations of the tower increase significantly. However, for a final assessment further case studies should be carried out.

7 Simultaneous feed-in management and inertial response with wind turbines

Publication 7 [100] analyses whether WTs can simultaneous supply IR and FIM. It is extension of publication 6 [39] described in chapter 6. Measurements of the grid frequency taken at WETI were added to the case study shown in Figure 29 and described in chapter 6.3. The grid support controller is updated as described in chapter 7.2. In addition, to the time domain simulations, the interaction of the two grid support controller is also analysed in the frequency domain. The study is also designed, performed and analysed mainly by Clemens Jauch.

7.1 Simulation model, control system and parameter

The simulation model and the baseline controller of the WT are identical to the description in chapter 6.1. The implementation of the extended grid support controller in the control system of the WT is shown in Figure 35. By contrast to publication 6, the time constant of the PT1 element representing the generator-converter unit is reduced from 150 ms to 25 ms and the parameter of the PI power controller changed accordingly. The provision of IR has no influence on the grid frequency, which is regarded as a disturbance in this study.

7.2 Controller grid support

IR is important for the angular stability in the grid and needs to be provided almost instantaneously. Furthermore, high ROCOFs indicate a severe situation for the entire synchronous area. By contrast, FIM mainly addresses local problems and acts on a longer time scale. Therefore, the provision of IR is prioritised over FIM as depicted in Figure 35. This should not be problematic, as the ROCOF typically varies around zero in a longer time frame (several seconds) and therefore is unlikely to interfere with the FIM controller as discussed in chapter 7.4.
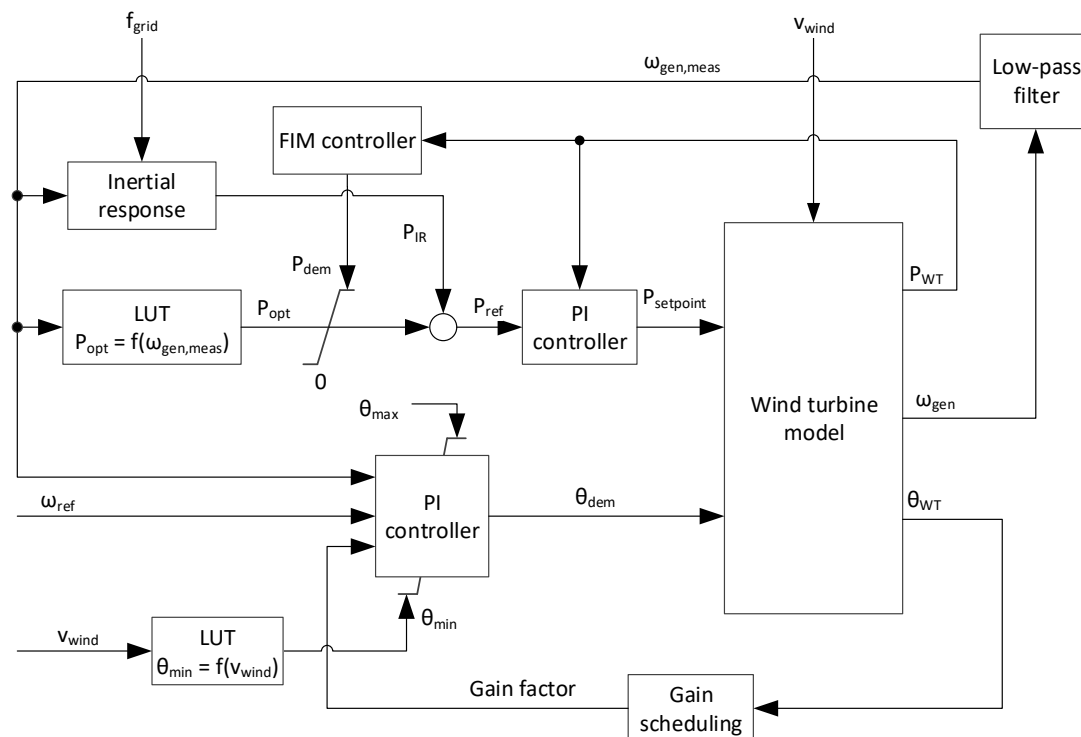
Figure 35 Implementation of the IR and FIM controller into the control system of the WT.

7.3   Analysed scenarios

The scenario described in chapter 6.3 is extended by the measured time traces of the grid frequency shown in Figure 36. The ROCOF derived from the measurements is typically smaller than ± 0.02 Hz/s. However, there are some peaks with ROCOF up to ± 0.48 Hz/s. Although, these may be caused by the measurement system [113], these were left in the time traces. When providing IR, WTs must measure the ROCOF online. Hence, some measurement error can be expected and should be considered when evaluating a controller. In order to account for the relatively strong Central European grid, two high inertia constant were emulated: H_{dem} = 6 s and H_{dem} = 12 s. Thus, the power changes are closer to those in a weaker grid with a higher volatility of the grid frequency.

For the analysis in the frequency domain, the WT system is linearized in upper part load. In this operating point, the WT is likely to cause congestions. At the same time, the variable H controller provides a strong IR. Furthermore, there is no excessive power in the wind as in full load operation, which could be used to provide additional power for IR. Therefore, IR is likely to have a strong effect on the rotational speed.
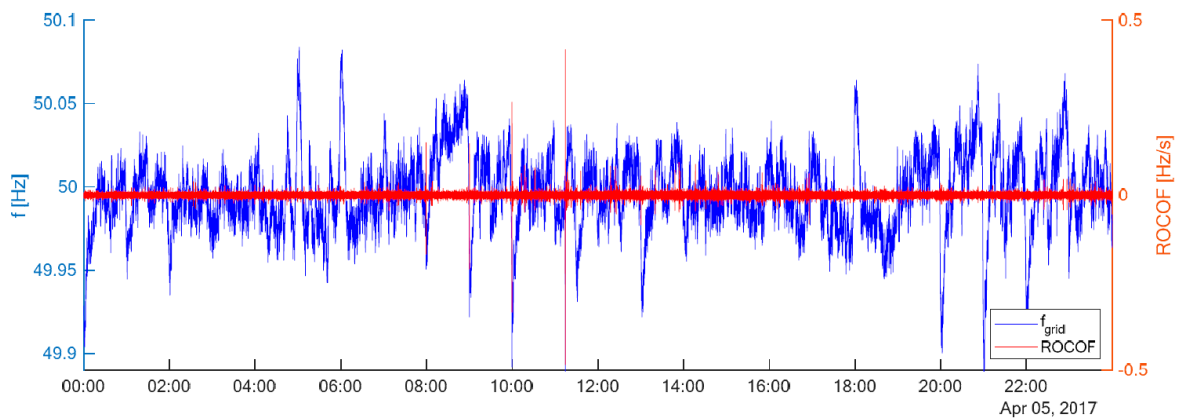
Figure 36 Time traces of the grid frequency (blue) and the ROCOF (red) used in publication 7. Figure by Jauch taken from [100].

7.4   Results

For the analysis in the frequency domain, the transfer function of the WT system from the power setpoint to the rotational speed of the generator is derived. Furthermore, the transfer functions of the P_{dem} controller (see Figure 31) and of the transformer are calculated. These transfer functions are compared with the frequency spectra of the main excitations from grid support, i.e. ROCOF for IR and P_C and Q_C for FIM (see Figure 37). The analysis reveals that the WT can mainly be excited by IR. The excitations from the IR are driven by the ROCOF and are high in the frequency band, in which the WT's rotational speed strongly reacts to changes of the power setpoint (1-3 Hz). By contrast, excitations from the FIM are mainly with a frequency below 0.1 Hz and therefore unproblematic. Furthermore, the P_{dem} controller has a small gain in the frequency band critical for the WT.

The effect of the simultaneous provision of IR and FIM for the WT is assessed with help of the relevant acceleration signals. The results indicate that the WT is not significantly stronger affected than by solely providing FIM (see chapter 5.5.4). Even for the scenario with H_{dem} = 12 s, the maxima and averages of lateral tower head accelerations and the drive train accelerations are only slightly increased.
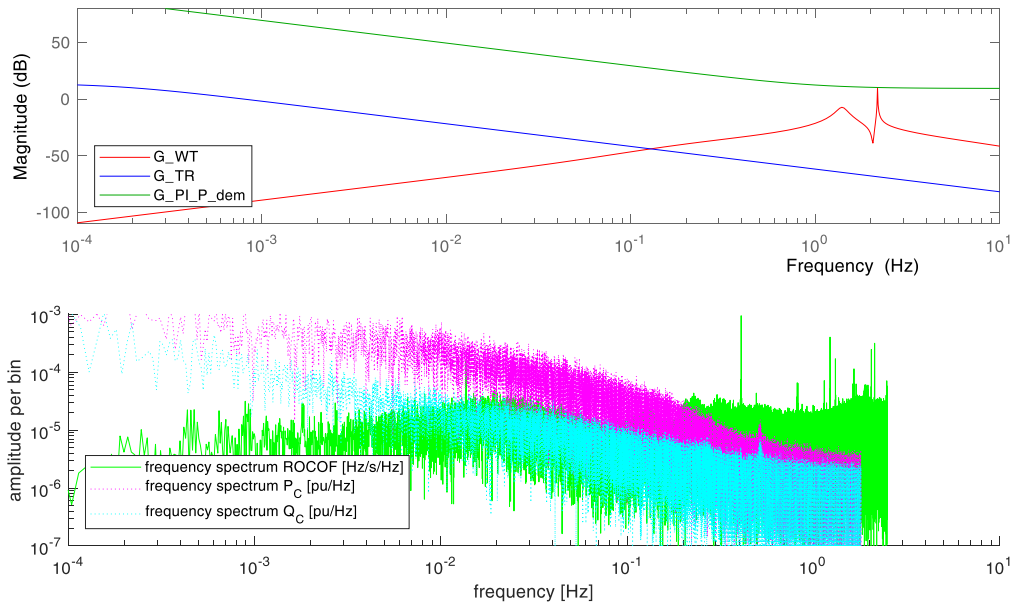
Figure 37 Bode plots of the transfer functions of the WT (G_WT, top, red), the power demand controller (GPI_P_dem, top green) and the transformer (G_TR, top, blue) in comparison to the frequency spectra of the different excitations: ROCOF (bottom, green), residual demand active power (P$_G$, bottom, magenta) and reactive power (QC, bottom, blue). Figure by Jauch taken from [100].

The positive effect of continuous FIM on the utilisation of the grid components was already shown in chapter 6.4. The effect on the grid by the additional IR provision is determined by the amount of energy, the WT exchanges with the grid irrespective of the direction of the power flow. The exchanged energy is compared to the theoretical value an idealized SG would deliver according to equation (8). A high inertia constant (H = 6 s) is assumed, which occurs only in some thermal power plants [19]. As the wind speed is low during the first half of the simulated scenario (see Figure 32), a WT equipped with the variable H controller will deliver little IR during this time. Hence, the analysis is carried out for both halves of the day separately (see Table 5). In the second half of the day, a WT with the same inertia constant exchanges 38 % less energy with the grid than a SG. In the first half of the day, IR is hardly active. When the demanded inertia constant is doubled, the WT exchanges 23 % more energy than the SG. It has to be kept in mind, that the ROCOF is very small in the chosen scenario. Whether a WT can reliably emulate such high inertia constants in more challenging situations remains to be shown, as it is significantly higher than the inertia constant of a typical WT.

Table 5 E$_{inertia}$ from an AC connected SG with H = 6 s, E$_{inertia}$ from the 5M with H$_{var}$ controller and H$_{dem}$ = 6 s and H$_{dem}$ = 12 s; reproduced with data from [100].

	5 April 2017	5 April 2017	5 April 2017
	00:00 – 24:00	00:00 – 12:00	12:00 – 24:00
E$_{inertia}$, SG, H = 6 s	88.2 kWh	41.5 kWh	46.6 kWh
E$_{inertia}$, WT, H$_{dem}$ = 6 s	33.1 kWh	4.33 kWh	28.7 kWh
E$_{inertia}$, WT, H$_{dem}$ = 12 s	66.1 kWh	8.66 kWh	57.5 kWh

8 Discussion and limitations

One major task of this thesis was to derive realistic scenarios, especially for the frequency support, as these have a major impact on the results of the simulations. The problem was addressed two folded: first by defining detailed scenarios of grid situations, which a WT experiences during the normal operation of the grid (publication 3). The scenarios are based on high-quality measurements of the frequency in the Indian grid, which can serve as an example for a future grid due to its relative weakness. Additionally, worst-case scenarios, which occur seldom, were analysed. An important case in this category is the well-known and well-documented ENTSO-E reference incident. However, while this case works well for dimensioning PFC, it is not very challenging for providing IR with WTs. Especially, the research on the blackout in Flensburg has shown, that system splits are much more important when analysing the interactions between WTs and the affected grid. System splits are the only situation with high relative power imbalances in the Central European grid. Hence, only during such splits high ROCOFs last for several seconds, i.e. relevant amounts of kinetic energy are fed into or drawn from the grid. A good example for the influence on the WT, are the overspeed problems in publication 4. These problems show that even reducing its power in the needed manner can be very challenging for WTs. Recent events in the Central European grid [60], [61] have shown that such grid incidents occur regularly and are therefore important when analysing frequency support by WTs.

Despite, the used analytical approach and the careful choice of the simulated scenarios, they can only serve as examples. A typical problem are grid frequency oscillations: these are typically caused by synchronously connected, rotating masses oscillating against each other. Hence, the periods of these oscillations depend on the structure of the grid and the synchronously connected masses, which are differ between grids and even in time. Furthermore, the effect on the WT depends on the exact WT model and in case of resonances on the eigenfrequencies of the components. For FIM, it is even more difficult to find suitable scenarios, as the effects not only depend on the structure of the high-voltage grid, but also of the medium-voltage grids and even on single grid components. Therefore, it was chosen to create fictional, yet realistic case using as much locally measurable data as possible.

Another issue is the measurement of the grid frequency. Measuring the grid frequency with a high precision and small time steps [28], [114] and prone to distortions of the voltage [113]. In most of the publications, the grid frequency is modelled as an external signal. The input signals are derived from high-quality measurements, which do not exist in a normal WT. Hence, the WTs will measure a different signal. This problem was addressed in publication 3. Although, the frequencies measured with standard equipment differed significantly from the original signals, the effects on the instantaneous power were much smaller and thus on the accelerations of the affected components were also smaller in most cases. However, the measurement system in the WT will have an impact on the capability to provide frequency support. In publication 4, the grid frequency is calculated in the grid model but the measurement of the frequency by the WTs was not modelled.

Another related issue is the use of filter. As there is very little information by TSOs, whether and to what extend filtering of the grid frequency is allowed, it was decided not to use filter in most publications. However, it has to be mentioned, that well-designed filter may greatly reduce the negative effects for WTs [111]. Furthermore, a slower adjustment of the WT power might be beneficial in some cases, due to the complex interaction between frequency support by WTs and by classic PFC [27]. In other cases, like the first two scenarios in publication 4, a fast adjustment of the power is the only chance to avoid a blackout. A similar benefit of a short reaction time has been shown in the literature, e.g. by the North American Electric Reliability Corporation [115]. The minimal reaction time

is limited by a reliable measurement of the ROCOF, as IR based on faulty measurements might be harmful for the grid [28]. Some manufacturer of measurement equipment claim to be able to measure a reliable ROCOF within approximately 60 ms [106]. Various OEMs claim, that a demanding frequency response (in terms magnitude and time) is likely to cost lifetime of the WTs [106]. It has to be stressed that this was not the case in the simulated scenarios, although some of them (e.g. publication 3) were very demanding. Nevertheless, it might be beneficial carefully balancing the required speed of the IR.

Most simulations for this thesis were conducted with a reduced order model of the WT [91]. Compared to the well-known OpenFAST [116], it uses a simplified aero-elastic model. Although, the simulation results showed a good agreement with FLEX5 simulations and field tests in general [49], the model might not capture all aerodynamic effects during transients. Especially, when the power has to be adjusted in large steps very quickly (e.g. after a system split), effects like dynamic stall or dynamic inflow may occur and are not represented appropriately. During such a situation, a more detailed model of the generator-converter unit might also be necessary. Furthermore, the model only considers the (most important) 1st eigenmodes of the most important WT components. However, this limitation has very likely no significant effect on the results of this thesis.

In order to assess the economic aspect of grid support, the change of the WT's energy yield was assessed various scenarios. Energy losses caused by FIM are being compensated (to a large extend) and can therefore be neglected. The change of the energy yield when providing IR differ between negligible changes [98], [100], and -0.3 % [102]. The addition of a feedforward loop for the pitch angle slightly increased the energy yield by 0.15 % compared to the standard variable H controller [104]. Additional investment costs for allowing grid support are only specified in one source known to the author. Such costs are expected to arise as WT OEMs have evaluate and enable the capability of their WTs to fulfil the grid code requirements. It states the additional capital costs for implementing a frequency support scheme in a wind farm is below 1 % for new wind farms and at least 2 % for retrofits [106]. While these numbers seem to be small, they might actually cost a considerable amount of the return on investment when margins are small [106]. In order to minimise these additional costs, TSOs should harmonise their requirements as much as possible.

A potentially high cost driver would be necessary adjustments of WT components to supply grid support. Publication 3 has shown that this might be necessary for some parts of the drive train when additional power is to be supplied at or near full load operation. Strengthening WT components due to increases of the mechanical loads is only necessary, if regular measurement errors cannot be avoided [49]. However, such adjustments are highly depending on the individual WT and are therefore very hard to quantify. If such costs occur, they are likely outweighed heavily by reduction of system costs as recently shown by Thiesen [25], [26] when considering the total system costs. Publication 1 has also shown that using storage units for IR would lead to an over-dimensioning of the power rating and is therefore a very costly alternative. Whether FFR provision with WTs is also cost-efficient is much harder to evaluate. When additional power is to be supplied in a similar manner to today's PFC, WTs must be curtailed before FFR can be delivered. Hence, the energy yield could suffer considerably, if the curtailment lasts for longer periods.

9   Conclusion

In this thesis, various aspects of grid support with WTs have been analysed. Detailed scenarios were developed to estimate the effect of the grid support on the WTs. Using these scenarios, the capability of WTs of providing frequency support and FIM was shown. This allows to the answer the research question with help of the sub-questions stated in the introduction.

1.   In which form should frequency support and FIM be provided in a future power system?

     The general concept of the controller used in this thesis is to provide grid services continuously. For FIM, this leads to a significant increase of the energy yield of the WT compared to the conventional FIM and a better use of the existing grid capacities. Thereby, unnecessary system costs can be avoided. Providing IR continuously instead of event based may help to stabilise the grid frequency in a future grid with little inertia. In such power systems even small power imbalances may lead to high ROCOFs. Therefore, the use of thresholds for an activation of IR may lead to higher frequency excursion than with a continuous provision. However, this theory could not be tested due to a lack of a comprehensive grid model. During the thesis the concept of the variable H controller was developed. Besides allowing a reliable provision of the IR, it also causes smaller load increases compared to IR provision with a fixed inertia constant [49]. The simulation results show that WTs are capable of providing FIM and IR continuously without unduly harm for the WTs, especially when the variable H controller is used for IR provision.

2.   What are reasonable scenarios to be considered when evaluating load changes by grid support with WTs?

     Finding a good scenario for FIM has been difficult, due to the strong influence of the local grid structure. Therefore, a fictional, yet realistic scenario has been used to evaluate the performance of the continuous FIM controller. In the analysed case, the accelerations of the tower in lateral directions and the pitch rate are slightly increased. The changes of other signals are negligible.

     For the analysis of the frequency support controller, data from various sources have been analyse to derive realistic scenarios. The simulations have shown that the provision of IR during the normal behaviour of the grid frequency has very little influence on the WT loads. Therefore, the scenario definition should focus on frequency events such as abrupt changes of the grid frequency, oscillations and extreme case like system splits. Unfortunately, these events are grid-specific in terms of magnitude and likelihood making an analysis by OEMs or academia very time consuming. It might be reasonable that TSOs define and publish such data in order to facilitate research and development of new controller. In the analysed scenarios, the mechanical loads of the WT are hardly affected even when very high inertia constants are demanded. The stable operation of the WT was only affected extreme cases, shown at the exemplary case of the grid islanding in Flensburg. This case shows, that even reducing the WT power for frequency support can be challenging, as there is very little reaction time, before the grid frequency causes a blackout.

3.   What are the economic consequences for WT operator?

     The analysis has shown that the decrease of the energy yield is very small. Furthermore, only small adjustments of WT components were needed to provide IR reliably. This may differ when

a different grid or a different WT is analysed. However, the mechanical loads did not increase significantly in the analysed scenarios. Hence, a replacement of WT components for IR due to load increases is not necessary.

The answers to the sub-questions above show that WTs are capable of providing grid support continuously at acceptable consequences. Considering the stated benefits for power systems in terms of reduction of system costs and grid frequency and voltage stabilisation, it can be concluded that WT should stabilise the grid to a higher extend than today.

However, there is also need for some additional research in the future. The effects of continuous FIM should be analysed in a different and larger power system. By doing so, the possible interactions between the excitations from the wind and from the grid side (through demanded power controller) can be analysed in detail. Furthermore, it should be analysed how a congestion at a high grid level (e.g. a substation between the medium and high voltage level) would affect the WTs connected the downstream grids. When such bottlenecks are carefully identified and monitored, a large number of WTs might benefit from the positive effects of continuous FIM. The continuous IR with WTs has been shown extensively. However, the rate of power change during extreme cases was higher than typical for a WT. Whether such drastic power changes are possible without overextending the capabilities of the generator-converter units should be shown in a higher order model of these components. Additionally, the effect of the feedforward loop on the WT dynamics shows a high variability depending on the prevailing wind conditions. It should be analysed how these variations are exactly caused by the turbulent wind and how the response of the WT can be improved in challenging wind conditions. Furthermore, it should be investigated how the analysed grid services can be provided best in a wind farm. As IR and FIM both change the active power of the WTs, it is also likely to change the flow in the wind farm. Thus, it might be beneficial to share the power changes unevenly between the WTs in the wind farm.

10 References

[1]   UN Framework Convention on Climate Change (UNFCCC) '7. d Paris Agreement', 2016. [Online]. Accessed: 30th Jan 2023. Available: https://treaties.un.org/doc/ Treaties/2016/02/20160215%2006-03%20PM/Ch_XXVII-7-d.pdf

[2]   International Energy Agency '*Renewable Energy Market Update*', 2022. Accessed: 30th Jan 2023. [Online]. Available: https://iea.blob.core.windows.net/assets/d6a7300d-7919-4136-b73a-3541c33f8bd7/RenewableEnergyMarketUpdate2022.pdf

[3]   Y. Zhou, D. D. Nguyen, P. C. Kjaer, and S. Saylors '*Connecting wind power plant with weak grid - Challenges and solutions*', in 2013 IEEE Power & Energy Society General Meeting, Vancouver, BC, 2013, pp. 1–7.

[4]   H. Bindner '*Power Control for Wind Turbines in Weak Grids*', RISØ NATIONAL LABORATORY, Project report JOR-3-CT95-0067, Dec. 1998. [Online]. Accessed: 30th Jan 2023. Available: https://cordis.europa.eu/docs/projects/files/JOR/JOR3950067/47698381-6_en.pdf

[5]   D. Lew, D. Bartlett, A. Groom, P. Jorgensen, J. O'Sullivan, R. Quint, B. Rew, B. Rockwell, and S. Sharma '*Getting to 100% renewables: operating experiences with very high penetrations of variable energy resources',* IET Renewable Power Generation, vol. 14, no. 19, pp. 3899–3907, Dec. 2020. doi: 10.1049/iet-rpg.2020.0573

[6]   ENTSO-E, '*Continental Europe Operation Handbook—P1—Policy 1: Load-Frequency Control and Performance*', Brussels, Belgium, 2009.

[7]   The European Commission, '*Commission Regulation establishing a network code on requirements for grid connection of generators',* vol. 2016/631. 2016.

[8]   P. Kundur, N. J. Balu, and M. G. Lauby '*Power system stability and control',* McGraw-Hill, 1994.

[9]   P. Tielens and D. Van Hertem, '*The relevance of inertia in power systems*', Renewable and Sustainable Energy Reviews, vol. 55, pp. 999–1009, Mar. 2016.

[10]   H. Thiesen and C. Jauch '*Determining the Load Inertia Contribution from Different Power Consumer Groups*', Energies, vol. 13, no. 7: 1588, Apr. 2020. doi: 10.3390/en13071588

[11]   R. Eriksson, N. Modig, and K. Elkington '*Synthetic inertia versus fast frequency response: a definition*', IET Renewable Power Generation, vol. 12, no. 5, pp. 507–514, Apr. 2018. doi: 10.1049/iet-rpg.2017.0370

[12]   M. Kurth and E. Welfonder '*Importance of the Selfregulation Effect within Power Systems*', IFAC Proceedings Volumes, vol. 39, no. 7, pp. 345–352, 2006. doi: 10.3182/20060625-4-CA-2906.00064

[13]   M. Scherer '*Frequency Control in the European Power System Considering the Organisational Structure and Division of Responsibilities*', ETH Zurich, 2016 [Online]. Accessed: 30th Jun 2022. Available: http://hdl.handle.net/20.500.11850/119865

[14]   E. Ørum, L. Haarla, M. Kuivaniemi, M. Laasonen, A.I. Bruseth, E.A. Jansson, A. Danell, K. Elkington, N. Modig '*Future System Inertia 2*' ENTSO-E Report; Brussels, Belgium, 2018.

[15]   H. Thiesen, C. Jauch, and A. Gloe '*Design of a System Substituting Today's Inherent Inertia in the European Continental Synchronous Area*', Energies, vol. 9, no. 8: 582, Jul. 2016, doi: 10.3390/en9080582

[16]   ENTSO-E '*Continental Europe Operation Handbook—P5—Policy 5: Emergency Operations*', Brussels, Belgium, 2010.

[17]   A. Ulbig and G. Andersson '*On operational flexibility in power systems*', in Power and Energy Society General Meeting, 2012 IEEE, 2012, pp. 1–8.

[18]   ENTSO-E, 'The inertia challenge in Europe - Present and long-term perspective', Brussels, Belgium, Aug. 2021, Accessed: 31st Jan 2023. [Online]. Available: https://eepublicdownloads.blob.core.windows.net/public-cdn-container/ tyndp-documents/TYNDP2020/FINAL/entso-e_TYNDP2020_Insight_Report_Inertia_2108.pdf.

[19]   A. Fernández-Guillamón, E. Gómez-Lázaro, E. Muljadi and A. Molina-García '*Power systems with high renewable energy sources: A review of inertia and frequency control strategies over time*' Renewable and Sustainable Energy Reviews, vol. 115: 109369, Nov. 2019. doi: 10.1016/j.rser.2019.109369

[20]   J. Matevosyan, C. Anderson, and W. Li '*ERCOT Future Synchronous Inertia Projections*', in Proceedings of the 16th Wind Integration Workshop, Berlin, 2017.

[21]   A. Ulbig, T. S. Borsche, and G. Andersson '*Impact of Low Rotational Inertia on Power System Stability and Operation*', IFAC Proceedings Volumes, vol. 47, no. 3, pp. 7290–7297, 2014. doi: 10.3182/20140824-6-ZA-1003.02615

[22]   Y. Wang, V. Silva, and A. Winckels, '*Impact of High Penetration of Wind and PV Generation on Frequency Dynamics in the Continental Europe Interconnected System*' in Proceedings of the 13th Wind Integration Workshop, Berlin, 2014.

[23]   F.M. Gonzalez-Longatt '*Impact of emulated inertia from wind power on under-frequency protection schemes of future power systems*', Journal of Modern Power Systems and Clean Energy*, 2015, doi:10.1007/s40565-015-0143-xich

[24]   M. Asmine, C.-E. Langlois, and N. Aubut '*Inertial Response from Wind Power Plants during a Frequency Disturbance on the Hydro-Québec System - Event Analysis and Validation*', in Proceedings of the 15th Wind Integration Workshop, Vienna, 2016, pp. 406 - 413

[25]   H. Thiesen and C. Jauch '*Potential of Onshore Wind Turbine Inertia in Decarbonising the Future Irish Energy System*', Applied Sciences, vol. 12, no. 6: 2984, Mar 2022, doi: 10.3390/app12062984.

[26]   H. Thiesen '*Power System Inertia Dispatch Modelling in Future German Power Systems: A System Cost Evaluation*', Applied Sciences, vol. 12, no. 16: 8364, Aug. 2022, doi: 10.3390/app12168364

[27]   N. Miller and S. Pajic '*Diverse fast frequency response services in systems with declining synchronous inertia*', in Proceedings of the 15th Wind Integration Workshop, Vienna, 2016.

[28]   ENTSO-E '*Frequency Measurement Requirements and Usage*', Final Version 7, Jan. 2018, [Online], Assessed: 19th Mar 2021, Available: https://eepublicdownloads.entsoe.eu/clean-documents/SOC%20documents/Regional_Groups_Continental_Europe/2018/TF_Freq_Meas_v7.pdf.

[29]   M. Joos and I. Staffell '*Short-term integration costs of variable renewable energy: Wind curtailment and balancing in Britain and Germany*', Renewable and Sustainable Energy Reviews, vol. 86, pp. 45–65, Apr. 2018. doi: 10.1016/j.rser.2018.01.009

[30]   M. Döring, K. Burges, and R. Kuwahata, '*Wind Curtailment – Assessment of Storage Options for Reduction of Yield Losses*', in Proceedings of the 13th Wind Integration Workshop, Berlin, 2014, pp. 703–708.

[31]   M. Frysztacki and T. Brown '*Modeling Curtailment in Germany: How Spatial Resolution Impacts Line Congestion*', in Proceedings of the 17th International Conference on the European Energy Market (EEM), Stockholm, Sweden, 2020, pp. 1–7.

[32]   K. Kollenda, A. Schrief, C. Biele, M. Lindner, N. Sundorf, A. Hoffrichter, A. Roehder, A. Moser, and C. Rehtanz '*Curative measures identification in congestion management exploiting temporary admissible thermal loading of overhead lines*', IET Generation, Transmission & Distribution, May 2022, pp. 3171 – 3183, doi: 10.1049/gtd2.12512

[33]   L. Bird, D. Lew, M. Milligan, E. Carlini, A. Estanqueiro, D. Flynn, E. Gomez-Lazaro, H. Holttinen, N. Menemenlis, A. Orths, P.B. Eriksen, J.C. Smith, L. Soder, P. Sorensen, A. Altiparmakis, Y. Yasuda, and J. Miller '*Wind and solar energy curtailment: a review of international experience*', Renewable and Sustainable Energy Reviews, Vol. 65, 2016, pp. 577-586, doi: 10.1016/j.rser.2016.06.082

[34]   Agora Energiewende '*The Integration Cost of Wind and Solar Power. An Overview of the Debate on the Effects of Adding Wind and Solar Photovoltaic into Power Systems*', Berlin, 2015, [Online], Assessed: 19th Mar 2021, Available: https://www.agora-energiewende.de/fileadmin/Projekte/2014/integrationskosten-wind-pv/Agora_Integration_Cost_Wind_PV_web.pdf

[35]   ENTSO-E '*Completing the map: Power system needs in 2030 and 2040*', Brussels, Technical report, [Online], Assessed: 19th Mar 2021, Available: https://eepublicdownloads.azureedge.net/tyndp-documents/IoSN2020/200810_IoSN2020mainreport_beforeconsultation.pdf

[36]   D. Lew, D. Stenclik, D. Bartlett, A. Groom, P. Jorgensen, J. O'Sullivan, R. Quint, B. Rew, B. Rockwell, and S. Sharma '*Secrets of Successful Integration: Operating Experience With High Levels of Variable, Inverter-Based Generation*', IEEE Power Energy Magazine, vol. 17, no. 6, Nov. 2019, pp. 24–34. doi: 10.1109/MPE.2019.2930855

[37]   P. Larscheid, M. Maercks, S. Dierkes, A. Moser, S. Patzack, H. Vennegeerts, J. Rolink, E. Wieben '*Increasing the hosting capacity of RES in distribution grids by active power control*', in proceedings of the International ETG Congress, Bonn 17-18 November 2015, [Online], Accessed 1st May 2019, Available: https://ieeexplore.ieee.org/stamp/stamp.jsp?tp=&arnumber=7388485&tag=1

[38]   M. Bons, J. Knapp, K. Steinbacher, et al., '*Verwirklichung des Potenzials der erneuerbaren Energien durch Höherauslastung des Bestandsnetzes und zügigen Stromnetzausbau auf Verteilnetzebene*', Dessau-Roßlau, Technical report FB000385, Dec. 2020, [Online], Accessed 1st May 2022, Available: https://www.umweltbundesamt.de/sites/default/files/medien/5750/publikationen/2020_12_14_cc_51-2020_zuegiger_ausbau.pdf

[39]   C. Jauch, A. Gloe, S. Hippel, and H. Thiesen '*Increased Wind Energy Yield and Grid Utilisation with Continuous Feed-In Management*', Energies, vol. 10, no. 7: 870, 2017. doi: 10.3390/en10070870

[40]   Ministerium für Energiewende, Landwirtschaft, Umwelt, Natur und Digitalisierung (MELUND) Schleswig-Holstein, '*Kurzbericht zum Engpassmanagement in Schleswig-Holstein*', 2018, [Online], Accessed 1st May 2022, Available: https://www.schleswig-holstein.de/DE/Fachinhalte/E/erneuerbareenergien/Bericht_Einspeisemanagement.pdf;jsessionid=CAD6BCDD96E9F0CFFB6472B2DA2B6E5F?__blob=publicationFile&v=1 (accessed on 01 May 2019)

[41]   J. Bömer, M. Doering, and K. Burges, '*Einspeisemanagement in Schleswig-Holstein*', Ministerium für Energiewende, Landwirtschaft, Umwelt und ländliche Räume des Landes Schleswig-Holstein, Kiel, POWDE12992, 2012.

[42]   J. F. Manwell, J. G. McGowan, and A. L. Rogers '*Wind energy explained: theory, design and application*', 2nd edition. Chichester: Wiley, 2011.

[43]   E. Hau '*Wind turbines: fundamentals, technologies, application, economics*', 3rd edition. Berlin: Springer, 2013.

[44]   R. Gasch and J. Twele, Eds. '*Wind power plants: fundamentals, design, construction and operation*', 2nd edition. Berlin Heidelberg: Springer, 2012.

[45]   S. Heier '*Grid integration of wind energy: onshore and offshore conversion systems*', 3rd edition. Chichester, West Sussex, United Kingdom: Wiley, 2014.

[46]   A. Gloe and C. Jauch '*Simulation Model Design and Validation of a Gearless Wind Turbine - For Fast Power Control to Enhance Congestion Management*', Wind Energy Technology Institute, Flensburg, Technical report, 2016, doi: 10.13140/RG.2.1.1697.5766

[47]   A. Gloe and C. Jauch '*Measurements of the dynamic response of a wind turbine to excitations from the wind*' presented at the WindAc, Cape Town, 2017, [Online], Accessed: 31st May 2022, Available: https://www.researchgate.net/publication/321168620_measurements_ of_the_dynamic_response_of_a_wind_turbine_to_excitations_from_the_wind.

[48]   S. Sieben 'Überprüfung der absoluten Blattwinkel und Schwingungstechnische Überprüfung Enercon E30', BerlinWind GmbH, Berlin, Technical report, Aug. 2019.

[49]   A. Gloe, C. Jauch, H. Thiesen, and J. Viebeg '*Inertial Response Controller Design for a Variable Speed Wind Turbine*', Wind Energy Technology Institute, Flensburg, Technical report, Mar. 2018, doi: 10.13140/RG.2.2.27846.57926

[50]   Hydro Québec TransÉnergie, '*Transmission provider technical requirements for the connection of power plants to the Hydro-Québec transmission system*', Feb 2009 [Online]. Accessed 3rd May 2016, Available: http://www.hydroquebec.com/transenergie/fr/commerce/ pdf/exigence_raccordement _fev_09_en.pdf.

[51]   Hydro-Québec TransÉnergie, '*Technical Requirements for the Connection of Generating stations to the Hydro-Québec Transmission System*', D-2018-145, Jan. 2019, [Online]. Accessed 3rd May 2016, Available: http://www.hydroquebec.com/transenergie/fr/commerce/pdf/ 2_Requirements_generating_stations_D-2018-145_2018-11-15.pdf

[52]   EirGrid '*EirGrid grid code. Version 6*', 2009, [Online]. Accessed 3rd May 2016, Available: http://www.eirgridgroup.com/site-files/library/EirGrid/GridCodeVersion6.pdf

[53]   EirGrid '*EirGrid grid code. Version 9*', 2020, [Online]. Accessed 3rd Feb 2022, Available: https://www.eirgridgroup.com/site-files/library/EirGrid/GridCodeVersion9.pdf

[54]   Red electrica '*Technical requirement for wind power and photovoltaic installations and any generating facilities whose technology does not consist on a synchronous generator directly connected to the grid*', 2008, [Online], Accessed: Dec 12, 2018, Available: https://www.aeeolica.org/uploads/documents/4535-separata-del-borrador-de-po122.pdf

[55]   Central Electricity Authority '*Technical Standards for Connectivity to the Grid (Amendment)*', 2019, [Online], Accessed: Dec 12, 2018, Available: https://cea.nic.in/wp-content/uploads/2020/02/notified_regulations.pdf

[56]   A. .Johnsen '*Grid Code Frequency Response Working Group Requirements for System Inertia*', 2013, [Online]. Accessed: 12th Dec 2018, Available: https://www.nationalgrideso.com/ sites/eso/files/documents/16916-Meeting%2011%20- %20System%20Inertia%20Presentation.pdf.

[57]   ENTSO-E '*Frequency Stability Evaluation Criteria for the Synchronous Zone of Continental Europe*', Mar. 2016, [Online]. Accessed: 27 Jan 2021, Available: https://eepublicdownloads.entsoe.eu/clean-documents/SOC%20documents/RGCE_SPD_ frequency_ stability_ criteria_v10.pdf

[58] ENTSO-E '*Connection Network Codes –Response to the comments received during the public consultation of Implementation Guidance Documents on Frequency Stability Parameters*', Jan. 2018, [Online]. Accessed: 27th Jan 2021, Available: https://eepublicdownloads.blob.core. windows.net/public-cdn-container/clean-documents/Network%20codes%20documents/ NC%20RfG/ENTSO-E_IGD_consultation_response.pdf

[59] A. Gloe, C. Jauch, and T. Räther '*Grid Support with Wind Turbines: The Case of the 2019 Blackout in Flensburg*', Energies, vol. 14, no. 6: 1697, 2021. doi: 10.3390/en14061697

[60] ENTSO-E '*Outage of French-Spanish interconnection on 24 July 2021*', 2021, [Online]. Accessed: 29th Jan 2022, Available: https://www.entsoe.eu/news/2021/08/20/outage-of-french-spanish-interconnection-on-24-july-2021-update/

[61] ENTSO-E '*System separation in the Continental Europe Synchronous Area on 8 January 2021*', 2nd update, Jan. 2021, [Online]. Accessed: 29th Jan 2022, Available: https://www.entsoe.eu/news/2021/01/26/system-separation-in-the-continental-europe-synchronous-area-on-8-january-2021-2nd-update/

[62] P. Godin, M. Fischer, H. Röttgers, A. Mendonca, and S. Engelken '*Wind power plant level testing of inertial response with optimised recovery behaviour*', IET Renewable Power Generation, vol. 13, no. 5, pp. 676–683, Apr. 2019. doi: 10.1049/iet-rpg.2018.5232

[63] J. Aho, P. Fleming, and L.Y. Pao '*Active power control of wind turbines for ancillary services: A comparison of pitch and torque control methodologies*', *in: Proceedings of the. American Control Conference*, Boston, 2016, pp 1407–12

[64] J. Aho, L.Y. Pao, and P. Fleming '*An active power control system for wind turbines capable of primary and secondary frequency control for supporting grid reliability*', in Proceedings of the 51st AIAA Aerospace Sciences Meeting*, Grapeville, 2013

[65] J. Aho, A. Buckspan, J. Laks, P. Fleming, Y. Jeong, F. Dunne, M. Churchfield, L.Y. Pao, and K. Johnson '*A tutorial of wind turbine control for supporting grid frequency through active power control*', in Proceedings of the American Control Conference, Montreal, 2012, pp. 3120–3131.

[66] E. Ela, V. Gevorgian, P. A. Fleming, et al. '*Active Power Controls from Wind Power: Bridging the Gaps*', NREL, Technical report NREL/TP-5D00-60574, Jan. 2014

[67] L. Holdsworth, J. B. Ekanayake, and N. Jenkins '*Power system frequency response from fixed speed and doubly fed induction generator-based wind turbines*', Wind Energy, vol. 7, no. 1, 2004, pp. 21-35 [68]   J. Morren, J. Pierik, and S. W. H. de Haan, 'Inertial response of variable speed wind turbines', *Electr. Power Syst. Res.*, vol. 76, no. 11, pp. 980–987, Jul. 2006. doi: 10.1016/j.epsr.2005.12.002

[69] G. Ramtharan, N. Jenkins, and J. B. Ekanayake, '*Frequency support from doubly fed induction generator wind turbines*', IET Renewable Power Generation, vol. 1, no. 1, 2007, p. 3,. doi: 10.1049/iet-rpg:20060019

[70] I. D. Margaris, S. A. Papathanassiou, N. D. Hatziargyriou, A.D. Hansen, and P. Sorensen '*Frequency Control in Autonomous Power Systems With High Wind Power Penetration*', IEEE Transactions on Sustainable Energy, vol. 3, no. 2, Apr. 2012, pp. 189–199,. doi: 10.1109/TSTE.2011.2174660

[71] C. Su and Z. Chen, '*Influence of wind plant ancillary frequency control on system small signal stability*', in IEEE Power and Energy Society General Meeting, San Diego, CA, 2012, pp. 1–8.

[72] R. You, B. Barahona, J. Chai, and N.A. Cutululis '*Frequency support capability of variable speed wind turbine based on electromagnetic coupler*', Renewable Energy, vol. 74, Feb. 2015, pp. 681–688. doi: 10.1016/j.renene.2014.08.072

[73]   Z. Zhang, Y. Wang, H. Li, and X. Su '*Comparison of inertia control methods for DFIG-based wind turbines*', in proceedings of the ECCE Asia Downunder, 2013, pp. 960–964

[74]   Z.-S. Zhang, Y.-Z. Sun, J. Lin, and G.-J. Li '*Coordinated frequency regulation by doubly fed induction generator-based wind power plants*', IET Renewable Power Generation, vol. 6, no. 1, 2012,. doi: 10.1049/iet-rpg.2010.0208

[75]   L.-R. Chang-Chien, W.-T. Lin, and Y.-C. Yin, '*Enhancing Frequency Response Control by DFIGs in the High Wind Penetrated Power Systems*', IEEE Transactions on Power Systems, vol. 26, no. 2, May 2011, pp. 710–718, doi: 10.1109/TPWRS.2010.2052402

[76]   F. Wilches-Bernal, J. H. Chow, and J. J. Sanchez-Gasca, '*A Fundamental Study of Applying Wind Turbines for Power System Frequency Control*', IEEE Transactions on Power Systems, vol. 31, no. 2, Mar. 2016, pp. 1496–1505. doi: 10.1109/TPWRS.2015.2433932

[77]   M. Hwang, E. Muljadi, J.-W. Park, P. Sorensen, and Y.C. Kang, '*Dynamic Droop–Based Inertial Control of a Doubly-Fed Induction Generator'*, IEEE Transactions on Sustainable Energy, vol. 7, no. 3, Jul. 2016, pp. 924–933. doi: 10.1109/TSTE.2015.2508792

[78]   J. Van de Vyver, J. D. M. De Kooning, B. Meersman, L. Vandevelde, and T.L. Vandoorn '*Droop Control as an Alternative Inertial Response Strategy for the Synthetic Inertia on Wind Turbines*', IEEE Transactions on Power Systems, vol. 31, no. 2, Mar. 2016, pp. 1129–1138. doi: 10.1109/TPWRS.2015.2417758

[79]   P. Moutis, E. Loukarakis, S. Papathanasiou, and N.D. Hatziargyriou '*Primary load-frequency control from pitch-controlled wind turbines*', in proceedings of the IEEE Bucharest PowerTech, Bucharest, Romania, 2009, pp. 1–7.

[80]   H. T. Ma and B. H. Chowdhury '*Working towards frequency regulation with wind plants: combined control approaches*', IET Renewable Power Generation, vol. 4, no. 4, 2010. doi: 10.1049/iet-rpg.2009.0100

[81]   A. Žertek, G. Verbič, and M. Pantoš '*Optimised control approach for frequency-control contribution of variable speed wind turbines*', IET Renewable Power Generation, vol. 6, no. 1, 2012. doi: 10.1049/iet-rpg.2010.0233

[82]   L. M. Castro, C. R. Fuerte-Esquivel, and J. H. Tovar-Hernandez '*Solution of Power Flow With Automatic Load-Frequency Control Devices Including Wind Farms*', IEEE Transactions on Power Systems, vol. 27, no. 4, Nov. 2012, pp. 2186–2195. doi: 10.1109/TPWRS.2012.2195231

[83]   K. V. Vidyanandan and N. Senroy '*Primary frequency regulation by deloaded wind turbines using variable droop*', IEEE Transactions on Power Systems, vol. 28, no. 2, pp. 837–846, May 2013. doi: 10.1109/TPWRS.2012.2208233

[84]   S. Wang and K. Tomsovic '*A Novel Active Power Control Framework for Wind Turbine Generators to Improve Frequency Response*', IEEE Transactions on Power Systems, vol. 33, no. 6, Nov. 2018, pp. 6579–6589. doi: 10.1109/TPWRS.2018.2829748

[85]   X. Zhang, X. Zha, S. Yue, et al. '*A Frequency Regulation Strategy for Wind Power Based on Limited Over-Speed De-Loading Curve Partitioning'*, IEEE Access, vol. 6, pp. 22938–22951, 2018. doi: 10.1109/ACCESS.2018.2825363

[86]   G. Joos '*Wind turbine generator low voltage ride through requirements and solutions'*, in 2008 IEEE Power and Energy Society General Meeting - Conversion and Delivery of Electrical Energy in the 21st Century, Pittsburgh, PA, USA, 2008, pp. 1–7 [Online]. Accessed 10.02.2021; Available: http://ieeexplore.ieee.org/document/4596605/

[87]   J. Wenske and U. Beckert '*Voltage-induced stresses during Low Voltage Ride Through (LVRT) in the drive train of wind turbines with DFIG*', presented at the International Conference on Renewable Energies and Power Quality, Santiago de Compostella, 2012, [Online]. Accessed 10th Feb 2021, Available: http://www.icrepq.com/papers-icrepq12.html.

[88]   P. A. Fleming, J. Aho, A. Buckspan, E. Ela, Y. Zhang, V. Gevorgian, , A. Scholbrock, L. Pao, and R. Damiani '*Effects of power reserve control on wind turbine structural loading: Structural loads analysis of power reserve control strategies for wind turbines*', Wind Energy, vol. 19, no. 3, Mar. 2016, pp. 453–469. doi: 10.1002/we.1844

[89]   X. Wang, W. Gao, A. Scholbrock, E. Muljadi, V. Gevorgian, J. Wang, W. Yan and H. Zhang '*Evaluation of different inertial control methods for variable-speed wind turbines simulated by fatigue, aerodynamic, structures and turbulence (FAST)*', IET Renewable Power Generation, vol. 11, no. 12, Oct. 2017, pp. 1534–1544. doi: 10.1049/iet-rpg.2017.0123

[90]   B. Fischer, M. Shan, P. Brosche, P. Loepelmann, A. Rezaeian, M.Sayed, and S. Hauptmann '*Abschlussbericht GridLoads*', Kassel, Stuttgart, Technical report, 2020, [Online]. Assessed: 17th Mar 2021, Available: https://www.mesh-engineering.de/images/Publications/ MesH/Abschlussbericht_GridLoads_final.pdf.

[91]   C. Jauch '*First Eigenmodes Simulation Model of a Wind Turbine - for Control Algorithm Design*', Wind Energy Technology Institute, Flensburg, Technical report, Sep. 2020, doi: 10.13140/RG.2.2.17192.19204.

[92]   J. Jonkman, S. Butterfield, W. Musial, et al. '*Definition of a 5-MW Reference Wind Turbine for Offshore System Development*', Technical report, NREL/TP-500-38060, Feb. 2009.

[93]   S. Øye '*FLEX4, Simulation of Wind Turbine Dynamics*', in State of the Art of Aerolastic Codes for Wind Turbine Calculations, Lyngby, Denmark: B. Maribo Pedersen, editor, 1996, pp. 71–76.

[94]   ENTSO-E '*Transparancy Platform*', 2016. [Online]. Assessed: 17th Mar 2016, Available: https://transparency.entsoe.eu/

[95]   H. Thiesen, A. Gloe, and C. Jauch '*Grid Frequency Data – WETI.*' OSF.io. Dec. 2021. doi: 10.17605/OSF.IO/JBK82

[96]   A. Gloe,H. Thiesen, C. Jauch '*Grid frequency analysis for assessing the stress on wind turbines*', in Proceedings of the 15th Wind Integration Workshop, Vienna, 2016.

[97]   M. Adeen, G. M. Jonsdottir, and F. Milano '*Statistical Correlation between Wind Penetration and Grid Frequency Variations in the Irish Network*', in 2019 IEEE International Conference on Environment and Electrical Engineering and 2019 IEEE Industrial and Commercial Power Systems Europe (EEEIC / I&CPS Europe), Genova, Italy, 2019, pp. 1–6.

[98]   H. Thiesen, A. Gloe, J. Viebeg and C. Jauch '*The Provision of Synthetic Inertia by Wind Turbine Generators: An Analysis of the Energy Yield and Costs'* in Proceedings of the 16th Wind Integration Workshop, Berlin, 2017.

[99]   German Weather Service '*Climate Data Center*', [Online]. Accessed: 27th Jan 2021, Available: https://cdc.dwd.de/portal/202007291339/mapview

[100]   C. Jauch and A. Gloe '*Simultaneous Inertia Contribution and Optimal Grid Utilization with Wind Turbines*' Energies, vol. 12, no. 15: 3013, 2019. doi: 10.3390/en12153013

[101]   Kries-Energietechnik '*Grid inspector IKI-50*', Data sheet [Online]. Accessed: 3rd April 2016. Available: https://www.kries.com/media/pdf/a7/28/fa/IKI_50_V6_d.pdf

[102]   A. Gloe, C. Jauch, B. Craciun, and J. Winkelmann '*Continuous provision of synthetic inertia with wind turbines: implications for the wind turbine and for the grid*', IET Renewable Power Generation, vol. 13, no. 5, pp. 668–675, 2019, doi: 10.1049/iet-rpg.2018.5263

[103]   A. Gloe, C. Jauch, B. Craciun, A. Zanter, and J. Winkelmann '*Influence of continuous provision of synthetic inertia on the mechanical loads of a wind turbine*' Energies. vol. 22, no. 15: 5185, 2021

[104]   A. Gloe '*Continuous grid frequency support with variable synthetic inertia and feedforward pitch angle adjustment*' in Journal of Physics: Conference Series, vol.2265, no. 3: 032105, 2022, doi: 10.1088/1742-6596/2265/3/032105.

[105]   A. Gloe, C. Jauch, B. Craciun, and J. Winkelmann '*Limitations for the continuous provision of synthetic inertia with wind turbines*', In Proceedings of the 16th Wind Integration Workshop, Berlin, 2017, pp. 442–447.

[106]   N. Miller, D. Lew, and R. Piwko '*Technology Capabilities for Fast Frequency Response*', Schenectady, NY, Technical report, Mar. 2017 [Online]. Accessed: 3rd Feb 2023. Available: https://www.aemo.com.au/-/media/files/electricity/nem/security_and_reliability/reports/2017/20170310-ge-ffr-advisory-report.pdf?la=en

[107]   Federal Network Agency '*Core energy market data register*'. [Online]. Accessed: 4th Mar 2021. Available: https://www.bundesnetzagentur.de/EN/Areas/Energy/Companies/CoreEnergyMarketDataRegister/CoreDataReg_node.html

[108]   IEC 61400-1 '*Wind energy generation systems - Part 1: Design requirements*', Feb. 2019.

[109]   M. Sessarego, N. Ramos-García, J. N. Sørensen, and W.Z. Shen '*Development of an aeroelastic code based on three-dimensional viscous-inviscid method for wind turbine computations*', Wind Energy, pp. 1145–1170, 2017. doi: 10.1002/we.2085

[110]   B. Badrzadeh '*Analysis of the South Australien Blackout*' in Proceedings of the 16th Wind Integration Workshop, Berlin, 2017.

[111]   F. Guo and D. Schlipf '*A spectral model of grid frequency for assessing the impact of inertia response on wind turbine dynamics', Energies*', vol.14, No. 9: 2492, 2021.

[112]   C. Jauch and A. Gloe '*Improved Feed-in Management with Wind Turbines*' in Proceedings of the 15th Wind Integration Workshop, Vienna, 2016.

[113]   H. Thiesen and C. Jauch '*Identifying electromagnetic illusions in grid frequency measurements for synthetic inertia provision*', in proceedings of the IEEE CPE-POWERENG 2019, 13th International Conference on Compatibility, Power Electronics and Power Engineering, April 2019 - Sonderborg, Denmark

[114]   E. Ørum, M. Kuivaniemi, M. Laasonen, A.I. Bruseth, E.A. Jansson, A. Danell, K. Elkington, N. Modig '*Nordic Report—Future System Inertia*' ENTSO-E Report; Brussels, Belgium, 2015.

[115]   North American Electric Reliability Cooperation 'Fast Frequency Response Concepts and Bulk Power System Reliability Needs', Atlanta, GA, USA, Mar. 2020. [Online]. Accessed: 7th Nov 2022. Available: https://www.nerc.com/comm/PC/InverterBased%20Resource%20Performance%20Task%20Force%20IRPT/Fast_Frequency_Response_Concepts_and_BPS_Reliability_Needs_White_Paper.pdf

[116]   J. Jonkman and M. Sprague 'OpenFAST Documentation', 12th Feb 2023 [Online]. Accessed: 8th Mar 2023. Available: https://openfast.readthedocs.io/en/main

Publications

Publication 1

Design of a System Substituting Today's Inherent Inertia in the European Continental Synchronous Area

Design of a System Substituting Today's Inherent Inertia in the European Continental Synchronous Area

Henning Thiesen *, Clemens Jauch and Arne Gloe

Wind Energy Technology Institute, Center for Sustainable Energy Systems Flensburg,
Flensburg University of Applied Sciences, Flensburg 24943, Germany; clemens.jauch@hs-flensburg.de (C.J.);
arne.gloe@hs-flensburg.de (A.G.)

* Correspondence: henning.thiesen@hs-flensburg.de; Tel.: +49-461-48161-441

Abstract: In alternating current (AC) power systems the power generated by power plants has to match the power drawn by consumers plus the system losses at any time. In the case of an imbalance between generation and consumption the frequency in the system deviates from its rated value. In order to avoid an unsuitable frequency, control power plants have to step in to level out this imbalance. Control power plants need time to adjust their power, which is why the inertial behaviour of today's AC systems is crucial for frequency control. In this paper it is discussed that the inertia in the European Continental Synchronous Area decreases due to the transition to renewable energy sources. This will become a problem for frequency control, which is why the provision of non-inherent inertia is proposed. This system consists of fast-responding energy storage. Its dimensions in terms of power and energy are determined. Since such non-inherent inertia requires investments a cost-efficient solution has to be found. Different technologies are compared in terms of the newly-introduced levelised cost of inertia. This paper concludes with the proposal that in future inertia should be traded and with the recommendation to use flywheels for this purpose, as these are the most cost-efficient solution for this task.

Keywords: energy storage systems; power system frequency control; power system stability; synthetic inertia; system inertia

---

1. Introduction

The threat of climate change consequences and the request to be independent from importing scarce fossil fuels, as well as the nuclear disaster in Fukushima, have led many countries to switch their energy generation to a generation based on renewable energy sources (RES). This transition takes place in the heating, transport, and electricity sectors. The European Union has ambitious targets in terms of RES and has taken a leading role with its "2030 climate and energy framework" [1]. At least 27% of the annual overall energy consumption in the European Union has to be covered by RES until 2030. By 2050 Germany wants to cover 80% of its annual gross electricity consumption by RES [2]. In order to reach such high penetration shares of RES, volatile generation types like wind turbines (WTs) and photovoltaic systems (PVs) will take an important part in future electricity generation.

One major challenge in this transition movement will be the future of power system stability. Power generation and consumption in an alternating current (AC) power system have to be balanced in every moment. The grid frequency is the indicator for the balance of power generation and consumption. Hence, an important part of power system stability is frequency control. Frequency control was, and still is, the task of conventional power plants. In order to keep frequency

deviations in an acceptable range, either RES have to take over this duty, or conventional must-run capacities have to remain in operation. However, keeping must-run capacities would contradict the energy transition. Due to the time which is needed until control power is fully activated, system inertia is required to limit frequency deviations and gradients. A major challenge in terms of frequency control by RES is the provision of power system inertia. WTs and PVs are connected to the grid by power electronics and therefore do not provide inherent inertia [3]. However, it is extensively discussed, that WTs are capable of providing so called synthetic inertia [4–7]. Currently, a research project regarding the provision of synthetic inertia using WTs and its effects on mechanical loads and costs is conducted at the Wind Energy Technology Institute (WETI), in collaboration with the WT manufacturer Suzlon Energy.

Cao et al. have studied the impact of variable system inertia on the performance of frequency based protection for the AC island system of the United Kingdom [8]. For a larger synchronous area Wang et al. have studied the impact of high penetration of variable RES in the European Continental Synchronous Area (ECSA) [9]. The German Energy Agency (DENA) has stated that until 2030 sufficient system inertia is available in the ECSA in order to react appropriately to frequency deviations in the event of an imbalance of 3 GW [10]. The main reasoning behind this statement is the great differences in the share of RES across the ECSA. A possible consequence of insufficient system inertia is the split of the grid into islands. These grid islands have to be controllable in terms of frequency stability. Such splits into electric islands occurred in September 2003 when Italy was disconnected and in November 2006 when the former Union for the Coordination of the Transmission of Electricity (UCTE) split into three islands [11,12]. After Italy was disconnected from the UCTE the grid frequency in Italy was temporarily stabilised at 49 Hz. It declined further for various reasons, which finally led to a system blackout. The incident in 2006 led to the split of the UCTE grid into three separate areas (west, northeast and southeast) with significant power imbalances. These imbalances caused under-frequencies in the west and southeast areas and an over frequency in northeast. Full synchronisation of the UCTE was achieved 38 min after the split.

One part of low rotational inertia in the power system relates to technical issues. While this is addressed extensively, a literature study has shown that the economical perspective of system inertia has only been researched superficial yet. Society and economy are highly dependent on electricity and its undisturbed provision due to an extensive use of electrical devices. Large frequency fluctuations or even blackouts might cause huge financial damages. Leahy and Tol evaluated the damage caused by blackouts for the private and the industrial sector in Ireland [13]. The same was done by Nooij et al. for the Netherlands [14] and by Growitch et al. for Germany [15]. Pelletier et al. analysed the development of system inertia in New Zealand and proposed a financial compensation/penalty system for generators providing sufficient or insufficient system inertia respectively. Based on the spread between the power system inertia constant and the individual inertia constant of each generator, a fee would have to be paid for generators providing insufficient inertia or a benefit would be received for generators providing sufficient inertia [16]. However, this proposal is not applicable due to a non-transparent calculation and a non-guarantee of sufficient system inertia, that is, a controllable power system.

The paper at hand emphasizes the importance of power system inertia for the ECSA for the purpose of frequency stability and provides a closer look on the economical side of inertia. Due to its decreasing nature, it is proposed that inertia should be a traded good in future power systems. Therefore, a physical trading unit is discussed and proposed. In a following step, an energy storage system is designed to provide synthetic inertia in order to maintain frequency stability in the ECSA as it is known today, and financially assessed. An obvious solution for maintaining system inertia appears to be idle operation of decommissioned conventional power plants. This option is not pursued here, because when decommissioning conventional power plants large masses are being disconnected from the turbine train and the inertia reduces significantly [10]. Although, synthetic inertia provision by RES and its impact on mechanical loads is currently researched at WETI, it is not part of this paper. It can be assumed that the provision of synthetic inertia by WTs increases mechanical stress and, therefore,

reduces the life expectancy of WTs. Alternatively the mechanical design has to be adapted, which leads to increased cost of energy from these WTs. As RES depend on the availability of primary energy sources (e.g., wind), storage units are unavoidable for the purpose of frequency stability at all times. Nevertheless, future research and finally a market for system inertia will determine, whether RES or storage units will be a proper and economical efficient solution.

In this paper Section 2 introduces the basic working principle of today's power system, the behaviour of the grid frequency in the event of a power imbalance, as well as the working principle of system inertia. Section 3 discusses and clarifies the unit in which futures system inertia should be traded, once the inherent inertia does no longer suffice for stable power system operation. In Section 4 an energy storage system for the provision of synthetic inertia is dimensioned with respect to power and energy and it is also modelled. Section 5 evaluates the costs of such a storage system. Additionally, levelised costs of inertia are introduced for the purpose of comparison. Section 6 sums up the results.

2. Power System Operation and the Influence of System Inertia

In present AC electrical systems, power generation and consumption have to be balanced in every moment. The grid frequency, f, indicates whether power generation and power consumption is balanced. The grid frequency is directly coupled to the rotational speed of all synchronous generators and all other rotating electric machines which are connected to the grid without power electronics. Depending on the synchronous region considered, the nominal grid frequency, f_0, is 50 Hz (like in the ECSA) or 60 Hz. A simple approach to describe the relation between power generation, power consumption, and the grid frequency is shown with Equation (1) [5].

$$\frac{\delta\omega}{\delta t} = \frac{T_{gen} - T_{load}}{J_{Sys}} \tag{1}$$

T_{gen} is the accumulated power generation torque, T_{load} is the torque of the total power consumption including grid losses and J_{Sys} the power system inertia. Power system inertia is the aggregated mass moment of inertia of all directly coupled rotational machines, i.e., mainly synchronous generators of conventional power plants. $\delta\omega/\delta t$ is the change of the rotational speed of these machines. The rotational speed of a generator is coupled to the grid frequency by $\omega = 2\pi f$. In the case of an unscheduled generation loss, $T_{gen} - T_{load}$ turns negative and the grid frequency decreases from its nominal value. In the case of a surplus of T_{gen}, the frequency increases.

System inertia refers to the lagging speed response of all coupled synchronous machines in an AC power system in the event of an imbalance between power generation and demand; hence, all synchronous machines can be seen as short-time accumulators. They dampen frequency deviations by storing or releasing kinetic energy.

$$E_{Kin} = \frac{1}{2} \cdot J \cdot \omega^2 \tag{2}$$

Equation (2) describes the relation between stored kinetic energy, the inertia of a machine, J, and the rotational speed ω. If the frequency decreases, the rotational speed of the machine decreases, kinetic energy is released and converted into additional electrical energy, which is fed into the grid. If the frequency increases, the opposite happens. It is the state of the art to describe the system resilience against frequency deviations by the inertia constant, H [17]. The inertia constant determines the duration a generating machine, theoretically, is able to provide its rated power solely from its stored kinetic energy, i.e., its speed decreases from rated to zero. See Equation (3):

$$H = \frac{E_{Kin}}{S_B} = \frac{J\omega^2}{2S_B} \tag{3}$$

where S_B is the rated power of the machine. Typical values for H are in the range of 2 s to 10 s [17].

Information about control energy and power in this paper refer to standards set by the European Network of Transmission System Operators of Electricity (ENTSO-E) [18,19]. In continental Europe

control energy and power is divided into three categories, namely Primary Control Reserve (PCR), Secondary Control Reserve (SCR), and Tertiary Control Reserve. PCR gets activated when frequency deviation exceeds ± 20 mHz from its nominal value f_0. It starts within a few seconds after the incident and has to be fully activated in no greater than 30 s. All power plants delivering PCR participate equally in the synchronous area. PCR has to be delivered until it is completely taken over by SCR and Tertiary Control Reserve (TCR) but at least for 15 min.

In summary, system inertia is an essential part for the functionality of present frequency control, as it provides PCR sufficient time to adjust its power. However, due to the increasing share of inverter based RES in power systems, system inertia decreases. Hence, in a future power system inertia has to be provided externally and suppliers have to be compensated for their expenses.

3. Determining Factors for Providing Non-Inherent Inertia in a Power System

As system inertia decreases, in future power systems the provision of non-inherent inertia becomes inevitable and has to be financially compensated. Consequently, a physical unit in which the good inertia can be traded has to be defined. Obvious choices would be power or energy—the units in which PCR and SCR are traded nowadays—or simply inertia. To find a reasonable unit, the ways of providing inertia in the future are analysed and compared with the behaviour of inertia today.

Grid frequency control must fulfil two targets:

1. The rate of change of frequency (ROCOF) has to be kept under 2 Hz/s [20–22]. If the ROCOF exceeds this threshold, ROCOF relays trigger.
2. The frequency must be kept within certain limits, e.g., 49–51.5 Hz in the ECSA [23]. Otherwise, load shedding is activated and parts of the grid are disconnected.

The performance of frequency control is assessed for the case of a sudden loss of a large power plant (3 GW), the so-called reference incident [18]. The reaction of the frequency in such an event is described by an imbalance of the torque ($\Delta T = T_{gen} - T_{load}$) and the system inertia (J_{Sys}) of Equation (1). Consequently, high system inertia allows limiting the absolute frequency excursion by ramping up the PCR power plants over a period of 30 s.

However, in a future grid system inertia has to be provided externally as the inherent inertia decreases. The system inertia in Equation (1) can be split into two independent inertias:

- Inertia provided by rotating loads (fans, pumps, etc.)—is assumed to vary with the load level and is assumed to decline in the future, as newly installed rotating loads are often connected via frequency converters.
- Inertia provided by synchronous generators—decreases with an increasing penetration of RES and varies with the load level of the grid.

It is assumed that, even in a system with 100% generation from RES, i.e., zero inertia from conventional power plants, a residual inertia, J_{res}, remains in the grid, which is the inertia provided by the loads, as well as hydro and biomass power plants. Usually, hydro and biomass power plants are RES which comprise AC connected synchronous generators. Figure 1 shows the power generation structure in continental Europe in the year 2015 [24]. The bottom part of Figure 1 shows RES equipped with synchronous generators (biomass and hydro power plants). Even though volatility is clearly visible, a certain base load of system inertia supplied by RES is obvious. Information drawn from such data can be used to predict J_{res}.

However, the decrease in the inertia in the future causes higher ROCOFs, which cannot be handled by the present frequency control method. Hence, additional system inertia has to be provided—so-called synthetic inertia. In contrast to today's inertia it will not necessarily be provided by rotating masses, but by any kind of very fast reacting generation or storage units. In contrast to PCR providing power plants, these units are assumed to respond instantaneously. If these units emulate the behaviour of today's inertia, the frequency control method will not have to be changed.
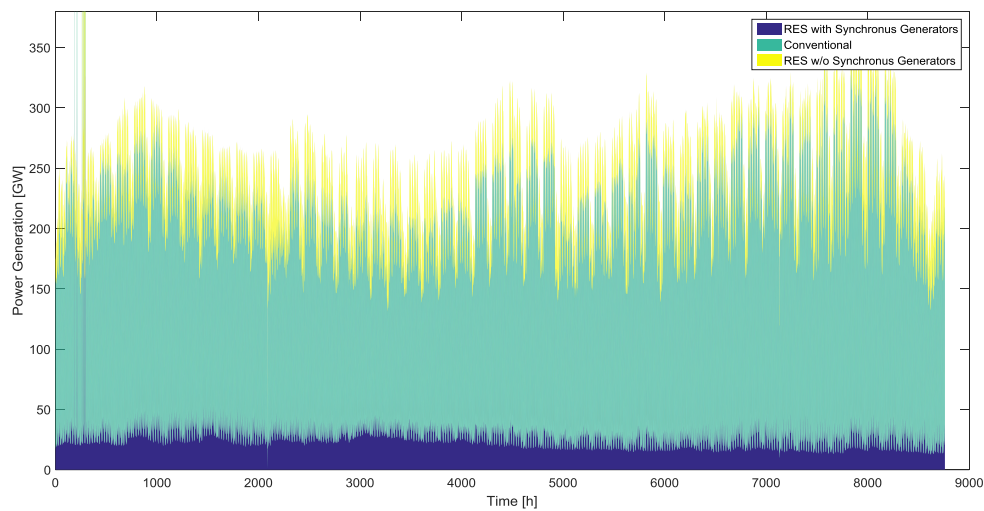
Figure 1. Power generation mix in the ECSA. Illustrated are RES with synchronous generator, conventional power plants and volatile RES without synchronous generators [24]. The horizontal axis shows the hours of the year 2015.

Today's inertia automatically exchanges power with the grid, whenever the grid frequency changes. The amount of power exchanged depends on the ROCOF and the frequency. The energy exchanged, is determined by the frequencies at the beginning and the end of the frequency excursion.

- Energy from system inertia: The provided energy is equal to the change of kinetic energy, which is stored in the rotating parts of the machines. The kinetic energy is described in Equation (2). Comparing the kinetic energies for two different frequencies, the difference can be described with Equation (4):

$$E_{Inertia} = E_{Kin} = \frac{1}{2} \cdot J_{Sys} \cdot \left(\omega_1^2 - \omega_2^2 \right) \tag{4}$$

- Power from system inertia: The feed-in power from inertia is the gradient of the kinetic energy, which is stored in the rotating parts of the machines. It can be calculated by differentiating Equation (2) with respect to time:

$$P_{Inertia} = \frac{\delta E_{Kin}}{\delta t} = J_{Sys} \cdot \omega \cdot \frac{\delta \omega}{\delta t} \tag{5}$$

Equation (5) shows, that the power provided by the system inertia depends on the frequency and the ROCOF. The provided power reduces the imbalance in the numerator of Equation (1) and counteracts the change of frequency and, therefore, limits the ROCOF.

From the paragraph above, it becomes obvious, that the traded unit should be inertia. If power was used instead, the amount of energy needed to limit the absolute change of frequency would be neglected (target 2 of the frequency control). By using energy instead, the instantaneous power response and therefore the ROCOF criteria (target 1 of the frequency control) would be neglected. As shown above, synthetic inertia could fulfil both targets at the same time by emulating today's inertia. In contrast to PCR, system inertia would be used almost anytime. This is a major difference between trading inertia and trading PCR power.

4. Dimension of a Storage System for the Provision of System Inertia

Potential bidders in a future scenario must dimension their units for the provision of synthetic inertia in terms of power and energy. As mentioned in the previous section, futures system inertia is a combination of the residual inertia, J_{res}, and the synthetic inertia, J_{SI}. In a first approach, established energy storage technologies are evaluated for the provision of synthetic inertia.

Each storage unit is connected to the electrical grid via a power conversion system (PCS). Assessed storage technologies in this paper are three types of battery storages (li-ion, lead acid, and sodium sulphur), supercapacitors, and flywheel storage systems. Power is provided almost instantaneously with a deployment time of 10 ms for flywheels and super capacitors and a deployment time of 5 ms for the battery storage systems after the detection of the imbalance [25]. The input signal for the PCS would be the grid frequency. Hence, a certain amount of inherent inertia needs to be provides by any kind of rotating mass, i.e., the residual inertia. Otherwise, the grid frequency would change instantaneously and infinitely steep, hence, it would not be possible to react appropriately. The amount of J_{res} needed is determined by the largest permitted ROCOF, i.e., $\delta f / \delta t = 2$ Hz/s. It can be calculated by rearranging Equation (1) and leads to 759,908 kg· m^2 for the standard loss of generation scenario in the ECSA (ENTSO-E reference incident). One part of J_{res} is provided from the consumer side and is, hence, unknown. Therefore, it is neglected and J_{res} is assumed to be supplied by rotating masses of hydro and biomass power plants only. Rearranging Equation (3) for S_B and using the inertia constant of a large hydro power plant ($H_{hydro} = 3$ s), as well as $J_{res} = 759,908$ kg· m^2 leads to an overall rated power of 12.49 GW for the ECSA [26]. Compared to the power feed-in from RES equipped with synchronous generators shown in Figure 1, it seems achievable, that futures J_{res} could be provided solely by such generation sources. It has to be noted that it is a conservative approach to assume a capacity factor of 100%, as it is unlikely that all synchronous generator based RES run at full load at any time.

In the next step, the amount of required synthetic inertia is determined with the help of frequency simulations. J_{SI} is increased stepwise, until the sum of residual (J_{res}) and synthetic inertia (J_{SI}) also meet the second frequency control target mentioned in Section 4. Figure 2 shows the time trace of the frequency based on the ENTSO-E reference incident applying J_{res}. The effects of SCR are not shown which is why the grid frequency levels out at 45 Hz. Once the imbalance is detected, power plants offering PCR start to adapt their power output. The additional power reduces the imbalance of the torque in the numerator of Equation (1). This results in a decreasing decline in the grid frequency. Figure 2 illustrates the fact that J_{res} alone does not limit the frequency to the threshold of 49 Hz. Hence, synthetic inertia is essential for frequency control. With simulations, the needed J_{SI} to stay above 49 Hz is determined to be 3.11×10^6 kg· m^2 for the ECSA. It is the spread between J_{res}, which results in the achievement of the first frequency control target and $J_{sys,min}$ which is the minimum amount of system inertia necessary to achieve both frequency control targets.
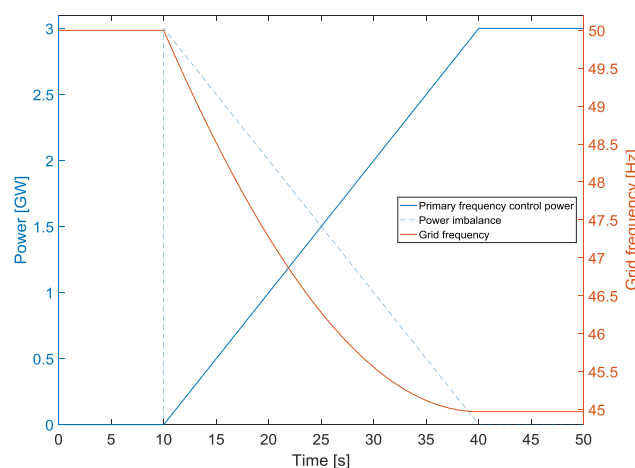
Figure 2. Simplified time traces of frequency and power in the event of the ENTSO-E reference incident and the minimum amount of inertia to reach the 2 Hz/s threshold.

The maximum power and energy needed from the energy storage system emulating the characteristics of present system inertia are calculated by adapting Equations (4) and (5). To calculate

the maximum power the highest allowed grid frequency (51.5 Hz) and the maximum ROCOF (2 Hz/s) are taken. Equation (6) shows the relationship where the frequency is expressed in terms of angular speed $\omega = 2 \cdot \pi \cdot f$. In Equation (6) P_{SI} results in 12.65 GW for the ECSA if J_{SI} is set to 3.11×10^6 kg·m^2 (derived above), if the maximum permissible frequency is set to $f = 51.5$ Hz and the maximum permissible ROCOF ($\delta f/\delta t = 2$ Hz/s) is applied.

$$P_{SI} = J_{SI} \cdot \omega \cdot \frac{\delta \omega}{\delta t} \tag{6}$$

The maximum needed energy for the provision of synthetic inertia is calculated using Equation (7):

$$E_{SI} = \frac{1}{2} \cdot J_{SI} \cdot \left(\omega_1^2 - \omega_2^2 \right) \tag{7}$$

Nowadays, synchronous generators provide energy by automatically adapting the kinetic energy in their rotation. The generators have to remain connected to the grid as long as the grid frequency is between 51.5 Hz and 47.5 Hz [23]. Hence, the kinetic energy, which is stored in the rotating masses has to be determined for a variation in rotational speed that results from a grid frequency variation from 51.5 Hz to 47.5 Hz. Applying these frequencies and J_{SI} as determined above, in Equation (7), leads to $E_{SI} = 2.43 \times 10^{10}$ Ws = 6.75 MWh. This is the minimum energy that a future energy storage systems providing synthetic inertia has to be able to supply.

In order to show the functionality of storage units providing synthetic inertia, their behaviour in the event of the ENTSO-E reference incident and the behaviour for current grid frequencies is modelled. As stated in the beginning of this section, five different types of storage units are assessed and grouped based on their deployment time. Figure 3a shows the time traces of the grid frequency and the ROCOF. The blue and solid red lines show the grid frequency and ROCOF, respectively, for the provision of synthetic inertia via storage units with a deployment time of 5 ms (li-ion, lead acid, and sodium sulphur). The dotted lines display the grid frequency and the ROCOF using storage units with a deployment time 10 ms (flywheel and super capacitors). Obviously, storage units with a slower deployment time lead to a lower grid frequency nadir. Figure 3b shows the power feed-in of the storage units. Storage units with a faster deployment time have a slightly higher power feed in. Nevertheless, both grouped storage systems are capable of providing the needed synthetic inertia as it is requested by the frequency control targets. Figure 4 displays the behaviour of the storage units responding to measured time series of the current grid frequency. Figure 4a shows the grid frequency of the ECSA on 3 March 2016 from 20:45 to 21:15. Figure 4b illustrates the power feed-in of both grouped storage units. As batteries are capable of providing power with a smaller time delay, the power feed-in is higher compared to storage units with a higher deployment time (flywheels and super capacitors). Figure 4c shows the state of charge (SOC) of both grouped storage units. At the beginning of the assessed frequency measurement, storage units are charged at a level of 61%. The SOC of storage units with a quicker response time (blue line) is slightly more volatile than the SOC of flywheels and super capacitors.

Storage systems can be located and controlled at different voltage levels [27]. As current conventional power plants, which are providing inertia today, are commonly connected to high voltage levels storage units providing synthetic inertia could be connected to the same voltage level. However, in order to minimise system losses a detailed assessment of the power flows in the grid has to be undertaken. Synthetic inertia covers gaps between supply and demand; therefore, the power that it exchanges with the grid travels to and from the generators and the consumers. The impedances through which this power travels have to be as low as possible. Hence, a generally applicable rule for the voltage level to which storage units providing synthetic inertia should be connected cannot be made. It has to be ensured that the grid capacity is sufficient for the power flow caused by synthetic inertia. The geographical allocation could be undertaken similar to today's allocation of PCR [19]. PCR is allocated based on the contribution coefficient of the various control areas. Nevertheless, future

development of the power system has to be considered regarding the geographical allocation of storage units.
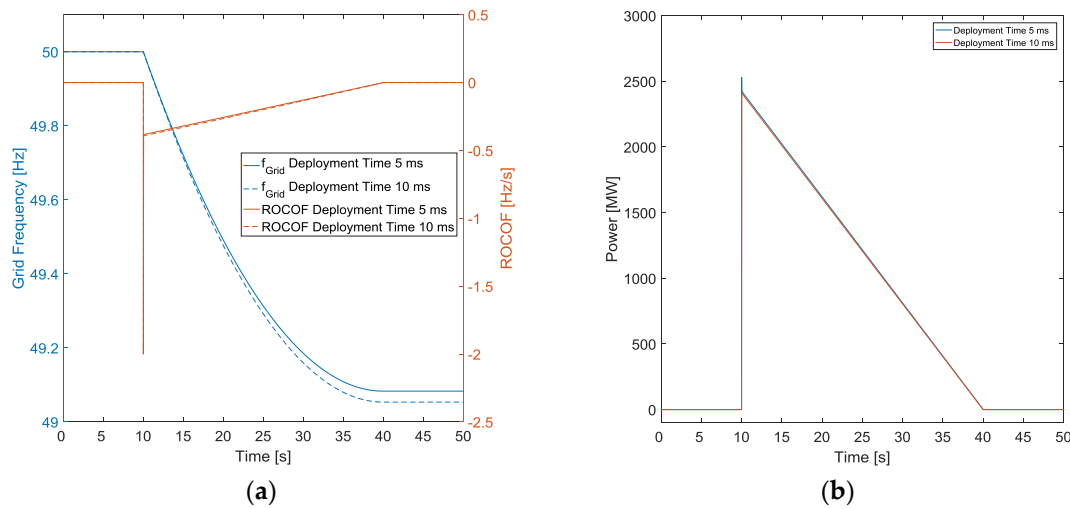
Figure 3. Grid frequency, ROCOF (**a**) and P_{SI} (**b**) time traces of the ENTSO reference incident under the influence of synthetic inertia provided via storage units with a deployment time of 5 ms and a deployment time of 10 ms.
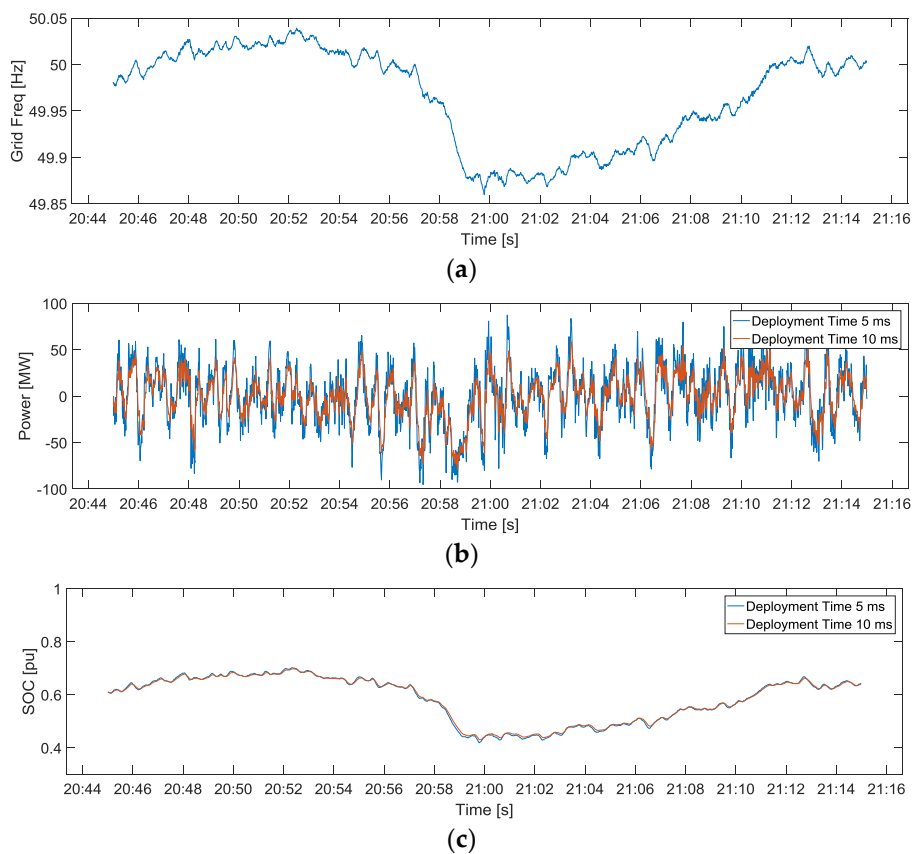
Figure 4. Modelled behaviour of storage units providing synthetic inertia. (**a**) shows the grid frequency of the ECSA on 3 March 2016; (**b**) shows the power feed in of storage units with a deployment time of 5 ms and a deployment time of 10 ms; and (**c**) shows the SOC of the assessed storage units.

5. Economical Evaluation of Power System Inertia

This section determines the economic costs involved for the provision of synthetic inertia by energy storage units. Therefore, different storage units are examined—three types of battery storages (li-ion, lead acid, and sodium sulphur), supercapacitors and flywheel storage systems. The storage systems are financially evaluated using the net present value (NPV) method. Currently, no market for system inertia exists. Consequently, only costs have been considered in the financial evaluation.

The NPV is calculated by taking the initial investment, I_t, and the cash flow, C_t, at time t. All cash flows are discounted with the target rate, r, which reflects the value of alternate usage of the investment as seen in Equation (8) [28]:

$$NPV = \sum_{t=0}^{T} \frac{I_t + C_t}{(1+r)^t} \tag{8}$$

The initial investment is the sum of the storage costs with respect to the needed power and capacity as well as for the costs for the PCS with respect to the power as listed in Table 1 [28–30]. The needed power and capacity are determined in the previous section. The cash flow consists of loan capital repayments, the interest payments and costs for operation and maintenance (O and M). These are represented in costs per year. The loan time of each investment is assumed to be three quarter of the life time of the energy storage unit and the interest rate is 7% [31]. Each storage unit has a unique life time. Hence, in order to achieve comparable results an examination time of 25 years is assumed. Once a storage technology reaches its expected lifetime, the same technology gets reinstalled. At the end of the examination time the remaining value of the system is being offset as a single revenue. The lifetime of a storage unit depends on a number of fixed charging/discharging cycles within a maximum given lifetime [32]. Due to present frequency characteristics in the ECSA full cycles are seldom achieved. Hence, the maximum lifetime is not affected by the number of charge/discharge cycles and the maximum given lifetime is used for calculations. The price level increases at a rate of 2% per annum.

It is common practice to compare different electricity generation technologies (conventional and renewables) using the levelised cost of electricity (LCOE) methodology [33–35]. Derived from the LCOE methodology, levelised cost of inertia (LCOI) is introduced, in order to introduce a parameter to compare different sources for the provision of synthetic inertia. Equation (9) displays how LCOI is calculated:

$$LCOI = \frac{\sum_{t=0}^{T} \frac{I_t + C_t}{(1+r)^t}}{\sum_{t=0}^{T} \frac{J_{SI}}{(1+r)^t}} \tag{9}$$

The LCOI represents the overall costs with respect to the amount of provided inertia in a certain period. It has been concluded in the third chapter, that neither power nor energy are suitable units for the provision of synthetic inertia. Likewise to the financial concept of PCR, the provision of synthetic inertia is compensated and not the actual utilisation similar to the recently proposed meter-based method [36]. In this case it is assumed that the tender period is one year. Hence, the unit is €/(kg· m^2· year).

Table 1 gives an overview of the used data. The information have been taken from [25,29,30]. The prices for PCSs are specified for an application at the distribution system [29]. As labelled, the upper rows of the table indicate the data used for the calculations; the lower rows contain the results.

The lowest NPV, i.e., the least cost solution, for the provision of synthetic inertia is found to be the flywheel storage unit with NPV = €7.19 billion. It is followed by supercapacitors with NPV = €8.24 billion and li-ion batteries with NPV = €8.82 billion. Also in terms of LCOI, the flywheel system is the cheapest technology with LCOI = 167.64 €/(kg· m^2· year), followed by supercapacitors and li-ion batteries.

Table 1. Data and result table for the economic evaluation (based on [25,29,30]).

		Lead Acid	Li-Ion	Sodium Sulphur	Super Capacitor	Flywheel
Data Used for Calculation						
Cost Storage (Power)	(€/kW)	175	175	175	15	300
Cost PCS	(€/kW)	155	155	155	270	-
Cost Storage (Capacity)	(€/kWh)	175	550	600	15,000	1,000
O & M	(€/(kW·years))	11.50	9	18	4	4
Life time	years	10	20	20	12	20
Results						
NPV	(billion€)	11.79	8.82	10.61	8.24	7.19
LCOI	(€/(kg·m^2·year))	275.22	205.64	247.48	192.12	167.64

6. Conclusions and Future Research

This paper emphasises the importance of system inertia and the necessity of synthetic inertia for future frequency control. Synchronous generators of conventional power plants are being replaced by RES equipped with frequency converters, which do not provide system inertia. System inertia is essential for frequency control as it limits the ROCOF and provides PCR with time to adjust its power.

In a future power system insufficient system inertia has to be compensated by the provision of synthetic inertia. Synthetic inertia is the behaviour of frequency converter equipped generation or storage units, emulating synchronous generators. This can be achieved by appropriate control strategies. The yet free of charge service inertia, has to be traded in a future power system due to additional costs for the provision of synthetic inertia. A suitable trading unit is inertia (kg·m^2), as it represents the behaviour of present synchronous machines regarding system inertia. Levelised cost of inertia (€/kg·m^2) is a suitable comparison parameter for the provision of inertia by different sources.

Different energy storage units are evaluated regarding the emulation of system inertia. As incomes for the provision are not yet assessable, only costs are considered. The NPV concludes, that the provision of synthetic inertia by a flywheel storage system is the least costly solution with overall system costs of €8.23 billion for the evaluated examination period. Adapting the newly introduced LCOI and assuming a tender period of one year leads to costs of 167.64 €/(kg·m^2·year) for the provision using flywheel storage systems.

A future market for inertia will presumably reduce costs for the provision of system and synthetic inertia. RES are capable of providing synthetic inertia, too [5,6,29,37]. Future research will indicate whether these sources are capable of providing synthetic inertia at lower costs then the evaluated storage systems in this work. Currently, a research project is conducted at the Wind Energy Technology Institute, in cooperation with the wind turbine manufacturer Suzlon Energy. In this project the provision of synthetic inertia with wind turbines is assessed in terms of performance and in terms of consequences for the mechanical loads, hence, costs. It has to be acknowledged though that RES generators, like wind turbines, cannot provide synthetic inertia permanently, but only at times of operation. Hence, alternative technologies, which are independent from the availability of prime energy, are inevitable.

Author Contributions: Henning Thiesen performed the research and wrote the paper. Clemens Jauch proposed the research idea, supervised the research and contributed with valuable discussions and scientific advice. Arne Gloe wrote Section 3, reviewed the paper and supported the research.

Conflicts of Interest: The authors declare no conflict of interest.

References and Notes

1. European Commission. *A Policy Framework for Climate and Energy in the Period from 2020 to 2030*; European Commission: Brussels, Belgium, 2014.

2. German Parliament. EEG: Erneuerbare-Energien-Gesetz vom 21. Juli 2014 (BGBl. I S. 1066), vierte Änderung. BGBl. I 2015 S. 2498, 2515. (In German)

3. Ulbig, A.; Borsche, T.S.; Andersson, G. Impact of low rotational inertia on power system stability and operation. In Proceedings of the 19th World Congress of the Internatonal Federation of Automatic Control (IFAC 2014), Capetown, South Africa, 24–29 August 2014.

4. Díaz-González, F.; Hau, M.; Sumper, A.; Gomis-Bellmunt, O. Participation of wind power plants in system frequency control: Review of grid code requirements and control methods. *Renew. Sustain. Energy Rev.* **2014**, *34*, 551–564. [CrossRef]

5. Keung, P.-K.; Li, P.; Banakar, H.; Ooi, B.T. Kinetic energy of wind-turbine generators for system frequency support. *IEEE Trans. Power Syst.* **2009**, *24*, 279–287. [CrossRef]

6. Gonzalez-Longatt, F.M. Impact of emulated inertia from wind power on under-frequency protection schemes of future power systems. *J. Mod. Power Syst. Clean Energy* **2016**, *4*, 211–218. [CrossRef]

7. Erlich, I.; Wilch, M. Primary frequency control by wind turbines. In Proceedings of the 2010 IEEE Power and Energy Society General Meeting, Minneapolis, MN, USA, 25–29 July 2010; pp. 1–8.

8. Cao, X.; Abdulhadi, I.; Emhemed, A.; Booth, C.; Burt, G. Evaluation of the impact of variable system inertia on the performance of frequency based protection. In Proceedings of the 12th IET International Conference on Developments in Power System Protection (DPSP 2014), Copenhagen, Denmark, 31 March–3 April 2014; pp. 1–6.

9. Wang, Y.; Silva, V.; Winckels, A. Impact of high penetration of wind and PV generation on frequency dynamics in the continental Europe interconnected system. In Proceedings of the 13th Wind Integration Workshop 2014, Berlin, Germany, 11–13 November 2014.

10. Rehtanz, C.; Greve, M.; Häger, U.; Hilbrich, D.; Kippelt, S.; Kubis, A.; Liebenau, V.; Noll, T.; Rüberg, T.; Schwippe, J.; et al. *Dena Ancillary Services Study 2030. Security and Reliability of a Power Supply with a High Percentage of Renewable Energy*; Deutsche Energie-Agentur GmbH (Dena)—German Energy Agency: Berlin, Germany, 2014.

11. UCTE. *Final Report of the Investigation Committee on the 28 September 2003 Blackout in Italy*; Union for the Coordination of the Transmission of Electricity (UCTE): Brussels, Belgium, 2004.

12. UCTE. *Final Report—System Disturbance on 4 November 2006*; Union for the Coordination of the Transmission of Electricity (UCTE): Brussels, Belgium, 2007.

13. Leahy, E.R.; Tol, S.J. An estimate of the value of lost load for Ireland. *Energy Policy* **2011**, *39*, 1514–1520. [CrossRef]

14. De Nooij, M.; Koopmans, C.; Bijvoet, C. The value of supply security: The costs of power interruptions: Economic input for damage reduction and investment in networks. *Energy Econ.* **2007**, *29*, 277–295. [CrossRef]

15. Growitsch, C.; Malischek, R.; Nick, S.; Wetzel, H. *The Costs of Power Interruptions in Germany—An Assessment in the Light of the Energiewende*; EWI Working Paper, 13/07; Institute of Energy Economics at the University of Cologne (EWI): Köln, Germany, 2013.

16. Pelletier, M.A.; Phethean, M.E.; Nutt, S. Grid code requirements for artificial inertia control systems in the New Zealand power system. In Proceedings of the 2012 IEEE Power and Energy Society General Meeting, San Diego, CA, USA, 22–26 July 2012; pp. 1–7.

17. Kundur, P.; Balu, N.J.; Lauby, M.G. *Power System Stability and Control*; McGraw-Hill: Alto, California, USA, 1994.

18. ENTSO-E. *Continental Europe Operation Handbook—P1—Policy 1: Load-Frequency Control and Performance*; ENTSO-E: Brussels, Belgium, 2009.

19. ENTSO-E. *Continental Europe Operation Handbook—Appendix 1. Load-Frequency Control and Performance*; ENTSO-E: Brussels, Belgium, 2004.

20. ENTSO-E. *ENTSO-E Draft Network Code for Requirements for Grid Connection Applicable to All Generators*; ENTSO-E: Brussels, Belgium, 2012.

21. ENTSO-E. *ENTSO-E Network Code for Requirements for Grid Connection Applicable to All Generators*; ENTSO-E: Brussels, Belgium, 2013.

22. 50Hertz GmbH, Amprion GmbH, TransnetBW GmbH, TenneT TSO GmbH. *Auswirkungen Reduzierter Schwungmasse Auf einen Stabilen Netzbetrieb*; 50Hertz Transmission GmbH: Berlin, Germany, 2014.

23. ENTSO-E. *Continental Europe Operation Handbook—P5—Policy 5: Emergency Operations*; ENTSO-E: Brussels, Belgium, 2010.

24. ENTSO-E. Data View. Actual Generation per Production Type, 2016. Available online: https://transparency.entsoe.eu/generation/r2/actualGenerationPerGenerationUnit/show (accessed on 3 April 2016).

25. Fuchs, G.; Luny, B.; Leuthold, M.; Sauer, D.U. *Technology Overview on Electricity Storage—Overview on the Potential and on the Deployment Perspectives of Electricity Storage Technologies*; ISEA—Institut für Stromrichtertechnik und Elektrische Antriebe, RWTH Aachen: Aachen, Germany, 2012.

26. Ørum, E.; Kuivaniemi, M.; Laasonen, M.; Bruseth, A.I.; Jansson, E.A.; Danell, A.; Elkington, K.; Modig, N. *Nordic Report—Future System Inertia*; ENTSO-E Report; ENTSO-E: Brussels, Belgium, 2015.

27. Gabash, A.; Li, P. On variable reverse power flow-part i: active-reactive optimal power flow with reactive power of wind stations. *Energies* **2016**, *9*, 121. [CrossRef]

28. Levy, H.; Sarnat, M. *Capital Investment and Financial Decisions*; Prentice-Hall: Essex, UK, 1986.

29. Schoenung, S.M.; Hassenzahl, W.V. *Long- vs. Short-Term Energy Storage Technologies Analysis—A Life-Cycle Cost Study—A Study for the DOE Energy Storage Systems Program*; Sandia National Laboratories: Albuquerque, NM, USA, 2003.

30. Leahy, M.J.; Connolly, D.; Buckley, D.N. *Wind Power Generation and Wind Turbine Design*; WIT Press: Southampton, UK, 2010.

31. Böttcher, J. *Finanzierung von Erneuerbare-Energien-Vorhaben*; De Gruyter: Oldenburg, Germany, 2009.

32. Gabash, A.; Li, P. Flexible optimal operation of battery storage systems for energy supply networks. *IEEE Trans. Power Syst.* **2013**, *28*, 2788–2797. [CrossRef]

33. Kost, C.; Mayer, J.N.; Thomsen, J.; Hartmann, N.; Senkpiel, C.; Philipps, S.; Nold, S.; Lude, S.; Saad, N.; Schlegl, T. *Levelized Cost of Electricity—Renewable Energy Technologies*; Fraunhofer Institute for Solar Energy System (ISE): Freiburg, Germany, 2013.

34. Ouyang, X.; Lin, B. Levelized cost of electricity (LCOE) of renewable energies and required subsidies in China. *Energy Policy* **2014**, *70*, 64–73. [CrossRef]

35. Branker, K.; Pathak, M.J.M.; Pearce, J.M. A review of solar photovoltaic levelized cost of electricity. *Renew. Sustain. Energy Rev.* **2011**, *15*, 4470–4482. [CrossRef]

36. Gabash, A. Flexible Optimal Operations of Energy Supply Networks with Renewable Energy Generation and Battery Storage. Ph.D. Thesis, Technischen Universität Ilmenau, Illmenau, Germany, 2013.

37. Zarina, P.P.; Mishra, S.; Sekhar, P.C. Deriving inertial response from a non-inertial PV system for frequency regulation. In Proceedings of the 2012 IEEE International Conference on Power Electronics, Drives and Energy Systems, Bengaluru, India, 16–19 December 2012.

Publication 2

Continuous provision of synthetic inertia with wind turbines: implications for the wind turbine and for the grid

Continuous provision of synthetic inertia with wind turbines: implications for the wind turbine and for the grid

Arne Gloe[1] ✉, Clemens Jauch[1], Bogdan Craciun[2], Jörg Winkelmann[2]

[1]Wind Energy Technology Institute, Flensburg University of Applied Sciences, Flensburg, Germany
[2]Department for Innovation and Strategic Research, SUZLON Energy Ltd, Rostock, Germany
✉ E-mail: arne.gloe@hs-flensburg.de

Abstract: In future power systems with little system inertia, grid operators will require the provision of synthetic inertia (SI) from renewable energy sources. Unlike today, grid operators may require continuous provision of SI. This can lead to an unwanted disconnection of wind turbine generators (WTGs) from the grid, and has the potential to cause a significant decrease of the energy yield and financial losses for the turbine operator. In order to avoid such situations a controller is proposed, which interprets the grid codes to the benefit of all parties involved. This can be achieved by a variable inertia constant, which changes with the operating point of the WTG. In this study, the behaviour of the variable inertia constant controller is described, assessed and verified with time domain simulations.

1 Introduction

Modern power systems with high penetration of inverter-based renewables are bound to exhibit little system inertia. In order to avoid unfavourable excursions of the grid frequency and high rates of change of frequency (ROCOFs), system operators will require the provision of synthetic inertia from renewables. This can be achieved by adjusting the power output depending on the measured ROCOF. Already today, some grid codes require the provision of synthetic inertia (SI) or some kind of fast frequency response during major frequency disturbances. The existing requirements are typically tailored to the system operator's specific needs and their individual control objectives. In other grids, like the Indian grid, frequency support by wind turbine generator (WTG) is currently under discussion [1]. Existing and proposed requirements are often vague when defining the exact terms for the provision of SI. This might lead to unwanted disconnection of WTGs, which contradicts the interest of the grid operator that SI is actually provided when needed. When the system inertia decreases further, SI might need to be provided reliably by WTGs at all operating points [2, 3].

This paper focuses on different control strategies for the continuous provision of SI. The controllers are tested with time domain simulations and real-time traces from measurements of the Indian grid frequency. For the controller design the grid codes analysed in Section 2 are interpreted such that unwanted behaviour of WTGs during SI provision is avoided. The controller is also tested in field tests and its effects on the WTG loads are estimated.

This work is structured as follows: In the Section 2, publications of grid operators are analysed and the requirements for WTGs are adapted for the provision of continuous SI. Based on these results, two control strategies are developed in Section 3 and the effect on the aerodynamics is discussed briefly. In Section 4, the simulation results in terms of controller performance and quantification of energy losses are shown. The last section presents the conclusions and indicates future work.

2 Requirements for synthetic inertia in grid codes

Some grid operators have been requiring the provision of SI by WTGs for a couple of years. Especially Hydro Québec TransÉnergie has well-documented experience with such requirement since they introduced it in 2005 [2].

For the current paper, various grid codes and publications of grid operators are analysed with respect to requirements for the provision of SI. The comparison shows a wide range how grid operators define the provision of SI. Three different types of requirements can be distinguished:

- Increase of the power output depending on the ROCOF. It is typically activated once the ROCOF exceeds a threshold. The power increase must be held constant for a specific time or can be slowly reduced to zero [4].
- Increase of the power output once a threshold for the frequency is exceeded. The power increase must be held constant for a specific time or can be slowly reduced to zero. Such a requirement is comparable to primary frequency control and not to the inertial response of a synchronous generator (SG) [1, 5].
- Emulation of the behaviour of a SG. The power increase is typically defined by an inertia constant stated by grid operator [2, 3].

The requirements are often designed to the need of the specific grid for which the grid code is drafted [6]. Furthermore, the SI requirements are often designed to handle extreme events and therefore are not suitable for continuous provision of SI which is studied in this paper. The only exception is the emulation of the behaviour of a SG, which can be applied in continuous operation. The behaviour of a SG is described by (1). The grid operator demands an inertia constant H_{dem} which must be emulated by renewables. This concept is called fixed H control in the rest of this paper.

$$P_{\text{SI, fixed } H} = -2 \cdot H_{\text{dem}} \cdot P_{\text{rated}} \cdot \frac{\text{ROCOF}}{f_{\text{grid}}} \quad (1)$$

Another problem with many existing grid codes is the lack of information, which would be needed for a clear interpretation of the stipulated requirements. This problem was recently addressed by European Network of Transmission System Operators for Electricity (ENTSO-E) [7]. In order to clearly define the provision of SI as given in (1) at least the following information is needed:

- Magnitude of required inertia constant H_{dem},

- Minimum measurement frequency and accuracy for the grid frequency f_{grid}. This information is particularly important as the ROCOF is used to calculate the power increase.
- Allowed delay time for the provision of SI,
- Potential deadbands for ROCOF and f_{grid}.

While the lack of information can be problematic during the development of a SI controller, it also leaves room for interpretation. The provision of SI typically causes a conflict of interests between the grid operator, who needs a reliable provision of SI to stabilise the grid frequency, and the WTG operator, who aims to maximise the energy yield of the WTG.

A common strategy for the provision of SI with WTGs is to change the rotational speed of the rotor. There is a variety of publications from different WTG manufacturer describing such a control strategy and the WTG behaviour during frequency response (e.g. [8, 9]). Furthermore, a comparison of different WTGs to a real frequency event can be found in a publication by Hydro Québec [6]. A change of the kinetic energy stored in the rotation of the WTG allows temporarily increasing the generated electrical power above the power in the wind. As a consequence, WTGs might run at non-optimal rotational speeds, which affects the aerodynamic power [10]. Drastic requirements for the provision of SI in combination with large ROCOFs can even lead to disconnection of WTGs from the grid if the rotational speed drops too much.

The provision of SI obviously has a negative impact on the WTG operator's interest to maximise the energy yield. A temporary disconnection of WTGs is also unfavourable for grid operators as it leads to the loss of generation during a grid disturbance. The SI provision requirements in the grid codes have to be interpreted in such a way that the interests of grid operators and WTG operators can be fulfilled.

A grid operator needs to maintain a minimum inertia constant in their grid in order to be able to control the grid frequency. In case WTGs are able to emulate the behaviour of SGs correctly, the needed inertia can either be provided by natural inertia of synchronously connected units or by WTGs with SI capabilities. The inertia of SGs is described by the inertia constant H and is typically in the range of 2–10 s [11]. When SGs are disconnected, their inertia contribution to the system is lost and has to be replaced by turbines providing SI. As long as the overall SI provided by WTGs is sufficient it is not important for the grid whether some WTGs provide large amounts of SI or many WTGs provide small amounts. However, it can make a huge difference for the WTGs as the operating point highly affects the capability of a WTG to provide SI.

Not all WTGs in a grid are in the same operating point at the same time. Grid operators currently consider this by defining a power limit below which WTGs do not have to provide SI [4, 5]. However, a lower limit for a reliable provision of SI strongly depends on the power vs. speed characteristic, the aerodynamics of the WTG and also on the available wind during and shortly after a frequency event. Hence, such a power limit must either be set to a high value (i.e. loosing much of the WTGs potential to provide SI) or it does not guarantee the provision of SI in all wind conditions. This problem can be overcome by the control method proposed in the following section.

3 Control strategies for inertia provision

A requirement for the continuous provision of SI should make sure that WTGs remain connected to the grid during frequency support while making sure that the WTG provides as much SI as possible in its current operating point. For variable speed WTGs this can be achieved by modifying (1) such that the inertia constant changes with the operating point as shown below:

$$P_{SI, varH} = -2 \cdot H_{var} \cdot P_{rated} \cdot \frac{ROCOF}{f_{grid}} \qquad (2)$$

As mentioned before, the kinetic energy stored in rotating masses of the WTG drive train is usually used to provide additional power for SI. Also the rotational speed of the WTG is crucial for effective
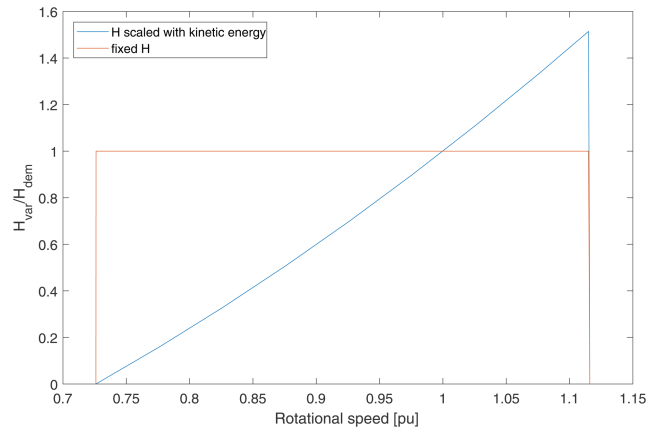
Fig. 1 *Comparison of the normalised variable and fixed inertia constants over the operating range of the WTG (best viewed in colour online)*

power production. Hence, it is reasonable to scale the variable inertia constant H_{var} with the kinetic energy as described in (3). The difference between the kinetic energy at the current speed (ω_{gen}) and the kinetic energy at cut-in speed (ω_{cut-in}) is available for SI without risking to disconnect the WTG from the grid. H_{var} is normalised such that the inertia constant H_{dem} defined by the grid operator is provided at rated speed (ω_{rated}). The change of the normalised variable inertia constant over the operating range is shown in Fig. 1.

$$\frac{H_{var}}{H_{dem}} = \frac{0.5 \cdot J_{WTG} \cdot (\omega_{gen}^2 - \omega_{cut-in}^2)}{0.5 \cdot J_{WTG} \cdot (\omega_{rated}^2 - \omega_{cut-in}^2)} \qquad (3)$$

Equation (2) and (3) ensure that every WTG contributes as much inertia as possible in the moment of a frequency event. The grid operator can be sure that sufficient inertia is present in their grid either provided by WTGs with high operating points, or by SG in case of a low wind situation. Thus, the negative effect on the energy yield is reduced as the full SI only has to be provided when there is sufficient wind to increase the power output and shutdowns of the WTGs are avoided. The controller concept presented in (2) and (3) is referred to as variable H controller in the rest of the paper.

Depending on the sign of the ROCOF WTGs either need to increase or decrease their power output. However, a decrease of the power output can easily be achieved, either by pitching the blades or running the WTGs at a non-optimal rotational speed. Therefore, the focus in this section is on power increases.

Control strategies for the provision of SI have been present in the literature for many years (e.g. [12, 13]). All have in common that the additional power needs to be provided from some kind of energy storage. There are three different options to provide the additional power:

- Throttling WTGs to release additional power in case of a frequency event. As major frequency events cannot be predicted, throttling the WTGs is not an option for continuous provision of SI. In addition to the high losses for the turbine operator, it is also very costly from a systems perspective.
- Using external energy storage in the WTG or the wind farm to provide additional power. If such a system is only used for the provision of SI, it might be much more expensive than the changing the controls of the WTG (see chapter 4.4 and [14]).
- Alternating the rotational speed of the WTG to provide the additional power for SI by tapping the kinetic energy stored in the drive train. This option does not require additional hardware. The implementation in the control system and the effects on the WTG are discussed in this section.

When the kinetic energy in the WTG rotation is used for the provision of SI according to (2), the power setpoint from the power vs. speed characteristic needs to be adjusted. Fig. 2 shows the
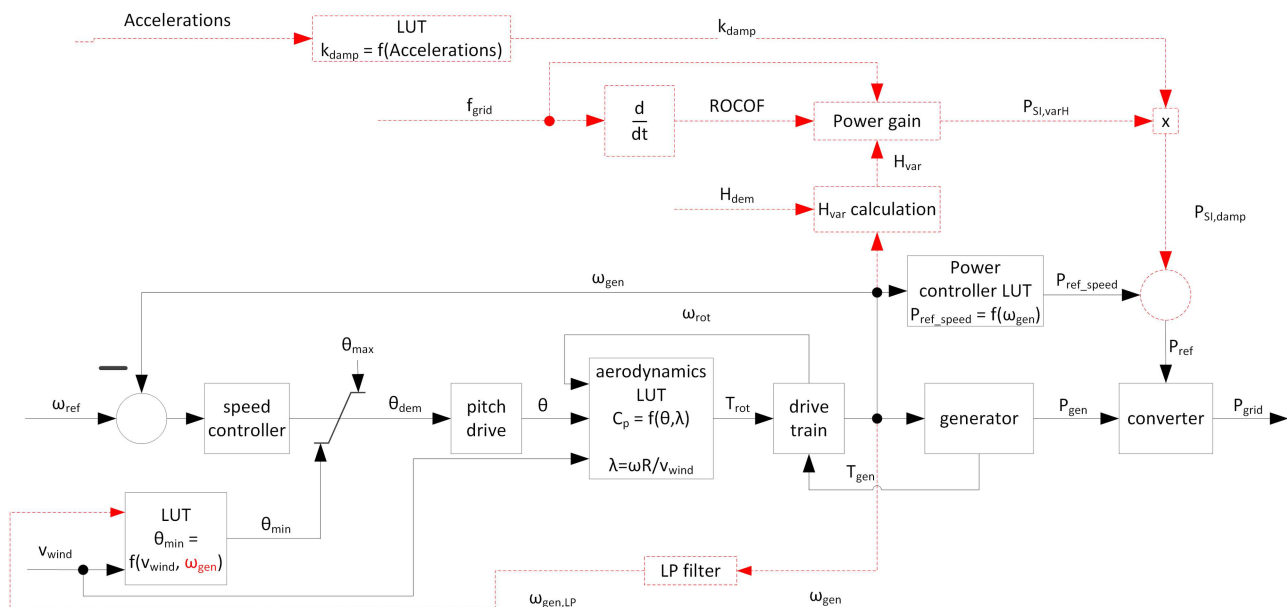
Fig. 2 *Simplified control circle of a variable speed WTG with SI control (red dashed lines) (best viewed in colour online)*
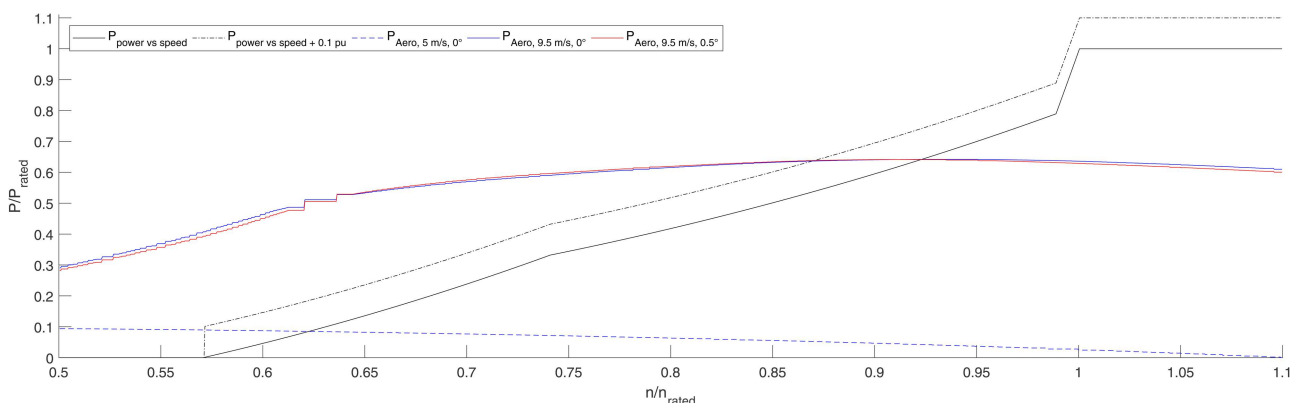

Fig. 3 *Power vs. speed characteristic and aerodynamic power (best viewed in colour online)*

simplified control circuit of a variable speed WTG. The elements which are added for the SI are shown as red dashed lines.

In addition to the power calculations it is proposed to monitor accelerations of some mechanical components of the WTG. If these accelerations exceed critical values it is assumed that they are caused by power variations from SI operation. Consequently, the SI contribution is dampened in order to protect the WTG. Furthermore, the aerodynamic losses are reduced by adding a rotational speed dimension to the minimum pitch angle table.

The aerodynamics are explained using data from [15, 16]. Figs. 3 and 4 show the power vs. speed characteristic and the aerodynamic power for two wind speeds and two pitch angles. Furthermore, the dashed–dotted black line indicates a constant power increase for SI of 0.1 pu over the whole speed range (SI calculation according to (1)). These figures and the explanations are meant to give a basic description of the aerodynamics during the provision of SI. Although, dynamic stall and dynamic inflow might have a strong influence on the aerodynamics these effects are neglected in this paper.

At part load the provision of SI will lead to a reduction of the rotational speed. It is assumed that the WTG is in steady state before the start of the frequency event (point B1 in Fig. 4*b* and that the wind speed is constant during the event.

The aerodynamic power is equal to the electrical power. When additional power is requested the electrical power is higher than the aerodynamic power (point B2 in Fig. 4*b*). The rotational speed decreases. As the WTG leaves its optimal aerodynamic operating point for this wind speed, the aerodynamic power decreases along with a decrease of the rotational speed (see blue curve in Fig. 4*b*). As the rotational speed decreases the pitch angle is slightly increased to reduce the aerodynamic losses. At the same time the

electrical power decreases as the power setpoint from power vs. speed characteristic drops. After a short time the WTG will reach a new equilibrium (point B3 in Fig. 4*b*). If the power increase from SI is offset by a power reduction from the power vs. speed characteristic, this new steady-state power is below the initial electrical power. The exact behaviour of the WTG largely depends on the aerodynamic design of the blades which determines the aerodynamic power vs. speed curves shown in Figs. 3 and 4.

In part load operation, the speed reduction can cause a disconnection of the WTG from the grid if the rotational speed falls below the cut-in speed (see Fig. 4*a*). The increase of the electrical power (jump from point A1 to A2 in Fig. 4*a*) causes a decrease of the rotational speed. At cut-in speed the electrical power (point A3 in Fig. 4*a*) is still above the aerodynamic power (point A4 in Fig. 4*a*). Hence, no new equilibrium is reached but the WTG is disconnected from the grid. The aerodynamic power increases in this example as the WTG is above the optimal tip-speed ratio before the start of the SI provision. The risk for a stop of the WTG highly depends on the initial operating point of the WTG, the requested power increase, the shape of the power vs. speed characteristic and the prevailing wind conditions. By adjusting the inertia constant to the operating point the risk of disconnecting the WTG from the grid is highly reduced.

In any of these cases, SI leads to suboptimal aerodynamic operating points. During part load operation the WTG tries to keep the inflow at the blades at a constant angle of attack (AoA). The speed decrease causes a higher AoA, which reduces the aerodynamic efficiency. This effect can be reduced by pitching the blades slightly towards feather position. However, the effect of a certain power increase on the rotational speed in turbulent wind is not known in advance. The pitch angle should not be altered
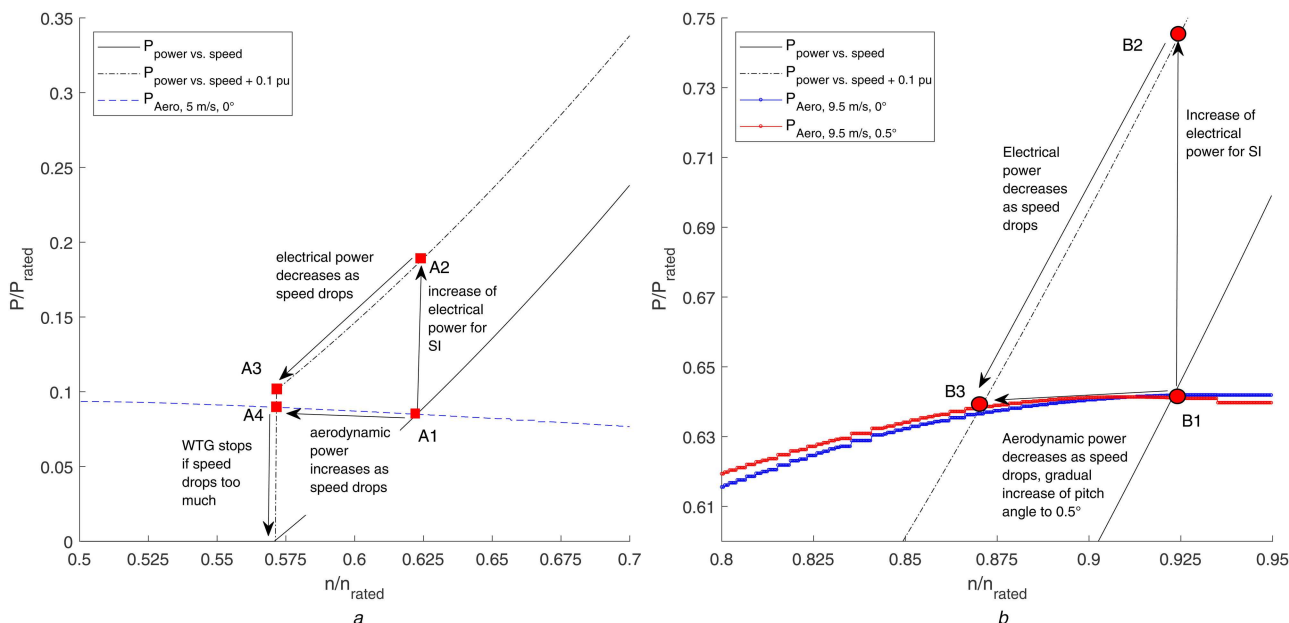
Fig. 4 *Excerpt from Fig. 3. Power vs. speed characteristic and aerodynamic power at lower part load (a) and medium part load (b) (best viewed in colour online)*

directly. Instead it is proposed to add a rotational speed dimension to the minimum pitch angle table (see Fig. 2). The optimal pitch angles for any combinations of wind speed and rotational speed can be derived with the aerodynamic tools during the design process of a WTG. In practice, such a two-dimensional minimum pitch angle requires reasonably accurate wind speed measurements.

The provision of SI can have strong effects on loads of some components of the WTG. As active power is used for SI, oscillations of the grid frequency may excite vibrations of WTG components. Most problematic are grid frequency oscillations with a frequency close to the eigenfrequency of a WTG component. As the drive train is affected directly by the changes of the electrical power, it is likely to be the most vulnerable component. Such excitations from SI can be limited by monitoring the accelerations or vibrations of critical components. Once critical thresholds are violated the magnitude of the $P_{SI,varH}$ is dampened (see Fig. 2). Thereby, the failure of a component caused by SI provision is unlikely while the WTG can provide the full SI during uncritical situations. Furthermore, unwanted interferences between the SI controller and other parts of the control system (e.g. drive train damper) can be minimised.

4 Controller tests with simulations

4.1 Used simulation model

The used simulation model focuses on the response of the WTG to the provision of SI. Measured and artificial time traces of grid frequency are used as input to the controller. Only the most relevant components of the model are introduced in this paper (see [17] for details). The parameters used in the model allow an adequate representation of a Suzlon DFIG WTG.

Each of the blades is modelled as two masses, one for each blade tip and one for each blade root. The two masses are connected with a spring damper system. The allowed degrees of freedom are translational motion in out-of-plane direction and rotation in in-plane direction. The aerodynamic forces are calculated with C_t and C_q look up tables individually for each blade. Therefore, the model can consider wind speed changes over the rotor plane. For each blade the thrust is split between the two masses with the majority acting on the blade tip masses, corresponding to the aerodynamic centre of gravity of the blade.

The shaft is represented by a spring and a damper connecting the low speed side inertia with the high speed side inertia. It allows one torsional degree of freedom representing the first torsional eigenfrequency of the shaft.

The behaviour of the generator and converter can sufficiently be approximated by a first-order lag (PT1 with a time constant of 40 ms) element as their time constants are much smaller than the time constants of the mechanical components.

The pitch system is modelled as depicted in Fig. 2 with a proportional–integral–derivative (PID) controller for the speed control and a PT1 element with a limitation on the slew rate representing the pitch drive.

4.2 Frequency measurements

The controller concepts are tested with different time traces of the grid frequency. For this purpose, frequency measurements from the Western Indian power system are analysed. The data was recorded following the IEC 61400 standard [18] with a state-of-the-art measurement system and a sample time of 20 ms. The measurements are classified in different categories. For each of the categories a likelihood of occurrence is estimated. These likelihoods of occurrence are needed for future load calculations.

In addition to the measured time traces the controller is also tested with the ENTSO-E reference case [19].

The demanded inertia constant H_{dem} is set to 6 s for all simulations shown in Section 4.

As the grid frequency is an input to the simulation model, interactions between the frequency measurements and the converter control during the provision of SI, which occurred in other studies (e.g. [20]), are not part of this study. It has been reported that the application of a virtual synchronous machine for the converter control reduces this problem and might be a control method for various grid integration problems [21].

4.3 Controller behaviour

The differences of the two controller and the risk of the stopping the WTG in unfavourable conditions as discussed in Section 3 are shown with the response of the controller to ENTSO-E reference case. Fig. 5 shows the inputs to the simulation. The behaviour of the controller is explained for three different wind scenarios. Such frequency events are one important aspect for controller design of the continuous provision of SI with WTG.

Fig. 6 shows the behaviour of the WTG at low wind speeds (average wind speed 5.4 m/s; average power 0.11 pu). With the fixed H controller the rotational speed of the WTG falls below the cut-in speed and the WTG is disconnected from the grid (see dotted lines in Fig. 6). The power increase only lasts for seconds. Due to the disconnection the power difference between fixed H controller and the WTG power without SI is negative for almost the entire
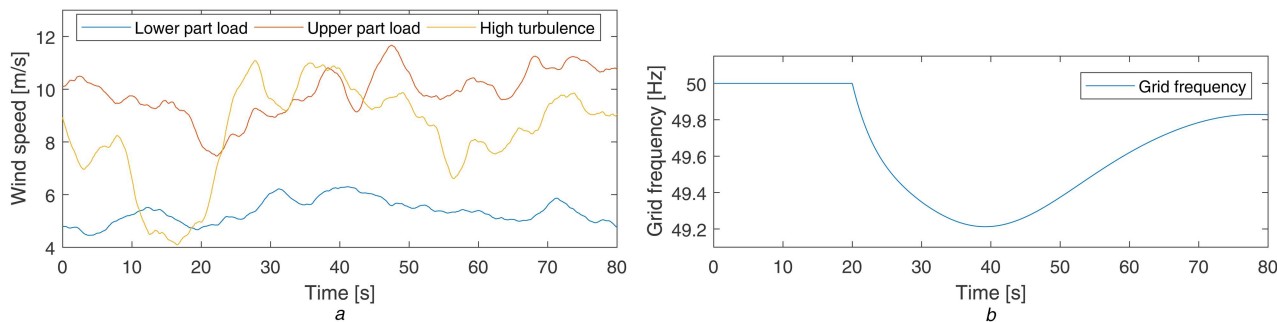
Fig. 5 *Time traces of wind speed (a) and grid frequency (b) for the discussed tests of the controller behaviour (best viewed in colour online)*
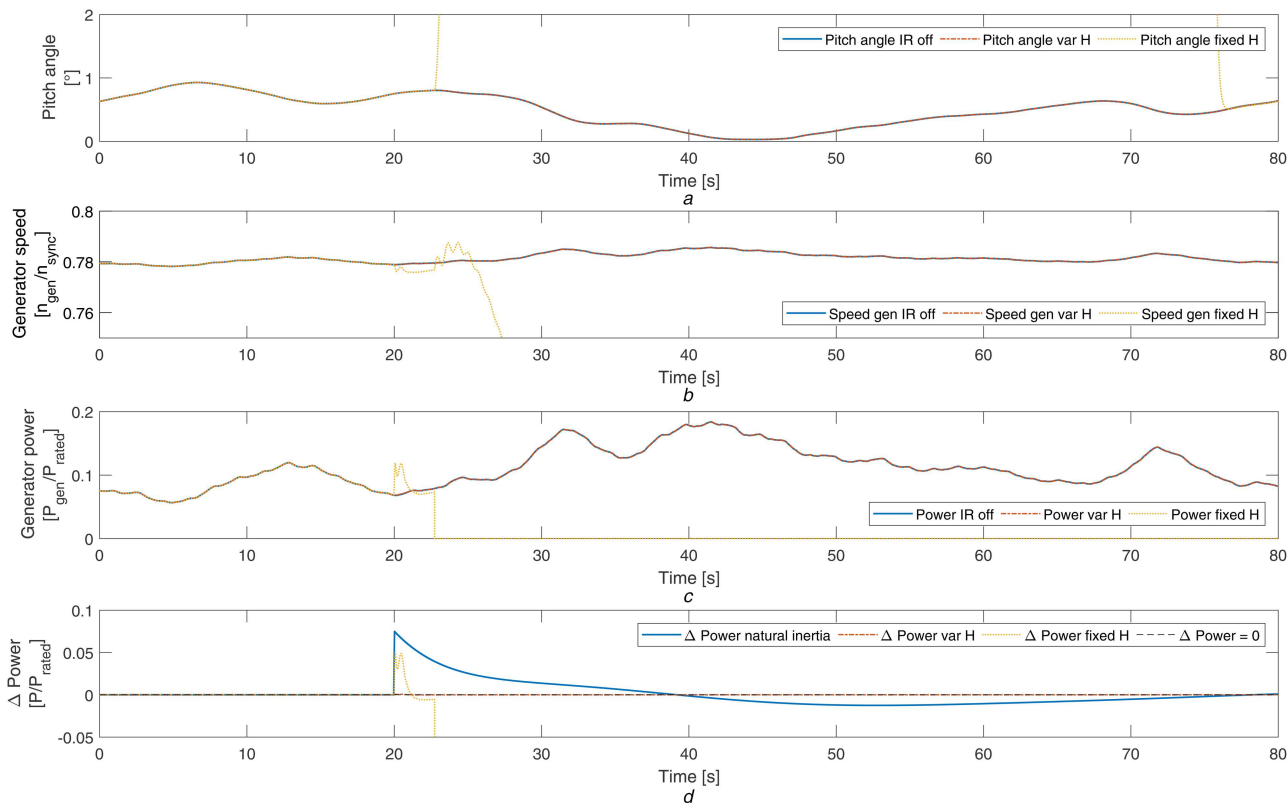
Fig. 6 *Simulation results for lower part load operation. Comparison of the pitch angle (a), the generator speed (b), and the generator power (b) for the variable H controller (dash–dotted lines), the fixed H controller (dotted lines), and with no SI (solid lines). In (d) the power differences are given for the variable H controller (dash–dotted line), fixed H controller (dotted line), and the theoretical value for a SG (solid line, according to (1)). Please note: the lines for the variable H controller are mostly covered by the lines of the disabled controller due to the very low power operating point (best viewed in colour online)*

simulation. The low rotational speed only allows a marginal increase of the power production with the variable H controller, which is not visible in Fig. 6. However, the WTG remains connected to the grid and continues to produce power as intended.

For higher wind speeds at upper part load operation (average wind speed 9.9 m/s; average power 0.69 pu) the differences between the fixed H controller and the variable H controller are much smaller (see Fig. 7). The initial power increase of both controllers is almost identical. The small power oscillations during the provision of SI are caused by drive train oscillations. In the recovery phase the power decrease for the variable H controller is smaller than for the fixed H controller as the WTG speed drops less. Hence, the average power of the variable H controller is higher than the one of the fixed H controller. As turbulent wind is used for the simulation, the pitch angle changes continuously for all three controller settings (SI off, variable H and fixed H, see Fig. 7a).

Both simulations shown in Figs. 6 and 7 are performed with relatively small turbulence intensities (TI = 0.08 and 0.12). However, even at good sites the wind can be much more turbulent. Fig. 8 shows the behaviour of the WTG in more turbulent, yet still realistic wind conditions (TI = 0.2, average wind speed 8.4 m/s, average power 0.53 pu). In this simulation a negative gust

coincides with the frequency event (see yellow line in Figs. 5a and b). Although the wind speed increases shortly after the event, the WTG is disconnected from the grid when the fixed H controller is used. The additional drop of the generator speed cannot be compensated. This simulation shows that the WTG may even disconnect at the relatively high average wind speed, if, due to the high turbulence, the frequency event happens at an unfavourable moment. The variable H controller enables the WTG to stay connected to the grid and provides a small amount of extra power for SI. This power increase causes a small decrease of the generator speed compared to the simulation with disabled SI controller. This speed difference compared to the WTG with disabled SI becomes visible at simulation time 29 s. At that moment the WTG enters a very steep part of the power vs. speed characteristic which amplifies the small speed decrease (0.001 pu) to a noticeable power decrease (0.015 pu). These speed differences also explain the power differences later in the simulation.

4.4 Energy losses

Although positive and negative power changes are equally likely when providing SI continuously, a reduction of the aerodynamic efficiency may negatively affect the power production. The
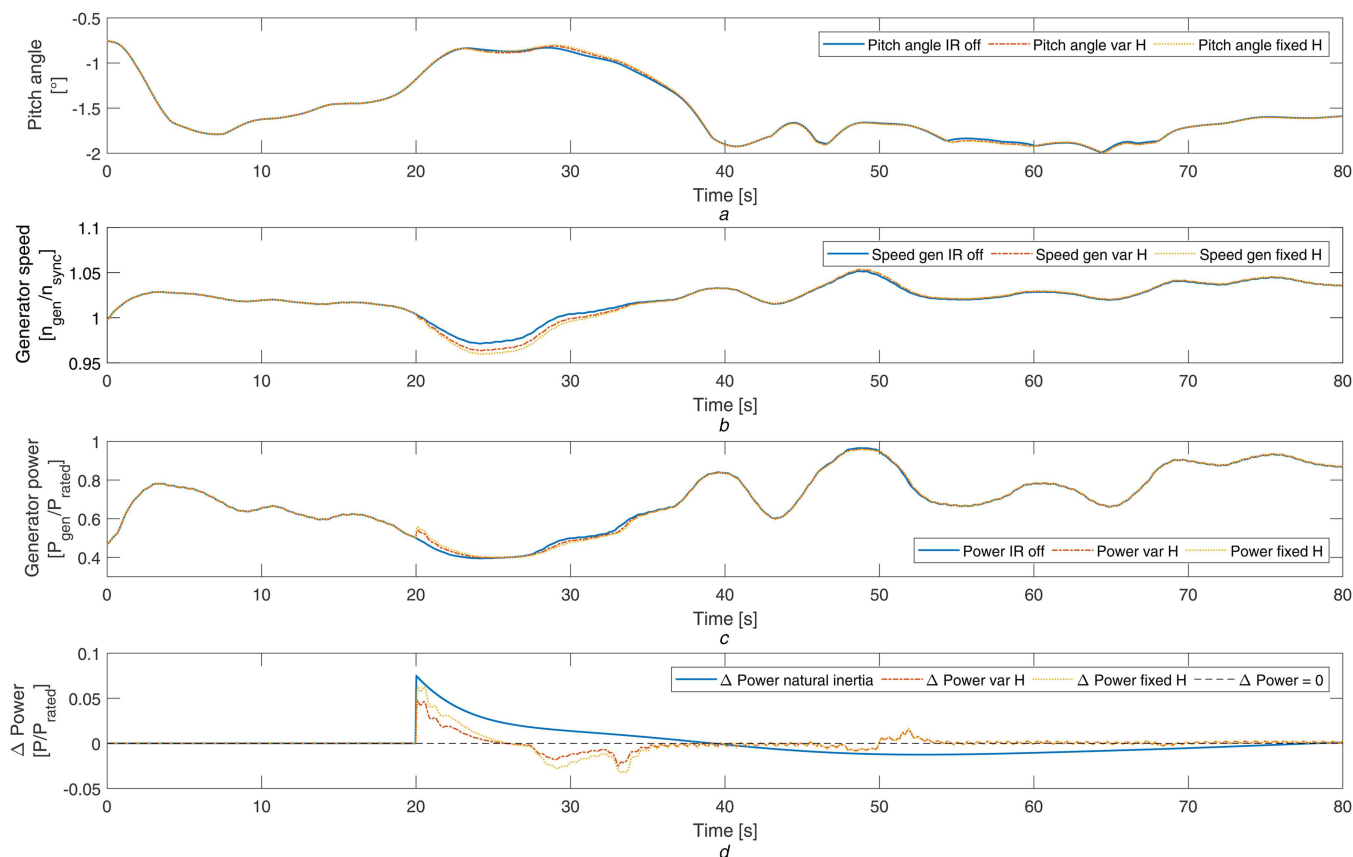
Fig. 7 *Simulation results for upper part load operation. Comparison of the pitch angle (a), the generator speed (b), and the generator power (b) for the variable H controller (dash–dotted lines), the fixed H controller (dotted lines), and with no SI (solid lines). In (d) the power differences are given for the variable H controller (dash–dotted line), fixed H controller (dotted line), and the theoretical value for a SG (solid line, according to (1)) (best viewed in colour online)*

continuous change of the generator power can prevent the WTG from reaching the optimal tip-speed ratio. This effect is quantified in a simulation over a full day. The power production of the WTG is compared for three different controller settings: variable H controller, constant H controller and disabled SI. The latter setting is called the reference case, in which the WTG only reacts to changes of the wind speed.

A measured time trace with a typical behaviour of the Indian grid frequency is chosen as input to the simulation. During the day, the frequency varies between 49.5 and 50.2 Hz (see Fig. 9b). The signal includes significant fast and slow changes of the measured frequency. The long simulation time ensures that these effects are fully considered.

The mentioned reduction of the aerodynamic efficiency is only relevant during part load operation and varies significantly with the operating point of WTG. Hence, a turbulent wind signal is chosen which varies between 4.5 and 11 m/s (TI = 0.1, see Fig. 9). The WTG must neither be disconnected from the grid due to SI nor reach full load operation as both situations would make a comparison of the aerodynamic efficiency meaningless. In order to facilitate the interpretation of the energy losses due to deterministic effects in the grid frequency (e.g. frequency drops in the early morning or increases in the evening) the mean wind speed is kept constant during the simulation.

Fig. 10 shows the results of the simulations. When compared to the reference case both SI controllers (variable H and the fixed H) produce ~0.3% less energy during the simulated 24 h. The energy difference between the variable H and the fixed H controller is negligible. Although power increases of up to 0.1 pu are requested during the simulation (see SG in Fig. 10b), the aerodynamic performance of the WTG is hardly affected for two reasons:

- High changes of the power (> 0.05 pu) are requested during times when the grid frequency oscillates with a high frequency (> 1 Hz). Hence, the additional power is needed for such a short time (several ms) that the rotational speed of the WTG is hardly

affected due to the inertia of the drive train. The histograms in Fig. 10b show how seldom these high power requests occur (<1.5% of the simulation time).

- The deep drops of the grid frequency, visible in Fig. 9b, are not caused by fast frequency events but by steady declines of the frequency over several minutes. Hence, the magnitude of the ROCOF and the corresponding requested power increase are very small. The rotational speed of the WTG is much more affected by the turbulent wind during these times than by the reaction to the declining grid frequency. Hence, there is no significant difference between the reference case and the simulations with an enabled controller during these times.

The simulations show that the continuous provision of SI has a minor effect on the energy yield for the chosen simulation inputs. In contrast to the expectations derived in chapter 3 there is no significant difference between the variable H and the constant H controller in terms of energy yield as the aerodynamic performance is hardly affected. However, different combinations of H_{dem}, ROCOF, wind speed, and operating point of the WTG are more likely to affect the aerodynamic performance. The interdependence of the inputs and the energy losses for the two control methods should be further elaborated in future research, where a large number of random input combinations should be simulated and evaluated. The current results show that the SI provision has little effect on a day with a typical frequency behaviour at the given wind speed. Severe frequency events, which may lead to a higher reduction of the aerodynamic performance, occur so seldom that they are not likely to decrease the energy production significantly. Therefore, like LVRT events today [22], such frequency events do not need to be considered when calculating the energy yield.

5 Conclusion

In this paper, a controller for the continuous provision of SI with WTGs is proposed, which interprets the grid codes to the
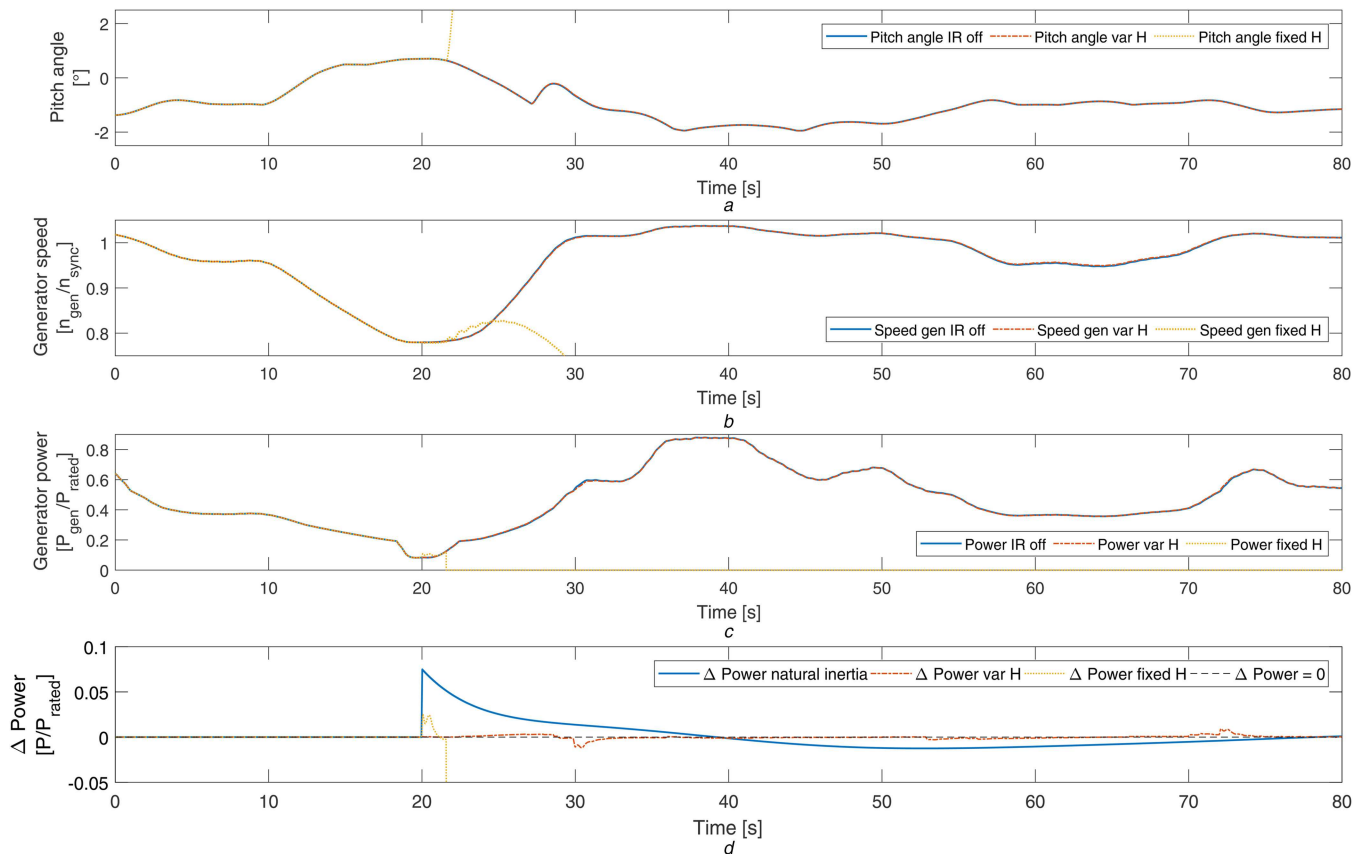
Fig. 8 *Simulation results for highly turbulent wind. Comparison of the pitch angle (a), the generator speed (b), and the generator power (b) for the variable H controller (dash–dotted lines), the fixed H controller (dotted lines), and with no SI (solid lines). In (d) the power differences are given for the variable H controller (dash–dotted line), fixed H controller (dotted line), and the theoretical value for a SG (solid line, according to (1)) (best viewed in colour online)*
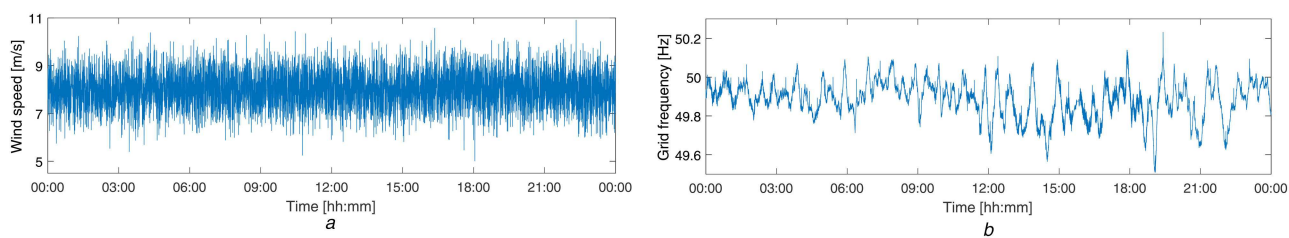
Fig. 9 *Time traces of wind speed (a) and grid frequency (b) for the quantification of the energy losses*
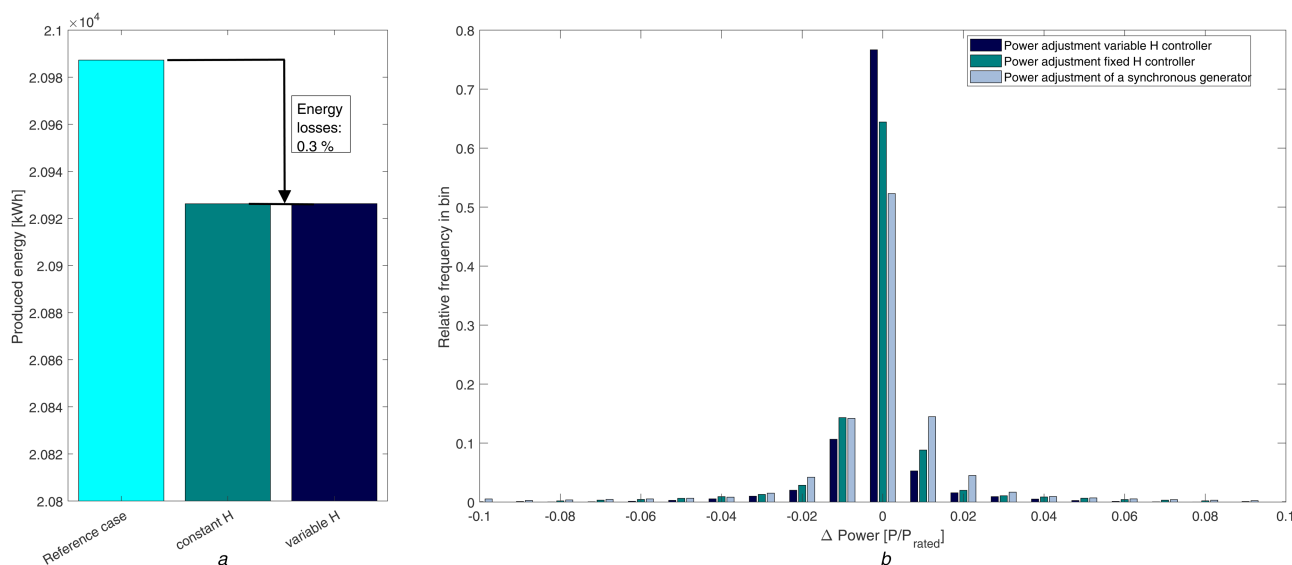
Fig. 10 *Simulation results for the quantification of the energy losses*
(a) Comparison of the energy production in the reference case (no SI), with constant *H* control, and variable *H* control, **(b)** Histogram of the power adjustments for SI of the fixed and variable H controller compared to the theoretical power adjustment of a SG

advantage of grid operators and WTG operators. The paper addresses the problem of SI at low wind speeds and in gusty wind conditions by scaling the inertia constant with the rotational speed of the WTG. This variable H controller allows a reliable provision of SI at all operating points of the WTG and thereby maximises the benefit for the grid operator.

Simulations show the behaviour of the controller under three different wind conditions. The simulation results prove the expected behaviour of the controller. An undesired disconnection of the WTG from the grid can be avoided when the variable *H* controller is used. Hence, the variable *H* controller also satisfies the needs of the operator of the WTG.

Simulations with a measured time trace of the Indian grid frequency shows that the effect of continuous provision of SI on the energy yield is negligible and therefore does not need to be considered in the calculation of the energy yield.

Future work is intended for analysing the impact of the SI controller on the loads of the WT with a more detailed simulation model and based on a detailed grid frequency analysis.

6 Acknowledgments

7 References

[1] Central Electricity Authority of India: 'Draft 2nd amendment in CEA (technical standards for connectivity to grid) regulations, 2007 as amended', New Dehli, 2016

[2] Hydro Québec TransÉnergie: 'Technical requirements for the connection of generation facilities to the hydro-québec transmission system. Supplementary requirements for wind generation', 2005. Available at http://www.hydroquebec.com/transenergie/fr/ commerce/pdf/eolienne_transport_en.pdf, accessed 12 December 2018

[3] Red electrica: 'Technical requirement for wind power and photovoltaic installations and any generating facilities whose technology does not consist on a synchronous generator directly connected to the grid', 2008. Available at https://www.aeeolica.org/uploads/documents/4535-separata-del-borrador-de-po122.pdf, accessed 12 December 2018

[4] Johnsen, A.: 'Grid code frequency response working group requirements for system inertia', 2013. Available at https://www.nationalgrideso.com/sites/eso/files/documents/16916-Meeting%2011%20-%20System%20Inertia%20Presentation.pdf, accessed 12 December 2018

[5] Hydro Québec TransÉnergie: 'Exigences techniques de raccordement de centrales au réseau de transport d'Hydro-québec', 2013. Available at http://publicsde.regie-energie.qc.ca/projets/208/DocPrj/R-3830-2012-B-0044-DemAmend-PieceRev-2013_11_29.pdf, accessed 12 December 2018

[6] Asmine, M., Langlois, C.-E., Aubut, N.: 'Inertial response from wind power plants during a frequency disturbance on the hydro-québec system – event analysis and validation'. Proc. 15th Int. Wind Integration Workshop, Vienna, 2016, pp. 406–413

[7] ENTSO-E: 'Need for synthetic inerta (si) for frequency regulation'. Technical Report, Brussels, Belgium, 2017. Available at https://consultations.entsoe.eu/system-development/entso-e-connection-codes-implementation-guidance-d-3/user_uploads/igd-need-for-synthetic-inertia.pdf, accessed 12 December 2018

[8] Godin, P., Fischer, M., Röttgers, H., *et al.*: 'Wind power plant level testing of inertial response with optimized recovery behavior'. Proc. 16th Int. Wind Integration Workshop, Berlin, 2017, pp. 436–441

[9] Ruttledge, L., Miller, N.W., O'Sullivan, J., *et al.*: 'Frequency response of power systems with variable speed wind turbines', *IEEE Trans. Sustain. Energy*, 2012, **3**, (4), pp. 683–691

[10] Fortmann, J.: 'Method for operating or controlling a wind turbine and method for providing primary control power by means of wind turbines'. U.S. Patent 7 528 496 B2, 5 May 2009

[11] Kundur, P.: '*Power system stability and control*' (McGraw-Hill Education, New York, 1994)

[12] Holdsworth, L., Ekanayake, J.B., Jenkins, N.: 'Power system frequency response from fixed speed and doubly fed induction generator-based wind turbines', *Wind Energy*, 2004, **7**, (1), pp. 21–35

[13] Morren, J., Pierik, J., Haan, S.W.H.D.: 'Inertial response of variable speed wind turbines', *Electr. Power Syst. Res.*, 2006, **76**, (11), pp. 980–987

[14] Thiesen, H., Viebeg, J., Gloe, A., *et al.*: 'The provision of synthetic inertia by wind turbine generators: an analysis of the energy yield and costs'. Proc. 16th Int. Wind Integration Workshop, Berlin, 2017, pp. 603–606

[15] Jonkman, S., Butterfield, S., Musial, W., *et al.*: 'Definition of a 5-mw reference wind turbine for offshore system development'. Technical Report NREL/TP-500-38060, National Renewable Energy Laboratory, Golden, Colorado, 2009. Available at http://www.nrel.gov/docs/fy09osti/38060.pdf, accessed 12 December 2018

[16] Marten, D., Wendler, J., Pechlivanoglou, G., *et al.*: 'QBlade: An open source tool for design and simulation of horizontal and vertical axis wind turbines', *Int. J. Emerg. Technol. Adv. Eng.*, 2013, **3**, pp. 264–269

[17] Jauch, C.: 'First eigenmode simulation model of a wind turbine'. Wind Energy Technology Institute, Flensburg, 2016. Available at https://www.researchgate.net/publication/312935476_First_Eigenmode_Simulation_Model_of_a_Wind_Turbine_-_for_Control_Algorithm_Design, accessed 12 December 2018

[18] Measurement and assessment of power quality characteristics of grid connected wind turbines IEC 61400-21, 2008

[19] ENTSO-E: 'P1 – policy 1 load-frequency control and performance', 2009. Available at https://www.entsoe.eu/fileadmin/user_upload/_library/publications/entsoe/Operation_Handbook/Policy_1_final.pdf, accessed 12 December 2018

[20] Duckwitz, D.: 'Performance of df/dt-based inertia control during emergency islanding'. Proc. 15th Int. Wind Integration Workshop, Vienna, 2016, pp. 659–663

[21] Roscoe, A.J., Yu, M., Dyśko, A., *et al.*: 'A VSM (virtual synchronous machine) convertor control model suitable for RMS studies for resolving system operator / owner challenges'. Proc. 15th Int. Wind Integration Workshop, Vienna, 2016, pp. 421–429

[22] Hau, E.: '*Wind turbines: fundamentals, technologies, application, economics*' (Springer, Berlin, 2013)

Publication 3

Influence of continuous provision of synthetic inertia on the mechanical loads of a wind turbine

A. Gloe, C. Jauch, B. Craciun, A. Zanter, and J. Winkelmann

Influence of Continuous Provision of Synthetic Inertia on the Mechanical Loads of a Wind Turbine

Arne Gloe [1],*, Clemens Jauch [1] , Bogdan Craciun [2], Arvid Zanter [3] and Jörg Winkelmann [2]

[1] Wind Energy Technology Institute, Flensburg University of Applied Sciences, 24943 Flensburg, Germany; clemens.jauch@hs-flensburg.de

[2] Innovation and Strategic Research, SUZLON Energy Ltd., 18057 Rostock, Germany; bogdan.craciun@suzlon.com (B.C.); joerg.winkelmann@suzlon.com (J.W.)

[3] Key Components, SUZLON Energy Ltd., 18057 Rostock, Germany; arvid.zanter@suzlon.com

* Correspondence: arne.gloe@hs-flensburg.de

Abstract: In many electrical grids, the share of renewable energy generation increases. As these generators are typically connected to the grid via inverters, the level of grid inertia decreases. Such grids may therefore suffer from high rates of change of frequency during power imbalances. Modern wind turbines can help in controlling the frequency in such grids by providing synthetic inertia. A controller to provide synthetic inertia with wind turbines was developed at the Wind Energy Technology Institute in collaboration with Suzlon Energy. For this controller the influence of providing synthetic inertia on the mechanical loads of the wind turbine is assessed for different grid frequency scenarios. Such a scenario-based load analysis has not been published before, especially as the scenarios are derived from real measurements. The effect of the loads strongly depends on the analyzed grid frequency behavior. Ten months of high quality grid frequency measurements of the Indian grid are analyzed in order to derive inputs for the load calculation. Different types of grid frequency abnormities are identified and categorized with respect to their severity. Based on the observed occurrences of the grid frequency abnormities, realistic scenarios for the load calculations are chosen. The load calculations are performed for a state-of-the-art Suzlon wind turbine generator. The load increases caused by the supply of synthetic inertia are calculated for individual components assuming an otherwise undisturbed power production of the wind turbine in turbulent wind. Furthermore, a hardware-in-the-loop test bench is used to show how the measured grid frequencies are actually perceived by the control system of a typical wind turbine. The original frequency data were recorded with high quality measurement equipment, which is faster and more accurate than a multi-function relay, often used in wind turbines. For exemplary time traces, the effect of the reduced measurement accuracy on the reaction of the wind turbine is shown. This aspect has not been investigated in the literature yet. The results show that wind turbines can provide synthetic inertia without a considerable effect on the lifetime of the wind turbine. However, there are still problems with providing synthetic inertia reliably at high power operating points, which have to be solved.

Keywords: frequency support; grid frequency analysis; mechanical loads; rate of change of frequency; synthetic inertia; wind turbine; wind turbine generator

1. Introduction

Modern power systems with high shares of inverter-based renewables are bound to exhibit little system inertia. In order to avoid unfavorable excursions of the grid frequency, and high rates of change of frequency (RoCoFs), system operators increasingly require the provision of grid frequency support from renewables. Such grid support is mandatory for instance in Ireland [1], Québec [2] and India [3]. The existing requirements are typically tailored to the system operator's specific needs and their individual control objectives. It has been shown for various countries that such demands can make future power systems

with high degrees of non-synchronous penetration more stable, e.g., in Ireland [4], the UK [5] and South Africa [6]. There are various strategies to support the grid frequency with wind turbine generators (WTGs) [7]. The frequency support is typically categorized in fast frequency response (a fast reacting frequency support service, which activates power proportionally to the grid frequency deviation—this is comparable to traditional primary frequency control) and the provision of synthetic inertia (reacting proportionally to the derivative of the frequency) [8]. In addition, there are various control schemes tailored to the needs of a specific grid operator, e.g., providing a predefined power increase for approximately ten seconds, if a frequency threshold is violated [9]. The provision of synthetic inertia with WTGs was first proposed in 2007 by Ramtharan et al. [10] In this paper, the effect of continuous provision of synthetic inertia (SI) with the so-called variable H controller [11] is researched, which improves the state-of-the-art concepts by considering the current operating point of the WTG. In comparison to an event-based activation of SI, continuous provision of SI stabilizes the grid also during smaller power imbalances in the grid. Hence, it may help stabilizing the frequency in future grids with little inertia.

Traditionally, WTG control aims to maximize the energy yield of the WTG while keeping the resulting structural loads at an acceptable level [12]. The main sources of WTG loads (aerodynamic, inertial and gravitational [13]) have traditionally been addressed by using a PI(D)-controller with gain scheduling for the speed and power control of the WTG [14]. Additionally, the drive train and the tower of the WTG are often protected by a drive train and tower damper, which modifies the power setpoint of the WTG to reduce the loads on these components [15]. More recent developments in WTG control use state estimation and sensor fusion [16,17], as well as self-learning algorithms [18,19], to improve the WTG control and to make it more robust. In addition to these purely control-based improvements, control concepts which require additional hardware have lately been proposed, e.g., Lidar-based systems [20], tuned-mass dampers in the tower [21] or a tunable flywheel in the rotor of the WTG [22]. Structural loads resulting from the electrical grid are traditionally limited to grid faults, e.g., a low-voltage ride through events, which result in high mechanical stress for the drive train [23,24]. Suzlon has been researching this topic for many years already [25]. During such events, the main goal is to protect the WTG while keeping it connected to the grid. By contrast, grid frequency support mainly aims to stabilize the frequency of the electrical grid. The control system of the WTG must therefore handle the dynamic excitation from the wind and, in addition, the dynamic excitation from the grid. These excitations from the grid must be quantified and might have to be considered in the load calculation of a WTG comparably to the excitations from the wind. While the effect of frequency support on the grid is well studied, there is little research on the consequences for the mechanical loads of the supporting WTGs. Fleming et al. [26] compared different derating strategies of the WTG for fast frequency control and calculated the effect on the WTG loads. The authors did not use specific frequency scenarios but assumed that the WTG remains in derated operation during its entire lifetime. Wang et al. [27] did a similar study for different synthetic inertia control methods, which were tested for two predefined frequency scenarios at two different wind speeds. Fischer et al. recently published a comprehensive report [28] on the interactions between the supply of various grid services and structural loading of the WTG, e.g., the effect of SI provision on the drive train [29]. However, there is a lack of publications, which combine scenarios based on real data (i.e., with a defined severity and frequency of occurrence) with a comprehensive load analysis. This is problematic, as the results of the load analysis largely depend on the analyzed scenarios. This paper aims to close this research gap by analyzing high quality data of the Indian grid frequency and defining scenarios for the load calculation from this analysis. A load calculation for a state-of-the-art Suzlon DFIG WTG is performed, which shows the effect of continuous provision of SI with the variable H controller in the defined scenarios. Furthermore, hardware-in-the-loop (HiL) tests are carried out, which show the grid frequency actually perceived by the WTG when an industry standard measurement system is used. In fact, the work presented

in the paper closes a critical gap in the development of wind turbines. Wind turbine manufacturers have to be able to assess the lifetime consumption, resulting from newly demanded services and excitations. Therefore, the presented analytical approach is chosen to quantify the excitations from the grid frequency. In this context, it is important to note that the grid frequency does not behave as stochastic as the wind. However, it does not behave deterministically either. Hence, there are three aspects which define the novelty of the paper: (I) simulation of comprehensive scenarios based on real grid frequency measurements for (II) a state-of-the-art WTG (III) considering the real measurement system of the WTG.

The rest of the paper is structured as follows: Section 2 of this paper describes the used frequency data set and the method to derive load simulation scenarios from it. Furthermore, the HiL setup and the simulation environment for the load calculations is outlined. Section 3 presents and discusses the results of the scenario definition, the hardware-in-the-loop test and the load calculations. Section 4 summarizes the findings.

2. Methodology, Measurement Setup, Data Analysis and Simulation Model

The methodology used in this paper is summarized in Figure 1. Scenarios for the load calculations are derived from high-quality recordings of the Indian grid frequency. These scenarios are tested for different wind conditions and controller settings in a Flex5 [30] WTG model. Based on these time domain results, the effect of frequency support on the WTG loads are calculated for the design load case 1.2 [31]. Furthermore, a representative subset of the frequency scenarios is tested in a HiL setup. These six modified time traces are also tested in the Flex5 model. The WTG reaction to the six HiL and the corresponding original scenarios are compared by analyzing accelerations of the most vulnerable WTG components. This allows estimating the effect of the real measurement system in the WTG on the controller-induced loads.
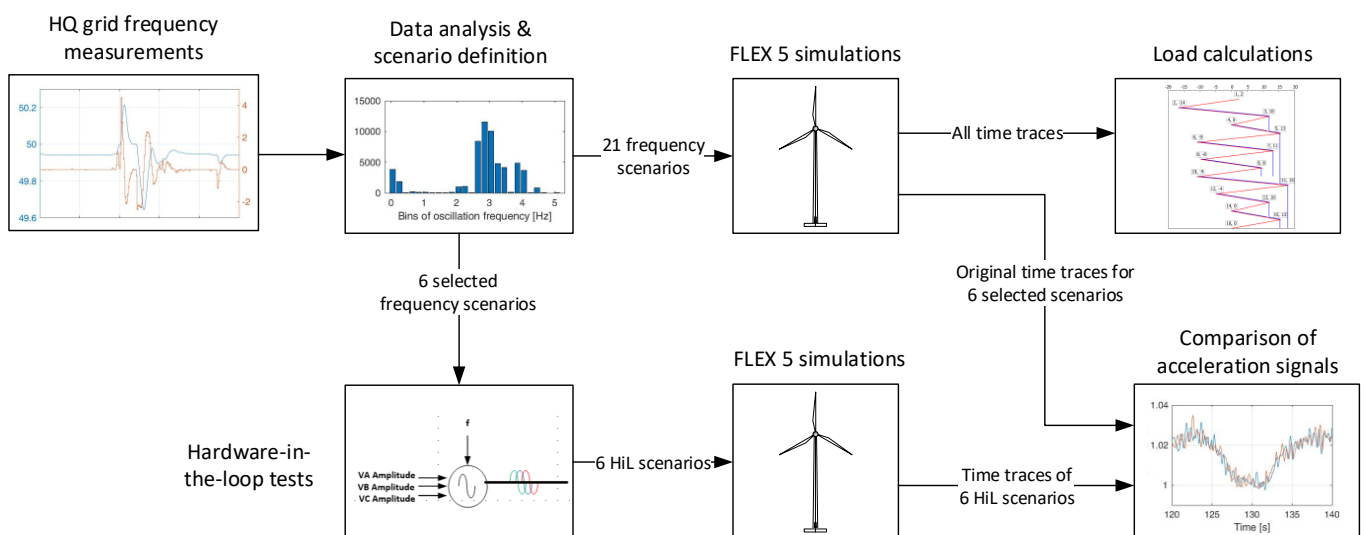
Figure 1. Overview of the used methodology.

After briefly introducing the variable H controller concept, the remainder of this section is structured along the three aspects of the load calculation: scenario definition, HiL tests and load simulation environment.

2.1. Variable H Controller

As this paper deals with the consequences of using the variable H controller, the concept of this controller is briefly introduced. The basic idea of the controller is that the grid operator defines an inertia constant (H_{dem}). The WTGs emulate the inertial response (IR) of a synchronous generator with the defined inertia constant, when the WTGs operate

at a rated speed (see Equations (1) and (2); [32]). However, unlike synchronous generators, the rotational speed of a WTG changes with its operating point. Therefore, the variable inertia constant scales with the operating point of the WTG in accordance with the available kinetic energy stored in its rotation (see Equation (2)). Hence, the WTG provides as much IR as possible in its current operating point, while minimizing the risk of reducing the WTG speed too much.

$$P_{SI} = -2 \cdot H_{var} \cdot P_{rated} \cdot \frac{RoCoF}{f_{grid}} \tag{1}$$

where P_{SI} is the power change for SI, P_{rated} is the rated power of the WTG and H_{var} is the variable inertia constant.

$$H_{var} = H_{dem} \cdot \frac{0.5 \cdot J_{WT} \cdot \left(\omega_{gen}^2 - \omega_{cut-in}^2\right)}{0.5 \cdot J_{WT} \cdot \left(\omega_{rated}^2 - \omega_{cut-in}^2\right)} \tag{2}$$

where H_{dem} is the inertia constant to be emulated as defined by the grid operator, ω_{gen} is the generator speed, $\omega_{cut\text{-}in}$ is the generator speed at which the WTG starts to produce power and ω_{rated} is the rated generator speed of the WTG.

The power controller of the WTG is modified by adding P_{SI} to the optimal power derived from the power-vs-speed characteristic of the WTG (see Figure 2). Therefore, P_{SI} directly influences the power reference of the WTG power controller and grid frequency abnormities may directly affect the WTG dynamics. Please note that, for the sake of clarity, Figure 2 does not show an additional controller mentioned in the introduction (e.g., drive train damper).
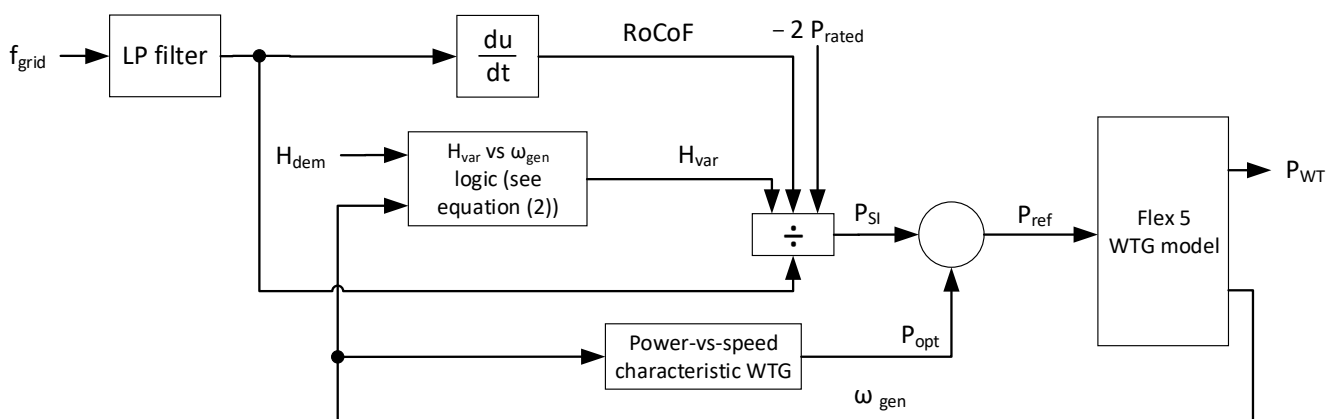
Figure 2. Power setpoint calculation and interaction with the WTG Flex5 model.

2.2. Grid Frequency Analysis and Scenario Definition

For the scenario definition, frequency measurements from the Western Indian power system are analyzed. The data were recorded between March 2015 and January 2016 following the then most recent IEC 61,400 standard [33] with a state-of-the-art measurement system and a sample time of 20 ms (in total 1,025,220,000 samples, equivalent to 237.3 days of uninterrupted measurements). The accuracy of the measurement system is 0.9 mHz. Hence, the smallest recognizable RoCoF is 0.045 Hz/s.

Load calculations in a previous project [34] showed that the effect of SI provision on WTG loads during normal frequency behavior is negligible. Therefore, the analysis focuses on two different abnormalities of the grid frequency, which are identified in the dataset:

1. Grid frequency oscillations: defined as periodic variations of the grid frequency. Oscillations are identified by a violation of a frequency-dependent amplitude thresholds in the frequency domain.
2. Events: defined as abrupt changes of the grid frequency. Events are identified by a violation of the threshold for the RoCoF ($|RoCoF| > 1$ Hz/s).

Both abnormities were also analyzed in the previous project. However, a regular pattern in frequency events was not addressed, which leads to a very high number of events (>25,000/year) and eventually to questionable results of the load calculation. The previous study also did not account for different amplitudes and frequencies of grid frequency oscillations as it was only used one scenario for this abnormity. Hence, in this study the recorded grid frequency measurements are analyzed in detail in order to derive detailed scenarios that are more realistic.

The times during which grid frequency oscillations occur are identified with the help of an analysis in the frequency domain. For that purpose, an amplitude threshold in the frequency domain is defined, which leads to a power setpoint variation (P_{SI}/P_{rated}) with an amplitude of at least 0.01 pu. To derive this threshold, Equation (1) can be solved for the minimum RoCoF leading to such a power variation using $f_{grid,0}$ = 50 Hz and $H_{var} = H_{dem}$ = 6 s [32]:

$$RoCoF_{min} = \frac{P_{SI}}{P_{rated}} \cdot \frac{f_{grid,0}}{-2 \cdot H_{var}} \tag{3}$$

The minimum RoCoF according to Equation (3) must be reached during a grid frequency oscillation. The general equation of a grid frequency oscillation (4) is used to derive the relation between the RoCoF and the amplitude and the frequency of the oscillation:

$$f_{grid}(t) = f_{grid,0} + A_{osc} \cdot \sin(2 \cdot \pi \cdot f_{osc} \cdot t) \tag{4}$$

where $f_{grid}(t)$ is the instantaneous grid frequency, $f_{grid,0}$ the center value of the grid frequency oscillation, A_{osc} the oscillation amplitude and f_{osc} the oscillation frequency.

Equation (4) can be derived with respect to time to calculate the RoCoF during the oscillation, $RoCoF_{osc}$:

$$RoCoF_{osc}(t) = A_{osc} \cdot 2 \cdot \pi \cdot f_{osc} \cdot \cos(2 \cdot \pi \cdot f_{osc} \cdot t) \tag{5}$$

The maximum RoCoF according to Equation (5) occurs when the cosine term is 1. Hence, Equation (5) can be simplified and solved for the amplitude of the grid frequency oscillation:

$$A_{osc} = \frac{RoCoF_{osc,max}}{2 \cdot \pi \cdot f_{osc}} \tag{6}$$

In order to derive the amplitude threshold in the frequency domain, the maximum RoCoF during the oscillation, $RoCoF_{osc,max}$, in Equation (6), is substituted by the minimum RoCoF according to Equation (3). Hence, the modified Equation (6) can be used as amplitude threshold in the frequency domain.

In order to find times with relevant grid frequency oscillations, the recorded grid frequency measurements are split into overlapping intervals (see Figure 3). The Fourier transform of each interval is compared to the amplitude threshold according to Equations (3) and (6). Intervals, for which a relevant oscillation is detected, are marked in green in Figure 3, while the others are marked in red. Whenever frequency oscillations in adjacent intervals are detected, these intervals are combined in a single time trace. For the example given in Figure 3, intervals 3 to 6 (and all further intervals until the end of the ongoing oscillation) are combined into a single time trace containing the full duration of the oscillation.

In order to define a reasonable number of scenarios for the load calculation, the detected time traces of grid frequency oscillations are binned with respect to the oscillation frequency. It is assumed that grid frequency oscillations with an oscillation frequency close to the eigenfrequency (f_{eigen}) of WTG components are more harmful to the respective component (due to resonance effects). Therefore, narrow frequency bins ($f_{eigen} \pm 10\%$) are used around the most important eigenfrequencies of the WTG. All other oscillations of the grid frequency are grouped and analyzed in three wider bins (see below). For the load analysis, the scenarios must be properly defined in terms of typical RoCoFs during the oscillation and the duration of the oscillation:

1. RoCoF during oscillation: The changes of the power setpoint for SI is directly proportional to the occurring RoCoF (see Equation (1)). Hence, a representative RoCoF has

to be defined for each oscillation bin. For this purpose, the weighted average of the RMS value of the RoCoF of all time traces in a bin is calculated. The duration of the individual time traces is used as a weighting factor. Longer time traces have therefore more influence on the average RoCoF than shorter time traces. The results are chosen as the representative RoCoF for the corresponding frequency bins.

2.   Duration of oscillation: A longer grid frequency oscillation may be more harmful to the WTG than a shorter one, especially when resonance may occur. Hence, a representative duration has to be defined for each frequency bin. For this purpose, the weighted average duration is calculated for each frequency bin. The RoCoF of the individual time traces is used as a weighting factor, as stronger oscillations are more harmful to the WTG than weaker ones. The resulting durations are chosen as the representative duration for the corresponding frequency bins.
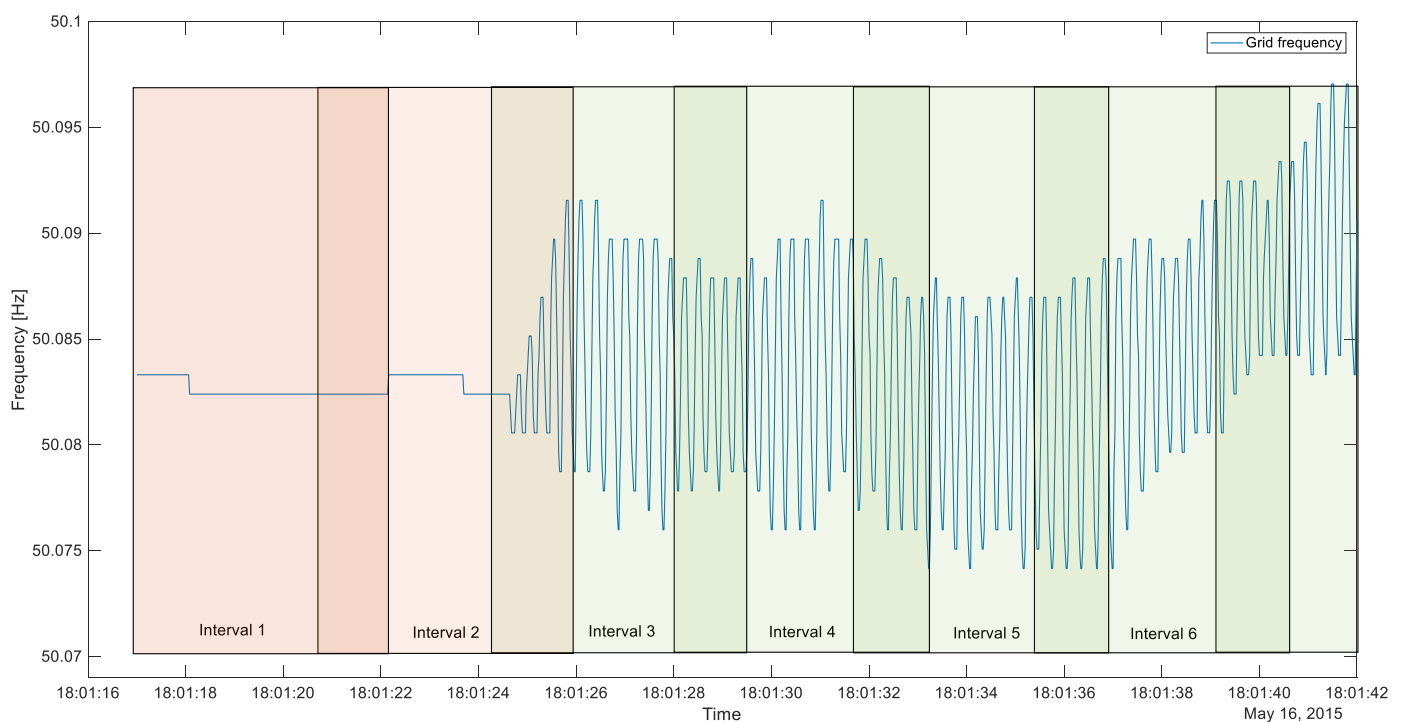
Figure 3. Example of a beginning grid frequnecy oscillation and the detection intervals. Red-shaded boxes mark intervals in which no oscillation is detected, while green-shaded boxes mark intervals with oscillations.

The analysis showed that the majority of the grid frequency oscillations occurred with an oscillation frequency between 2.6 Hz and 4.6 Hz (see Figure 4). Furthermore, there is a second cluster with an oscillation frequency below 0.4 Hz. The lack of oscillations with a frequency between 0.4 Hz and 2.6 Hz is actually beneficial, as most eigenfrequencies of the vulnerable components of the considered WTG are within this frequency range. Hence, scenarios for WTG components only have to be defined for the 1st eigenfrequency of the tower and for the 2nd bending eigenfrequency of the blades (see Table 1). It has to be noted that the eigenfrequencies of the relevant component may differ depending on the WTG design, which would influence the choice of scenarios. For this particular WTG, five scenarios are defined which represent grid frequency oscillations in the load analysis (see Table 1). In addition to the three properties described above, the total duration of the time traces in each oscillation bin is given in Table 1 and is used as a likelihood of occurrence (i.e., % of measurements in which such oscillations occur). The time traces for the scenarios were chosen such that the representative RMS value of the RoCoF and the representative duration as defined above are met.
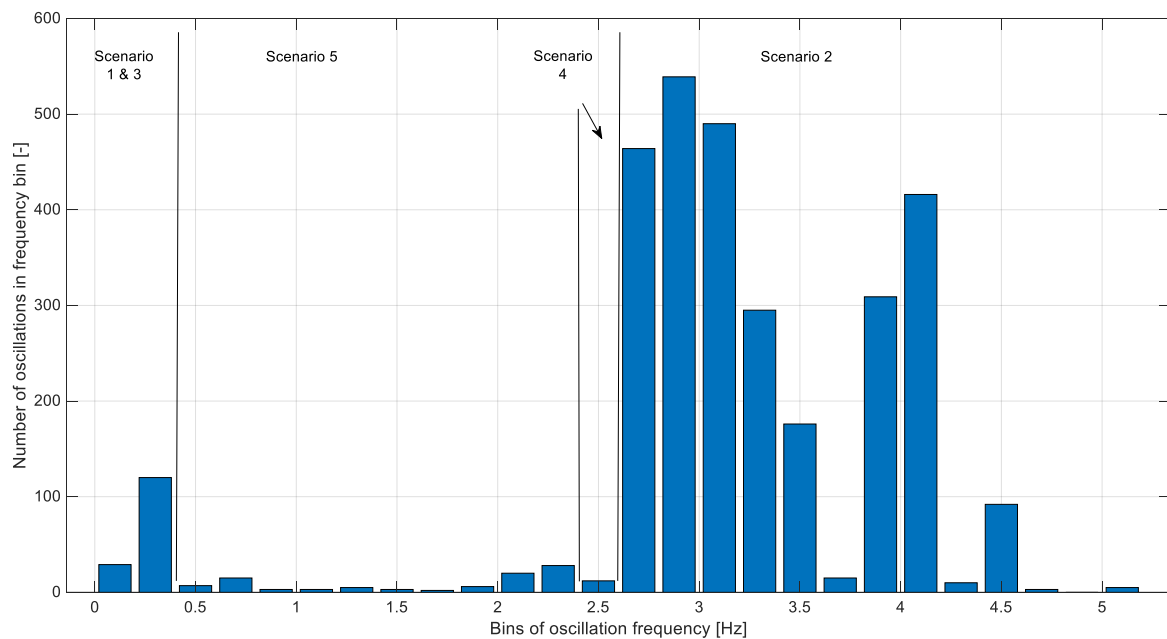
Figure 4. Number of detected periods with grid frequency oscillation with respect to the binned oscillation frequency (bin width 0.2 Hz). Number of the scenario, which represents the accumulated oscillations.

Table 1. Overview of identified scenarios to represent grid frequency oscillation in the load analysis.

Scenario Number	Oscillation Frequency	RoCoF$_{RMS}$	Duration	Likelihood of Occurrence	Comment for Scenario
1	0.26 Hz	0.1 Hz/s	77 s	0.007%	Low frequency oscillation
2	2.73 Hz	0.09 Hz/s	20 s	0.21%	High frequency oscillation
3	0.3 Hz	0.07 Hz/s	22 s	0.004%	Tower 1st eigenfrequency
4	2.4 Hz	0.127 Hz/s	61.7 s	0.008%	Blade 2nd bending eigenfrequency
5	2–2.3 Hz [1]	0.103 Hz/s	24 s	0.004%	Oscillations with a frequency between scenario numbers 3 and 4

[1] The dominant frequency changes during the oscillation period.

The second abnormity considered in this analysis are frequency events. Figure 5 shows an example of a frequency event, which occurred during the measurement campaign. The grid frequency increases temporarily to 50.2 Hz before dropping to 49.65 Hz within 500 ms and immediately returning to 49.95 Hz. The RoCoF threshold (± 1 Hz/s) is violated several times during the event, both in a negative and a positive direction.

Events can be detected in the recorded grid frequency measurements by a violation of the RoCoF threshold. The properties of the detected events are analyzed in order to derive scenarios for the load calculation. For this purpose, the events are categorized based on three criteria:

1. Event type: An event occurs every twenty minutes in the recorded grid frequency measurements. The exact reason for these regular events is unknown, but it is likely caused by the measurement setup and is called an expected event. All other events are called unexpected events (e.g., see Figure 5). While the expected events may be avoided with a different measurement system, the other events are likely to be measured with any kind of system. For this study, only the unexpected events are considered in the load calculation.

2. Duration: During most events, the RoCoF threshold is violated several times during a short period, typically less than 500 ms. These events are called singular events,

e.g., a steep drop of the grid frequency followed by an immediate return to the steady state value. Sometimes, multiple singular events occur with very short pauses (e.g., see Figure 5) causing multiple excitations of the WTG before the WTG can return to its steady state operating point. Such multiple excitations are potentially more harmful for the WTG. Hence, such multiple events are considered separately in the load analysis. The event shown in Figure 5 is classified as a long event as the RoCoF threshold is violated several times between 13:06:05 and 13:06:06 and again at 13:06:07.5.

3. Maximum and minimum RoCoF: It is assumed that extreme RoCoFs are more harmful for the WTG. A combination of maximum and the minimum RoCoF is used to categorize individual events into clusters (see Figure 6).
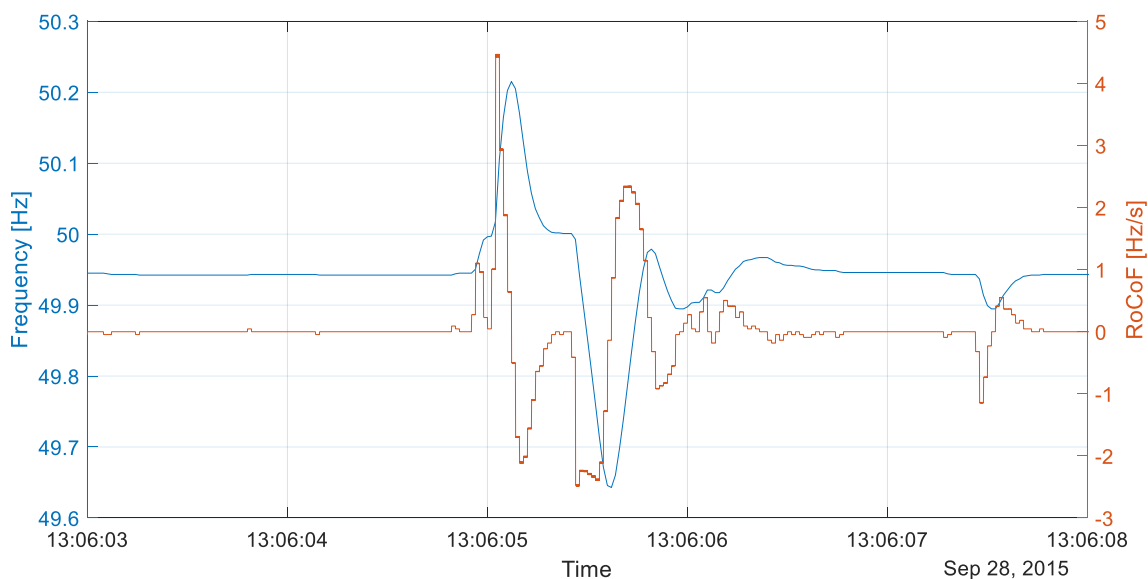
Figure 5. Example for an event of the grid frequency during which the RoCoF threshold is violated several times in a short period.

There were 2131 unexpected events detected in the analyzed data. These events are clustered with respect to the maximum and minimum RoCoF for two different durations (see Figure 6a–c). During 6.5% of the events extreme RoCoFs occurred (see Figure 6a) for which the detected grid frequency changed by up to -158 Hz/s and $+90$ Hz/s. These events were assigned to five clusters (see Figure 6a). The majority of the events showed smaller RoCoFs up to ± 5 Hz/s for short events and up to ± 10 Hz/s for long events. These events were grouped in detailed clusters: three clusters for long events (see Figure 6c) and seven cluster for short events (see Figure 6b). Even though the RoCoFs for these events are small in comparison to the extreme events in the data set, they still have a drastic effect on the power setpoint of a WTG providing SI.

For each cluster, a representative time trace of the grid frequency is chosen as a scenario for the load calculations (see Table 2). The only exception is cluster one, for which two separate time traces are chosen as the cluster contains many short and many long events. The number of detected events in the recorded grid frequency measurements is used to derive the expected number of events per year for each cluster. Data equivalent to 237.3 days of uninterrupted measurements are recorded, hence the scaling factor to 365 days is 1.54. As the measurement campaign only recorded data between March 2015 and January 2016, the data are also checked for seasonality effects, e.g., they are caused by the Indian monsoon. For the data at hand, no such effects stand out: grid frequency oscillations and events occurred with a similar likelihood throughout the months. Hence, a linear scaling seems appropriate.
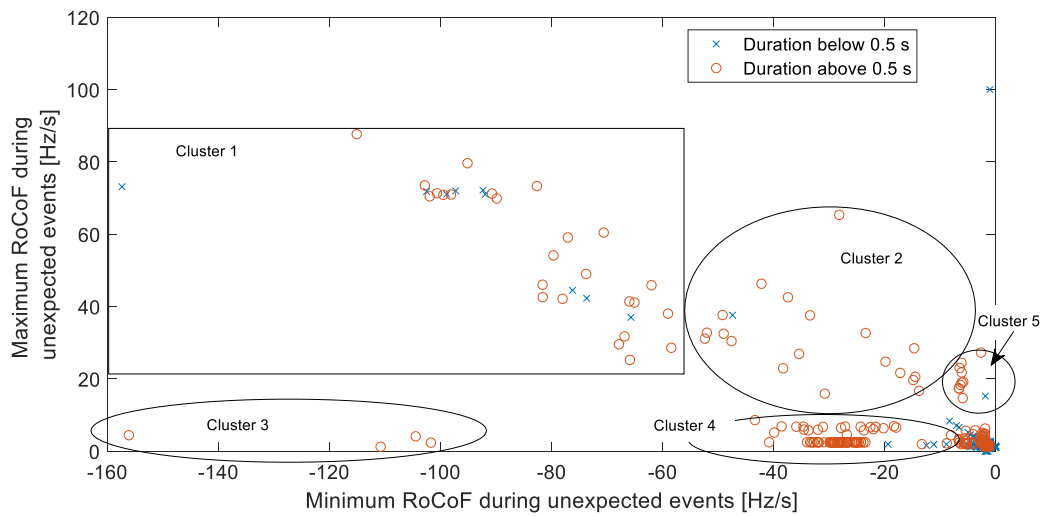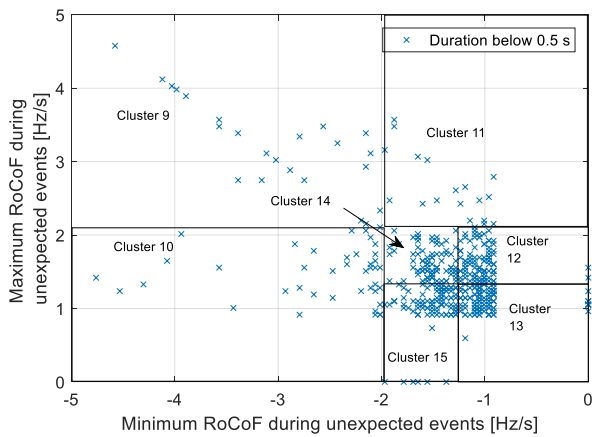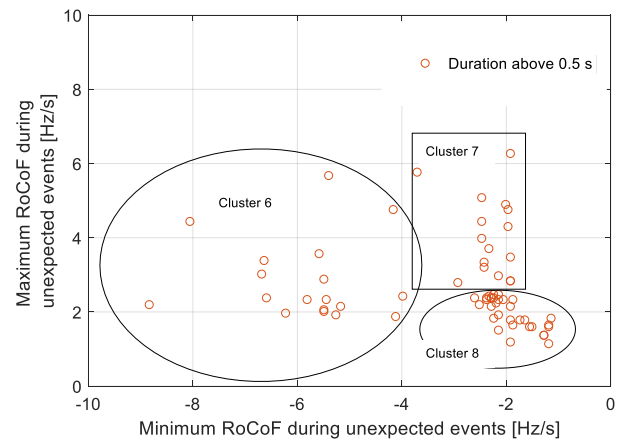
Figure 6. Cluster of grid frequency events depending on the maximum and minimum ocurring RoCoFs and the event duration. (**a**) Short and long event for very high RoCoFs. (**b**) Short events for smaller RoCoFs. (**c**) Long events for smaller RoCoFs. (**b**,**c**) are an excerpt from (**a**) giving a detailed view of events with less extreme RoCoFs.

Table 2. Overview of identified event scenarios for the load analysis.

Scenario Number	Cluster	Upper Limit Minimum RoCoF	Lower Limit Minimum RoCoF	Lower Limit Maximum RoCoF	Upper Limit Maximum RoCoF	Duration	Number of Events in Dataset	Number of Events Per Year
6	1	-50 Hz/s	-120 Hz/s	25 Hz/s	90 Hz/s	long	27	42
7	1	-50 Hz/s	-120 Hz/s	25 Hz/s	90 Hz/s	short	9	14
8	2	-10 Hz/s	-50 Hz/s	15 Hz/s	75 Hz/s	long	19	29
9	3	-100 Hz/s	-160 Hz/s	0 Hz/s	20 Hz/s	long	4	6
10	4	-10 Hz/s	-50 Hz/s	0 Hz/s	15 Hz/s	long	77	118
11	5	0 Hz/s	-10 Hz/s	10 Hz/s	50 Hz/s	long	10	15
12	6	-4 Hz/s	-10 Hz/s	0 Hz/s	6 Hz/s	long	17	26
13	7	0 Hz/s	-4 Hz/s	2.5 Hz/s	10 Hz/s	long	16	25
14	8	0 Hz/s	-4 Hz/s	0 Hz/s	2.5 Hz/s	long	33	51
15	9	-2 Hz/s	-5 Hz/s	2 Hz/s	5 Hz/s	short	27	42
16	10	-2 Hz/s	-5 Hz/s	0 Hz/s	2 Hz/s	short	74	114
17	11	0 Hz/s	-2 Hz/s	2 Hz/s	5 Hz/s	short	41	63
18	12	0 Hz/s	-1.25 Hz/s	1.25 Hz/s	2 Hz/s	short	129	198
19	13	0 Hz/s	-1.25 Hz/s	0 Hz/s	1.25 Hz/s	short	548	843
20	14	-1.25 Hz/s	-2 Hz/s	1.25 Hz/s	2 Hz/s	short	108	166
21	15	-1.25 Hz/s	-2 Hz/s	0 Hz/s	1.25 Hz/s	short	244	375

The defined grid frequency scenarios are used in HiL tests and a Flex 5 simulation. Both setups are introduced in the following sections.

2.3. Hardware-in-the-Loop Tests Experimental Setup

The analyzed time traces of the grid frequency were measured with a high-quality measurement system, which is not available in a standard WTG. Hence, the WTG will measure a different frequency in an identical grid situation. In order to reduce the uncertainty, which arises from the different measurement systems, HiL tests of exemplary time traces are conducted (for scenarios 1, 2, 4, 7, 8 and 10). As the chosen time traces include typical characteristics of the time traces of all scenarios, the HiL tests are representative for all cases. For the HiL tests, the measured frequency signal is converted into three analogue AC voltage signals using a Typhoon HIL 602 [35], which are then measured by the original multi-function relay (MFR) of the WTG and processed in the original Bachmann [36] controller hardware (see Figure 7). The sample rate of the analogue inputs and outputs of the Bachmann controller is 1 ms. The frequency signal is sent to the Typhoon using an analog signal with the same sample rate. The Typhoon HIL 602 has a 1 µS simulation time step and the analogue output is updated with the same rate. The sampling of the Typhoon HIL 602 can go down even to 20 ns. The MFR measures the grid frequency every 10 ms and submits its measurements to the Bachmann controller via a CAN connection.
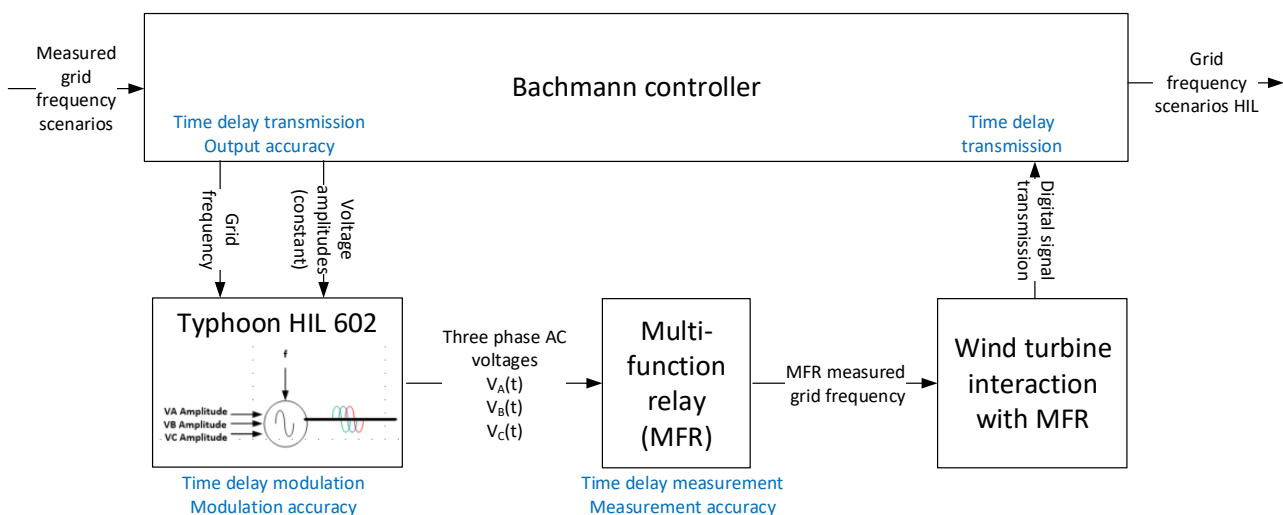
Figure 7. Measurement setup of the HiL tests and indication of the occuring accuracy issues and time delays.

However, these HiL tests can only reduce the uncertainty as it is inherently assumed that the grid frequency was measured perfectly. Furthermore, the output signal of the Bachmann controller has a limited accuracy and the created voltage signals are near perfect sinusoidal curves with a limited modulation accuracy. By contrast, the transmission of the MFR signal to the Bachmann controller does not limit the accuracy of the measured signal. The results of frequencies measured in the HiL tests are presented and discussed in Section 3.1. The resulting time traces are used in the FLEX 5 simulations (described in the following section) and are compared to the frequency time traces measured by the high-quality system to check whether the WTG reaction is affected by the limitation of its measurement system.

2.4. Wind Turbine Simulation Model and Load Calcualtions

The load calculations are based on time domain simulations of a novel DFIG WTG of the 3.x MW class, which will be introduced into the market in the near future. Due to the novelty of this WTG, the technical details, which may be published, are limited. The simulations are conducted with a Flex5 [30] model for the mechanical part of the

WTG. The model has 20 degrees of freedom (4 for each blade, 2 for the main shaft, 6 for the tower). A second order model of the generator-converter unit is also implemented in Flex5. The power controller is modelled in Matlab/Simulink. It calculates a power setpoint, P_{ref}, which is passed on to the generator-converter model in Flex5 (see Figure 2). The time traces of the grid frequency are processed with a low-pass (LP) filter with a cut-off frequency of 10 Hz. The cut-off frequency is set in accordance with the ENTSO-E recommendations [37]. The calculated power setpoint, P_{ref}, is limited by a maximum allowed power and a maximum allowed torque to protect the electrical and the mechanical part of the drive train. The maximum allowed power change for synthetic inertia, P_{SI}, is set to $\pm$ 0.3 pu. The simulation time step is 10 ms.

For the variable H controller, a demanded inertia constant, H_{dem}, has to be defined. In reality, this value would be defined by the transmission system operator. For the study at hand two different inertia constants are chosen, which have to be emulated by the WTG: 6 s, which allows a comparison to previously published results [34], and 12 s, which may be necessary to allow a stable grid operation in extreme situations (high shares of non-synchronous generation and large power imbalances [38,39]). In another previous study, 12 s has also been applied to maintain sufficient grid inertia in a turbulent part load wind [40].

The dynamic behavior of the WTG for the scenarios of the grid frequency as listed in Tables 1 and 2 is simulated in turbulent wind with a 0.17 turbulence intensity at 15 m/s wind speed. The simulated wind speeds are chosen such that an extrapolation to the full operating range of the WTG is possible. For the load calculation, the reactions of the WTG at different wind speeds are weighted based on a Weibull distribution to represent a site with an average wind speed of 7.3 m/s. In post-processing, these results are compared to the dynamic behavior without frequency support to calculate the load increases caused by the SI provision over the lifetime of the WTG (20 years). Hence, 10^7 load cycles are assumed. The analysis is carried out only for normal operation of the WTG (design load case 1.2 [31]).

The loads are analyzed for so-called sensors. Each sensor represents a one-directional torque or force at a certain segment of the WTG model. Hence, there are six sensors for each analyzed segment. Flex 5 uses different coordinate systems for the different segments of the WTG. An overview of the different coordinate systems used in Flex 5 is given in Sessarego et al. [41] For this analysis, the tower is represented by five segments (tower top, tower segment 1–3, and foundation), and the nacelle by three segments (main bearing, yaw bearing, and hub center). Furthermore, each blade root is analyzed individually. Hence, the loads are analyzed for 66 sensors in total.

The results of the time domain simulations and the load calculation are discussed in Sections 3.2 and 3.3, respectively.

3. Hardware-in-the-Loop and Simulation Results, Load Analysis, and Discussion

In the first part of this section, the results of the HiL tests are shown. This is followed by the time domain response of the WTG to exemplary frequency inputs, and finally the last section shows the results of the load calculations.

3.1. Hardware-in-the-Loop Test Results and Discussions

The conducted HiL tests show the performance of a measurement system used in a real WT. To allow an easier comparison among grids with a different steady-state frequency, the frequencies and RoCoFs in Figures 8–10 are shown as normalized frequencies (base value 50 Hz). The varying time delay between the originally measured frequencies and those modelled in the HiL tests are caused by the HiL measurement setup and would not affect the mechanical loads of the WTG or the capability of the WTG to provide SI in a real grid.
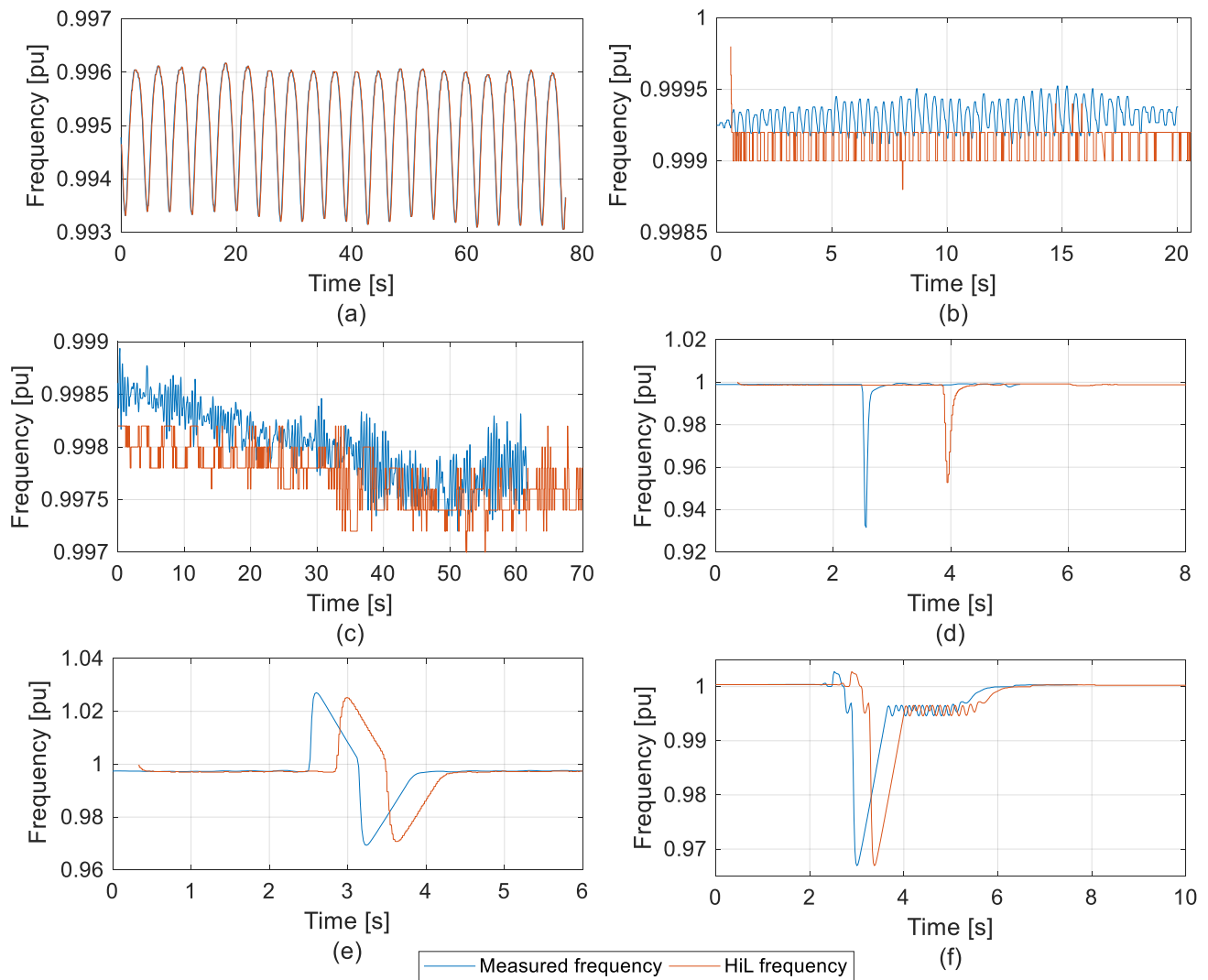
Figure 8. Comparison of the normalized measured frequency (blue) with the normalized frequency modelled in the hardware-in-the-loop test (orange) for scenario 1 (**a**), scenario 2 (**b**), scenario 4 (**c**), scenario 7 (**d**), scenario 8 (**e**), and scenario 10 (**f**).

The chosen time traces for the HiL tests allow a sufficient representation of the major characteristics of the frequency behavior for all scenarios defined in Section 2.1. The tests show that grid oscillations with a high frequency and small amplitudes cannot be measured reliably due to the limited accuracy of the measurement system. Hence, the simulation results for scenarios 2, 4 and 5 may differ from the reaction of a real WT (see Figure 8b,c). The time traces retrieved from the HiL tests are fundamentally different from the originally measured ones, especially when looking at the RoCoF (see Figure 9).

In contrast, slow oscillations with a higher amplitude occurred (see Figure 8a). Furthermore, high frequency oscillations can be measured if the amplitude is sufficiently high (see oscillations after the event in Figure 8f). Events can also be measured very well by the MFR (see Figure 8d–f). An exception is the nadir of frequency event for scenario 7, which is underestimated by approximately 2% (see Figure 8d). This may be caused by the short time the frequency stays in the nadir in combination with a very steep drop and rise, which may not be fully captured by the limited sampling time of the measurement system.
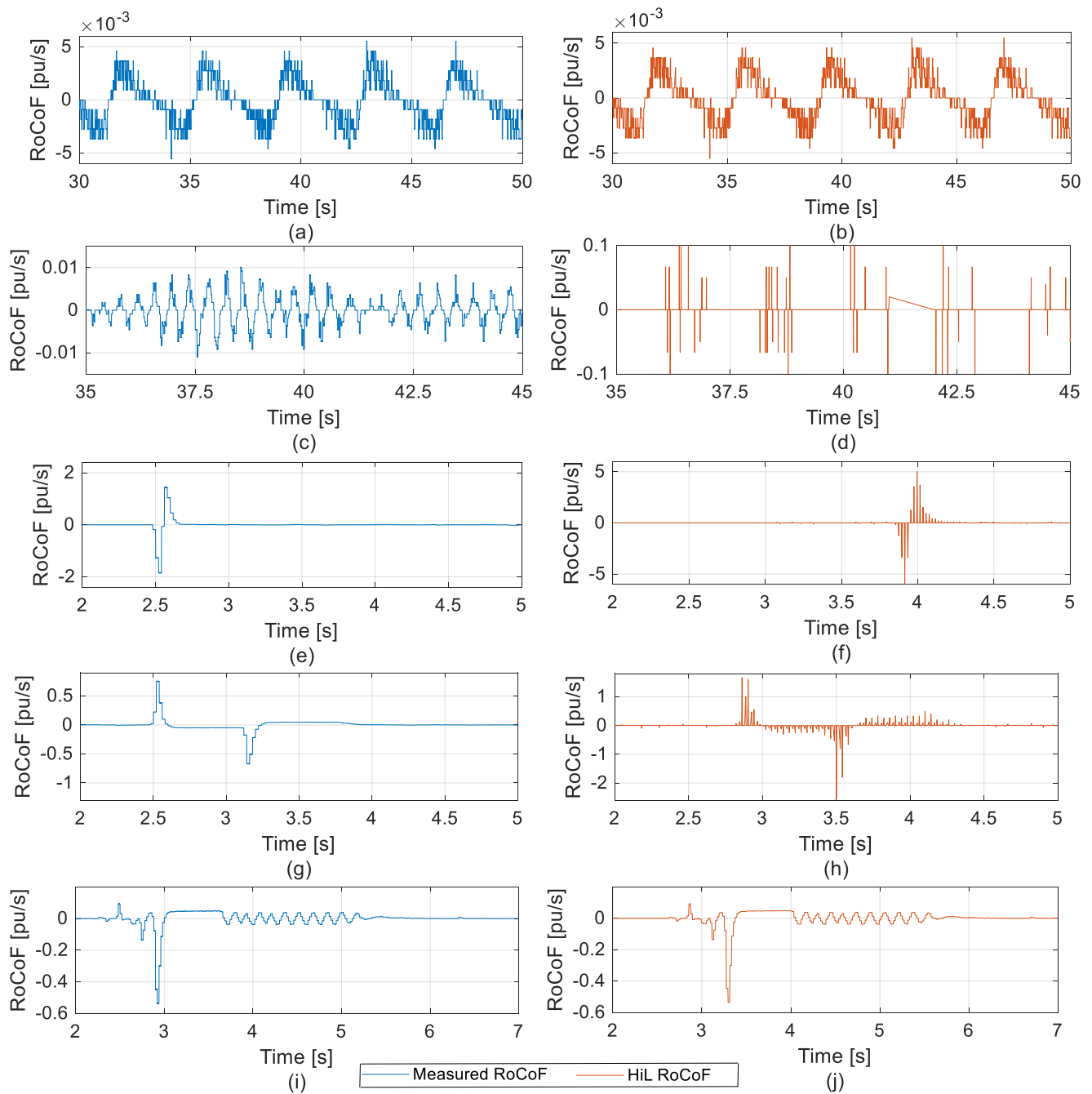
Figure 9. Comparison of the measured RoCoF (blue) with the RoCoF modelled in the hardware-in-the-loop test (orange) for parts of the time traces for scenario 1 (**a**,**b**), scenario 4 (**c**,**d**), scenario 7 (**e**,**f**), scenario 8 (**g**,**h**) and scenario 10 (**i**,**j**). Scenario 2 is shown in Figure 10.

For the IR of the WTG, the RoCoF is more important than the absolute value of the grid frequency (see Equation (1)). To allow an easier comparison between the original and the HiL signals, only parts of the scenario time traces are shown in Figure 9. When looking at the RoCoF, the limited sampling time of the measurement system in the HiL tests becomes also relevant for scenario 8 (see Figure 9g,h)). As the MFR updates its output slower than the Bachmann controller reads its input, the RoCoF alternates between 0 Hz/s and very high RoCoF values (see Figure 9d,f,h)). This effect is reduced by the LP filter used in the SI controller (see Figure 10). The slower and less extreme scenarios 1 and 10 are by contrast captured extremely well by the WTGs measurement system even when looking at the RoCoF (see Figure 9a,b,i,j).
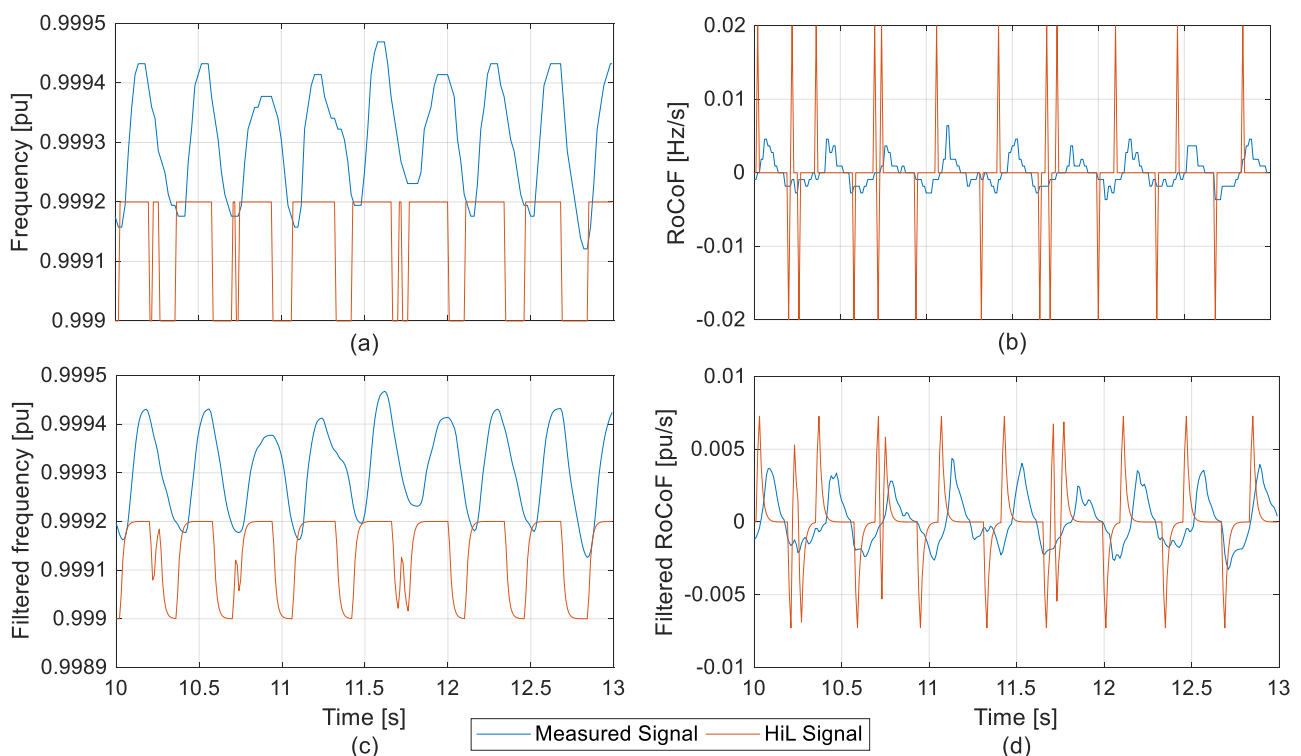
Figure 10. Comparison of the original frequencies and RoCoFs (blue) and HiL signals (orange) for a part of the time trace of scenario 2. (**a**) Shows the originally measured and the HiL frequency, (**b**) the corresponding RoCoFs to the signals in (**a**), (**c**) filtered version of the originally measured and the HiL frequency, and (**d**) the corresponding RoCoFs to the signals in (**c**). Time axes of (**c**,**d**) are valid for the above subplots as well.

The measured frequency signals are not used directly in the load simulations but are filtered with an LP filter with a cut-off frequency of 10 Hz (see Section 2.4). The RoCoF is calculated from these filtered signals. For the exemplary time traces of scenario 2, Figure 10 shows a comparison of the filtered measured and filtered HiL signals. Filtering the signals significantly decreases the RoCoF differences (see Figure 10b,d). The peaks of the HiL RoCoFs are reduced by a factor of 2.5 and are much closer to the peaks of the measured signals. However, the sinusoidal behavior of the signals is replaced by the LP filter response to the arbitrary jumps in the frequency (see Figure 10c,d).

For scenario 2 and 10, the WTG reaction to the HiL and the corresponding original time traces is shown and discussed in the next section. Furthermore, the acceleration of WTG components are compared for all scenarios, which are analyzed in the HiL tests.

3.2. Wind Turbine Simulations

In order to get an idea of the WTG reaction to the different frequency signals, time traces are shown and discussed for two exemplary scenarios. Furthermore, the differences between the measured frequency and the frequency generated in the HiL test is shown and discussed. Acceleration signals are analyzed for all scenarios for which HiL time traces are available. All simulations in this chapter are conducted with a demanded inertia constant, H_{dem} = 12 s.

Figure 11 shows the reaction of the WTG to scenario 2, a fast oscillation of the grid frequency with a small amplitude (see Figure 10). The offset of the power setpoint, P_{SI} (see Figure 2), varies between ± 0.06 pu with a period of 0.37 s for the measured frequency signal (see blue line in Figure 11b). For the HiL frequency signal, the power setpoint varies almost arbitrarily between ± 0.19 pu (see red line in Figure 11b). This behavior is caused by the limitations of the measurement system as discussed in the previous section. However, a large part of the differences is reduced by the reaction of the generator-converter unit

to the setpoint changes. Hence, the differences in the generator power (see Figure 11c) are much smaller and for some parts of the time traces are almost negligible (e.g., 102 s to 106 s). As the WTG uses kinetic energy stored in the drive train to provide SI, the differences in the generator speed (see Figure 11d) follow the same pattern as the generator power. The generator speed oscillates almost sinusoidally as the physical inertia of the drive train dampens the sharper peaks of the generator power oscillations. The period of the oscillation resembles the period of the grid frequency variations. In the final seven seconds of the frequency oscillation, the WTG IR is occasionally limited by the maximum allowed drive train torque, thus limiting the generator power setpoint. Such limitations occurred for very short intervals: The longest duration of an ongoing limitation is 0.1 s. The total duration of all torque limitations in scenario 2 is 0.7 s (measured frequency signal) and 0.5 s (HiL signal). Such torque limitations also occur for other scenarios in high wind conditions and hamper the capability of the WTG to provide a reliable frequency support in high wind operating points.
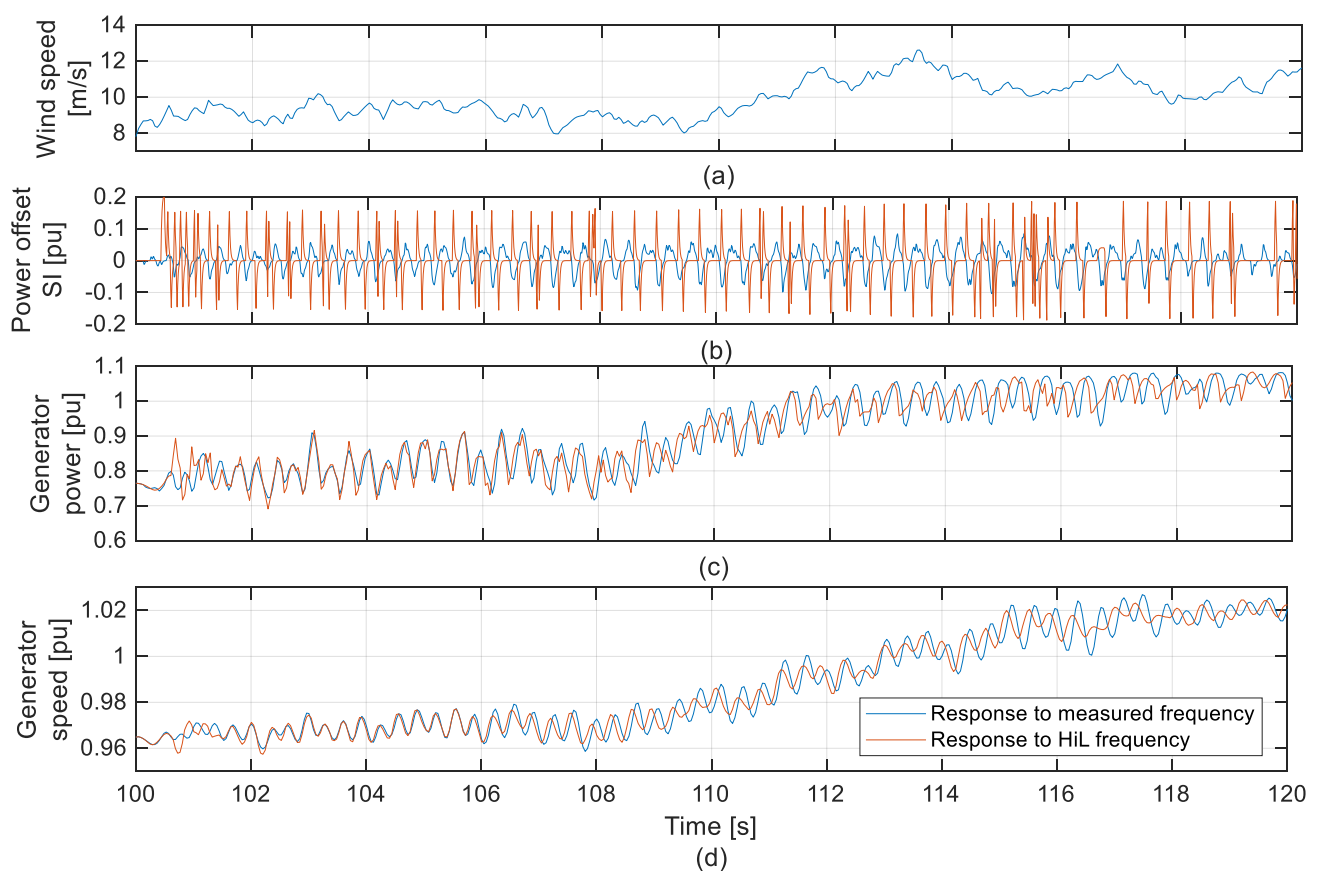
Figure 11. WTG reaction to scenario 2 for the measured frequency (blue) and the HiL frequency. (**a**) Wind speed, (**b**) power offset for SI provision, (**c**) generator power and (**d**) generator speed. Time axis of (**d**) is valid for the above subplots as well.

Figure 12 shows an example of the WTG's reaction to a severe frequency event. The IR is here often limited by the maximum allowed power offset for SI provision ($\pm$0.3 pu, see Figure 12b). The event and the following oscillation of the grid frequency causes drastic changes of the generator power, and consequently, of the generator speed (see Figure 12c,d). The different reactions of the WTG to the measured and the HiL frequency signal are mainly caused by the time delay of the HiL signal (appr. 0.4 s) and therefore slightly different wind conditions and operating points of the WTG. The grid frequency and the RoCoF for the two signals are almost identical (see Figures 8 and 9). Figure 12c,d also shows that the aerodynamic performance of the WTG is hardly affected by the drastic power changes, as the operating points of the WTG for both signals are almost identical

within one second after the last power offset for SI occurred. Furthermore, the results show the capability of the WTG to change its power output extremely fast: the maximum power gradient is close to ±4 pu/s (see changes of generator power between 102.5 s and 104 s in Figure 12).
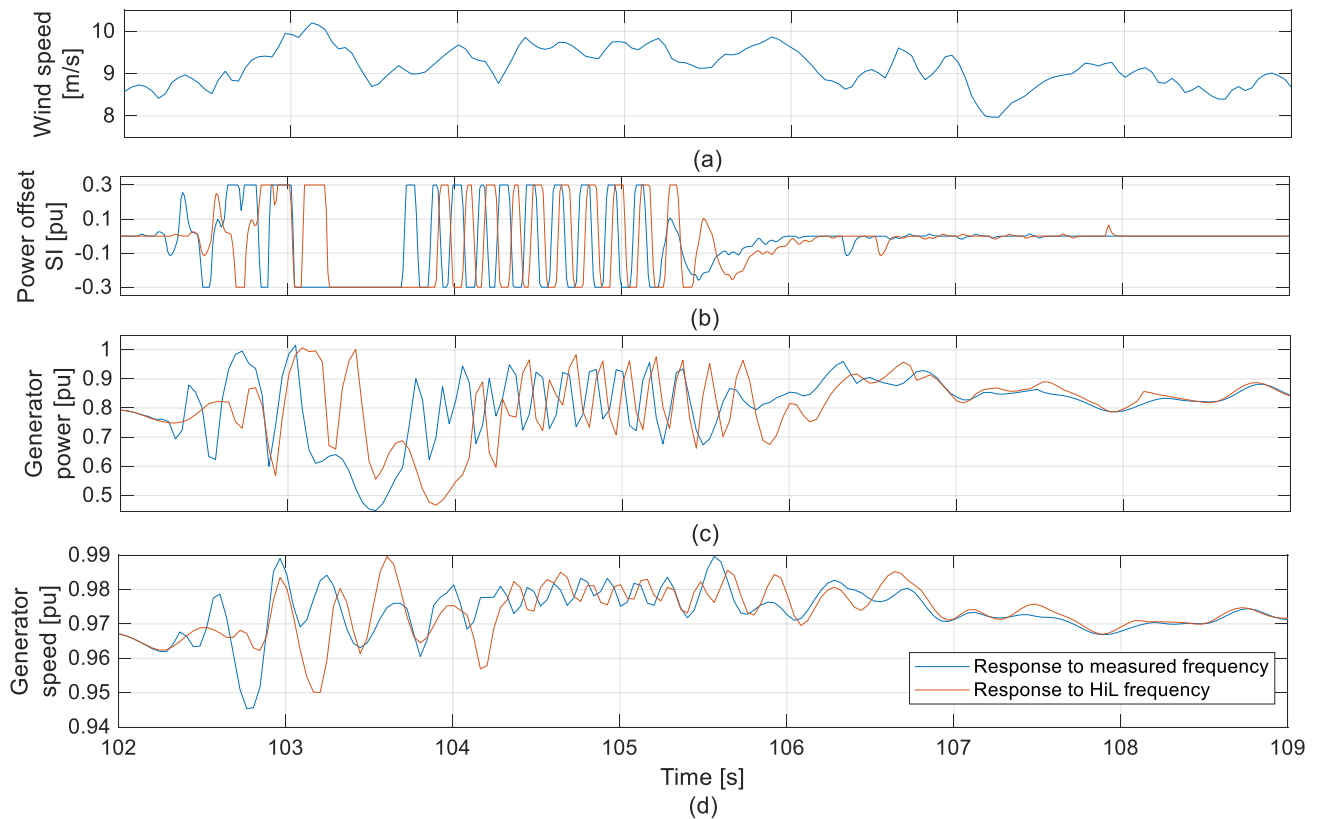
Figure 12. WTG reaction to scenario 10 for the measured frequency (blue) and the HiL frequency. (**a**) Wind speed, (**b**) power offset for SI provision, (**c**) generator power and (**d**) generator speed. Time axis of (**d**) is valid for the above subplots as well.

Such drastic changes of the applied electrical torque leads to heavy excitations of the drive train. Furthermore, drastic changes of the aerodynamic operating point may cause tower head motions. This may affect the lifetime of the WTG, which is discussed in detail in Chapter 3.3 for the measured frequency signals. In order to compare the HiL to the original frequency signals, the effect of IR on the WTG is estimated by comparing acceleration signals of the drive train and the tower head. The signals are chosen based on the results of a previous study [34]. The standard deviation of these signals is calculated for the original and the HiL scenarios and compared to the standard deviation during periods without SI provision in identical wind conditions.

Table 3 shows that the tower is much less affected than the drive train. In the for–aft direction, scenario 4 leads to the highest increase of the standard deviation for the originally measured signal. However, as scenario 4 represents a fast oscillation of the grid frequency, the effect is strongly reduced by the limitations of the WTG measurement system. When looking at the HiL frequency, the WTG is affected strongest in scenario 8. This scenario is characterized by a sharp increase in the frequency, followed by a longer decline and a longer rise of the frequency, which is well measurable in the HiL test (see Figure 8). Hence, the WTG shortly reduces its power, before it increases it for a longer time (approximately 0.7 s) and then reduces it again. This leads to a change of the WTG thrust, which causes a for–aft motion in the tower. For the side–side acceleration, the changes vary between 0.3% and 13%. Overall, the changes for the tower acceleration are small and can be neglected even for the extreme scenarios used in this study.

Table 3. Change of the standard deviation of the analyzed acceleration signals for six scenarios.

Scenario Number	Tower Head Acceleration (Fore−Aft)		Tower Head Acceleration (Side−Side)		Drive Train Acceleration	
	Meausred Frequency	HiL Frequency	Meausred Frequency	HiL Frequency	Meausred Frequency	HiL Frequency
1	−6.7%	2.9%	2.9%	2.7%	3.5%	8.8%
2	3.2%	0.1%	1.7%	0.8%	133.6%	86.1%
4	18.1%	−0.2%	6.9%	0.3%	204.1%	57.2%
7	0.8%	3.6%	9.5%	13.0%	308.1%	222.4%
8	4.9%	−0.9%	5.7%	4.4%	202.7%	232.9%
10	2.5%	−0.7%	6.7%	6.7%	254.3%	253.2%

In contrast to the tower acceleration, the drive train acceleration is strongly affected by all scenarios apart from scenario 1 (slow oscillation of the grid frequency). In scenario 1, the power setpoint for SI varies slowly and with a smaller magnitude than the power variations arising from the turbulent wind. Hence, the drive train acceleration is only slightly increased. The fast oscillations of the grid frequency (scenarios 2 and 4) lead to a very high increase in the drive train accelerations. However, this increase is strongly reduced for the HiL time traces. The instantaneous peaks in the SI power offset (see Figure 11b, orange line and Figure 10) do not fully show in the generator power (see Figure 11c) as the generator-converter unit changes its operating point with some time delay. Hence, the drive train is less often excited and the speed becomes more stable. This behavior is strongest towards the end of scenario 2 (see Figure 11d). Grid frequency events (scenario 7, 8 and 10) strongly increase the drive train acceleration. For scenarios 8 and 10, there is no relevant difference between the measured and the HiL frequency. For scenario 7, there is a considerable reduction, but the increase remains at a high level. This is in line with the observation that grid frequency events can be captured very well by the WTG measurement system (see Figure 8). Hence, events, as well as fast oscillations, may strongly affect the WTG lifetime. The magnitude of this effect is quantified in the following section.

3.3. Load Analysis

The measurement and control system of each WTG differs and the analysis of the accelerations (see Table 3) shows that the measurement system is likely to reduce the loads of SI provision for the WTG. Hence, following a conservative approach, the originally measured frequencies are used in the load calculation. The loads are calculated for the SI provision case (i.e., for the scenarios listed in Tables 1 and 2). The resulting loads are compared to the loads without SI provision. The calculations are done for two demanded inertia constants: 6 s and 12 s.

For each sensor, the damage equivalent loads (DELs) of the frequency support case are divided by the damage equivalent loads of the reference case. These calculations are performed for various Woehler line exponents as these exponents are material depending (e.g., 4 is the relevant coefficient for steel towers while 10 is used for concrete towers). In addition, the load duration distribution (LDD) is calculated for the drive train to estimate the load increase for the rotating components (e.g., gearbox).

Table 4 shows the results of the load calculations. The data shows that the provision of SI has a negligible effect on the WTG loads. As expected, the highest increase is observed for the torsion in the drive train (sensor MzR1) due to the frequent changes of the generator torque. Furthermore, there are some smaller effects on the tower. There are no significant changes of the DELs for the blades. The increases for the LDD calculations of the drive train are also very small.

Table 4. Load changes for sensors with an increase of more than 0.1% caused by the provision of SI.

Sensor Name [41]	Sensor Description	Calculation Method	Woehler Coefficient	Load Increase, H_{dem} = 6 s	Load Increase, H_{dem} = 12 s
MzR1	Mainbearing torque	DEL	m = 4	0.21%	0.27%
MzR1	Mainbearing torque	DEL	m = 8	0.14%	0.65%
Mx	Tower top torsional moment	DEL	m = 10	0.12%	0.12%
My	Tower bottom fore–aft bending	DEL	m = 4	0.24%	0.20%
Mz	Tower bottom side–side bending	DEL	m = 4	0.17%	0.17%

There are various effects which explain the small increases of the loads, although extreme scenarios have been modelled. The requested power changes are typically very short and are often followed by another pulse in the opposite direction (increases/decreases). Hence, the generator-converter unit does not always reach the new operating point before an opposed signal starts. Therefore, the drive train speed changes little. Even for a longer power pulse, as in scenario 10, the drive train speed only oscillates with an amplitude of 0.02 pu (see Figure 12). Although frequency events occur regularly (2131 expected events per year, see Table 2), each event is only a few seconds long and hence the overall effect on the annual loads is small. Furthermore, the observed oscillations in the grid frequency (see Table 1) are not in the range of the eigenfrequency of the drive train. Hence, there are no resonance issues for the directly affected components of the WTG. This might be different for a different WTG or in a different grid, as the dominant oscillation frequencies are grid-specific [42]. During the simulations for scenario one, there were also no resonance issues for the tower. This can be partially explained by the aerodynamic damping through the wind speed changes for such a slow oscillation and partly by the shape of the time traces of the RoCoF, which only resemble a sinusoidal form (see Figure 9a,b).

There are also controller-related aspects, which explain the small effect on the WTG loads. The variable H controller was designed to make sure that the WTG provides more IR when the grid needs it and the WTG can provide it (i.e., high wind speeds and high instantaneous shares of inverter-based renewables [11]). Hence, during lower wind speeds, which occur regularly for onshore WTG, the WTG provides little IR and experiences and therefore there are also small changes in the loads. The load reduction by using a variable instead of a fixed inertia constant was shown in a previous study [34]. Furthermore, the torque limitation in the controller occasionally prevents an additional power supply by the WTG. While this has a positive effect on the WTG loads, it can be problematic for the grid when such a limitation occurs during a critical state of the grid. This problem is particularly important to overcome, as during high wind periods the grid is most likely to need SI provision from WTGs. During high wind periods, conventional power plants tend to shut down, especially when the high wind period lasts for a day or longer [43]. Hence, there is little conventional inertia in the grid causing a high demand for SI to stabilize the grid frequency. Therefore, WTGs should be able to supply SI reliably in these conditions. The full capability of the WTG to provide SI has to be ensured, e.g., by strengthening the drive train to allow higher torques. That may be achieved by replacing limiting components such as the coupling between the gearbox and the generator. A higher maximum torque is in return likely to increase the loading of the drive train. However, it is still expected be in an order of magnitude, which does not make a complete redesign of the drive train necessary. The peaks in the demanded torque are directly related to calculation method for the RoCoF used in this study. It is chosen to create a worst-case, yet realistic scenario for the WTG. The effect of other methods or parameters on the magnitude of the RoCoF and consequently on the loads resulting from SI provision have not been studied. One critical parameter is the high cut-off frequency of the used LP filter. While this is backed by an ENTSO-E publication [37], the details of the RoCoF calculation still vary between different grid operators. Even in the cited document, different measuring time windows for the

RoCoF calculation are discussed. Any kind of averaging would result in smaller RoCoFs leading to smaller power offsets for SI provision and consequently to smaller maximum torque values. However, such an averaging would also lead to a delayed IR. Whether a faster or a slightly delayed but more robust response is favorable may depend on the particular grid in which SI is to be provided [44]. Hence, this topic is very critical: it may need to be discussed with the individual grid operator and will be investigated further in the future.

4. Conclusions

The effect of SI provision on the loads of a state-of-the-art WTG is shown for comprehensive scenarios, which are based on the measurements of the Indian grid frequency. The detailed scenario definition allows a more realistic assessment of the dynamic excitations from SI provision and the resulting load increases than in previous studies. The study shows that supplying SI is marginally affecting the drive train. Other components of the WTG are de-facto unaffected. Hence, SI provision does not have to be prominently addressed in the load calculation of a WTG, although the RoCoFs of the analyzed grid abnormities are very high and much larger than in previous studies [26–29]. The high RoCoFs are plausible as the Indian grid is considerably weaker than European grids and may therefore serve as an example for a future grid with higher shares of renewables, i.e., grids with little inertia. Furthermore, the RoCoF was calculated for short time intervals, which automatically leads to higher RoCoFs. However, the results are limited to the specific setup of the study as frequency analysis would differ for each grid (e.g., the frequency of inter-area-oscillations differ). This may lead to resonance problems if the eigenfrequencies of the WTG are close to the frequencies of the inter-area-oscillations. In addition, the results depend on the used controller and the design of the WTG. Furthermore, the measurement system of each WTG differs slightly, which would result in differences in the measured frequencies and differences in the SI provision of the WTG. Finally, the effect of an increased torque limitation on the loads is not considered in this study as it depends on the limitations of the new drive train components. However, the load increases are so small and the researched RoCoFs so high, that a different study setup is unlikely to change the results fundamentally.

In addition to the effects on the fatigue loads discussed in this study, SI provision may also lead to generator overspeed in extreme situations (e.g., system splits [39]). This problem may be overcome with a feedforward path to the speed controller. Such a control modification allows us to adapt the pitch angle faster and thus help to mitigate overspeeding due to SI provision. The exact design of the feedforward control is part of future research. Additionally, the effects of different RoCoF calculation methods and filter parameter on peaks of the electrical torque and the consequences for the SI provision will be studied in the future.

Considering all the limitations above, it is concluded that the continuous provision of SI can be achieved with a state-of-the-art WTG without significant effects on the lifetime of the WTG. This may help to stabilize future grids with little inertia.

Author Contributions: A.G.: conceptualization, methodology scenario definition, literature review, data analysis grid frequency, development of SI controller, visualization, writing—original draft preparation; C.J.: conceptualization, development of SI controller, discussions and comments, writing—review and editing; B.C.: conceptualization, methodology and conducting hardware in the loop tests; A.Z. implementation SI controller, conducting WTG simulations for load analysis, writing—review and editing J.W.: provision of data and resources, writing—review and editing. All authors have read and agreed to the published version of the manuscript.

Institutional Review Board Statement: Not applicable.

Informed Consent Statement: Not applicable.

Data Availability Statement: The data used in this study are confidential and are therefore not available to the public.

Conflicts of Interest: The authors declare no conflict of interest.

References

1. EirGrid. EirGrid Grid Code. Version 9. December 2020. Available online: https://www.eirgridgroup.com/site-files/library/EirGrid/GridCodeVersion9.pdf (accessed on 15 January 2021).
2. Hydro-Québec TransÉnergie. Technical Requirements for the Connection of Generating Stations to the Hydro-Québec Transmission System. D-2018-145, January 2019. Available online: http://www.hydroquebec.com/transenergie/fr/commerce/pdf/2_Requirements_generating_stations_D-2018-145_2018-11-15.pdf (accessed on 15 January 2021).
3. Central Electricity Authority. Technical Standards for Connectivity to the Grid (Amendment). 2019. Available online: https://cea.nic.in/wp-content/uploads/2020/02/notified_regulations.pdf (accessed on 15 January 2021).
4. O'Sullivan, J.; Rogers, A.; Flynn, D.; Smith, P.; Mullane, A.; O'Malley, M. Studying the Maximum Instantaneous Non-Synchronous Generation in an Island System—Frequency Stability Challenges in Ireland. *IEEE Trans. Power Syst.* **2014**, *29*, 2943–2951. [CrossRef]
5. Yu, M.; Roscoe, A.J.; Dysko, A.; Booth, C.; Ierna, R.; Zhu, J.; Urdal, H. Instantaneous penetration level limits of non-synchronous devices in the British power system. *IET Renew. Power Gener.* **2017**, *11*, 1211–1217. [CrossRef]
6. Chown, G.; Wright, J.; van Heerden, R.; Coker, M. System inertia and Rate of Change of Frequency (RoCoF) with increasing non-synchronous renewable energy penetration. In Proceedings of the 8th Southern Africa Regional Conference, Cape Town, South Africa, 14–17 November 2017.
7. Díaz-González, F.; Hau, M.; Sumper, A.; Gomis-Bellmunt, O. Participation of wind power plants in system frequency control: Review of grid code requirements and control methods. *Renew. Sustain. Energy Rev.* **2014**, *34*, 551–564. [CrossRef]
8. Eriksson, R.; Modig, N.; Elkington, K. Synthetic inertia versus fast frequency response: A definition. *IET Renew. Power Gener.* **2017**, *12*, 507–514. [CrossRef]
9. Godin, P.; Fischer, M.; Roettgers, H.; Mendonca, A.; Engelken, S. Wind power plant level testing of inertial response with optimised recovery behaviour. *IET Renew. Power Gener.* **2019**, *13*, 676–683. [CrossRef]
10. Ramtharan, G.; Jenkins, N.; Ekanayake, J.B. Frequency support from doubly fed induction generator wind turbines. *IET Renew. Power Gener.* **2007**, *1*, 3. [CrossRef]
11. Gloe, A.; Jauch, C.; Craciun, B.; Winkelmann, J. Limitations for the continuous provision of synthetic inertia with wind turbines. In Proceedings of the 16th Wind Integration Workshop, Berlin, Germany, 25–27 October 2017; pp. 442–447.
12. Manwell, J.F.; McGowan, J.G.; Rogers, A.L. *Wind Energy Explained: Theory, Design and Application*, 2nd ed.; Wiley: Chichester, UK, 2011.
13. Hansen, M.O. *Aerodynamics of Wind Turbines*, 3rd ed.; Routledge: London, UK, 2015. [CrossRef]
14. Hau, E. *Wind Turbines: Fundamentals, Technologies, Application, Economics*, 3rd ed.; Springer: Berlin, Germany, 2013.
15. Fleming, P.A.; Van Wingerden, J.-W.; Scholbrock, A.K.; Van Der Veen, G.; Wright, A.D. Field testing a wind turbine drive-train/tower damper using advanced design and validation techniques. In Proceedings of the 2013 American Control Conference, Washington, DC, USA, 17–19 June 2013; pp. 2227–2234. [CrossRef]
16. Rahim, N.A.; Khyam, M.O.; Li, X.; Pesch, D. Sensor Fusion and State Estimation of IoT Enabled Wind Energy Conversion System. *Sensors* **2019**, *19*, 1566. [CrossRef]
17. Ritter, B.; Schild, A.; Feldt, M.; Konigorski, U. The design of nonlinear observers for wind turbine dynamic state and parameter estimation. *J. Phys. Conf. Ser.* **2016**, *753*, 052029. [CrossRef]
18. Saenz-Aguirre, A.; Zulueta, E.; Fernandez-Gamiz, U.; Ulazia, A.; Teso-Fz-Betoño, D. Performance enhancement of the artificial neural network–based reinforcement learning for wind turbine yaw control. *Wind. Energy* **2019**, *23*, 676–690. [CrossRef]
19. Jie, W.; Jingchun, C.; Lin, Y.; Wenliang, W.; Jian, D. Pitch control of wind turbine based on deep neural network. *IOP Conf. Ser. Earth Environ. Sci.* **2020**, *619*, 012034. [CrossRef]

20. Schlipf, D. *Lidar-Assisted Control Concepts for Wind Turbines*; University of Stuttgart: Stuttgart, Germany, 2016. [CrossRef]

21. Gaur, S.; Elias, S.; Höbbel, T.; Matsagar, V.; Thiele, K. Tuned mass dampers in wind response control of wind turbine with soil-structure interaction. *Soil Dyn. Earthq. Eng.* **2020**, *132*, 106071. [CrossRef]

22. Jauch, C. Grid Services and Stress Reduction with a Flywheel in the Rotor of a Wind Turbine. *Energies* **2021**, *14*, 2556. [CrossRef]

23. Joos, G. Wind turbine generator low voltage ride through requirements and solutions. In Proceedings of the 2008 IEEE Power and Energy Society General Meeting—Conversion and Delivery of Electrical Energy in the 21st Century, Pittsburgh, PA, USA, 20–24 July 2008; pp. 1–7. Available online: http://ieeexplore.ieee.org/document/4596605/ (accessed on 10 February 2021).

24. Wenske, J.; Beckert, U. Voltage-induced stresses during Low-Voltage Ride Through (LVRT) in the drive train of wind turbines with DFIG. *Renew. Energy Power Qual. J.* **2012**, *1*, 1094–1099. [CrossRef]

25. Arbeiter, M.; Hopp, M.; Huhn, M. LVRT Impact on Tower Loads, Drivetrain Torque and Rotational Speed—Measurement Results of a 2-MW Class DFIG Wind Turbine. *Energies* **2021**, *14*, 3539. [CrossRef]

26. Fleming, P.A.; Aho, J.; Buckspan, A.; Ela, E.; Zhang, Y.; Gevorgian, V.; Scholbrock, A.; Pao, L.; Damiani, R. Effects of power reserve control on wind turbine structural loading. *Wind. Energy* **2015**, *19*, 453–469. [CrossRef]

27. Wang, X.; Gao, W.; Scholbrock, A.; Muljadi, E.; Gevorgian, V.; Wang, J.; Yan, W.; Zhang, H. Evaluation of different inertial control methods for variable-speed wind turbines simulated by fatigue, aerodynamic, structures and turbulence (FAST). *IET Renew. Power Gener.* **2017**, *11*, 1534–1544. [CrossRef]

28. Fischer, B.; Shan, M.; Brosche, P.; Loepelmann, P.; Rezaeian, A.; Sayed, M.; Hauptmann, S. Abschlussbericht GridLoads, Kassel, Stuttgart, Technical Report. 2020. Available online: https://www.mesh-engineering.de/images/Publications/MesH/Abschlussbericht_GridLoads_final.pdf (accessed on 17 March 2021).

29. Fischer, B.; Duckwitz, D.; Shan, M.; Sayed, M.; Rezaeian, A. On Interactions of Drive Trains in Wind Farms Providing Power System Inertia. In Proceedings of the Wind Energy Science Conference, Cork, Ireland, 17–20 June 2019. Available online: https://www.researchgate.net/publication/334030049_On_interactions_of_drive_trains_in_wind_farms_providing_power_system_inertia (accessed on 17 March 2021).

30. Øye, S. FLEX4, Simulation of Wind Turbine Dynamics. In *State of the Art of Aeroelastic Codes for Wind Turbine Calculations*; Pedersen, B.M., Ed.; Technical University of Denmark: Lyngby, Denmark, 1996; pp. 71–76.

31. International Electrotechnical Commission. *IEC 61400-1, Wind Energy Generation Systems—Part 1: Design Requirements*; International Electrotechnical Commission: Geneva, Switzerland, 2019.

32. Gloe, A.; Jauch, C.; Craciun, B.; Winkelmann, J. Continuous provision of synthetic inertia with wind turbines: Implications for the wind turbine and for the grid. *IET Renew. Power Gener.* **2019**, *13*, 668–675. [CrossRef]

33. International Electrotechnical Commission. *IEC 61400-21, Wind Energy Generation Systems—Part 21: Measurement and Assessment of Power Quality Characteristics of Grid Connected Wind Turbines*; International Electrotechnical Commission: Geneva, Switzerland, 2008.

34. Gloe, A.; Jauch, C.; Thiesen, H.; Viebeg, J. *Inertial Response Controller Design for a Variable Speed Wind Turbine*; Technical Report; Wind Energy Technology Institute: Flensburg, Germany, 2018.

35. Typhoon HIL. Typhoon HIL602, Product Brochure. Available online: https://www.typhoon-hil.com/doc/products/Typhoon-HIL602-brochure.pdf (accessed on 1 July 2021).

36. Bachmann Electronic. 'System Overview', Product Brochure. 2019. Available online: https://www.bachmann.info/uploads/tx_sbdownloader/systemoverview_11_2019_en.pdf (accessed on 1 July 2021).

37. ENTSO-E. 'Frequency Measurement Requirements and Usage', Final Version 7. 2018. Available online: https://eepublicdownloads.entsoe.eu/clean-documents/SOC%20documents/Regional_Groups_Continental_Europe/2018/TF_Freq_Meas_v7.pdf (accessed on 19 March 2021).

38. Fernández-Guillamón, A.; Gómez-Lázaro, E.; Molina-García, Á. Extensive frequency response and inertia analysis under high renewable energy source integration scenarios: Application to the European interconnected power system. *IET Renew. Power Gener.* **2020**, *14*, 2885–2896. [CrossRef]

39. Gloe, A.; Jauch, C.; Räther, T. Grid Support with Wind Turbines: The Case of the 2019 Blackout in Flensburg. *Energies* **2021**, *14*, 1697. [CrossRef]

40. Jauch, C.; Gloe, A. Simultaneous Inertia Contribution and Optimal Grid Utilization with Wind Turbines. *Energies* **2019**, *12*, 3013. [CrossRef]

41. Sessarego, M.; Ramos-García, N.; Sørensen, J.N.; Shen, W.Z. Development of an aeroelastic code based on three-dimensional viscous-inviscid method for wind turbine computations. *Wind. Energy* **2017**, *20*, 1145–1170. [CrossRef]

42. Domínguez-García, J.L.; Gomis-Bellmunt, O.; Bianchi, F.D.; Sumper, A. Power oscillation damping supported by wind power: A review. *Renew. Sustain. Energy Rev.* **2012**, *16*, 4994–5006. [CrossRef]

43. Matevosyan, J.; Anderson, C.; Li, W. ERCOT Future Synchronous Inertia Projections. In Proceedings of the 16th Wind Integration Workshop, Berlin, Germany, 25–27 October 2017.

44. Miller, N.; Pajic, S. Diverse fast frequency response services in systems with declining synchronous inertia. In Proceedings of the 15th Wind Integration Workshop, Vienna, Austria, 15–17 November 2016.

Publication 4

Grid Support with Wind Turbines: The Case of the 2019 Blackout in Flensburg

Article

Grid Support with Wind Turbines: The Case of the 2019 Blackout in Flensburg

Arne Gloe [1,*], Clemens Jauch [1] and Thomas Räther [2]

1   Wind Energy Technology Institute, Flensburg University of Applied Sciences, 24943 Flensburg, Germany; clemens.jauch@hs-flensburg.de

2   Stadtwerke Flensburg GmbH, Grids, 24939 Flensburg, Germany; thomas.raether@stadtwerke-flensburg.de

*   Correspondence: arne.gloe@hs-flensburg.de

Abstract: The work presented in this paper aims to show how modern wind turbines can help to control the frequency in a small grid which suffers from large power imbalances. It is shown for an exemplary situation, which occurred in Flensburg's distribution grid in 2019: a major blackout, which occurred after almost two hours in islanding operation, affecting almost the entire distribution grid, which supplies approximately 55,000 households and businesses. For the analysis, a wind turbine model and a grid support controller developed at the Wind Energy Technology Institute are combined with real measurements from the day of the blackout to generate a fictional yet realistic case study for such an islanding situation. For this case study, it is assumed that wind turbines with grid support functionalities are connected to the medium voltage distribution grid of the city. It is shown to what extent wind turbines can help to operate the grid by providing grid frequency support in two ways: By supplying synthetic inertia only, where the wind turbines can help to limit the rate of change of frequency in the islanded grid directly after losing the connection to the central European grid. In combination with the primary frequency control capabilities of the wind turbines (WTs), the disconnection of one gen set in the local power station might have been avoided. Furthermore, wind turbines with primary frequency control capabilities could have restored the grid frequency to 50 Hz shortly after the islanding situation even if the aforementioned gen-set was lost. This would have allowed connecting a backup medium voltage line to the central European grid and thereby avoiding the blackout.

Keywords: system split; blackout; frequency support; wind turbines; synthetic inertia; primary frequency control

1. Introduction

Modern power systems with high penetration of inverter-based renewables are bound to exhibit little system inertia [1]. To avoid unfavorable excursions of the grid frequency and high rates of change of frequency (RoCoFs), system operators will require the provision of grid frequency support from renewables. Such grid support is already mandatory in some grids for instance in Ireland [2], Québec [3], or India [4]. To fulfill these requirements, wind turbine (WT) manufacturers, as well as academics, have developed various methods of grid support for WTs. Control options developed by manufacturers are usually tailored to the needs of a specific grid (e.g., Enercon for Hydro-Québec [5]) while academia follows a more general approach. A good overview of current control strategies to provide synthetic inertia and primary frequency response is given by Díaz-González et al. [6] and by Fernández-Guillamón et al. [7]. In an electrical grid large power imbalances i.e., the difference between generation and consumption, can cause heavy excursions of the grid frequency. Such contingencies may be caused by the failure of a large power plant, a large line but also by a system split. The ENTSO-E regards a system split as a major threat for the continental European grid [8]. In case of a system split, the power imbalances may reach up to 40%

of the generated power [9]. Just recently the European grid was split into two parts during which a blackout could be avoided [10]. However, a system split may cause a devastating blackout as in Italy 2003 (affecting 56 Million people) [11]. Blackouts may also be triggered by a combination of market effects and technical problems as recently seen in Texas [12]. In addition to technical solutions, a different market design may also help to mitigate such imbalance situations: Borowski [13] proposes a different model for the electricity market which may send price signals depending on the local situation and thus helping during times of high imbalances. Blackouts may have devastating economic effects: Yamashita et al. report a range for the lost gross domestic product between \$3.53 and \$39.7 for every undelivered kWh [14].

System splits may also occur locally, leaving a local, islanded grid without connection to the rest of the system. Such an incident occurred in Flensburg on 9 January 2019. On that morning, Flensburg's electricity demand was covered by two coal-fired gen sets (Generator 7 & 9) and one combined cycle gen set in the local power station, of the latter only the gas-fired gen-set (Generator 12) was connected to the grid (see Figure 1).
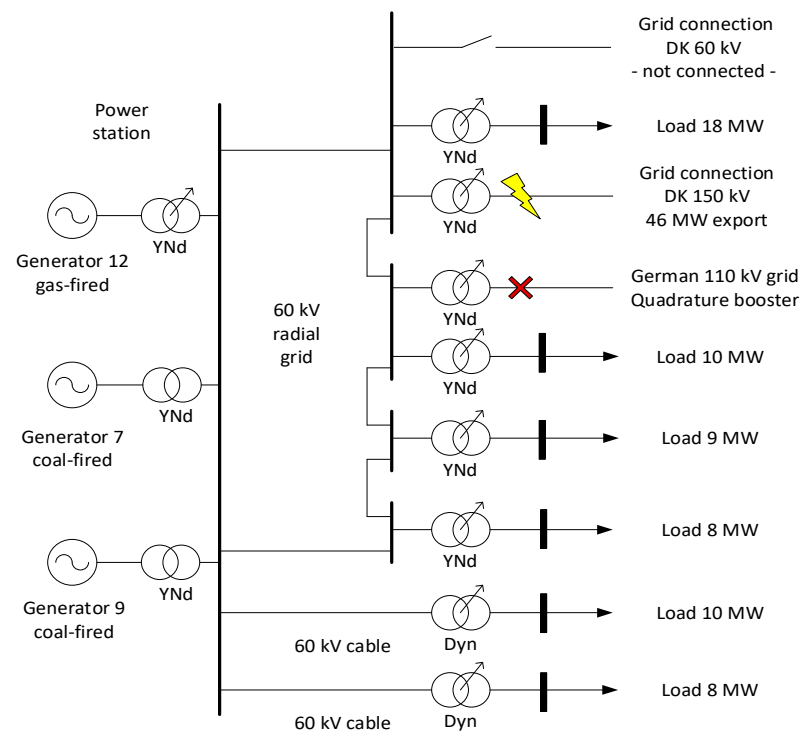
Figure 1. Schematic depiction of the distribution grid in Flensburg, the connected generators, export lines, and the aggregated loads shortly before the blackout on 9 January 2019.

Stadtwerke Flensburg (SWFL) operates the power station as well as the distribution grid in Flensburg. While exporting a large share of the generated power to Denmark, the connection to the Danish grid was lost due to a cable failure. Consequently, the connection to the German grid was also lost, leaving the islanded grid with a large power surplus. This caused a strong acceleration of the generator rotors resulting in a high RoCoF (see Figure 2b), which in return triggered protection systems of Generator 12. Such a combination of an initial event and following failures of other grid components has been often observed during a major blackout in the past [14].
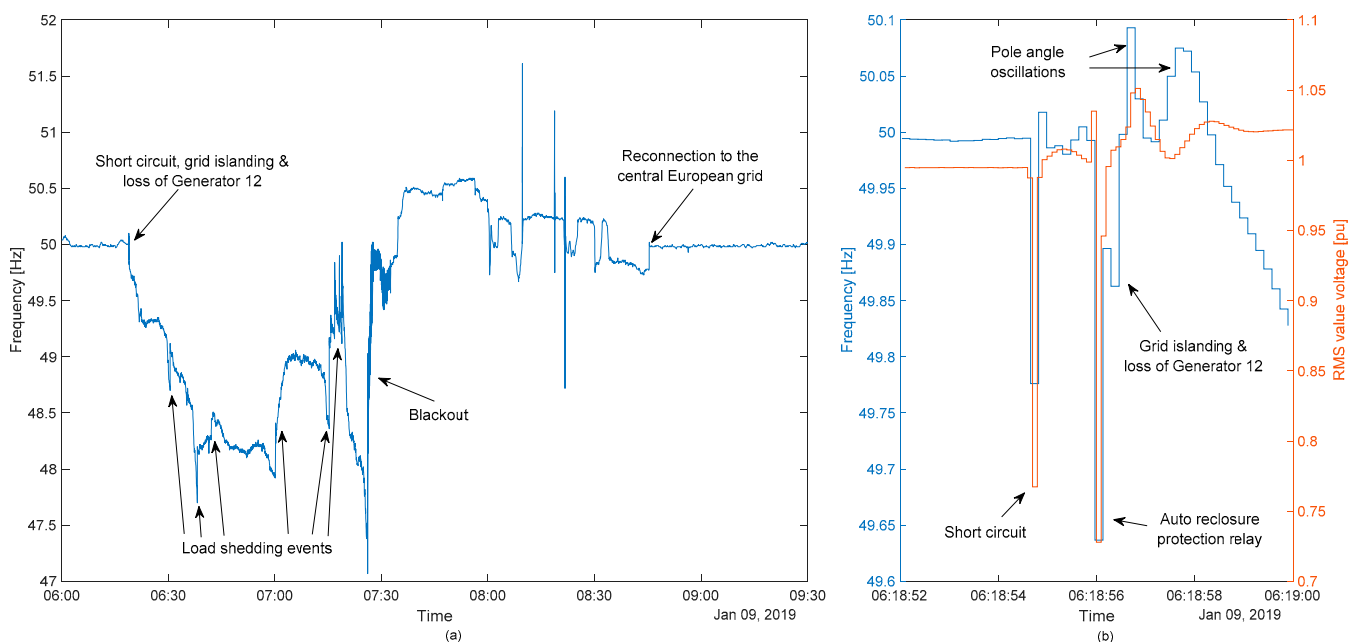
Figure 2. (**a**) Grid frequency measured at the Flensburg power station on 9 January 2019. (**b**) Grid frequency and root mean square (RMS) value of the grid voltage measured at the Wind Energy Technology Institute (WETI) during the initial event on 9 January 2019.

Loosing Generator 12 was problematic as this generator unlike the two remaining generators is capable of providing primary frequency control (PFC). The loss of Generator 12 and the increase of the electricity consumption in the morning hours caused a power deficit. Consequently, the grid frequency slowly (see Figure 2a). Over the next 75 min, the SWFL used cascaded load shedding for parts of the city to stabilize the frequency but eventually had to disconnect almost all remaining customers from the grid. After stabilizing the grid frequency, a backup connection to Denmark was engaged to reconnect to the central European grid and to end the blackout, approximately three hours after the initial incident (see Figure 2a).

This paper investigates whether wind turbines (WTs) with grid support capabilities would have been able to prevent the blackout. For this purpose, it is assumed that WTs would have generated a part of the electricity on 9 January 2019; the power plant's production would have been accordingly lower. In three different scenarios, the WTs would be equipped with different functionalities to support the grid frequency. The goal is to avoid the blackout either by keeping Generator 12 synchronized with the grid or by a fast reconnection via the back-up line to the Danish 60 kV grid.

There is plenty of literature on grid support with WTs. However, these publications usually test the developed controller with reference cases (e.g., [15]) or focus on a comprehensive study of grid behavior rather than the WT behavior [16]. Ela et al. study the WT dynamics during system disturbances with measured data but the considered data lacks the severity of a blackout event [17]. Therefore, this paper aims to close this gap by using real data of a severe incident in combination with a reasonable model to study the WT dynamics. Furthermore, the performance of the variable H controller developed at the Wind Energy Technology Institute (WETI) is shown during a localized event in a small grid. This allows not only accessing the control performance with respect to the WT but also with respect to grid frequency stabilization with little uncertainty for the wind conditions and grid participants.

Section 2 of this paper describes the used WT model, the controller capabilities, and the applied grid model. Furthermore, the blackout event and the simulated scenarios are described in detail. Section 3 presents and discusses the simulation results. Section 4 summarizes the findings.

2. Materials and Methods

2.1. Detailed Description of the Blackout

Historically, the local grid in Flensburg has a strong connection to the Danish grid via a large 150 kV cable/line connection to the Aabenraa power station. Furthermore, there is a 110 kV connection to the German grid via one phase angle regulating transformer (quadrature booster) and a 60 kV back-up connection to the Danish distribution grid (see Figure 1). The power station in the city consists of four gen-sets: three coal-fired steam turbines and one combined cycle gas turbine.

In the early hours of 9 January 2019, approximately 57% of the generated electricity was consumed in the city while the rest was exported to Denmark via the aforementioned 150 kV cable-line connection (see Figure 1). Generator 7 & 9 (coal-fired) and Generator 12 (gas-fired) produced the power.

At 06:18:55 there was a short-circuit between one of the phases in the 150 kV cable and earth. Protection relays triggered and isolated the faulty phase immediately (see Figure 2b). Approximately one second later an automatic reclose of the circuit breakers was attempted. As the short-circuit remained, the complete 150 kV cable was isolated by automatically opening the circuit breakers (see Figure 2b). Consequently, the connection to the German high-voltage grid was also lost and the distribution grid worked as an islanded grid with a massive surplus (approximately 43%) of generated power. This caused a strong acceleration of the generator rotors resulting in a high RoCoF (up to 1.8 Hz/s), which in return triggered protection systems of Generator 12. Hence, Generator12 disconnected itself from the grid approximately 70 ms after losing the 150 kV connection to Denmark. The sudden changes of the electrical torque caused oscillations in the generator rotors of the two remaining generators as typical for a directly connected synchronous generator after a sudden change of the operating point [18]. As Generator 7 & 9 did not work at rated active power at the moment of islanding, their power could be increased (see Table 1). This allowed stabilizing the frequency for some time (see Figure 2a). However, after approximately 15 min the electricity demand rose so much that cascaded load shedding was inevitable. The exact load shedding sequence is described in Thiesen and Jauch [19].

Table 1. Specifications and operating points of the generator and the local consumers.

Grid Participants	Power at Moment of Islanding	Rated Power	Inertia [1]	Number of Pole Pairs
Generator 7 (coal-fired gen-set)	29.6 MW	33 MW	2293 kg·m^2	1
Generator 9 (coal-fired gen-set)	31.3 MW	36 MW	2223 kg·m^2	1
Generator 12 (gas-fired gen-set)	49.1 MW	49 MW	7320 kg·m^2 (referred to grid speed)	2
Local consumers	63 MW	-	1216 kg·m^2	-
Power export	47 MW	-	-	-

[1] The sources of the reported inertias are described in Section 2.3.1.

After the cascaded load shedding did not decrease the power demand sufficiently to increase the grid frequency back to 50 Hz, the SWFL disconnected almost the entire city. In the next 80 min, the operating points of the generators were adjusted such that the grid frequency eventually stabilized and the 60 kV back-up connection to Denmark could be engaged to resynchronize with the central European grid. In this paper, three strategies are researched, which could have helped to avoid the blackout. All scenarios work with a fictive case in which part of the power in the islanded system is produced by WTs instead of by the fossil-fueled power station:

- Scenario I: WTs supplying synthetic inertia (SI) could have lowered the high RoCoF, which occurred immediately after the system split. This might have kept the gas-fired gen-set connected to the grid and thereby the grid frequency could have been controlled because Generator 12 is capable of PFC.
- Scenario II: As in scenario I, the goal is to keep Generator 12 connected to the grid. In addition to scenario I, the WTs also supply PFC. As there was an excess of power in the islanded grid the WTs could have reduced their power rapidly and thus allowing a longer reaction time for Generator 12 than in scenario I.
- Scenario III: In this scenario, losing Generator 12 is accepted. The goal is to increase the grid frequency back to 50 Hz in the first minutes after the system split and keep it there long enough to allow a reconnection with the central European grid via the 60 kV back-up connection to Denmark (see Figure 1). To achieve that the WTs must be able to provide PFC and they must be curtailed before the event. This scenario is similar to the situation in Ireland, where the system operator is allowed to require such curtailment during times of volatile grid frequency [2]. WT curtailment due to feed-in management is common in the federal state surrounding Flensburg [20]. Hence, in strong wind conditions, some level of curtailment is to be expected, which may be used for PFC provision. As in scenarios I & II, the WTs also provide SI.

2.2. Grid Model, Wind Turbine Model, and Frequency Support Controller

The behavior of the WT, its capability to provide frequency support in extreme situations, and the consequences for the WTs are the focus of this paper. Hence, a complex model of the WT is used in combination with a simple model of the grid for representing the behavior of the grid frequency.

2.2.1. Grid Model

In an AC power system, the grid frequency depends on the balance of generated and consumed power as well as the inertia of the grid [18]. The relation can be expressed by the so-called swing equation:

$$\frac{\delta f_{grid,t}}{\delta t} = \frac{P_{gen,t} - P_{load,t}}{4 \, \pi^2 \cdot f_{grid,t} \cdot J_{grid,t}} \tag{1}$$

where $\delta f_{grid,t}/\delta t$ is the RoCoF, $P_{gen,t}$ is the sum of all generated (and imported) power, $P_{load,t}$ is the sum of all consumed (and exported) power, $f_{grid,t}$ is the grid frequency and J_{grid} is the sum of the inertia of all grid participants. The generation and consumption changes constantly. By contrast, the grid frequency changes typically only in a small interval (in extreme cases $+/- 800$ mHz [9]) and is therefore almost constant. The grid inertia changes only whenever grid participants (generators or rotating loads) are connected or disconnected. Furthermore, a self-regulation factor is considered for the loads: its power changes with 2%/Hz which is in line with ENTSO-E recommendations [9].

2.2.2. Wind Turbine Model and Frequency Support Controller

The WTs are simulated with the so-called 1st eigenmodes model developed at the WETI [21]. The model allows simulating the most important degrees of freedom of a WT, i.e., two-directional motions of tower and blades, as well as the torsional movement of the drive train. The flywheel in the model of the WT rotor [21] is disabled, such that the model represents a state-of-the-art WT. Furthermore, the power controller is adapted as described below to allow providing SI with the variable-H controller [22] and PFC as defined in the Irish grid code [2]. In this study, the parameters of the NREL 5 MW research WT are used [23].

The power controller of the WT is modified to allow SI and PFC provision (see Figure 3). Hence, the power reference for the WT is calculated using three terms as explained below (see also three shaded areas in Figure 3).
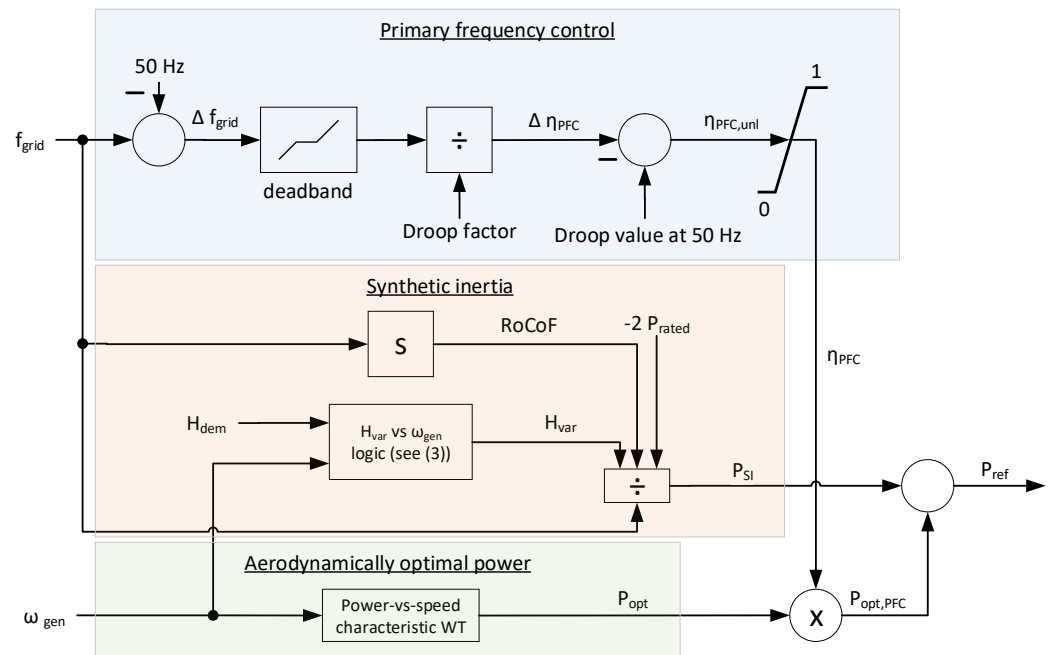
Figure 3. Block diagram of the power reference for the WT including grid frequency support (primary frequency control (PFC) and synthetic inertia (SI)).

- Power-vs-speed characteristic: If a WT operates in part load, there is an optimal combination of generator speed and generator power to maximize the aerodynamic performance of the WT. If all grid support functionalities are disabled, the power setpoint of the WT is determined by the optimal power (P_{opt}).
- SI provision: Whenever a non-zero RoCoF is detected the WT alters its power output from the optimal aerodynamic value to support the grid frequency. To provide a reliable SI provision and safe operation of the WT the variable H controller is used [22]. The power change is described by Equation (2) [22]:

$$P_{SI} = -2 \cdot H_{var} \cdot P_{rated} \cdot \frac{RoCoF}{f_{grid}} \qquad (2)$$

where P_{SI} is the power change for SI, H_{var} is the variable inertia constant and P_{rated} is the rated power of the WT. The variable inertia constant scales with the operating point of the WT in accordance with the available kinetic energy stored in its rotation (see (3); [22]).

$$H_{var} = H_{dem} \cdot \frac{0.5 \cdot J_{WT} \cdot \left(\omega_{gen}^2 - \omega_{cut-in}^2 \right)}{0.5 \cdot J_{WT} \cdot \left(\omega_{rated}^2 - \omega_{cut-in}^2 \right)} \qquad (3)$$

where H_{dem} is the inertia constant to be emulated as defined by the grid operator, ω_{gen} is the generator speed, ω_{cut-in} is the generator speed at which the WT starts to produce power, and ω_{rated} is the rated generator speed of the WT.

Figure 4a depicts the transient behavior of the WT during a negative RoCoF event. The WT leaves the steady-state value (point 1) by producing additional power (point 2). As the electrical power is temporarily higher than the aerodynamic power, the WT uses some of the kinetic energy stored in its rotation and the generator slows down (point 3). The power output of the WT is still higher than the optimal value according to the power-vs-speed characteristic but not necessarily higher than in point 1. When SI is no longer needed the WT falls back to the power-vs-speed characteristic (point 4). Assuming stable wind conditions the WT would return to point 1 as the aerodynamic power is now higher than the electrical power. Obviously, the exact behavior of the WT

depends on several factors, most prominently the wind conditions and the severity of the frequency event. More detailed explanations of the aerodynamics during the transient operation of the WT can be found in [22].

- PFC: In addition to SI, the WT also provides PFC for scenarios II & III. The controller is modeled based on the requirements in the Irish grid code during frequency-sensitive mode [2]. The grid operator is allowed to curtail the WTs to a certain percentage of the available power. This allows increasing the power output of the WT whenever the grid frequency drops below the insensitivity band (see Figure 5). The curtailment of the WTs is lowered in accordance with the so-called droop characteristic. For high frequencies, the curtailment is increased. The curtailment factor resulting from this power-vs-frequency characteristic is hereafter called η_{PFC} and is used to scale the output of the power-vs-speed characteristic. When the WT is curtailed in part-load operation, a prolonged curtailment will cause the WT to run at super optimal speed as the aerodynamic power exceeds the electrical power (see the shaded area in Figure 4b). Furthermore, a prolonged curtailment imposes a significant financial burden on the WT operator due to the lower energy yield.
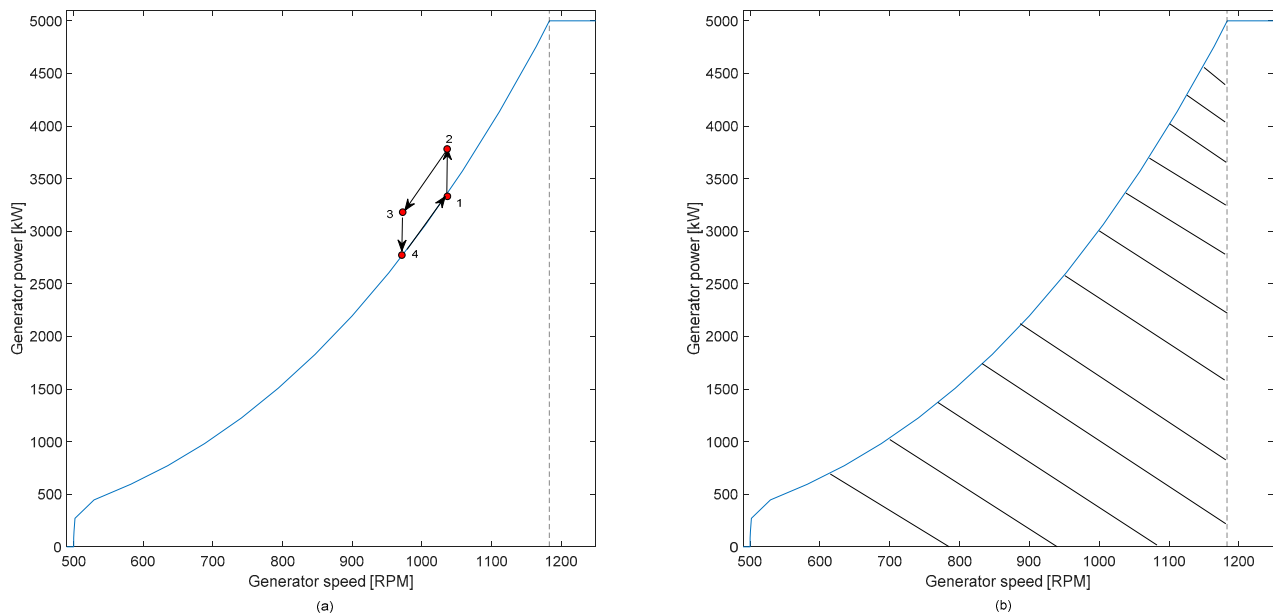
Figure 4. Power-vs-speed characteristic (blue line) of the NREL 5 MW wind turbine (WT) [23]. (**a**) The black quadrangle depicts the transient behavior of the WT when supplying SI. (**b**) The black shaded area depicts typical operating points of the WT when operating in curtailed mode with the simulated PFC controller.

When the grid frequency support is activated, the power reference of the WT, P_{ref}, is calculated as a combination of the three effects described above: (see (4) and Figure 3):

$$P_{ref} = P_{opt} \cdot \eta_{PFC} + P_{\mathrm{SI}} \tag{4}$$

The PI controller is used to derive the setpoint for the generator-converter model (PT1 element) from the power reference (see Figure 6 and [24]). The parameters for the generator-converter model and the PI power controller are taken from [24].
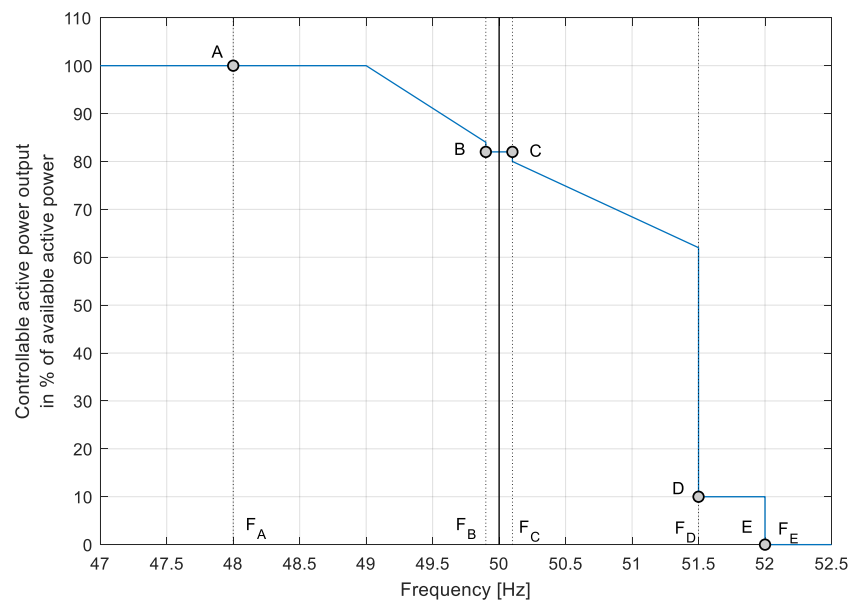
Figure 5. PFC requirements during frequency sensitive mode in the Irish grid code [2].
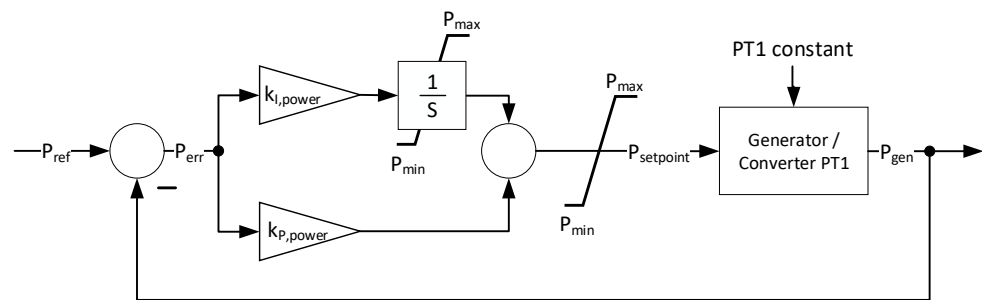

Figure 6. Block diagram of the power controller and the generator-converter model.

2.3. Detailed Scenario Description and Used Data

For the scenario development, data provided by the SWFL are combined with measurements taken at WETI. Table 2 gives an overview of the settings used in the different scenarios. The simulations for scenarios I & II start shortly before the initial short-circuit (see Figure 2b). By contrast, scenario III starts after the transient phase of the grid frequency (see Figure 2b), as the frequency measurement is unreliable during the voltage dips [25] and afterward dominated by the pole angle oscillations.

The assessment criteria for the three scenarios are:

- Scenario I: the instantaneous RoCoF falls below 1 Hz/s within 70 ms.
- Scenario II: the instantaneous RoCoF falls below 1 Hz/s within 70 ms & the grid frequency stays below 51.5 Hz for at least 30 s.
- Scenario III: the grid frequency can be increased to 50 Hz and be stabilized within 50 Hz +/− 10 mHz for as long as possible.

For all scenarios, various simulations were conducted to define the minimum number of WTs, which still allowed fulfilling the assessment criteria (see Table 2). To fulfill these criteria, the WTs have to provide a high share of the power production in scenarios I & II. The simulation time is adapted to the assessment criteria of the scenarios. In addition, the effect of the frequency support on the WTs are shown.

Table 2. Overview of simulated scenarios and the used simulation and controller settings.

Category	Scenario I	Scenario II	Scenario III
Scenario goal	Keep Generator 12 connected to the grid	Keep Generator 12 connected to the grid	Stabilize f_{grid} close to 50 Hz
Assessment criteria	Time until RoCoF falls below 1 Hz/s	Time until frequency reaches 51.5 Hz	Time until frequency reaches 49.99 Hz Time within frequency insensitivity 50 Hz $+/-$ 10 mHz
Active controller	SI	SI & PFC	SI & PFC
Simulation time	20 s	60 s	200 s
Power imbalance	Power export of lost export line	Power export of lost export line	Calculated from grid frequency measurements
Grid inertia	13,052 kg·m^2	13,052 kg·m^2	5732 kg·m^2
Number of WTs	8	10	2
Share of WTs in power production	35%	44%	15%
Wind characteristic	turbulent	turbulent	turbulent
Average wind speed	13 m/s	13 m/s	13 m/s
Turbulence intensity	12%	12%	12%
H_{dem}	12 s	12 s	12 s
Curtailment factor η_{PFC} before event	Not used	1 (no curtailment)	0.9
Droop factor	Not used	2%	2%
Frequency insensitivity	Not used	10 mHz	0 mHz

2.3.1. Scenario Inputs

For each scenario, the power imbalance (i.e., the imbalance before the fictional WT power is added) and the grid inertia must be defined to solve (1), which allows calculating the grid frequency. Furthermore, the wind inputs must be defined.

The inertias of Generator 7 & 9 as listed in Table 1 are known from technical documentation provided by SWFL. This is also true for the inertia of the generator rotor of Generator 12. However, the inertia of the gas turbine had to be estimated with help of the known weight [26] and an assumed distance of the mass center to the rotational axis. The estimated inertia constant for the gas-fired gen-set (5.9 s) is in line with inertia values of gas-fired gen-sets reported in the literature [27]. The inertia provided by the loads is known from Thiesen and Jauch [19].

While the power production of the different generators at the power station is well known, there is a lot of uncertainty in the data for the loads. The data of the current measurements are mainly taken on the low-voltage side of the controllable transformer (see Figure 1) while the voltage measurements are taken on the high voltage side. Hence, the power imbalance cannot be calculated from the power calculated using these measurements. However, the power export is exactly known and can be used as an initial power imbalance for scenarios I & II. The power imbalance occurs once the export line to Denmark is fully disconnected (second nadir in the voltage measurements in Figure 2b). A constant power imbalance assumes that the power of the generators and the loads remain constant during the simulation. This is a conservative approach: a PFC power adjustment of Generator 12 as well as self-regulation of the loads would decrease the power imbalance and help to stabilize the grid frequency.

For scenario III, the self-regulation of the loads would hinder bringing the grid frequency back to 50 Hz. Hence, the load must be calculated from the available data and scaled with the grid frequency during the simulation. In a first step, the power imbalance can be calculated with the known grid inertia and the frequency measurements taken at WETI (f_{meas}) by solving (1) for the power imbalance. As the power production of Generator 7 & 9 is directly measured, the load is given as the difference between the total power production and the power imbalance (see (5) and Figure 7). Figure 7 shows how slowly the

frequency declines. Hence, the calculated load power is most of the time slightly higher than the generator power but also falls below it occasionally.

$$P_{load,t} = P_{gen,t} - \frac{f_{f_{meas,\,t+1}} - f_{f_{meas,\,t}}}{\Delta t} \cdot 4\,\pi^2 \cdot f_{meas,t} \cdot J^J_{grid,t} \tag{5}$$
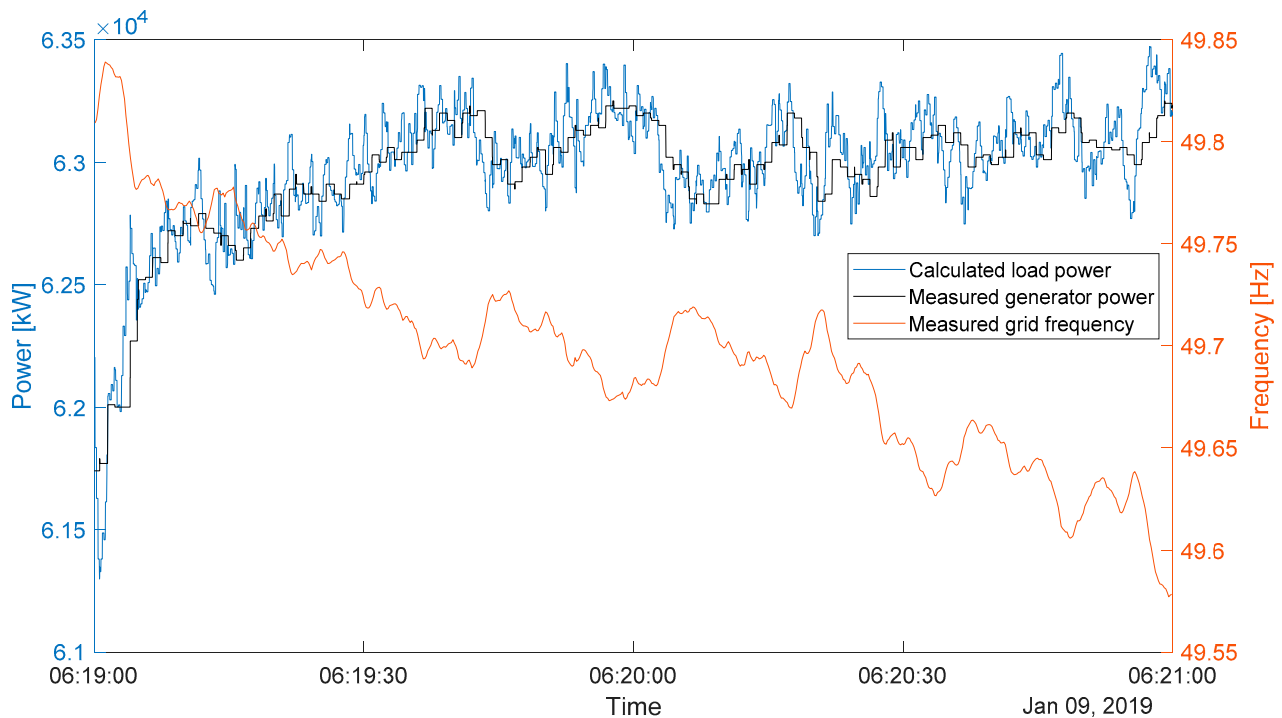
Figure 7. Example of the load power, calculated with the measured generator power and the grid frequency measured at WETI.

Data provided by German Metrological Service, Deutscher Wetterdienst, is used to model the wind conditions in Flensburg on 9 January 2019. The hourly mean wind speed at the time of the system split was 7.9 m/s in 10 m height [28]. The wind speed at hub height can be calculated with a logarithmic wind profile [29]. It is assumed that the roughness length, z_0, is 0.35 m, which is a reasonable value for the landscape and topography in the area around Flensburg [29]. Using this data the mean wind speed at the hub height (90 m) is 13 m/s. Furthermore, the turbulence intensity is assumed 0.12, which is also a reasonable value for the region. In a previous project, the measured turbulence intensity for 13 m/s average wind speed at the campus in the outskirts of Flensburg was 0.17 (based on the measurements in 50 m height) [30]. In the same project, the roughness length for the site was estimated at 1.7 m, which is a very turbulent site. Hence, the lower TI is reasonable due to the higher hub height [31] and the lower turbulence, which can be expected outside the city. Individual WTs are simulated by using independent turbulence seeds for each WT.

Currently, there is no large-scale WT directly connected to Flensburg's distribution grid. Therefore, the analyzed scenarios are fictional. However, as the distribution grid also comprises some of the surrounding villages and dwellings, it seems feasible that WTs could be connected to the grid. Currently, there are several WTs with 25 MW installed capacity within a 10 km radius around the city center [32]. Furthermore, the installation of an additional 25 MW is planned [32]. These WTs are connected to a different medium voltage grid but show the potential for WT installations in close proximity to the city with cable length comparable to the ones in the existing grid.

2.3.2. Controller and Simulation Settings

For the frequency support controller, some settings must be chosen which are in reality defined by the transmission system operator. A reasonable approach is to choose an inertia constant, which the WTs have to emulate, in a similar range of fossil-fueled or hydroelectric power stations [33]. However, with increasing penetration of non-synchronous generation, higher inertia constants may need to be demanded to safely operate a grid in challenging situations [34]. It has also been shown that WTs can be safely operated with emulated inertia constants as high as 6 s [35] or even 12 s [24]. For this study, the demanded inertia constant was set to 12 s, which is in line with the aforementioned [24] and the findings in [34] for such high power imbalances.

Reducing the RoCoF to a value below 1 Hz/s in such a short time (100 ms) is very difficult, as the WTs have to react very fast. While the generator-converter-units have a very fast reaction time, the PI controller naturally dampens such drastic power changes. When the original settings as reported in [24] are used, the behavior of the PI controller is dominated by the anti-wind-up (AWU) loop of the integrator. Therefore, the power of the WT falls too slow to reduce the RoCoF below the threshold in the designated time. The original AWU considers the proportional controller output when limiting the integrator, such that the sum of the proportional and integral terms is the minimum power, P_{min} (0 W). This has been changed such that the integrator is set to P_{min}. As the sum of the proportional and integral terms can be negative, the limiter adjusts the controller output in such cases (see Figure 6).

The PFC controller settings are chosen in accordance with the requirements stated in the Irish grid code [2]. It has to be noted that these settings can change during the operation of the WTs depending on the status of the grid [2]. Especially the curtailment factor η_{PFC} valid for 50 Hz is adopted depending on the expected grid situation. Hence, a curtailment of the WTs as needed for scenario III would only be present in specific situations, when the grid is vulnerable. However, WTs can also be curtailed for other reasons, e.g., feed-in management, which occurs regularly in the federal state surrounding Flensburg [20]. Hence, some level of curtailment would have been likely considering the strong wind conditions on the day of the blackout even though the grid islanding was not foreseeable. In the third scenario of this study, the WTs were curtailed to 90% of the available power before the frequency event happened. For scenario II, no curtailment is needed as the power output has to be reduced to provide PFC. The droop factor is set to 2%, which is on the lower end of the range mentioned in [2] and [36] and causes a strong reaction to frequency deviations. The frequency insensitivity, i.e., the minimum detected deviation of the grid frequency for the controller to react, is set to 10 mHz [36] in scenario II and to 0 mHz in scenario III to facilitate bringing back the grid frequency to 50 Hz in the latter scenario.

3. Results

The results of the simulations show that it is theoretically possible to achieve the assessment criteria of the three scenarios with help of WTs. The results are discussed individually for each scenario below.

3.1. Scenario I

In this scenario, the eight simulated WTs lower the RoCoF below the 1 Hz/s threshold within 17 ms by reducing their power output (see Figure 8a–d). Hence, the RoCoF threshold could be reached in time even considering a time delay for detecting the frequency event due to measurement and signal processing delays in the WT. However, as the WTs only provide SI, the frequency support is not sufficient to stop the rise of the grid frequency. Hence, Generator 12 is likely to disconnect from the grid as soon as the grid frequency reaches 51.5 Hz approximately 1.5 s after the start of the islanding event (see Figure 8e,f). This time is obviously too short for the gas-fired gen set to activate its own frequency support.
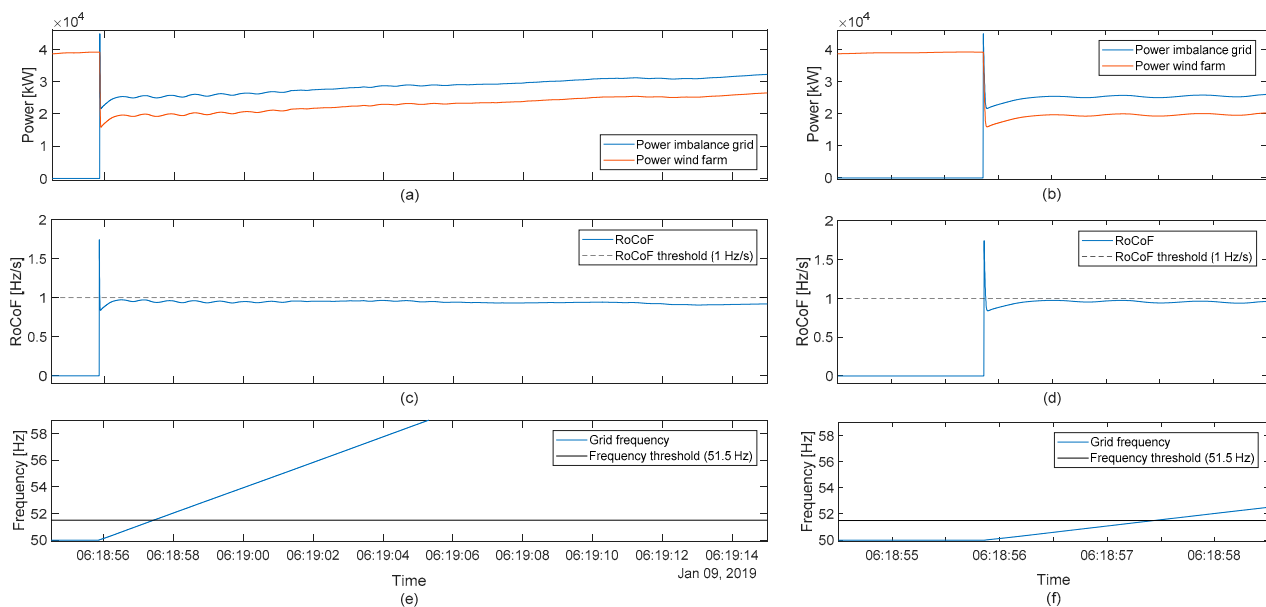
Figure 8. Results of scenario I: Power imbalance in the islanded grid and power of the simulated wind farm for (**a**) the full simulation time and (**b**) a zoom to the time of the event; (**c**,**d**) RoCoF and RoCoF threshold; (**e**,**f**) grid frequency and frequency threshold. Time axes of (**e**,**f**) are valid for the above subplots as well.

The massive frequency support provides a heavy burden for the drive trains of the WTs. The almost instantaneous power reduction causes a strong temporary imbalance between the accelerating aerodynamic torque and the decelerating electrical torque. Hence, the generator speed rises rapidly and starts to oscillate with the 1st torsional eigenfrequency of the drive train (see Figure 9b). As a result, the pitch angle also oscillates. These oscillations last for approximately 10 s with decreasing magnitude. As the power setpoint of the WT is linked to the generator speed, the WT power also oscillates (see Figure 9b).

Furthermore, the WT is at risk of shutting down due to overspeed. A typical value for the allowed overspeed is in the range of 10% [30,35] and is marked in Figure 9b. The shown WT experienced a gust shortly before the event. Hence, the generator speed is already high and the pitch not at a steady-state value when the frequency support is demanded. As a result, the generator speed instantaneously exceeds the overspeed threshold. As this occurs only for various milliseconds, the WT would probably stay connected to the grid, which is favorable for a reliable frequency response [22]. For WT 5, 6 & WT 8 however, the power reduction coincides with stronger gusts causing longer periods of overspeed (see Figure 10 and Table 3). Depending on the settings in the WTs safety systems, this may cause an emergency stop of the WTs. Figure 10 also depicts the simulation results of the least affected WT 2. It is clearly visible how the negative gust at the time of the frequency event helps to avoid an extreme overspeed situation.

3.2. Scenario II

For scenario II, PFC is activated and the number of grid-connected WTs is raised to ten to keep the grid frequency below 51.5 Hz. As in scenario I, the RoCoF is pushed below the 1 Hz/s threshold in time by a rapid reduction of the power of the wind farm (i.e., 16 ms, see Figure 11a–d). As the power reduction persists, the grid frequency is stabilized within a few seconds and stays stable during the rest of the simulation (see Figure 11e,f).
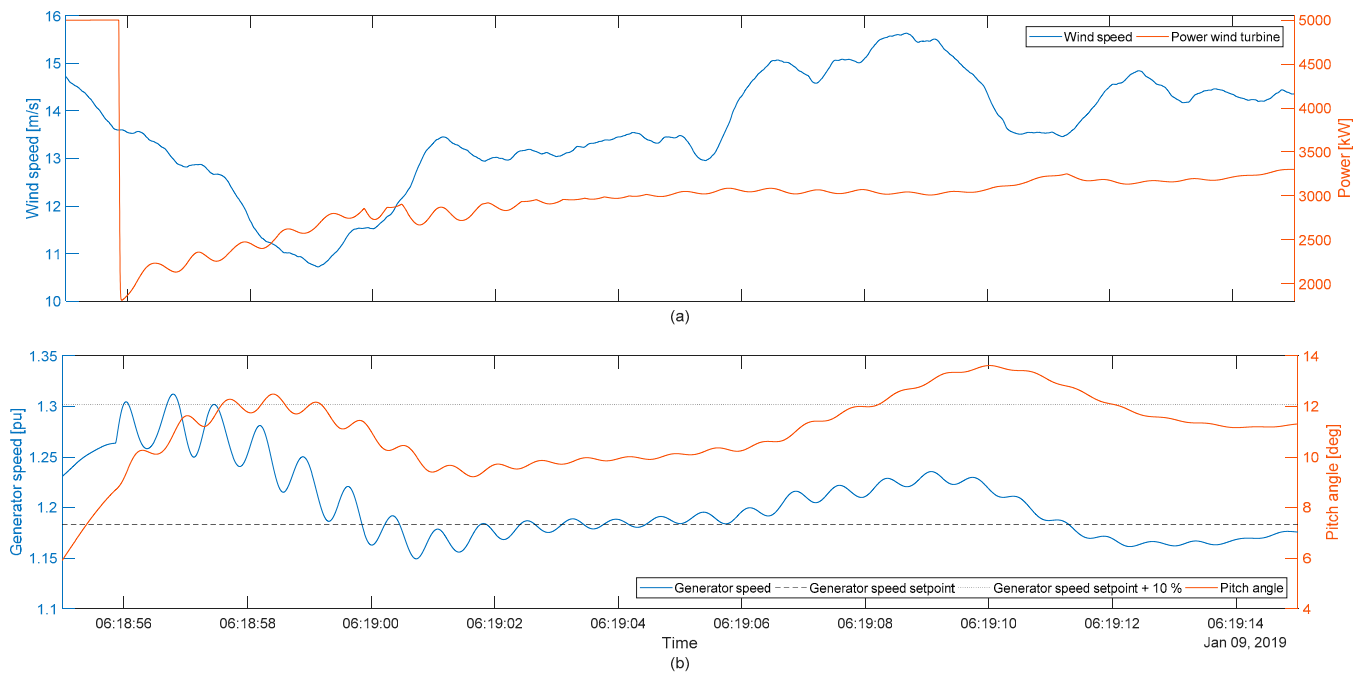
Figure 9. Results of scenario I for the 1st simulated WT: (**a**) Wind speed at hub height and electrical power of the WT; (**b**) generator speed, speed setpoint, overspeed threshold and pitch angle.
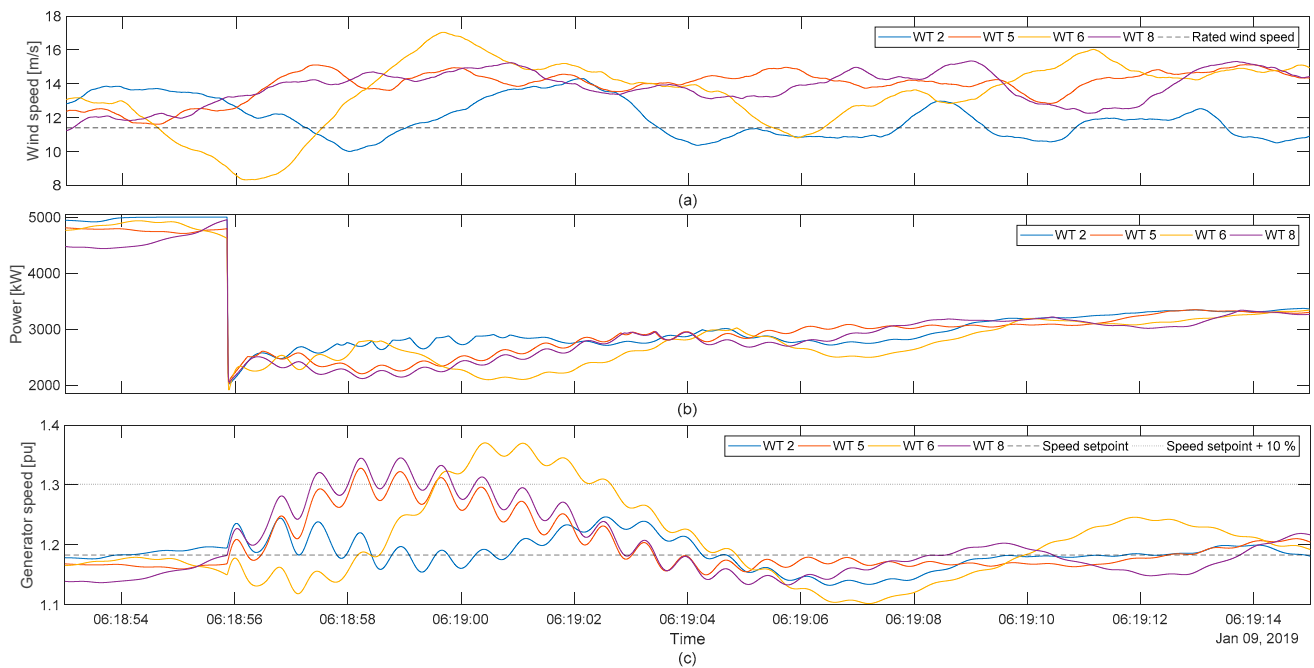
Figure 10. Simulation results of scenario I for four WTs: (**a**) Wind speed and rated wind speed; (**b**) Generator power; (**c**) generator speed, speed setpoint, and overspeed threshold. The time axis of (**c**) is valid for the above subplots as well.

Figure 12 shows how the SI and PFC work together to allow stabilizing the grid frequency: in the first moments after the system split, the SI controller provides a very fast frequency response, which decreases as the RoCoF approaches 0 Hz/s. The depicted PFC modification factor lowers the WTs power setpoint (see (4)) as the grid frequency rises. Eventually, an equilibrium is reached once the frequency response of the wind farm balances the power in the grid. To bring back the frequency to 50 Hz, more WTs would be

needed. However, the stable frequency should allow keeping the gas-fired gen-set grid connected and using its frequency response to stabilize the grid frequency at 50 Hz.

Table 3. Results of scenario I. Maximum speed and duration in overspeed for all simulated WTs.

WT Number	Maximum Generator Speed [% of Rated Speed] [1]	Duration in Overspeed [ms]
1	110.7	316
2	104.8	0
3	107.4	0
4	110.7	184
5	111.6	864
6	115.8	3090
7	108.2	0
8	113.3	1995

[1] Rated generator speed is 1.183 pu.
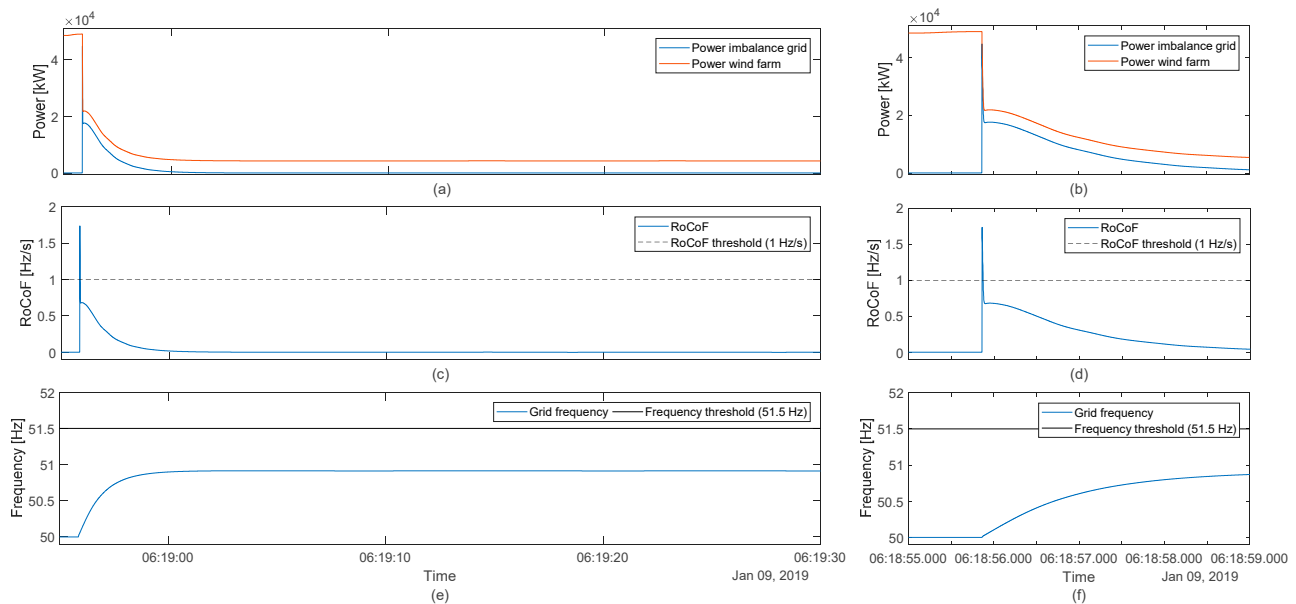
Figure 11. Results of scenario II: power imbalance in the islanded grid and power of the simulated wind farm for (**a**) the full simulation time and (**b**) a zoom to the time of the event; (**c,d**) RoCoF and RoCoF threshold; (**e,f**) grid frequency and frequency threshold. Time axes of (**e,f**) are valid for the above subplots as well.

As in scenario I, most of the WTs experience overspeed situations in the first seconds after the system split. The maximum generator speed and the duration for which the generator speed exceeds 110% of the rated speed are given in Table 4. Both values increased in comparison with scenario I. The increase is caused by the PFC, which keeps the generator power at a low level (see Figures 12 and 13). As the pitch drive needs some time to adjust the pitch angle, overspeed occurs for most WTs. This problem is worsened when the frequency support coincides with a positive gust.

Examples of such coincidences are depicted in Figure 13. The WT 5, WT6, and WT8 experience a strong gust starting shortly before the power reduction for frequency support. Hence, the increase of the aerodynamic torque coincides with the decrease of the electrical torque. Consequently, the drive train is strongly accelerated. Furthermore, the drastic change of the electrical torque causes drive train oscillations with the 1st torsional eigenfrequency (see Figure 13c). The speed controller slows down the generator speed to rated speed after approximately 10 s and can stabilize the speed even though the WT operates at a low power setpoint and experiences heavy gusts. As in Figure 10 the least

affected WT2 is also depicted. For this WT the highest speed occurs at the end of a gust starting shortly after the initial event. The power reduction at this time of the event is dominated by PFC, which explains the increase of the maximum speed compared to scenario I (see Figure 12).
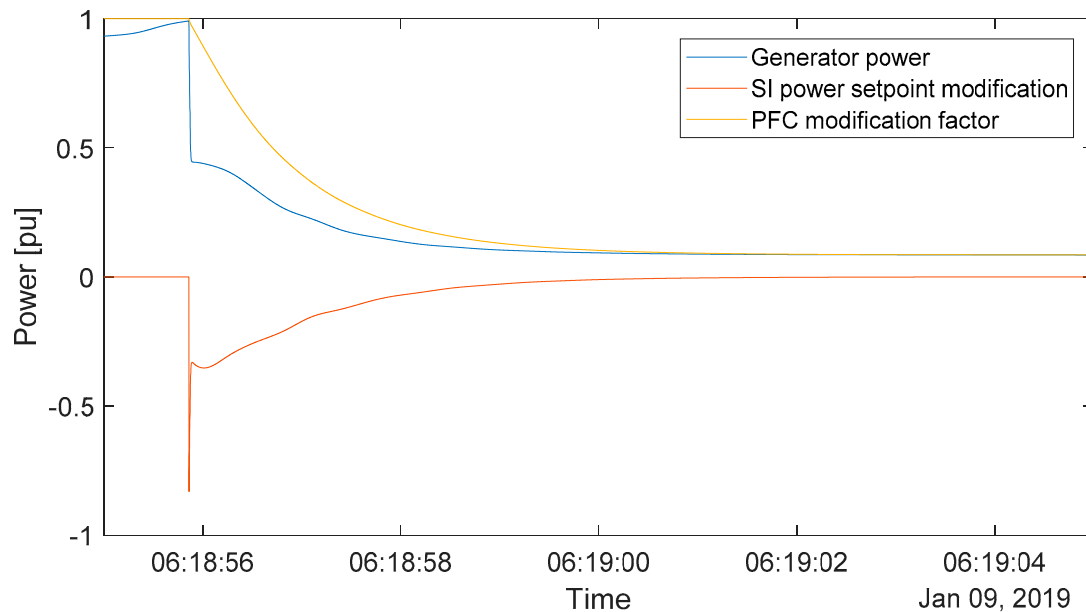

Figure 12. Results for scenario II. Generator power and the two frequency support functions: SI and PFC.

Table 4. Results of scenario II. Maximum speed and duration in overspeed for all simulated WTs.

| WT Number	Maximum Generator Speed [% of Rated Speed] [1]	Duration in Overspeed [ms]
1	111.1	517
2	106.2	0
3	109.6	0
4	112.2	1296
5	113.6	2791
6	119.5	3901
7	110.7	542
8	115.2	3951
9	112.8	2105
10	108.3	0

[1] Rated generator speed is 1.183 pu.

3.3. Scenario III

As in scenario II, PFC and SI controller are active. The number of grid connected WTs is reduced to two and a pre-event curtailment to 90% of the available power is introduced. Hence, the wind farm is allowed to produce 9000 kW when the grid frequency is at 50 Hz. The results show that the WTs can bring the grid frequency back to 49.99 Hz within 15 s after the event by increasing the power up to 9500 kW (see Figure 14a,c). The RoCoF is limited to approximately +/− 0.05 Hz/s, which is a low, unproblematic value. The axes scales for Figure 14a are chosen such that it becomes visible how the power imbalance in the grid is dominated by the power output of the wind farm. The load fluctuations and the changing power production of the power plant are comparable small for most of the time. Due to the turbulent wind, the PFC controller fails to keep it in the 50 Hz +/− 10 mHz tolerance band during negative gusts (see Figure 14a,c). The effects of the strongest gusts are shown in Figure 15: The drop of the wind farm power causes a drop in

the grid frequency. Consequently, the PFC controller allows the WTs to generate as much power as possible for the WTs ($\eta_{PFC} = 1$). This helps to bring back the grid frequency to the tolerance band around 50 Hz. After the initial recovery, the grid frequency is only for five seconds below 49.9 Hz, which is the threshold for possible load shedding. After reaching the tolerance band, the grid frequency is for 56 s out of the remaining 185 s simulation within the tolerance band (appr. 30% of the time). This could have been increased by heavily increasing the number of grid-connected WTs. However, in this scenario, a small share of WTs on the power production is deliberately chosen to show the strong effect PFC provision of a few WTs may have on grid frequency stabilization.
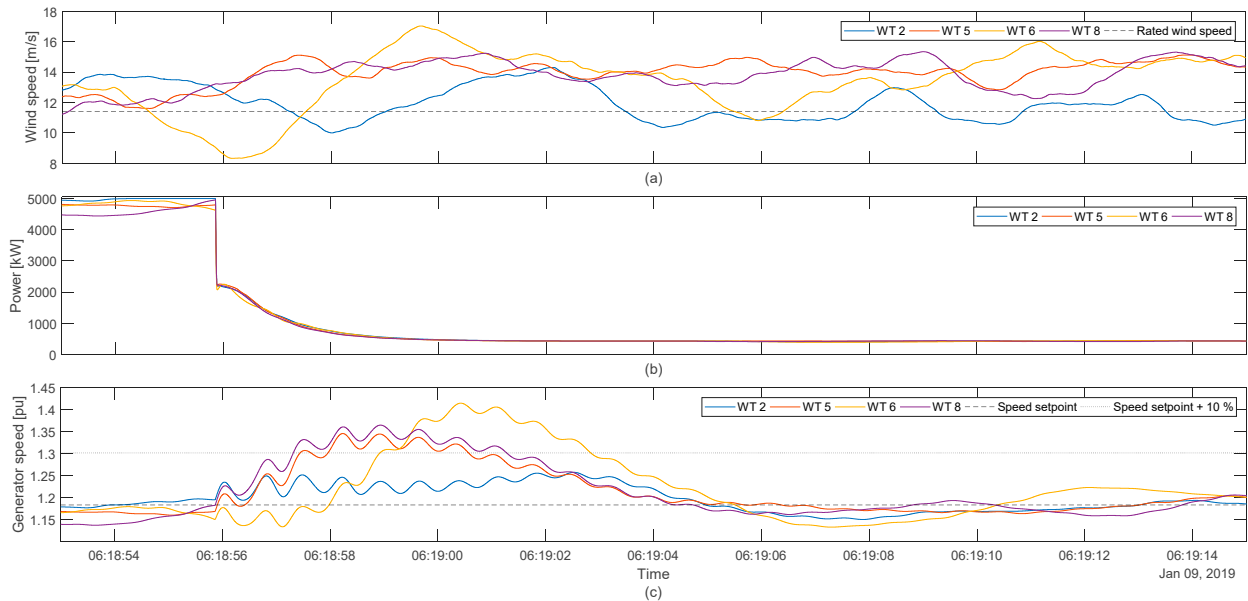
Figure 13. Simulation results of scenario II for 4four WTs: (**a**) Wind speed and rated wind speed; (**b**) Generator power; (**c**) generator speed, speed setpoint, and overspeed threshold. The time axis of (**c**) is valid for the above subplots as well.
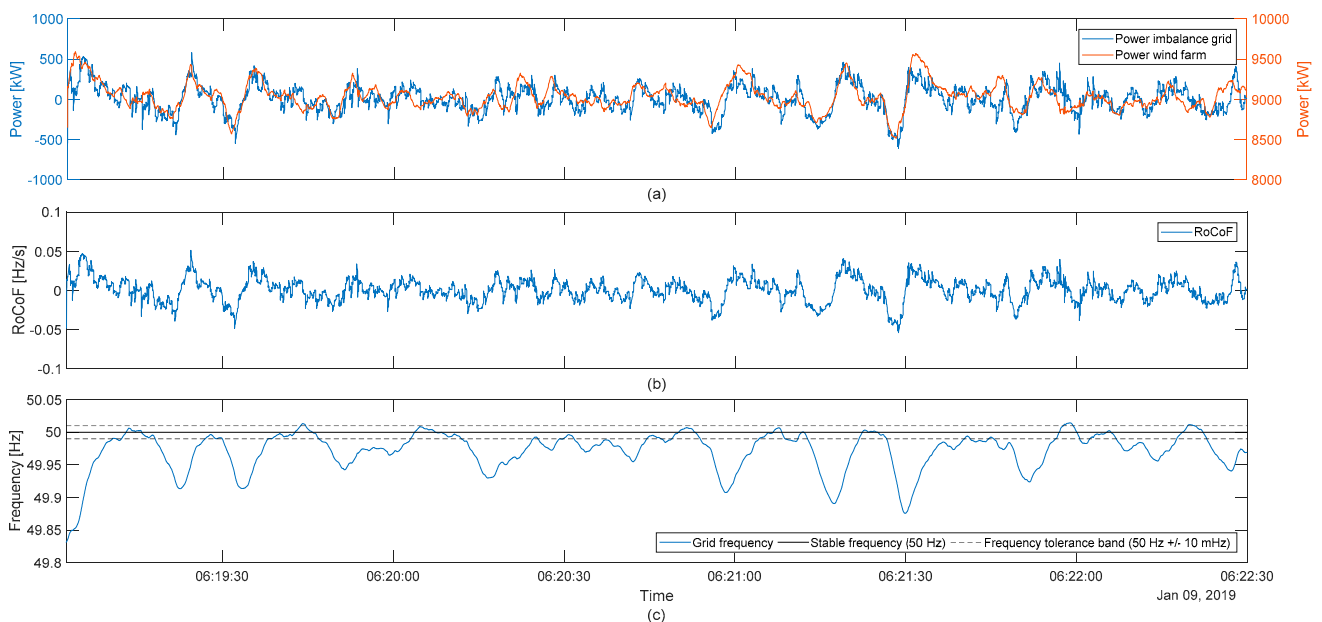
Figure 14. Results of scenario III: (**a**) power imbalance in the islanded grid and power of the simulated wind farm; (**b**) RoCoF; (**c**) grid frequency, stable frequency, and frequency tolerance band.
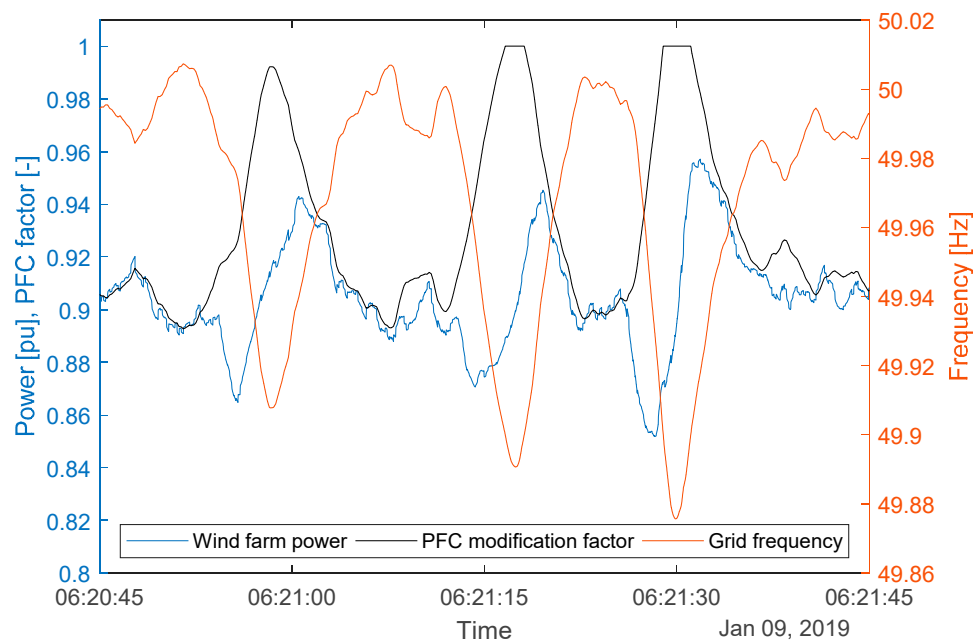
Figure 15. Results of scenario III: Wind farm power (pu base = 10 MW), PFC modification factor η_{PFC}, and grid frequency during negative wind gusts.

4. Discussion

The results show that WTs would have been able to support the grid to some extent. The provision of SI could have lowered the RoCoF below a critical threshold within milliseconds and thus have lowered the consequences for the conventional power station. However, as the frequency rises too fast above the 51.5 Hz threshold, it would not have been possible to keep the gas-fired gen-set (Generator 12) connected to the grid. The grid could have been stabilized if the number of WTs were increased to ten and the WTs would provide PFC in addition to SI. In this case, the WTs would have been able to balance the power in the grid effectively and limit the frequency to 50.8 Hz. Keeping Generator 12 synchronized would have allowed using its PFC functionalities to bring the grid frequency back to 50 Hz and to stabilize it. This would have allowed reconnecting to the central European grid. In this case, the blackout would have been avoided. However, both scenarios require a large share of the power being produced with WTs. In the third scenario, a much smaller part of the power production would have been provided by WTs. The small number of individual WTs in combination with the small grid makes the power balance in the grid very sensitive to gusts. The regular gusts prevent the WTs to keep the grid frequency continuously within the tolerance band. The effect of the gusts would be smaller in a larger wind farm, as spatial smoothing effects occur in larger wind farms [37]. The ongoing development of various energy storage systems [38] could make local storage systems affordable and thus help smooth the power production further. Finally, even the inertia of the WT rotor in combination with advanced control could be used to smooth the power output [39,40]. However, even in the shown scenario, the grid frequency stays very close to or in the tolerance band for longer periods. Thus, a reconnection to the central European grid might have been possible and the blackout may have been avoided.

The first two scenarios have no direct financial implication for the WT operation. Although the continuous provision of SI alters the power setpoint of the WT, the consequences for the WT performance are negligible [22]. The PFC in scenario II requires no pre-event curtailment and is therefore financially negligible. By contrast, scenario III requires a pre-event curtailment by 10%. Such a prolonged curtailment solely for frequency support is very costly. However, in the region around Flensburg curtailment due to feed-in management is very common. It may be possible to use such curtailed WTs as a

PFC reserve as the time scope of frequency support and feed-in management differ [24]. Hence, a temporary frequency support would most likely not compromise the safety of the affected grid.

The overspeed problem, which occurred in scenarios I & II, could be addressed by directly integrating the speed controller in the frequency response logic. Another option would be to use Lidar data to foresee gusts and thus reduce overspeed. Whether both options yield better results and stable control of the WT may be part of future research.

Although the frequency support provides a heavy burden for the drive train, it is unlikely to cost much lifetime. Lifetime is influenced by fatigue loads and extreme loads. A system split occurs seldom. Therefore, the frequency response during such an event is unlikely to cause significant fatigue loads. Furthermore, the change of the electrical torque for frequency response is slower than during low-voltage-ride-through (LVRT), which is a typical extreme burden for the drive train [41,42]. Hence, frequency support in the researched scenario is unlikely to be more significant than LVRT events and consequently neither for fatigue nor for extreme loads relevant.

5. Conclusions

For three fictive, yet realistic scenarios, it has been shown to what extent WTs could have helped to avoid the blackout in Flensburg on 9 January 2019. WTs solely providing SI would not have been sufficient for keeping the grid frequency in an acceptable band. Hence, the WTs would also need to provide PFC. As expected the frequency support comes at a price: namely possible overspeed and speed oscillation issues when the power output is heavily reduced and a need for pre-event curtailment when the power is to be increased. Possible mitigation strategies have to be researched to weaken these effects.

While the study focuses on the real situation in Flensburg on the day of the event, the findings are also relevant for other cases. The power imbalance in the grid matches the worst-case scenario for a system split defined by ENTSO-E very well. The exact behavior of a WT during frequency support depends strongly on its operating point thus the shown effects are limited to similar wind conditions. Whether WTs in part-load operation (providing a similar share of the power production) could have stabilized the grid frequency is likely but not shown in the paper. This is due to the attempt to stick as closely as possible to the real situation in Flensburg on 9 January 2019.

Further limitations of the results concern the used grid model. As the focus of the paper is on the WT dynamics power balances are used to calculate the RoCoF and the grid frequency. Furthermore, the measurement of the grid frequency is not modeled which could affect the efficiency of the grid frequency support and certainly would have delayed the power reduction in scenarios I & II. However, as the assessment criterion (RoCoF < 1 Hz/s) is reached approximately 50 ms before the goal, a successful stabilization of the grid frequency is likely for scenario II. Finally, the reconnection to the Central European grid is not modeled but the research shows to what extent this reconnection could have been facilitated and a successful reconnection would have been likely. Hence, it is concluded that a blackout could have most likely been prevented for scenarios II & III through the grid support of the WTs.

Author Contributions: A.G.: conceptualization, methodology, literature review, data analysis, development and implementation of the model, conducting the simulation, visualization, writing—original draft preparation; C.J.: conceptualization, development of the wind turbine simulation model, discussions and comments, writing—review and editing; T.R.: provision of data and information on the blackout, writing—review and editing. All authors have read and agreed to the published version of the manuscript.

References

1. Tielens, P.; van Hertem, D. The relevance of inertia in power systems. *Renew. Sustain. Energy Rev.* **2016**, *55*, 999–1009. [CrossRef]
2. EirGrid. EirGrid Grid Code. Version 9. December 2020. Available online: https://www.eirgridgroup.com/site-files/library/EirGrid/GridCodeVersion9.pdf (accessed on 15 January 2021).
3. Hydro-Québec TransÉnergie. Technical Requirements for the Connection of Generating Stations to the Hydro-Québec Transmission System. D-2018-145, January 2019. Available online: http://www.hydroquebec.com/transenergie/fr/commerce/pdf/2_Requirements_generating_stations_D-2018-145_2018-11-15.pdf (accessed on 15 January 2021).
4. Central Electricity Authority. Technical Standards for Connectivity to the Grid (Amendment). 2019. Available online: https://cea.nic.in/wp-content/uploads/2020/02/notified_regulations.pdf (accessed on 15 January 2021).
5. Godin, P.; Fischer, M.; Röttgers, H.; Mendonca, A.; Engelken, S. Wind power plant level testing of inertial response with optimised recovery behaviour. *IET Renew. Power Gener.* **2019**, *13*, 676–683. [CrossRef]
6. Díaz-González, F.; Hau, M.; Sumper, A.; Gomis-Bellmunt, O. Participation of wind power plants in system frequency control: Review of grid code requirements and control methods. *Renew. Sustain. Energy Rev.* **2014**, *34*, 551–564. [CrossRef]
7. Fernández-Guillamón, A.; Gómez-Lázaro, E.; Muljadi, E.; Molina-García, Á. Power systems with high renewable energy sources: A review of inertia and frequency control strategies over time. *Renew. Sustain. Energy Rev.* **2019**, *115*, 109369. [CrossRef]
8. ENTSO-E. Connection Network Codes—Response to the Comments Received during the Public Consultation of Implementation Guidance Documents on Frequency Stability Parameters. January 2018. Available online: https://eepublicdownloads.blob.core.windows.net/public-cdn-container/clean-documents/Network%20codes%20documents/NC%20RfG/ENTSO-E_IGD_consultation_response.pdf (accessed on 27 January 2021).
9. ENTSO-E. Frequency Stability Evaluation Criteria for the Synchronous Zone of Continental Europe. March 2016. Available online: https://eepublicdownloads.entsoe.eu/clean-documents/SOC%20documents/RGCE_SPD_frequency_stability_criteria_v10.pdf (accessed on 27 January 2021).
10. ENTSO-E. System separation in the Continental Europe Synchronous Area on 8 January 2021. 2nd Update. January 2021. Available online: https://www.entsoe.eu/news/2021/01/26/system-separation-in-the-continental-europe-synchronous-area-on-8-january-2021-2nd-update/ (accessed on 27 January 2021).
11. UCTE. Final Report of the Investigation Committee on the 28 September 2003 Blackout in Italy. Technical Report. April 2004. Available online: https://eepublicdownloads.entsoe.eu/clean-documents/pre2015/publications/ce/otherreports/20040427_UCTE_IC_Final_report.pdf (accessed on 3 March 2021).
12. Everhart, K.; Gergely, M. Severe Power Cuts in Texas Highlight Energy Security Risks Related to Extreme Weather Events. IEA, Paris. February 2021. Available online: https://www.iea.org/commentaries/severe-power-cuts-in-texas-highlight-energy-security-risks-related-to-extreme-weather-events (accessed on 3 March 2021).
13. Borowski, P.F. Zonal and Nodal Models of Energy Market in European Union. *Energies* **2020**, *13*, 4182. [CrossRef]
14. Yamashita, K.; Joo, S.K.; Li, J.; Zhang, P.; Liu, C.C. Analysis, control, and economic impact assessment of major blackout events. *Eur. Trans. Electr. Power* **2008**, *18*, 854–871. [CrossRef]
15. Yuxin, Z.; Xuemin, Z.; Shengwei, M.; Deming, X.; Shuai, W.; Rui, S. Blackout risk analysis and control of power system integrated with wind farm. In Proceedings of the 2016 Chinese Control and Decision Conference (CCDC), Yinchuan, China, 28–30 May 2016; pp. 876–882. Available online: http://ieeexplore.ieee.org/document/7531107/ (accessed on 3 March 2021).
16. Yan, R.; Saha, T.K.; Bai, F.; Gu, H. The Anatomy of the 2016 South Australia Blackout: A Catastrophic Event in a High Renewable Network. *IEEE Trans. Power Syst.* **2018**, *33*, 5374–5388. [CrossRef]
17. Ela, E.; Gevorgian, V.; Fleming, P.; Zhang, Y.C.; Singh, M.; Muljadi, E.; Scholbrook, A.; Aho, J.; Buckspan, A.; Pao, L.; et al. *Active Power Controls from Wind Power: Bridging the Gaps*; NREL, Technical Report NREL/TP-5D00-60574; National Renewable Energy Lab. (NREL): Golden, CO, USA, 2014.
18. Kundur, P.; Balu, N.J.; Lauby, M.G. *Power System Stability and Control*; McGraw-Hill: New York, NY, USA, 1994.

19. Thiesen, H.; Jauch, C. Determining the Load Inertia Contribution from Different Power Consumer Groups. *Energies* **2020**, *13*, 1588. [CrossRef]

20. Ministerium für Energiewende, Landwirtschaft, Umwelt, Natur und Digitalisierung (MELUND) Schleswig-Holstein. Bericht zum Engpassmanagementin Schleswig-Holstein. Kiel. December 2020. Available online: https://www.schleswig-holstein.de/DE/Landesregierung/Themen/Energie/Energiewende/Strom/pdf/berichtEngpassmanagement.pdf?__blob=publicationFile&v=3 (accessed on 4 February 2021).

21. Jauch, C. *First Eigenmodes Simulation Model of a Wind Turbine—For Control Algorithm Design*; Technical Report; Wind Energy Technology Institute: Flensburg, Germany, 2020. [CrossRef]

22. Gloe, A.; Jauch, C.; Craciun, B.; Winkelmann, J. Continuous provision of synthetic inertia with wind turbines: Implications for the wind turbine and for the grid. *IET Renew. Power Gener.* **2019**, *13*, 668–675. [CrossRef]

23. Jonkman, J.; Butterfield, S.; Musial, W.; Scott, G. *Definition of a 5-MW Reference Wind Turbine for Offshore System Development*; Technical Report, NREL/TP-500-38060; National Renewable Energy Lab. (NREL): Golden, CO, USA, 2009.

24. Jauch, C.; Gloe, A. Simultaneous Inertia Contribution and Optimal Grid Utilization with Wind Turbines. *Energies* **2019**, *12*, 3013. [CrossRef]

25. Kušljevic, M.D.; Tomic, J.J.; Jovanovic, L.D. Frequency Estimation of Three-Phase Power System Using Weighted-Least-Square Algorithm and Adaptive FIR Filtering. *IEEE Trans. Instrum. Meas.* **2010**, *59*, 322–329. [CrossRef]

26. Hagerstål, T.; Wikner, J. *Development & Operational Experience with SGT-800, a Siemens 45 MW Industrial Gas Turbine for Various Appications*; Technical Report; Siemens Industrial Turbomachinery AB: Finspong, Sweden, 2006.

27. Tielens, P.; van Hertem, D. Grid Inertia and Frequency Control in Power Systems with High Penetration of Renewables. Presented at the Young Researchers Symposium in Electrical Power Engineering, Delft. 2012. Available online: https://lirias.kuleuven.be/retrieve/182648 (accessed on 4 February 2021).

28. German Weather Service. Climate Data Center. Available online: https://cdc.dwd.de/portal/202007291339/mapview (accessed on 27 January 2021).

29. Manwell, J.F.; McGowan, J.G.; Rogers, A.L. *Wind Energy Explained: Theory, Design and Application*, 2nd ed.; Wiley: Chichester, UK, 2011.

30. Gloe, A.; Jauch, C. *Simulation Model Design and Validation of a Gearless Wind Turbine—For Fast Power Control to Enhance Congestion Management*; Technical Report; Wind Energy Technology Institute: Flensburg, Germany, 2016. [CrossRef]

31. Jauch, C.; Gloe, A.; Hippel, S.; Thiesen, H. Increased Wind Energy Yield and Grid Utilisation with Continuous Feed-In Management. *Energies* **2017**, *10*, 870. [CrossRef]

32. Federal Network Agency. Core Energy Market Data Register. Available online: https://www.bundesnetzagentur.de/EN/Areas/Energy/Companies/CoreEnergyMarketDataRegister/CoreDataReg_node.html (accessed on 4 March 2021).

33. Hydro Québec TransÉnergie. Transmission Provider Technical Requirements for the Connection of Power Plants to the Hydro-Québec Transmission System. February 2009. Available online: http://www.hydroquebec.com/transenergie/fr/commerce/pdf/exigence_raccordement_fev_09_en.pdf (accessed on 3 May 2016).

34. Fernández-Guillamón, A.; Gómez-Lázaro, E.; Molina-García, Á. Extensive Frequency Response and Inertia Analysis under High Renewable Energy Source Integration Scenarios: Application to the European Interconnected Power System. *IET Renew. Power Gener.* **2020**, *14*, 2885–2896. [CrossRef]

35. Gloe, A.; Jauch, C.; Thiesen, H.; Viebeg, J. *Inertial Response Controller Design for a Variable Speed Wind Turbine*; Technical Report; Wind Energy Technology Institute: Flensburg, Germany, 2018. [CrossRef]

36. The European Commission. *Commission Regulation Establishing a Network Code on Requirements for Grid Connection of Generators*; European Commission: Brussels, Belgium, 2016; Volume 631.

37. Li, P.; Banakar, H.; Keung, P.K.; Far, H.G.; Ooi, B.T. Macromodel of spatial smoothing in wind farms. *IEEE Trans. Energy Convers.* **2007**, *22*, 119–128. [CrossRef]

38. Koohi-Fayegh, S.; Rosen, M.A. A review of energy storage types, applications and recent developments. *J. Energy Storage* **2020**, *27*, 101047. [CrossRef]

39. Abedini, A.; Nasiri, A. Output Power Smoothing for Wind Turbine Permanent Magnet Synchronous Generators Using Rotor Inertia. *Electr. Power Compon. Syst.* **2008**, *37*, 1–19. [CrossRef]

40. Jauch, C. Controls of a flywheel in a wind turbine rotor. *Wind Eng.* **2016**, *40*, 173–185. [CrossRef]

41. Joos, G. Wind turbine generator low voltage ride through requirements and solutions. In Proceedings of the 2008 IEEE Power and Energy Society General Meeting—Conversion and Delivery of Electrical Energy in the 21st Century, Pittsburgh, PA, USA, 20–24 July 2008; pp. 1–7. Available online: http://ieeexplore.ieee.org/document/4596605/ (accessed on 10 February 2021).

42. Wenske, J.; Beckert, U. Voltage-Induced Stresses during Low Voltage Ride through (LVRT) in the Drive Train of Wind Turbines with DFIG. Presented at the International Conference on Renewable Energies and Power Quality, Santiago de Compostella. 2012. Available online: http://www.icrepq.com/papers-icrepq12.html (accessed on 10 February 2021).

Publication 5

Continuous grid frequency support with variable synthetic inertia and feedforward pitch angle adjustment

Continuous grid frequency support with variable synthetic inertia and feedforward pitch angle adjustment

Arne Gloe

Wind Energy Technology Institute, Flensburg University of Applied Sciences, 24943 Flensburg, Germany
Email: arne.gloe@hs-flensburg.de

Abstract. Grid frequency support by wind turbines is increasingly demanded by grid operators around the globe. By meeting these requirements, the wind turbines leave their optimal operating point and may even be pushed out of their safe operating range during severe grid events. In the past years, the Wind Energy Technology Institute developed a controller for grid frequency support in collaboration with Suzlon Energy. This work seeks to improve this controller by adding a pitch angle adjustment depending on the operating point of the wind turbine and the power adjustment for grid support. The controller performance is analysed for three scenarios and for the whole operating range of the NREL 5 MW WT. Simulations show, that the adjustment lowers the risk for overspeed at the cost of an increased pitch rate. By contrast, the aerodynamic efficiency is not increased by the additional control loop. The effect on the tower depends heavily on the wind situation during and shortly after the grid frequency support event.

1. Introduction

In response to higher shares of inverter connected generators, many grid operators increase their demand for system services to be provided by wind turbines (WTs), for instance in Ireland [1], Québec [2] or India [3]. The existing requirements are typically tailored to the system operator's specific needs and their individual control objectives. Future power systems with high degrees of non-synchronous penetration can achieve power system stability by WTs providing grid frequency services. This has been shown for several countries e.g. Ireland [4], the UK [5], or South Africa [6]. In addition, there can be economic incentives from a systems perspective: using synthetic inertia (SI) of WT can help to lower the must-run capacity of expensive conventional power plants [7].

The frequency support is typically categorized in SI (reacting proportionally to the derivative of the frequency) and fast frequency response (FFR, reactivating proportionally to the grid frequency deviation) [8]. In addition, there are various control schemes tailored to the needs of a specific grid operator, e.g. providing a predefined power increase for approximately ten seconds, if a frequency threshold is violated [9]. All have in common that the WT's active power is altered.

The effect of active power control strategies for frequency support [10] and its effects on the WT loads [11] have been studied extensively by working groups at NREL and University of Colorado. Their work focuses on the optimal control strategy when the WT is curtailed to allow primary and secondary frequency control [12].

The provision of SI with WTs was first proposed in 2007 by Ramtharan et al. [13] and developed further in the following years [14]. Over the past years, the Wind Energy Technology Institute and

Suzlon Energy have developed a so-called variable H controller. The variable H controller enables WTs to provide SI with respect to its capability in the current operating point. This is an improvement over other SI controller [15]. The kinetic energy stored in the rotation of the WT is used to modify the power setpoint according to the grid's need. Thus, the WT leaves its optimal operating point in the prevailing wind conditions. It has been shown, that the variable H controller can provide SI reliably in various grid situations while keeping the increase of the mechanical loads at a minimum [16].

This work analyses the performance of continuous grid frequency support with a variable SI and an additional loop for the pitch angle for the NREL 5 MW WT [17]. The additional loop is called feedforward loop as it seeks to minimize the impact of a grid frequency support on the WT's speed before it actually appears. Thus, the impact of grid support on the WT in extreme grid situations should be minimized. It is also investigated whether the feedforward controller can improve the aerodynamic efficiency during grid frequency support. The modified controller is evaluated by estimating the effect of the changes on the mechanical loads by analyzing the rotor and tower acceleration as well as the pitch rate. Furthermore, the energy production is analyzed from the WT's as well as from the grid's perspective.

The rest of the paper is structured as follows: section 2 describes the modifications of the controller and the simulated scenarios. Section 3 presents the results and a conclusion based on these results is drawn in section 4.

2. Control system and simulated scenarios

2.1. Control system and simulation model
The first subsection describes the general idea, how the pitch angle should be adjusted to help the WT during grid frequency support and how the needed parameters are derived. The second subsection explains the intended controller behavior for different combinations of grid support and WT operating points. The last subsection describes how the controller is implemented in the NREL baseline control system.

2.1.1. Feedforward controller concept. When the power setpoint is adapted to the grid's needs, the WT leaves its optimal operating point. In case of a decrease of the WT power, the adjustment may lead to high drive train accelerations and eventually to overspeed situations. In this case, the decreasing aerodynamic efficiency actually helps to limit the drive train acceleration. However, during severe events an increase of the pitch angle might be needed to support this effect when the WT operates close or at its rated rotational speed. In case of a power increase, the decreasing aerodynamic efficiency hampers the return to steady-state operation. In such a situation, the pitch angle could be adjusted to reduce the loss of aerodynamic efficiency.

However, the change of the grid frequency and of the wind speed in the next seconds are typically both unknown. While the change of the wind speed can be predicted and compensated to some degree with a Lidar system [18], the grid frequency cannot be predicted. In an ideal scenario, the rotational speed, ω_{gen}, would be kept constant. Theoretically, this could be achieved by varying the pitch angle such, that the aerodynamic torque, T_{aero}, changes in a similar magnitude as the electrical torque (see equation (1)). During grid support the electrical torque deviates from its optimal value, $T_{elec,opt}$ by a grid support term, $T_{elec,GS}$. The angular acceleration, $\dot{\omega}_{gen}$, depends on the difference between aerodynamic and electrical torque as well as the inertia of the WT drive train, J_{WT}.

$$\dot{\omega}_{gen} = \frac{T_{aero} - (T_{elec,opt} + T_{elec,GS})}{J_{WT}} \qquad (1)$$

The needed change of the pitch angle can be calculated from the pitch sensitivity of the WT in its current operating point. When calculating the pitch sensitivity, it has to be distinguished between WT operation in region 1.5, 2, 2.5 and 3 as defined by Jonkman et al. [17]. For the operation in region 3 the pitch sensitivity is published by Jonkman et al. [17]. For regions 2 & 2.5, the pitch sensitivity in the steady-state operating points is calculated with c_P coefficients published by Jonkman and Hippel on the

NREL forum [19] (see Figure 1). It shows values for positive and negative pitch angle adjustments as the effects on the aerodynamics differ significantly for most operating points. Please note: The pitch sensitivity in region 2 for a negative pitch angle adjustment is calculated for a tip-speed-ration (TSR) of 7.0 as 0° is the optimal pitch angle at the optimal TSR and pitch angle decreases are needed if the speed drops.
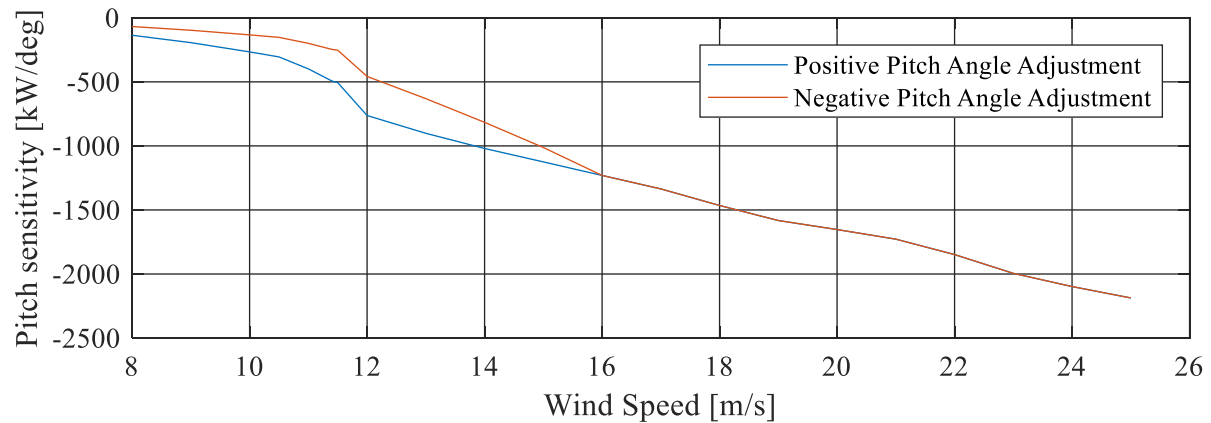

Figure 1 Pitch sensitivity vs wind speed for steady-state operating points.

The needed change of the pitch angle, θ_{ff}, is calculated based on the so derived pitch sensitivity in the current operating point, $\delta P_{aero}/\delta\theta$, (see Figure 1) and the power adjustment for grid support, $P_{dem,GS}$ (see equation (2)). The pitch sensitivity is chosen based on the steady-state operating point estimated by the rotational speed and the pitch angle control signal calculated in the feedback speed controller.

$$\theta_{ff} = \frac{P_{dem,GS}}{\frac{\delta P_{aero}}{\delta\theta}\big|_{WT,operating\ point}} \qquad (2)$$

2.1.2. Intended controller behavior. In region 3, the available power in the wind theoretically allows a constant generator speed. Here, the challenge is to control the pitch angle such that the WT operates as close as possible to rated speed even when responding to extreme grid situations. Figure 2 shows the aerodynamic efficiency of the WT, c_P, for some selected pitch angles and TSRs.
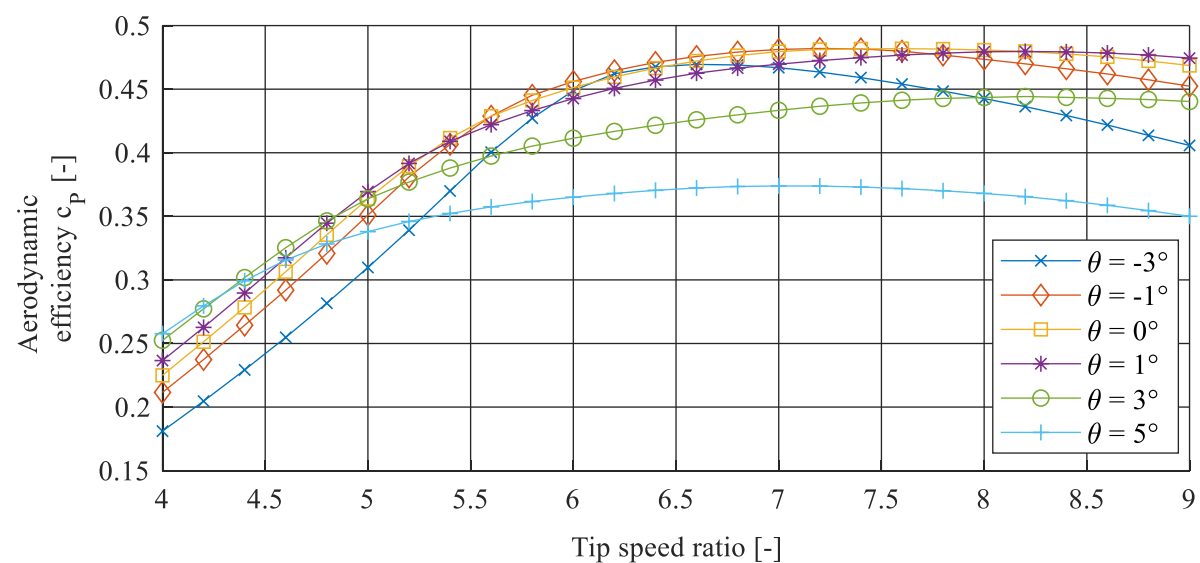

Figure 2 Aerodynamic efficiency vs TSR for various pitch angles.

In region 3 the TSR is typically below 7 and the pitch angle is positive. During power increases, the pitch angle should be decreased to avoid dropping out full load operation due to a declining rotor speed. In Figure 2 this would e.g. mean to move from the light blue, $\theta = 5°$ line towards the green, $\theta = 3°$ while the TSR decreases at the same time. In the opposite situation, where the WT power is reduced, the aerodynamic efficiency must be lowered by increasing the pitch angle quickly to avoid overspeed.

In region 2, the WT typically operates at the optimal tip speed ratio, TSR = 7.55 and at the optimal pitch angle, $\theta = 0°$, which is also the minimum allowed pitch angle. When the WT power is increased, the TSR drops. The pitch angle should then be adjusted to negative values, which allow maintaining a better angle of attack and thus help to lower the aerodynamic losses. Therefore, the minimum pitch angle, θ_{min}, also has to be adjusted by the feedforward controller. However, as Figure 3 shows, there is little room for improvement. It reveals that for reasonable decreases of the TSR a decrease of the pitch angle below 0° improves the efficiency by less than 1 % and pitch angles below -1° are hardly ever beneficial. The same logic applies for region 2.5, in which the steady-state TSR varies between 7 (at rated speed) and 7.55. Hence, for region 2 and 2.5 the minimum pitch angle is adjusted to $0° >= \theta_{min} >= -1°$.

When the WT's power is reduced in region 2, the TSR increases and the declining aerodynamic efficiency helps the WT to return to its steady-state operating point. The risk of overspeed has been observed, if the steady-state generator speed exceeded 85 % of rated speed. This risk intensifies in region 2.5 as the WT typically operates at suboptimal speed. Hence, the aerodynamic efficiency slightly increases if the generator speed increases (see yellow line in Figure 2).

A special case is the operation in region 1.5: the WT runs in super-optimal speed during steady-state operation. Hence, the speed-depending change of the aerodynamic efficiency will help the WT to return to the steady-state operation point. Thus, the pitch angle does not have to be adjusted.
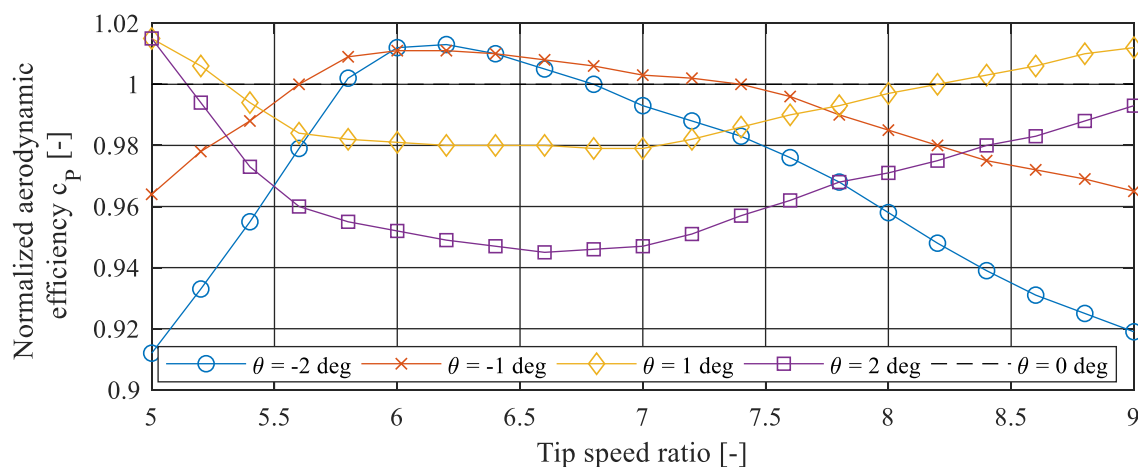

Figure 3 Aerodynamic efficiency vs TSR for various pitch angles normalized with respect to the efficiency at $\theta = 0°$ pitch angle.

2.1.3. Implementation of feedforward controller in NREL baseline controller and WT model. The modified controller is implemented into the so-called 1st eigenmodes model developed by Jauch [20] with the parameters and the baseline controller of the NREL 5 MW reference WT [17]. The control loop of the reference WT is changed by adding grid support functionalities including the feedforward loop (see Figure 4). The grid frequency support block consists of controller for the supply of SI and FFR. The SI controller uses the variable H concept. The FFC leads to a frequency depending derating of the WT similarly to the percentage derating strategy described by Fleming et al. [11]. The used grid frequency support controller is described in detail in Gloe et al. [21] supplemented by a notch filter for the RoCoF as proposed by Guo and Schlipf [22].

The newly added feedforward pitch angle control is shown in detail in Figure 5. The feedforward controller heavily affects the actual pitch angle, θ_{WT}. Hence, the control signal of the feedback speed controller, θ_{FB}, and the filtered generator speed of the WT, $\omega_{gen,LP}$, are used to estimate the WT's operating point and to determine the pitch sensitivity. In order to avoid unnecessary pitch maneuver, a deadband is introduced such that a modified power signal $P_{dem,GS,lim}$ is used for the feedforward pitch angle calculation. For the calculation, the power signal is set to zero between $\pm$ 0.5 % of the rated WT power, P_{rated}. Between $\pm$ 0.5 % and $\pm$ 1 % of P_{rated} it is linearly faded in. Over $\pm$ 1 % of P_{rated}, $P_{dem,GS}$ is used unchanged in the pitch angle calculation. The values are chosen according to experience gained in a previous project with Suzlon Energy [16]. Furthermore, the minimum pitch angle has to be adjusted as described in section 2.1.2.

In addition to the aforementioned signals, the block diagrams in Figure 4 and 5 depicts the wind speed, v_{wind}, the grid frequency, f_{grid}, the reference speed, ω_{ref}, the speed error, ω_{error}, the speed depending power setpoint, $P_{dem,speed}$, the maximum pitch angle, θ_{max}, the overall power setpoint, P_{dem}, and the overall pitch angle setpoint, θ_{dem}.
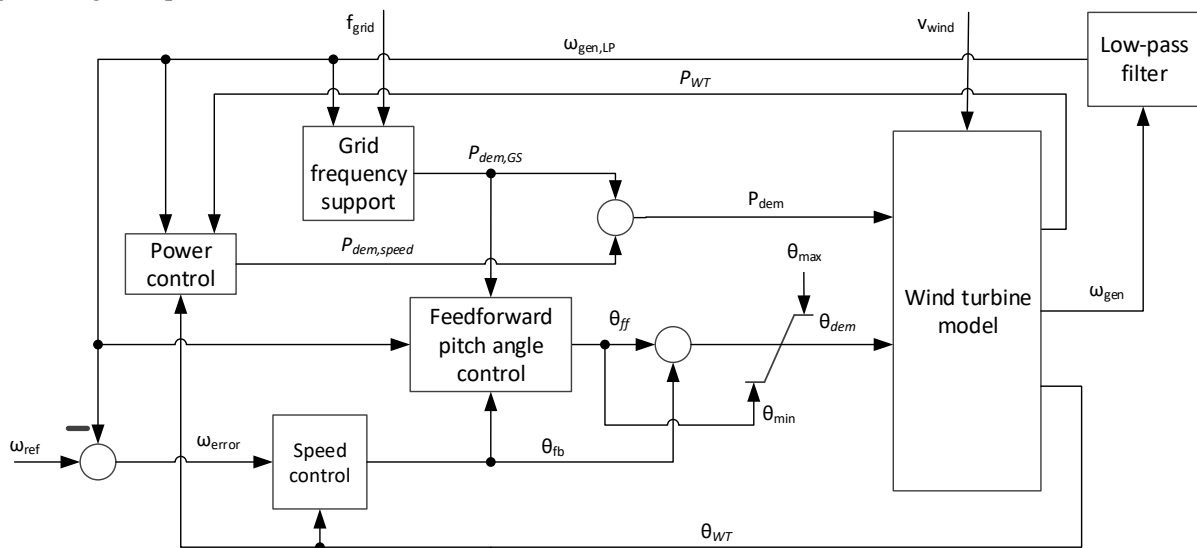

Figure 4. Modified block diagram of the NREL baseline controller to allow grid frequency support.
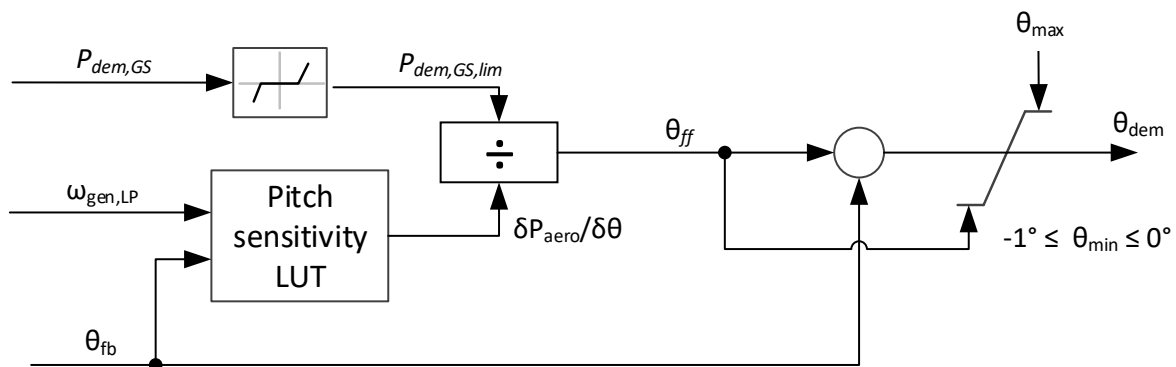
Figure 5 Block diagram of the feedforward pitch angle calculation and the integration into the overall control system.

2.2. Analysed wind and frequency scenarios

The effect of grid support on the loads of a WT heavily depends on the assumed scenarios. An exact estimation of the effect is particularly difficult as behavior of the electrical grids depends on a number of technical (e.g. share and structure of conventional power plants) and economic aspects (e.g. market

design) and also changes with time. These aspects make an estimate how often frequency support services of WTs are demanded by the grid operators very difficult. Therefore, this paper focuses on three scenarios, which mean to cover some of the most important grid situations:

    a) System split: System splits are extreme scenarios. However, recent years show that they occur regularly on a continental scale [23], [24] and occasionally locally [21]. The controller is tested with a simulated case based on real measurements in Flensburg [21].

    b) ENTSO-E reference incident: The required power for primary frequency response in an electrical grid is typically based on the loss of the biggest contingency. In the central European grid this is given by the simultaneous loss of two large power plants, in total 3,000 MW [25]. This is typically called the ENTSO-E reference case. The grid frequency behaviour for this situation is simulated with an inertia constant of 3 s, which is the minimum inertia constant to keep the European grid controllable [26]. Here, only the SI controller is active as reliable FFR provision would require a pre-event curtailment of the WT.

    c) Normal operation: during most of the time, the grid only experiences small power imbalances, which cause the grid frequency to fluctuate around its nominal value. These fluctuations are depending on the grid inertia and vary therefore with the share of wind power on the power production [27]. Measurements of the grid frequency in Ireland during high wind power production [28] are used for the normal operation scenario. During this scenario, the feedforward loop should hardly be active as the RoCoF typically oscillates around zero and therefore does not cause speed changes.

Each frequency scenario is tested at six wind speeds covering the WT control regions 2, 2.5 and 3. For the grid frequency scenario c) with stochastic frequency changes, three different turbulence seeds are used. By contrast, the frequency event scenarios a) and b) occur at a certain simulation time. Hence, 20 seeds are used to analyse the WT's response in various wind conditions for these scenarios.

3. Results

The simulation results are shown and discussed for the three frequency scenarios separately. In all shown cases, the WT provides grid frequency support and its behaviour with an activated & deactivated feedforward controller is compared.

The main purpose of the scenario a) is to show the capability of the feedforward controller to avoid overspeed situations. The WT has to reduce its power almost instantaneously to allow controlling the grid frequency in the islanded grid. Figure 6 shows exemplary time traces of selected signals for an average wind speed of 11.5 m/s and two turbulence seeds (orange and blue lines). The solid and the dashed lines indicate the WT's behaviour with activated & deactivated feedforward controller respectively. The sudden power decrease and thus the loss of generator torque not only accelerates the drive train but also excites it to oscillate with its eigenfrequency. While the damping of the oscillations are not controller depending, the overspeed of the WT is effectively reduced in the cases with activated feedforward control. Furthermore, the WT is capable of holding the reduced power setpoint very well in all cases.
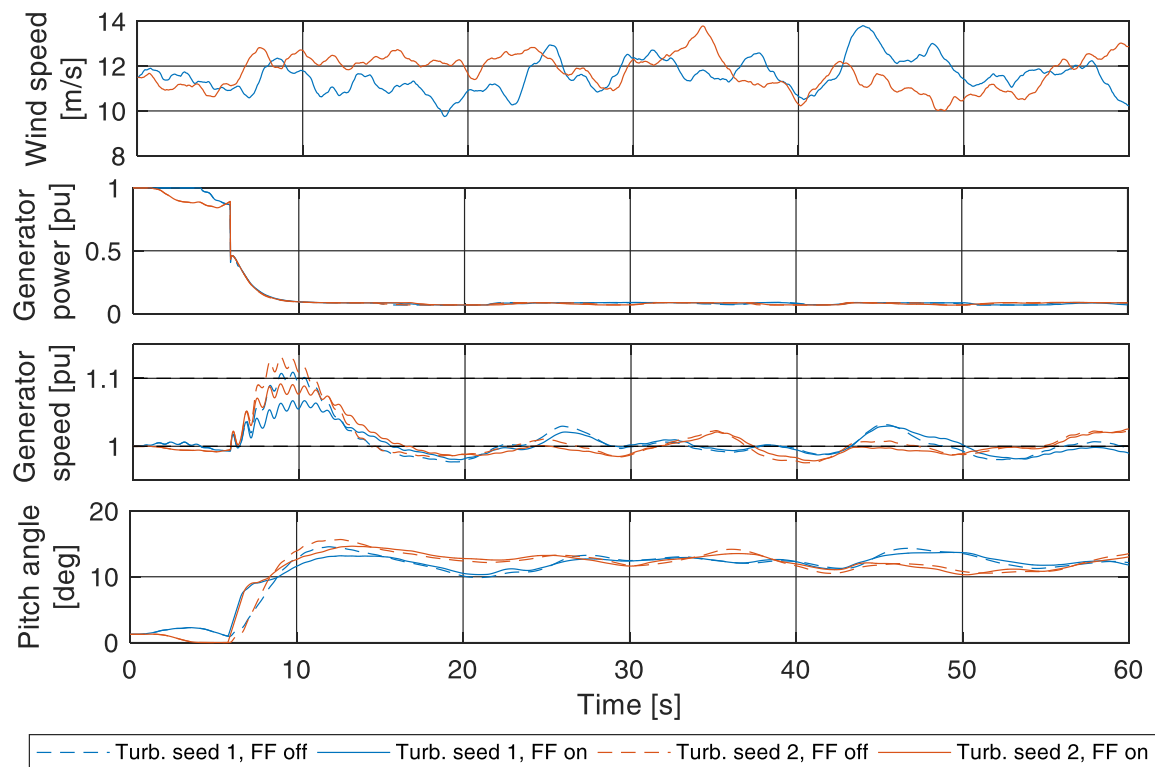
Figure 6 Time traces of selected WT signals for scenario a) at 11.5 m/s average wind speed. Colored dashed and solid lines show the results for feedforward control disabled and enabled respectively. Black dashed in the generator speed diagram mark rated speed and 10 % overspeed.

As stated in section 2.2., six different average wind speeds and twenty turbulence seeds are simulated for scenario a) and b). To give an overview over all simulations, the controller performance is evaluated with help of boxplots.

In scenario a), the maximum generator speed and the rotor acceleration are effectively reduced for nearly all wind speeds and turbulence seeds (see Figure 7, top left and right): In 19 % of simulations with deactivated feedforward controller the maximum speed of the WT exceeded 1.1 pu, a typical limit for an emergency stop of the WT. When the feedforward controller is activated, all of these situations can be avoided. The maximum observed speed over all simulations is 1.092. This positive influence on WT speed comes at the price of a strong increase of the RMS pitch rate (see Figure 7, bottom right). Especially, in region 2 and 2.5 the pitch rate increases heavily. While this is needed in region 2.5 to avoid the overspeed, the normal WT speed can keep the WT below 10 % overspeed without the help of the additional loop in region 2. Another burden for the WT is the increase of the fore-aft tower head acceleration (Figure 7, bottom left). The influence is strongest in region 2.5 as here the pitch angle dependency of the thrust force is maximal. Hence, the high pitch rate directly after the power reduction (see Figure 6) causes a strong decrease of the thrust. However, the effect of the tower depends strongly on the turbulence seed as shown in Figure 7. An analysis of the simulation time traces reveals, that the tower suffers most when there is a gust during or shortly after the power reduction (e.g. as shown by turbulence seed 2 in Figure 6). When the wind stays approximately constant, the tower head acceleration does not change significantly or can even be reduced. Furthermore, a possible emergency stop of the WT is not modelled, which would increase also the tower head acceleration and the pitch rate in case of a severe overspeed situation (i.e. in scenarios in which feedforward is deactivated).
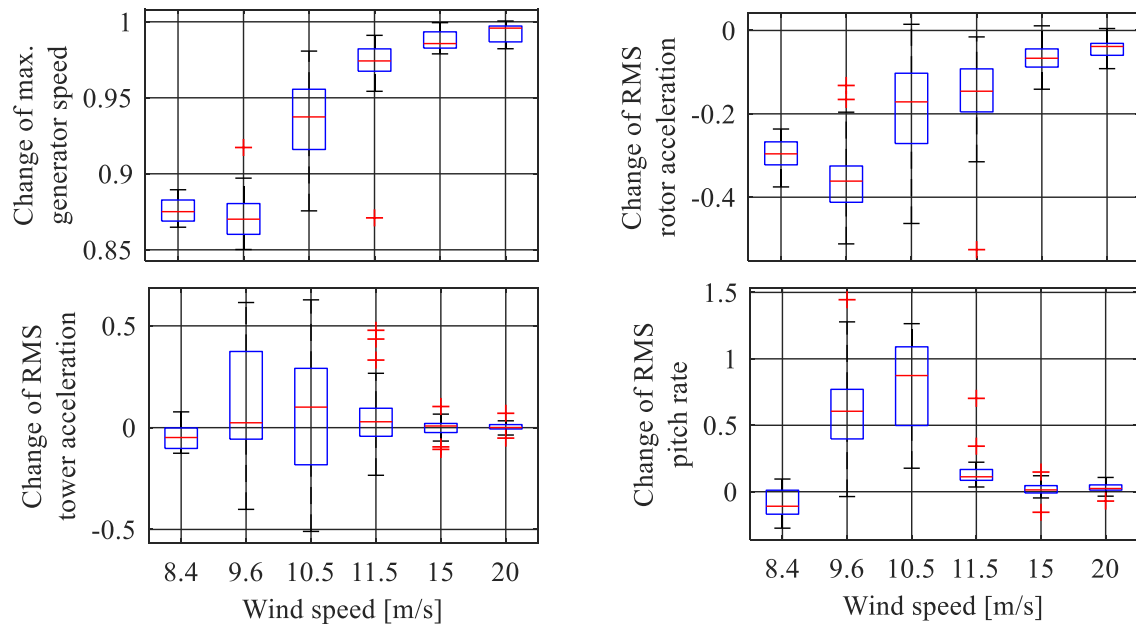
Figure 7 Changes of the maximum generator speed (top left), the rotor acceleration (top right), the fore-aft tower acceleration (bottom left) and the pitch rate (bottom right) when feedforward control is activated for all turbulence seeds in scenario a). Boxplots show the median (red line), upper and lower quartiles (box), typical range (whiskers), and outliners (red crosses).

The purpose of scenario b) is to investigate, whether the feedforward controller can help to improve the aerodynamic efficiency when the WT power is increased. The simulation results show that the current controller fails to increase the average generator power in region 2 and 2.5 (see Figure 8, top left). During most simulations, the turbulent wind caused regular deviations from steady-state operating points. Thus, pitch angle decreases just caused minimal gains in aerodynamic efficiency. Furthermore, over the cause of several seconds, the changes in the power of the wind outweighed the power increase for frequency support thus making such a support ineffective. That might be different for other frequency scenarios with a longer and stronger power increase like the islanding of the Iberian peninsula [24]. For higher average wind speeds, there are typically minimal increases of the average generator power as the feedforward controller helps to keep the WT in region 3. As the average generator power remains nearly constant, there is no significant benefit from the additional control loop for the grid.

The pitch rate and the rotor acceleration are significantly increased for all average wind speeds except for the 15 m/s and 20 m/s cases (Figure 8, top and bottom right). For 8.4 m/s and 9.6 m/s relative increases of the pitch rate cannot be displayed, as the WT does not pitch when the feedforward control is deactivated. The absolute increase is approximately 0.16 deg/s for all turbulence seeds at these wind conditions. The influence of the tower acceleration is comparatively small (Figure 8 bottom left). The strongest decreases occur when the decreased pitch angle during the frequency event helps to stabilise the thrust force during a negative wind gust. The highest increases occur when a positive gust coincides with the frequency event.
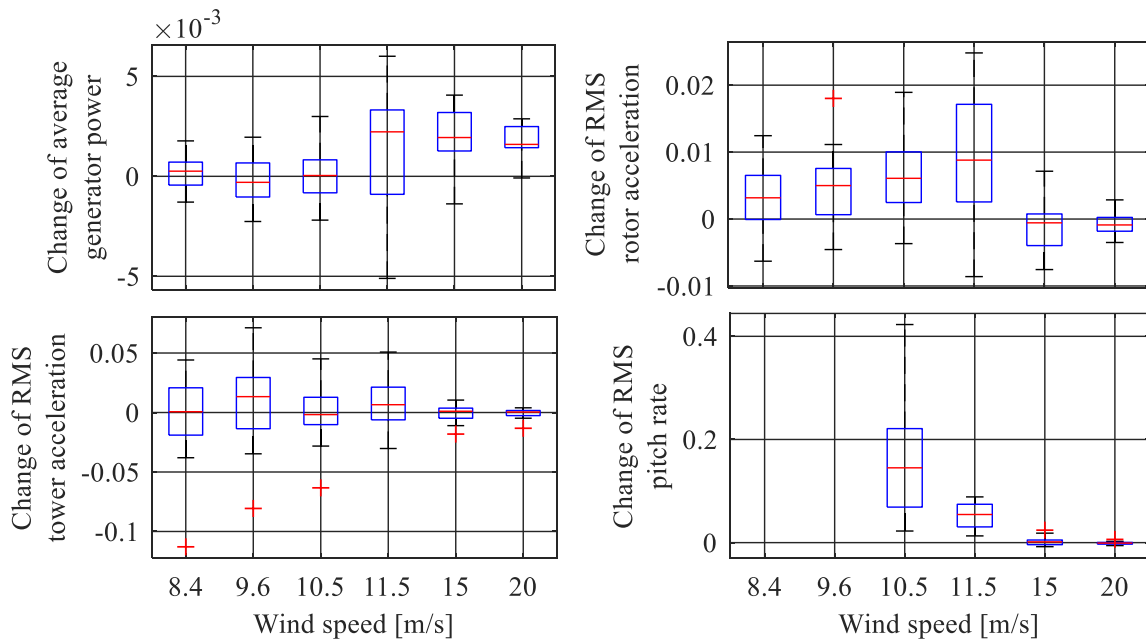
Figure 8 Changes of the average generator power (top left), the rotor acceleration (top right), the fore-aft tower acceleration (bottom left) and the pitch rate (bottom right) when feedforward control is activated for all turbulence seeds in scenario b). Boxplots show the median (red line), upper and lower quartiles (box), typical range (whiskers), and outliners (red crosses).

The purpose of scenario c) is to investigate, whether the feedforward controller causes unnecessary loads during a normal behaviour of the grid frequency. In such a situation, the WT only provides little grid support. Therefore, the pitch angle should only be changed occasionally. In the simulations, the RMS value of the pitch rate changes less 0.5 % at 10.5 m/s and even less 0.1 % for all other wind speeds. The average generator power slightly increases by approximately 0.15 % for all cases. All other signals change by less than 0.01 %. Hence, it can be concluded that the controller works as intended in this scenario.

4. Conclusions

In the presented work, a forward loop for the pitch angle is added to an existing grid frequency support controller. The theoretical idea of the controller is explained with help of a TSR and pitch angle depending aerodynamic efficiency. The modified controller is tested for the NREL 5 MW WT with three different grid frequency scenarios, exemplary covering some of the most important grid situations.

The study shows that the controller is capable of effectively protecting the WT from overspeed when its power is drastically reduced during extreme grid events. Furthermore, the rotor acceleration is decreased in this situation, thus reducing the negative impact on the drive train. However, the pitch rates are significantly increased during extreme grid scenarios, which might also be a burden for the WT. The grid will benefit from the increased reliability of the WT grid support, if emergency stops are avoided.

By contrast, there is no significant impact on the aerodynamic efficiency and thus the produced energy when additional power for grid frequency support is supplied. In the simulated scenarios, the rotor acceleration is also increased. Hence, it can be concluded that for the simulated scenarios and the analysed WT, the feedforward loop should not be used to increase the aerodynamic efficiency, especially not in part load operation. This might be different, if the blades of different WT react stronger to a suboptimal angle of attack.

The effect on the tower head accelerations strongly depends on the wind conditions during the frequency event. The negative consequences are strongest when the frequency event coincides with a

positive wind gust. Hence, it might be beneficial to combine the controller with a Lidar feedforward control to minimize the effect of grid frequency support on the WT.

References

[1]   EirGrid 2020 EirGrid grid code. Version 9. Available from: https://www.eirgridgroup.com/site-files/library/EirGrid/GridCodeVersion9.pdf

[2]   Hydro-Québec TransÉnergie 2019 Technical requirements for the connection of generating stations to the Hydro-Québec transmission system Available from: http://www.hydroquebec.com/transenergie/fr/commerce/pdf/2_Requirements_generating_stations_D-2018-145_2018-11-15.pdf

[3]   Central Electricity Authority 2019 Technical standards for connectivity to the grid (Amendment). Available from: https://cea.nic.in/wp-content/uploads/2020/02/notified_regulations.pdf

[4]   O'Sullivan J, Rogers A, Flynn D, Smith P, Mullane A and O'Malley M. 2014 Studying the maximum instantaneous non-synchronous generation in an island system—frequency stability challenges in Ireland. *IEEE Trans Power Syst.* **29** 6 pp 2943–51.

[5]   Yu M, Roscoe AJ, Dyśko A, Booth CD, Ierna R, Zhu J and Urdal H. 2017 Instantaneous penetration level limits of non-synchronous devices in the British power system *IET Renew Power Gen* **11** 8 pp. 1211–17.

[6]   Chown G, Wright J, van Heerden R and Coker M. 2017 System inertia and rate of change of frequency (RoCoF) with increasing non-synchronous renewable energy penetration. *Cigré 2017: 8th Southern Africa Regional Conf.* (Cape Town: Cigré) pp. 32 – 43.

[7]   Thiesen H and Jauch C 2022 Potential of onshore wind turbine inertia in decarbonising the future Irish energy system. A*pplied Sciences*. **12** 6 2984.

[8]   Eriksson R, Modig N and Elkington K. 2018 Synthetic inertia versus fast frequency response: a definition. *IET Renew Power Gen*. **12** 5 pp 507–14.

[9]   Godin P, Fischer M, Röttgers H, Mendonca A and Engelken S. 2019 Wind power plant level testing of inertial response with optimised recovery behaviour. *IET Renew Power Gen*. **13** 5 pp 676–83.

[10] Aho J, Fleming P and Pao LY. 2016 Active power control of wind turbines for ancillary services: A comparison of pitch and torque control methodologies. *In: Proc. American Control Conf.* (Boston: IEEE) pp 1407–12.

[11] Fleming PA, Aho J, Buckspan A, Ela E, Zhang Y, Gevorgian V, Scholbrock A, Pao L and Damiani R. *2016* Effects of power reserve control on wind turbine structural loading: Structural loads analysis of power reserve control strategies for wind turbines. *Wind Energy* **19** 3 pp 453–69.

[12] Aho J, Pao L and Fleming P. 2013. An active power control system for wind turbines capable of primary and secondary frequency control for supporting grid reliability. In: *Proc. 51st AIAA Aerospace Sciences Meeting* (Grapeville: Aerospace Research Central).

[13] Ramtharan G, Jenkins N and Ekanayake JB. 2007 Frequency support from doubly fed induction generator wind turbines. *IET Renew Power Gen*. **1** 1 pp 3-9.

[14] Fernández-Guillamón A, Gómez-Lázaro E, Muljadi E and Molina-García Á. 2019 Power systems with high renewable energy sources: A review of inertia and frequency control strategies over time. *Renew Sustain Energy Rev*. **115** 109369.

[15] Gloe A, Jauch C, Craciun B and Winkelmann J. 2019 Continuous provision of synthetic inertia with wind turbines: implications for the wind turbine and for the grid. *IET Renew Power Gen*. **13** 5 pp 668–75.

[16] Gloe A, Jauch C, Craciun B, Zanter A and Winkelmann J. 2021 Influence of continuous provision of synthetic inertia on the mechanical loads of a wind turbine. *Energies*. **22** 14 5185.

[17] Jonkman J, Butterfield S, Musial W and Scott G. 2009 Definition of a 5-MW reference wind turbine for offshore system development. Report No.: NREL/TP-500-38060.

[18] Schlipf D, Fleming P, Haizmann F, Scholbrock A, Hofsäß M, Wright A and Cheng P W. 2014 Field testing of feedforward collective pitch control on the CART2 using a nacelle-based lidar scanner. *J. Phys.: Conf Ser*. **555** 012090.

[19] Jonkman J and Hippel S. 2015 NREL 5-MW reference turbine - cp, cq, ct coefficients. Available from: https://wind.nrel.gov/forum/wind/viewtopic.php?f=2&t=582

[20] Jauch C. 2020 First eigenmodes simulation model of a wind turbine - for control algorithm design Available from: https://www.researchgate.net/publication/344154941_First_Eigenmodes _Simulation_Model_of_a_Wind_Turbine_-_for_Control_Algorithm_Design

[21] Gloe A, Jauch C and Räther T. 2021 Grid support with wind turbines: the case of the 2019 blackout in Flensburg. *Energies*. **14** 6 1697.

[22] Guo F and Schlipf D. 2021 A spectral model of grid frequency for assessing the impact of inertia response on wind turbine dynamics. *Energies*. **14** 9 2492.

[23] ENTSO-E. 2021 System separation in the Continental Europe synchronous area on 8 January 2021 Available from: https://www.entsoe.eu/news/2021/01/26/system-separation-in-the-continental-europe-synchronous-area-on-8-january-2021-2nd-update/

[24] ENTSO-E. 2021 Outage of French-Spanish interconnection on 24 July 2021 Available from: https://www.entsoe.eu/news/2021/08/20/outage-of-french-spanish-interconnection-on-24-july-2021-update/

[25] ENTSO-E. 2009 Continental Europe operation handbook - P1 - policy 1: Load-Frequency control and performance [C] Available from: https://eepublicdownloads.entsoe.eu/clean-documents/pre2015/publications/entsoe/Operation_Handbook/Policy_1_final.pdf

[26] Wang Y, Silva V and Winckels A. 2014 Impact of high penetration of wind and PV generation on frequency dynamics in the Continental Europe interconnected system. In: *Proc. Wind Integration Workshop 2014* ed U Betancourt and T Ackermann (Berlin: Energynautics).

[27] Adeen M, Jonsdottir GM and Milano F. 2019 Statistical correlation between wind penetration and grid frequency variations in the Irish network. In: *Proc. 2019 IEEE Int. Conf. EEEIC / I&CPS Europe* (Genova: IEEE) pp. 1–6.

[28] Mele FM, Ortega A, Zarate-Minano R and Milano F. 2016 Impact of variability, uncertainty and frequency regulation on power system frequency distribution. In: *Proc 2016 PSCC* (Genova: IEEE) pp 1-8.

Publication 6

Increased Wind Energy Yield and Grid Utilisation with Continuous Feed-In Management

C. Jauch, A. Gloe, S. Hippel, and H. Thiesen

Increased Wind Energy Yield and Grid Utilisation with Continuous Feed-In Management

Clemens Jauch *, Arne Gloe, Sebastian Hippel and Henning Thiesen

Wind Energy Technology Institute, Flensburg University of Applied Sciences, Kanzleistraße 91-93, Flensburg 24943, Germany; arne.gloe@hs-flensburg.de (A.G.); sebastian.hippel@hs-flensburg.de (S.H.); henning.thiesen@hs-flensburg.de (H.T.)

* Correspondence: clemens.jauch@hs-flensburg.de; Tel.: +49-461-805-1660

Abstract: This paper presents a study to assess how wind turbines could increase their energy yield when their grid connection point is not strong enough for the rated power. It is state of the art that in such situations grid operators impose feed-in management on the affected wind turbines, i.e., the maximum power is limited. For this study a 5 MW wind turbine is introduced in a small grid that has only limited power transfer capabilities to the upstream power system. Simulations of one particular day are conducted with the electric load, the temperature, and the wind speed as measured on that day. This simulation is conducted twice: once with the 5 MW wind turbine controlled with conventional feed-in management, and a second time when its power is controlled flexibly, i.e., with continuous feed-in management. The results of these two simulations are compared in terms of grid performance, and in terms of mechanical stress on the 5 MW wind turbine. Finally, the conclusion can be drawn that continuous feed-in management is clearly superior to conventional feed-in management. It exhibits much better performance in the grid in terms of energy yield and also in terms of constancy of voltage and temperature of grid equipment. Although it causes somewhat more frequent stress for the wind turbine, the maximum stress level is not increased.

---

1. Introduction

In the transition from conventional (mostly thermal) power production to renewable energy sources (dominated by wind power), the expansion of the power system can often not keep pace with the installation of wind power plants. Historically grown power systems based on conventional generation are usually centralised. The power is produced in relatively few locations and the task of the power system is to deliver the electric energy to the dispersed consumers. Wind turbine (WT) generators, on the other hand, are inevitably scattered across a wider area. In order to maximise the energy yield and in order to minimise the impact on the inhabitants of a country, wind turbines (WTs) are usually installed in rural areas; ideally far away from residential areas. Hence, the transition to wind power asks for substantial changes in the power system. Many power lines, which were historically built for delivering power one way, now experience alternating power flow directions. A sparsely dimensioned power system in a rural area might need to be reinforced massively, to be able to take on the power produced by WTs.

Since power system reinforcements are very expensive and time consuming, grids which are affected by massive growth of wind power installation are usually insufficiently dimensioned. Historically, power system equipment is often only used to 70% of its rating, to avoid undue wear and tear and to maintain redundancy. In contrast to this, grids that are heavily penetrated by wind power, in peak times operate at their limits. Instead of dimensioning the power system to be able

to take on any conceivable amount of power from the installed WTs, the power feed-in from these WTs is limited in order to avoid overloading the power system components. This mechanism is called feed-in management [1]. While wind power is often fed into the distribution grid, sometimes also the upstream transmission grid is congested requiring feed-in management [2]. In Germany the amount of unused energy from feed-in management was 1581 GWh in 2014 and 77.3% of this would have been generated by WTs. A figure of 96% of unused renewable energy was wasted by feed-in management in the northern states, most of it in the state of Schleswig-Holstein [3]. In 2015 the amount of unused energy rose to 4722 GWh, the share of wind power increased to 87.3% [4].

To reduce the dissipation of wind power, continuous feed-in management was already proposed some years ago [5]. A German grid operator currently tests slow continuous feed-in management [6] and it has been investigated whether this approach can also be adapted to other grids [7]. The idea of continuous feed-in management is to continuously adapt the power feed-in of WTs to the currently prevailing loading of the considered grid. Experience gathered so far shows that power system expansions are necessary only to a small extent if the power control from WT is carried out more flexibly. Further it would be advantageous if the permissible voltage range could be expanded [7].

In areas which are short of free land for wind power installations, the available land needs to be utilised to the maximum extent. Hence, the rated power of each WT is as large as possible to minimise the number of installed WTs. Large power generally means large rotor diameters. In countries that are densely populated also rural areas are affected by settlements. The inevitable proximity of WTs to settlements demands a reduction of their visible impact. Consequently, the installed WTs with large rotor diameters are often installed on very short towers. Also this trend can be observed in Schleswig-Holstein.

Although traditional (conventional) feed-in management is done in a very conservative manner, it induces stress on the affected WTs [8]. Hence, in this paper continuous feed-in management is applied and it is assessed whether this approach, which is a lot more favourable for the power system, causes a noticeable increase in stress for the WT [8]. In order to do this assessment a realistic case study is presented here. It is assumed that a 5 MW WT has been installed at the university campus in Flensburg, in the state of Schleswig-Holstein (northern Germany) and that this WT feeds into the grid of the campus. The voltage in the campus grid, and the loading of the transformer, which is assumed to be the link to the upstream grid, are researched. The rating of the grid connection transformer is chosen such that it poses a limitation for the wind power infeed, depending on the current load and the current infeed of the already existing equipment on campus Flensburg. The purpose of this study is to find the additional stress from continuous feed-in management when the WT operates under very demanding, but yet realistic conditions. It is the intention of the authors to avoid undue preference of continuous feed-in management. Therefore, the excitations continuously inflicted on the WT are chosen to be as large as possible. This way, any additional excitations from feed-in management are bound to cause obvious problems for the WT.
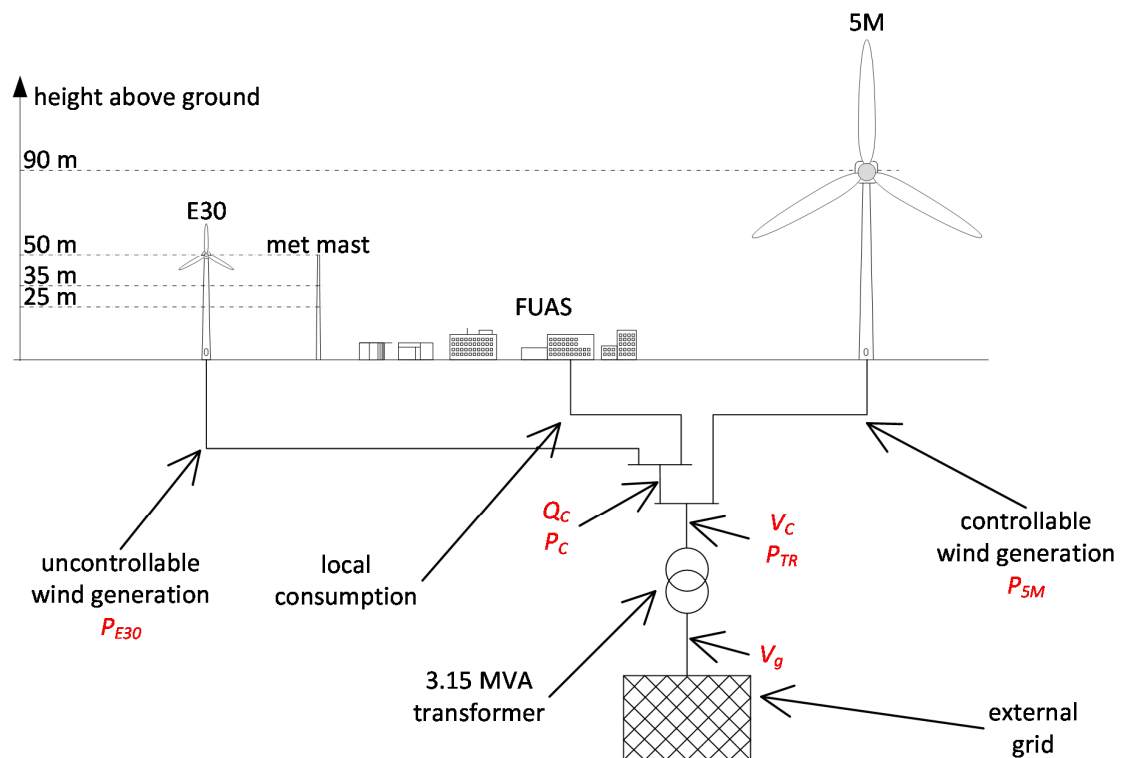
2. Case Study

2.1. General Setup and Reasoning

In the considered case study it is assumed, that the combination of supply and demand on campus Flensburg is supplemented with a massive increase of installed wind power. Hence, a 5 MW WT is assumed to have been installed in the vicinity of campus Flensburg and this WT feeds its power into the campus grid. The connection between the campus grid and the external grid is assumed to be made of a 3.15 MVA transformer. This has a sufficient rating most of the time, but it is prone to get overloaded in times of low demand and high wind speeds. This configuration replicates the situation in many grids, which are heavily penetrated with wind power and which become regularly congested because the installed wind power capacity exceeds the capacity of the grid equipment. At the same time this configuration replicates the situation common for areas that are short of available land for

wind power installations. As mentioned in Section 1 "Introduction", this leads to installation of as few as possible WTs (to save space) with as large as possible rotors (to maximise the energy yield) that are installed on as short as possible towers (to minimise the effect on the people living in the vicinity). Consequently, the WT considered in this case study is the NREL 5 MW reference turbine (5M) [9].

Figure 1 illustrates the setup of the case study of campus Flensburg with Flensburg University of Applied Sciences (FUAS). This drawing is to scale in the vertical dimension to illustrate how the heights of the different installations relate to each other. Also shown is the single line diagram of the grid connection with variable names (in red letters) of electrical quantities as they are presented in measurements and simulations later in this article.

Figure 1. Setup of case study of campus Flensburg supplemented by a 5 MW wind turbine (WT) with connection to the external grid.

In order to have a representative situation, the electrical consumption, the wind speed and ambient temperature was measured on an arbitrary week day during the semester. The day chosen was 5 April 2017. The prevailing conditions on this day are discussed in Section 2.3 "Load Profile" and Section 2.5 "Wind Measurement".

2.2. Campus Flensburg

Campus Flensburg hosts two universities, namely FUAS and Europa-Universität Flensburg. In total approximately 10,000 students study on campus Flensburg. These two universities share some facilities on campus like the library, canteen, lecture hall and chapel. For billing and redundancy reasons the two universities have separate grid connections. The grid connection of FUAS supplies all lecture theatres, laboratories, and administration buildings of FUAS. Of the shared facilities it supplies the canteen and the chapel. Apart from this load, there is also some generation that feeds into the grid connection point of FUAS: a 1.6 kW rooftop photovoltaic generator, a 6 kW Easywind WT and a 240 kW Enercon WT. The Enercon WT has a rotor diameter of 30 m (this WT in the following text is called E30). Next to the E30 there is a met mast that measures the wind at three different heights, up to the hub height of the E30 (50 m). Section 2.5 "Wind Measurement" provides more information about

the met mast. Figure 1 shows the met mast and buildings of FUAS; most of these are three and four story buildings.

2.3. Load Profile

The load profile of campus Flensburg is mainly determined by the teaching activities at the two universities. It is low during the night and it peaks during the normal lecturing hours. Figure 2 shows the time traces of active and reactive power, P_C and Q_C respectively, at the grid connection point. Hence, P_C can be considered the residual load of the campus Flensburg. On the time axis in Figure 2, and in all following plots showing time traces, the time starts with 00:00 on 5 April 2017 and ends at 00:00 on 6 April 2017. Also shown in Figure 2 is the active power of the E30, P_{E30}, as this covers some of the load. The power factor of the E30 is always controlled to be unity ($\cos\phi = 1$), and the active power is purely determined by the prevailing wind speed. Therefore, the measured wind speed is shown in Section 2.5 "Wind Measurement". The increasing wind speed and the decreasing demand eventually lead to power being fed into the external grid (negative P_C) every now and then after about 16:00.
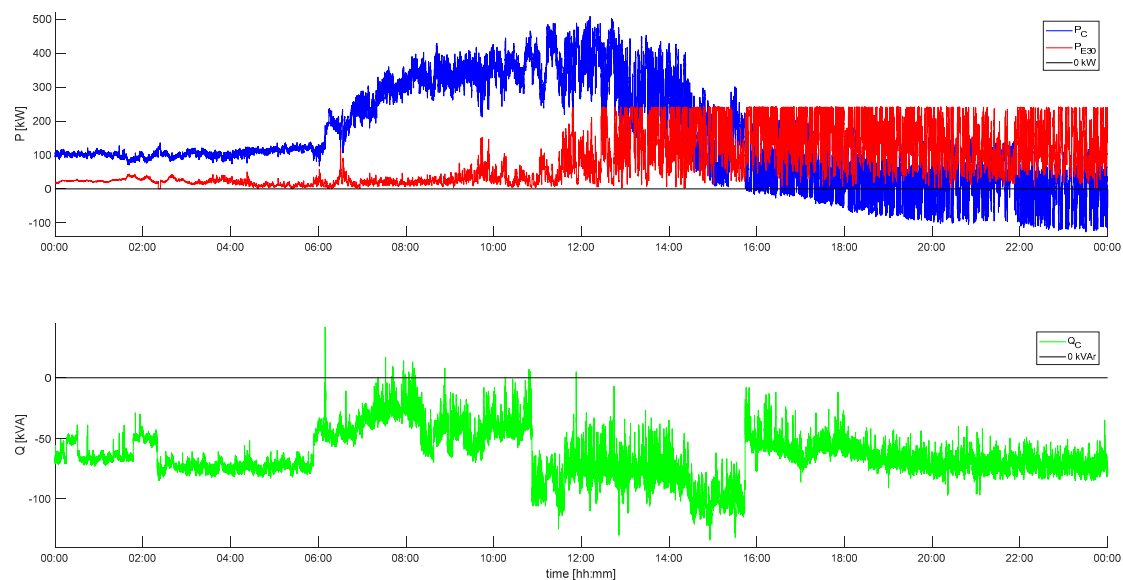

Figure 2. Power measurements on campus Flensburg on 5 April 2017.

2.4. Wind Turbine Model

As introduced above, the WT to feed extra power into the campus grid was chosen to be the NREL 5 MW WT (5M). The properties of this WT are publicly available and well documented [9]. The goal is to simulate the interaction of this WT with the grid (see Section 2.7 "Connection to External Grid") by supplementing it with the applicable controllers (see Section 2.8 "Power Control"). Therefore, the mechanical dynamics of the 5M are translated to fit the 1st eigenmode model of a WT [10], which exhibits relatively little complexity but retains the most dominant mechanical dynamics. This model represents the first eigenmodes of the tower, the blades in in-plane and in out of plane direction, and the first torsional eigenmode of the drive train. At the same time this model allows easy extension with grid connection and additional controllers.

The need for a short tower, as discussed in the Introduction, leads to a relatively high 1st eigenfrequency of the tower. At the same time the short tower causes severe wind shear across the rotor plane. This is discussed further in Section 2.5 "Wind Measurement".

The aerodynamics of the rotor blades are modelled with lookup tables of the aerodynamic power coefficient and the aerodynamic thrust coefficient for the individual blades. An aeroelastic representation of the rotor applying a blade element momentum model and a stochastic wind field

in front of the rotor is omitted for the sake of simplicity and ease of use of the model. As outlined in Section 1 "Introduction" it is the intention of this study to find the worst possible additional stress for the WT when burdened with continuous feed-in management. For this purpose artificial excitations are added to the wind speed signal inflicted on the WT; for more details see Section 2.6 "Wind Model". Previously conducted measurements at the E30 on campus Flensburg showed that the natural turbulences at the site and the rotational sampling of the rotor do not provide extreme excitations [11]. Hence, this relatively simple model was used, as it allows artificial addition of excitations via the wind speed signal.

In addition to the reduction of the model to the first eigenmodes, the blade parameters are a simplification of the structural dynamics of the 5M blades, because the whirling modes [12] are neglected. Also the fact that the stiffness of the blades of the 5M is a function of the rotor speed [12] is neglected. This simplification is deemed justifiable as in this study the focus is on grid connected operation. Hence, the maximum error that can be experienced is 0.03 Hz in flapwise direction and 0.007 Hz in edgewise direction. Therefore, the stiffness that applies at rated speed is used throughout the whole speed range [10].

The eigenfrequencies that are represented by the 1st eigenmode model are visualized in the Campbell diagram in Figure 3.
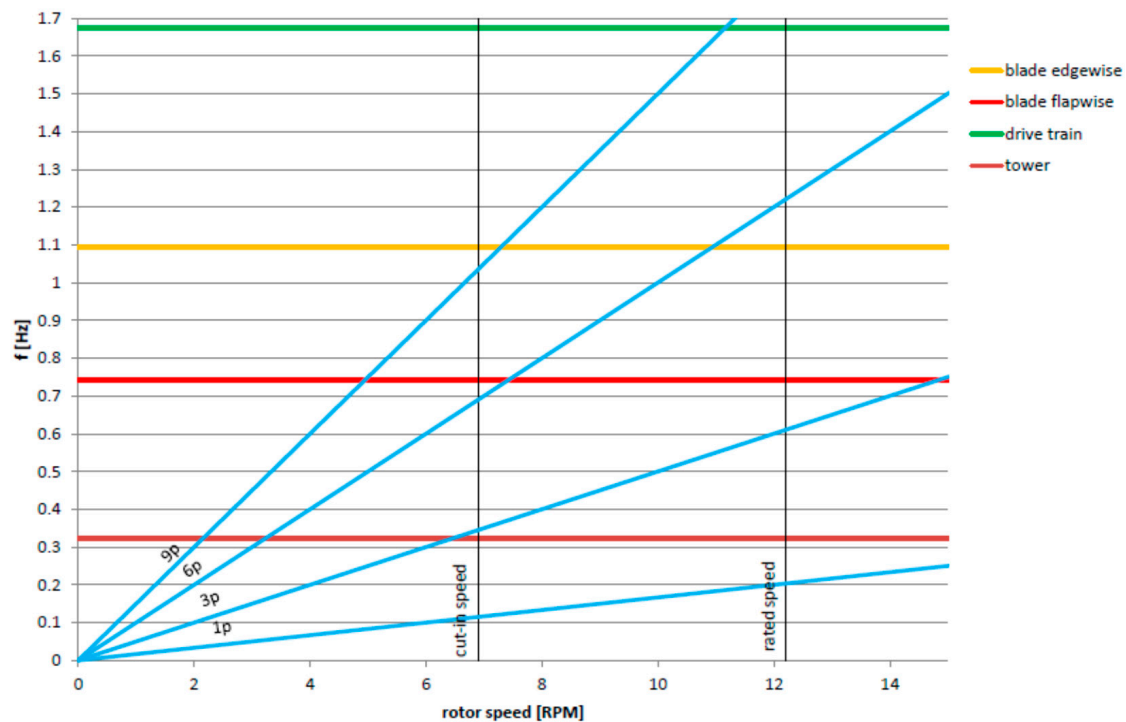

Figure 3. Campbell diagram with eigenfrequencies of 5M WT as implemented in the 1st eigenmode model.

The speed controller of the 5M WT with its gain scheduling is as documented by Jonkman et al. [9]. In order to be able to adjust the power infeed flexibly to the requirements resulting from the loading of the grid connection transformer, a feed-in management controller is needed. This controller is introduced in Section 2.8 "Power Control", further below.

2.5. Wind Measurement

The met mast on campus Flensburg allows the wind speed to be measured at 25 m, 35 m and 50 m above ground, see Figure 1. This met mast is equipped with ultrasonic anemometers that collect measurements with a frequency of up to 10 Hz [11]. Figure 4 shows the wind speed measured on 5 April 2017. It can be seen that the wind speed is low in the morning hours and increases considerably in the afternoon (after 11:00), which has a noticeable effect on the residual load shown in Figure 2.
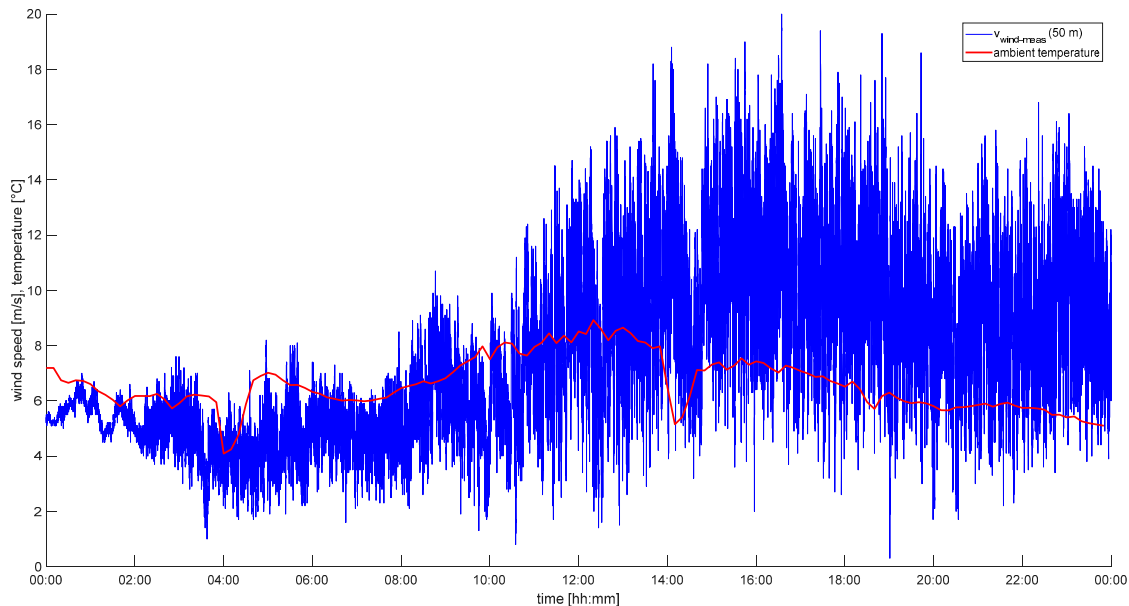
Figure 4. Wind speed at 50 m above ground (hub height of the E30) and temperature on campus measured on 5 April 2017.

Based on the measured wind speed v_1 at height z_1, Equation (1) allows the wind speed v_2 at a different height z_2 to be calculated. In Equation (1) z_0 is the roughness length of the considered area, which is $z_0 = 1.7$ m for campus Flensburg. Applying the measured wind speed at hub height of the E30 ($z_1 = 50$ m), the wind speed at different heights, z_2, that are swept by the rotor of the 5M WT, e.g., hub height ($z_2 = 90$ m) can be derived [13], see Figure 5. It is to be appreciated that Equation (1) only yields reliable results when z_0 is small, or z_2 is not much larger than z_1. Hence, comparing the hub height of the E30 with the hub height and blade length of the 5M it is questionable whether Equation (1) should be applied. In particular since z_0 on campus Flensburg is so large due to the complexity of the terrain, partly caused by buildings and vegetation (z_0 is derived from measurements recorded over several years and confirmed by different measurement technologies). However, for the sake of this case study Equation (1) is applied nonetheless as it worsens the wind shear to which the 5M is exposed, see next section.

$$v_2(z_2) = v_1(z_1) \cdot \frac{\ln\left(\frac{z_2}{z_0}\right)}{\ln\left(\frac{z_1}{z_0}\right)} \tag{1}$$

With measurements from the met mast, which were recorded over several years, also the turbulence intensity, *TI*, can be computed according to Equation (2) [11]. *TI* contains the standard deviation of the wind speed, $\sigma_{wind,10\,min}$, and the mean wind speed, $v_{wind,10\,min}$, each of 10-min-intervals.

$$TI = \frac{\sigma_{wind,10min}}{v_{wind,10min}} \tag{2}$$

th the height above ground. Applying this reasoning
and ... which allows extrapolating *TI* to the heights swept
by t ... firmed with the long term measurements conducted
witl ... e seen in Figure 5.

(**a**)

(**b**)
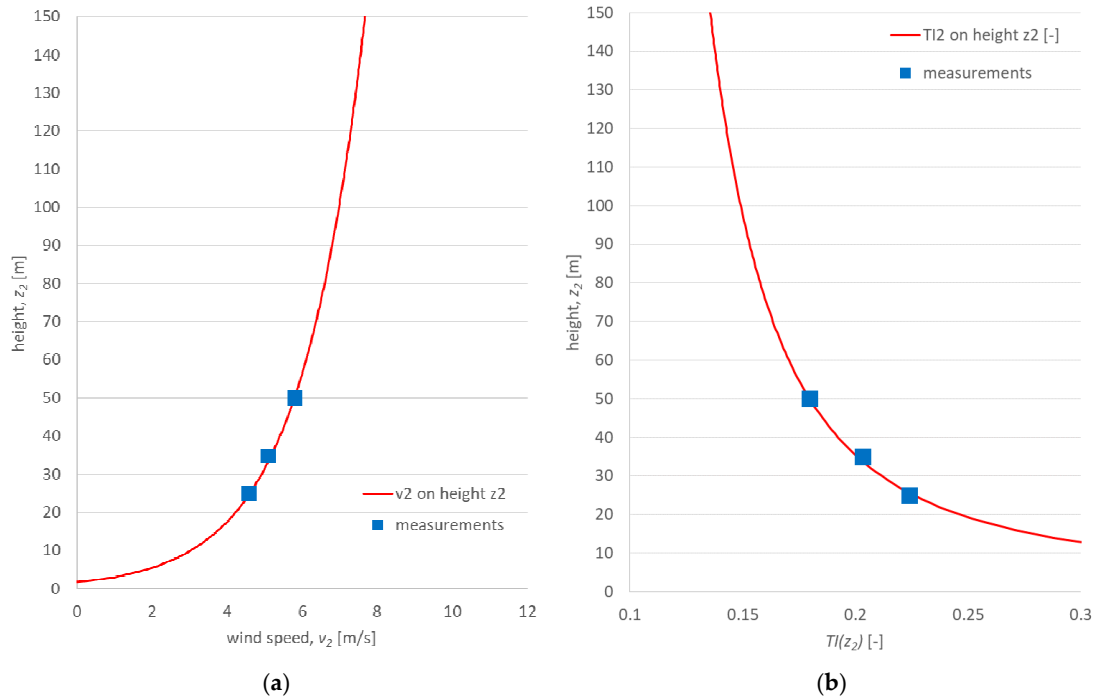
Figure 5. Measured and extrapolated wind speed (**a**) and turbulence intensity, *TI*; (**b**) versus height above ground, z_2.

With this information about the wind conditions at the site of campus Flensburg a wind model can be designed, as discussed in the following section.

$$TI_2(z_2) = TI_1(z_1) \cdot \frac{\ln\left(\frac{z_1}{z_0}\right)}{\ln\left(\frac{z_2}{z_0}\right)} \tag{3}$$
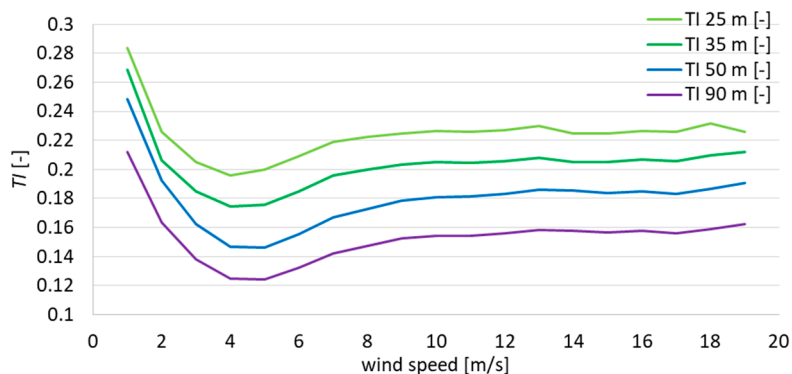

Figure 6. Computed from measurements and extrapolated turbulence intensity, *TI*, versus wind speed.

2.6. Wind Model

Since in this study the simple 1st eigenmode model of the 5M WT is applied, only one single wind speed time series is needed as input. Inside this WT model the wind speed time series is manipulated to account for the wind speed variations arising from wind shear across the rotor plane, rotation, and vibrations of WT components [10]. Hence, the wind speed time series that is input to this model has to be suitable for the hub height of the 5M, i.e., 90 m. The basis for the simulated wind speed is the wind speed measurement of the met mast 50 m above ground. In this way the simulated wind speed signal fits the scenario of the measurement. It has to be kept in mind that the measured electric power, P_C, is affected by the uncontrollable wind power of the E30. The 5M is assumed to be located in the vicinity of the E30; hence, the time trace of the wind speed for the 5M has to be similar to that of the E30.

The purpose of the wind model is twofold: (i) to generate a wind speed signal that is realistic for the considered scenario; and (ii) the wind speed variations need to cause the worst possible continuous and realistic excitations for the WT components. Note that the goal of this study is also to assess the additional mechanical stress from continuous feed-in management.

In the wind model (illustrated in Figure 7) the measured wind, $v_{\text{wind\_meas}}$, is transformed to 90 m, $v_{\text{wind\_meas\_trans}}$, (Equation (1) with $z_1 = 50$ m and $z_2 = 90$ m). Then, this wind speed is filtered with a second order low pass filter (PT2) with a filter time constant $T_{\text{filter}} = 5$ s, leading to $v_{\text{wind\_meas\_filt}}$. This retains the low frequency components, i.e., the overall wind speed behaviour is comparable to other sites in the vicinity of the met mast. However, by low pass filtering also the *TI* decreases, which is fine as *TI* is lower at 90 m than at 50 m (see Figure 5). Figure 6 shows *TI* as computed from measurements of the met mast on campus Flensburg and as extrapolated to 90 m for the different wind speeds.
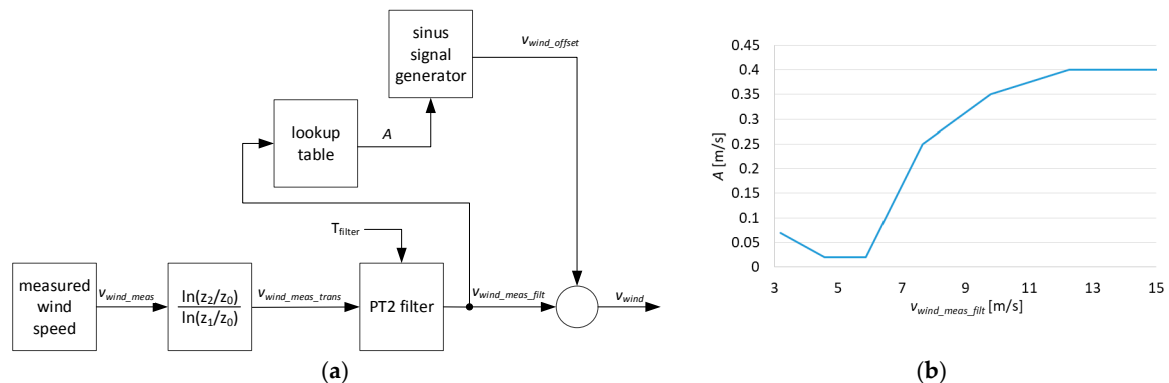

Figure 7. (**a**) Block diagram of wind model; (**b**) content of lookup table $A = f(v_{\text{wind\_meas\_filt}})$.

Low pass filtering reduces the *TI* below the desired values (*TI* at 90 m for the different wind speeds as shown in Figure 6), which leaves room for further wind speed variations. These are accomplished by offsetting $v_{\text{wind\_meas\_filt}}$ with a combination of sine waves ($v_{\text{wind\_offset}}$) whose frequencies are chosen to be identical with the four dominant eigenfrequencies of the WT components, as shown in Figure 3. The reason for this approach is that, as mentioned above, the wind signal shall cause the worst possible stress for the WT. These eigenfrequencies are f_{bf}, f_{be}, f_{t}, f_{dt} in Equation (4) (listed in the Appendix A) and t is the time in seconds.

$$v_{\text{wind\_offset}} = A(v_{\text{wind\_meas\_filt}}) \cdot [(\sin(2 \cdot \pi \cdot f_{\text{bf}} \cdot t) + \sin(2 \cdot \pi \cdot f_{\text{be}} \cdot t) + \sin(2 \cdot \pi \cdot f_{\text{t}} \cdot t) + \sin(2 \cdot \pi \cdot f_{\text{dt}} \cdot t)] \quad (4)$$

The magnitude, $A(v_{\text{wind\_meas\_filt}})$, in Equation (4) is a function of the filtered measured wind speed, in order to achieve the desired *TI* for the different wind speeds (see Figure 6). Figure 7 shows that *A* is implemented as lookup table in the wind model.

Figure 8 shows an exemplified time trace of the wind speed signals in the wind model.
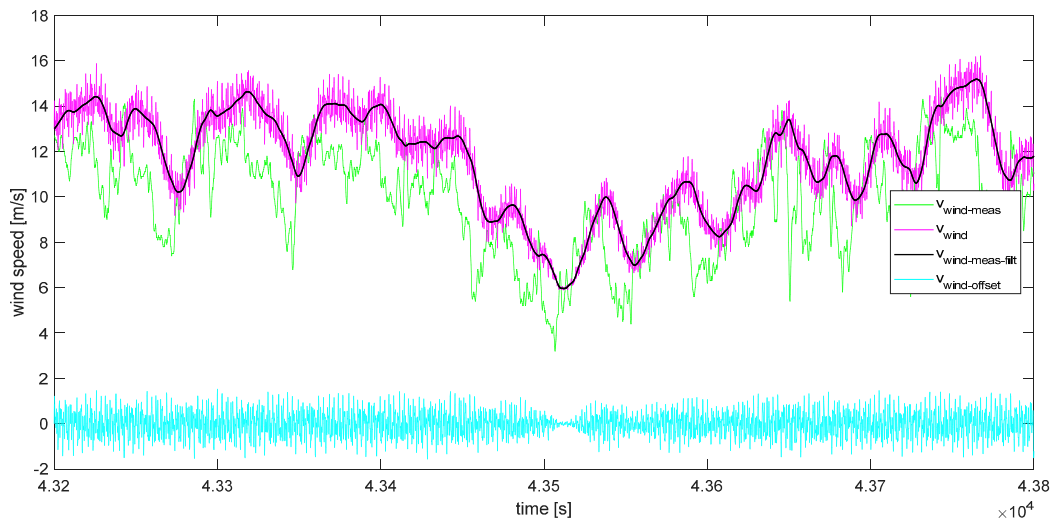
Figure 8. Measured wind speed at 50 m, filtered, extrapolated and offset wind speed at 90 m in the 10 Min interval at midday on 5 April 2017.

Figure 9 shows the frequency spectra of the wind speed time series measured at the met mast at 50 m above ground, v_{wind_meas}, (Figure 9 top) and of the wind speed signal from the wind model, v_{wind}, (Figure 9 bottom). The frequency spectrum of v_{wind_meas} must not be compared with frequency spectra that can be found in literature, as it is generated only from the 24 h time series used in the simulation discussed here. The frequency spectrum of v_{wind} clearly exhibits the four frequencies imposed by the wind model.
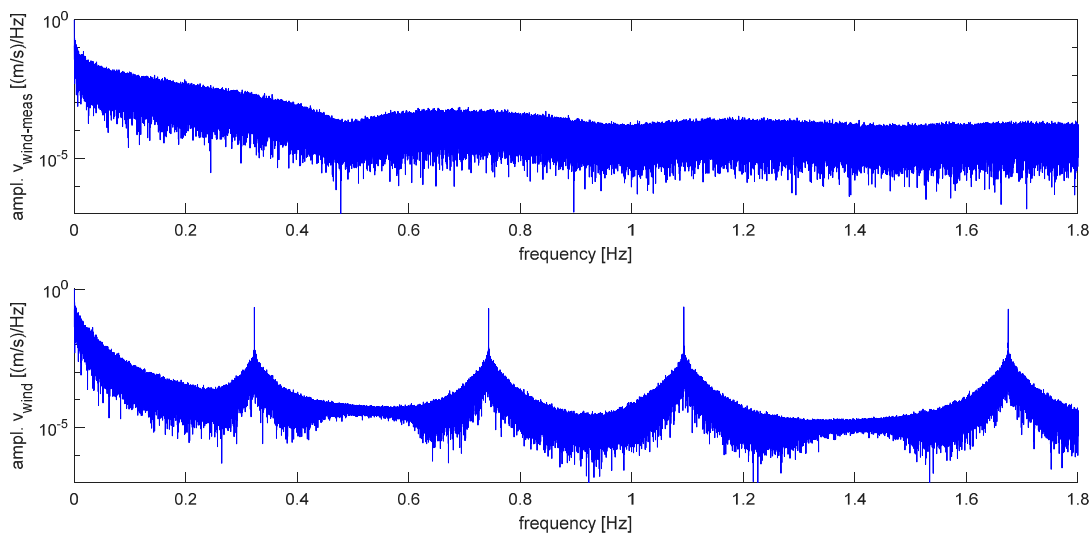
Figure 9. Frequency spectrum of wind speed measured at 50 m (**top**) and of the wind speed signal input to the 5M (**bottom**).

2.7. Connection to External Grid

In this case study, the grid on campus Flensburg is assumed to be connected to the external grid via a 3.15 MVA oil-immersed transformer [14]. The thermal behaviour of this transformer is modelled with a PT1 filter, as commonly suggested in the literature [15]. Whenever a transformer produces losses, P_L, its temperature, ϑ_{TR}, rises with respect to the ambient temperature, $\vartheta_{ambient}$. These losses are partially stored in the heat capacity of the material and partially dissipated via the cooling surface of the transformer, A_{cool}. In Equation (5) the first term represents the thermal power that is stored in

the heat capacity whenever the temperature ϑ_{TR} changes; where c_{TR} is the specific heat capacity and m_{TR} is the mass of the transformer. The second term represents the power that is dissipated via A_{cool} whenever cooling air with a certain heat transfer coefficient, α_{TR}, and a certain temperature difference, $\Delta\vartheta_{TR}$, is in contact with A_{cool}.

$$P_L = c_{TR} \cdot m_{TR} \cdot \frac{d\vartheta_{TR}}{dt} + \alpha_{TR} \cdot A_{cool} \cdot \Delta\vartheta_{TR} \tag{5}$$

Solving Equation (5) for $\Delta\vartheta_{TR}$ leads to Equation (6).

$$\Delta\vartheta_{TR} = \vartheta_{TR} - \vartheta_{ambient} = \Delta\vartheta_1 \left(1 - e^{-\frac{t}{\tau}}\right) \tag{6}$$

With $\Delta\vartheta_1$ being the steady state temperature difference between transformer and ambient air. This is the temperature difference needed to dissipate all P_L via A_{cool}.

$$\Delta\vartheta_1 = \frac{P_L}{\alpha_{TR} \cdot A_{cool}} \tag{7}$$

The time constant, τ, in Equation (6) represents the time it takes to charge the heat capacity of the transformer:

$$\tau = \frac{c_{TR} \cdot m_{TR}}{\alpha_{TR} \cdot A_{cool}} \tag{8}$$

The absolute temperature of the transformer, ϑ_{TR}, (Equation (6)) should be kept below ϑ_{TR_max} = 50 °C at all times in order to protect the transformer from overheating and the oil from excessive deterioration.

The electrical behaviour of this transformer is modelled as an impedance, $Z_{TR} = (R_{TR} + jX_{TR})$, which can be derived from name plate data. The methodology is as documented in Gloe and Jauch 2016 [11], the name plate data is listed in the Appendix A and the resulting impedance is Z_{TR} = (4.7891 + j 18.3897) Ω. The loss power, P_L, is the power that arises from the current flowing through R_{TR}.

In order to utilise the power transfer capability of the transformer to the full extent, i.e., in order to minimise the heat losses from current flowing through the transformer, the reactive power in the campus grid is controlled such that $\cos\phi$ = 1. Hence, the reactive power that arises in the campus grid, Q_C shown in Figure 2, has to be levelled out by the 5M. This can be achieved independent of the wind speed, as the frequency converter can generate and absorb reactive power independently of active power.

The active power fed into the transformer has to be limited such that the maximum steady state voltage in the campus grid does not exceed 110% of the rated voltage (in per unit (pu) this is 1.1 pu). Otherwise the usability of the voltage would be jeopardised. Hence, the power fed through the transformer, P_{TR}, has to be controlled with respect to the voltage in the campus grid, V_C, and with respect to ϑ_{TR}. This is discussed in the following section.

2.8. Power Control

The power that flows through the transformer, P_{TR}, comprises the uncontrollable power infeed of the E30 WT, P_{E30}, minus the local power consumption of the campus, which results in P_C, plus the controllable wind power of the 5M WT, P_{5M} (see Figure 1). Hence, P_{TR} has to be controlled such that neither the transformer gets overheated, nor the voltage limits are violated. Figure 10 shows the block diagram of the cascaded power control circuit; where in the outer loop P_{max_TR} is the power that would be permissible at a currently prevailing transformer temperature. While the transformer is cold, P_{max_TR} could be large enough to lead to an unacceptable voltage (V_C > 1.1 pu). Therefore, the power setpoint needs to be limited, $P_{max\_TR\_lim}$, to the value that leads to the maximum permissible voltage

drop, $P_{max\_TR\_volt}$. V_C is not only determined by the voltage drop across the transformer, but also by the voltage in the outer grid, V_g.
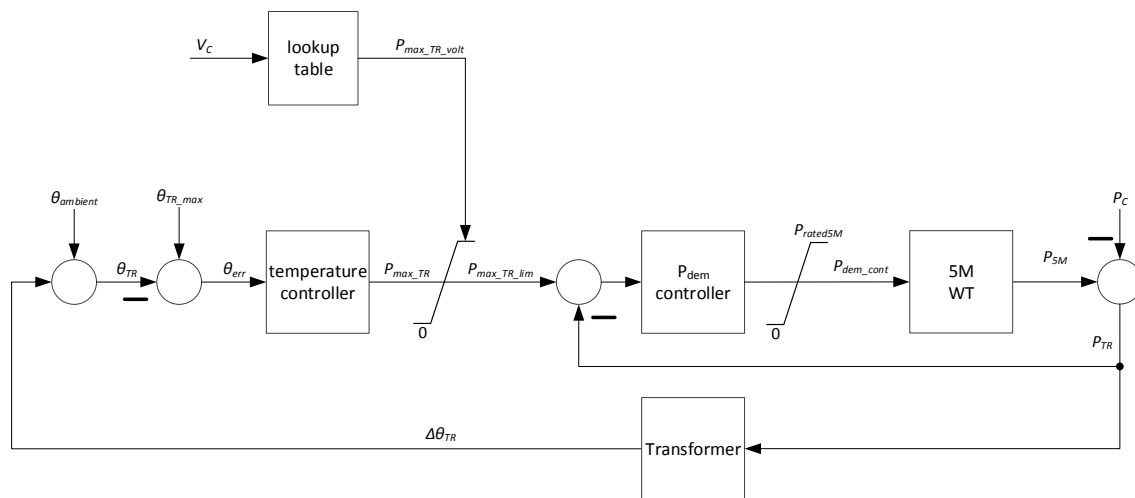
Figure 10. Power control circuit that maximises the power infeed while maintaining a healthy transformer temperature and an acceptable voltage in the campus grid.

The inner loop in the block diagram in Figure 10 controls the power setpoint of the 5M, P_{dem_cont}. In the inner loop the residual load, P_C, is a disturbance. The temperature controller in the outer loop is slow, as it interacts with the long thermal time constant of the transformer, τ. The inner control loop is faster, as the response of the WT is also fast. The gains of these proportional-integral (PI) controllers and the content of the lookup table $P_{max\_TR\_volt} = f(V_C)$ are listed in Appendix A.

3. Simulation of Feed-In Operation

With the simulation model introduced in the previous sections the scenario of 5 April 2017 can be simulated. When simulating the situation of campus Flensburg, the voltage in the outer grid, V_g, has to be defined, because V_C is not only determined by the voltage drop across the transformer, but also by V_g. In the absence of measurements of the voltage in the outer high voltage grid, V_g is assumed to be a constant 1.015 pu. This is a conservative assumption as the voltage in the high voltage grid is most likely higher when there is also high wind power infeed in neighbouring grid regions. As outlined in Section 1 "Introduction", Flensburg is located in northern Schleswig-Holstein. This region is characterised by good wind resources, massive wind power installations, relatively little consumption, and very limited power transfer capabilities to export wind power. North of Schleswig-Holstein is Denmark, which is comparably congested with wind power. With the North Sea to the west and the Baltic to the east the only option to export power is via limited lines to the continental European grid in the south. Hence, at times of high wind speeds the voltage in the transmission grid is most likely well beyond rated. However, V_g is assumed to be only moderately beyond its rated value as otherwise the comparison between conventional and continuous feed-in management would become trivial as is discussed in the following section.

3.1. Conventional Feed-In Management

Conventional feed-in management refers to the way feed-in management is conducted in Germany today. Feed-in management allows power system operators to throttle WTs to 60%, 30% or 0% of their rated power. This power demand is derived remotely by the power system operator and is relayed to those WTs, which have to limit their power infeed to the demanded value. The two controllers shown in Figure 10 are abandoned in case of conventional feed-in management. The power demand for the WT, P_{dem}, is in reality provided by the power system operator via a communication link. In the

simulation shown here P_{dem} is generated with the algorithm illustrated in Figure 11, which represents the methodology with which power system operators conduct feed-in management. The precise algorithm that translates thermal loading of equipment and voltage into P_{dem}-values is not disclosed by power system operators. It is, however, known that the P_{dem}-steps are 60%, 30% or 0% of their rated power and that the P_{dem}-values are updated only every 10 min. The intention behind this approach is to keep the power system stable with the least possible control effort.

The algorithm in Figure 11 follows the following logic: The relation between voltage and P_{dem}-values is assumed to be identical to the shape of the lookup table in Figure 10 (and as listed in Appendix A) but translated to discrete steps. The relation between transformer temperature and P_{dem}-values is in the style of the temperature control in Figure 10 but also translated to discrete steps. Note that in Figure 11, as well as in all following figures showing power, the unit for power is per unit (pu), with the rated power of the 5M being the power base.
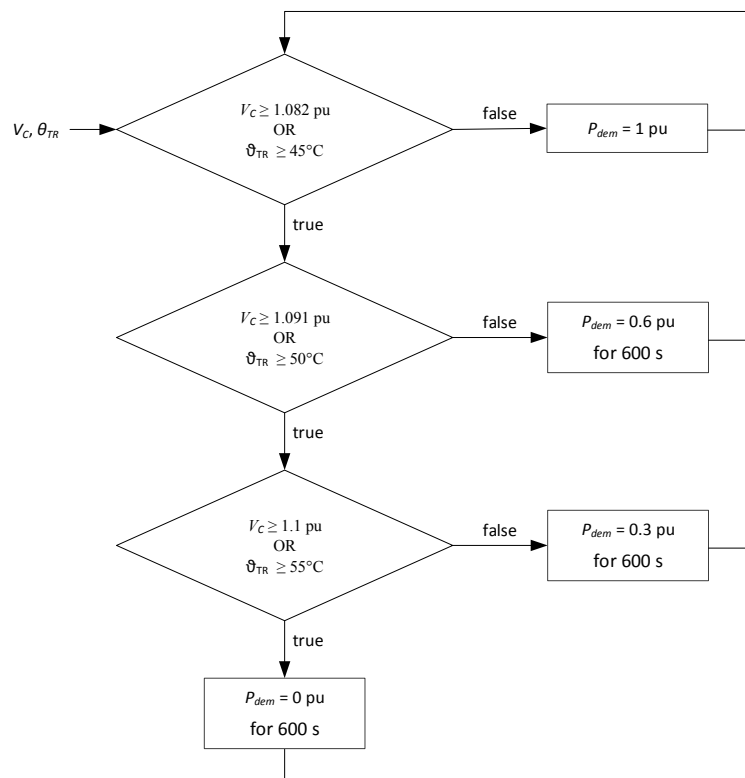

Figure 11. Flow chart of conventional feed-in management.

As in reality, the derivation of the P_{dem}-values is done in a conservative manner in case of conventional feed-in management. P_{dem} is set to values lower than necessary resulting from the current situation in the power system. Looking at the historical data of feed-in management in Schleswig-Holstein provided by the power system operator, it can be seen that it is very common to set P_{dem} precautionary to low values and keep it low for very long times [16]. In the conventional feed-in management simulations shown here, this precautionary approach is avoided. Consequently, the maximum energy infeed that could be achieved with conventional feed-in management can be found. Also, as mentioned in the previous section, the voltage in the outer grid is assumed to be only 1.5% above its rated value. This assumption also serves the purpose of finding the maximum energy yield. In contrast to this approach, high resolution measurements of the voltage in the high voltage grid would have been necessary. Since such measurements are not available, a constant value of V_g has to be assumed. Due to the large discrete steps in which P_{dem} is varied, a high value of V_g would lead to $P_{dem} = 0$ pu most of the time. This would make a comparison between conventional

and continuous feed-in management trivial, at least in terms of energy yield. In terms of mechanical loads a comparison would become impossible, as conventional feed-in management would lead to standstill of the WT. Hence, with a large constant value of V_g continuous feed-in management would look unduly superior.

Simulating the scenario with the given wind speed, temperature (Figure 4) and local residual load (Figure 2) leads to the behaviour of the 5M as shown in Figure 12 where it is controlled with conventional feed-in management. Figure 12 reveals that when the wind speed increases after 12:00 the transformer temperature is the primary cause for reducing P_{dem}. After 14:30 the local load decreases, and P_C eventually becomes negative because P_{E30} dominates the local consumption. In this situation V_C demands reducing P_{dem}. V_C reaches up to 8.3% above its rated value. Due to the long periods of reduced P_{dem} (at least 10 consecutive minutes) the transformer cools down such that its temperature is no longer the bottle neck. The cooling down of the transformer is further supported by the dropping ambient temperature (Figure 4). During the whole second half of the day, i.e., when feed-in management operation is necessary, the transformer is not utilised to its full potential. The transformer temperature even drops down to 21 °C. In such situations the loading of the transformer could be increased if also the reactive power would be controlled in order to control V_C. This option is not pursued here, as it is not part of conventional feed-in management in reality either.
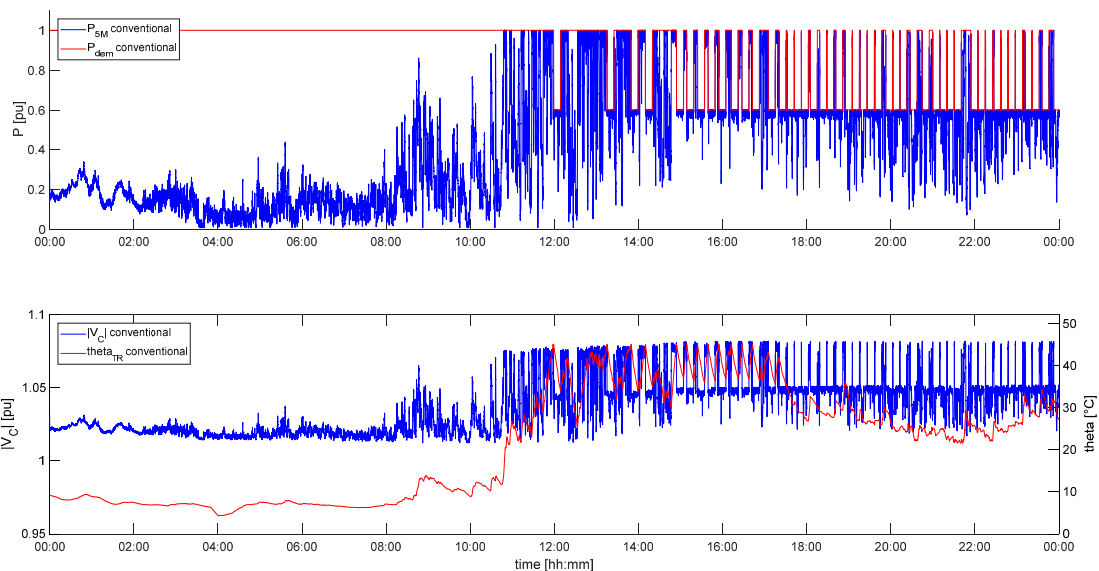
Figure 12. Simulation of case study with conventional feed-in management.

3.2. Continuous Feed-In Management

When the scenario is simulated with continuous feed-in management controlling the 5M, the response is as shown in Figure 13. As soon as feed-in management becomes necessary, commencing at 10:47, the power of the 5M is reduced to limit the voltage to 7.3% above its rated value. This limitation in power slows down the heating up of the transformer. However, eventually the transformer reaches its maximum temperature of 50 °C, such that both the voltage and the temperature are addressed with continuous feed-in management. Later, beyond 15:45, when P_C becomes negative, the wind speed drops (Figure 4), leading to more frequent dips in power, while in periods of high wind speed the voltage still needs to be limited. This high variability in power, in combination with the long thermal time constant of the transformer, leads to a cooling down of the transformer to almost 30 °C. Again, reactive power control is not pursued here to allow a fair comparison with conventional feed-in management.
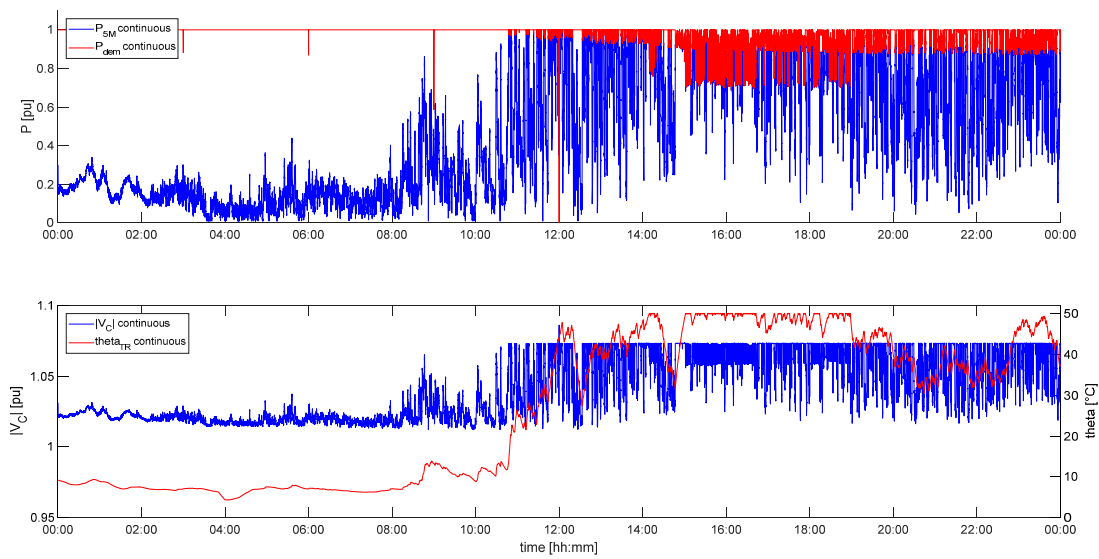
Figure 13. Simulation of case study with continuous feed-in management.

As can be seen in the next section the scope of this article is not limited to the assessment of energy yield, but it also comprises the assessment of mechanical loads on the WT.

4. Comparison of Feed-In Management Strategies

The two different feed-in management strategies can be assessed from two perspectives: from the power system's point of view and from the WT's point of view. Hence, the following subsections compare the effects that conventional and continuous feed-in management have on the power system and on the WT, i.e., the 5M.

4.1. Effects on the Power System

Since the primary purpose of wind power installations is the feed-in of electric energy, the energy yield is compared first. Figure 14 shows the energies that are fed into and consumed from the grid of campus Flensburg on 5 April 2017. The local consumption (3.67 MWh), which is partially provided by the E30 (1.97 MWh), is only a minor fraction of the energy produced by the 5M. Controlling the 5M with continuous feed-in management yields 57.1 MWh, which is 13.5% more than with conventional feed-in management.
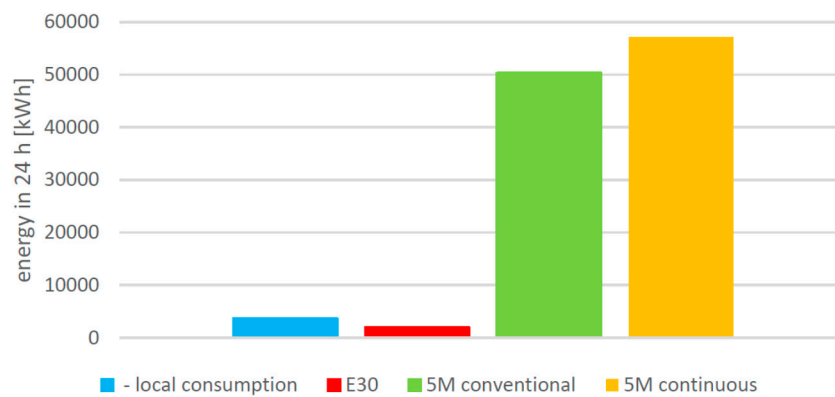

Figure 14. Comparison of energies fed into and consumed from the campus grid during the 24 h scenario.

It has to be pointed out however, that the numbers of MWh are not transferable to other cases as they apply only to the scenario considered here. These numbers do, however, allow the conclusion to be drawn that continuous feed-in management increases the energy yield substantially. The difference in energy yield would be even more striking were the voltage in the outer high voltage grid, V_g, assumed to be higher. In this case conventional feed-in management would lead to P_{dem} = 0.3 pu or even 0 pu most of the time. The same would apply when conventional feed-in management were to be conducted in the same precautionary manner, with the goal to minimise the control effort, as can be observed in reality [16]. Continuous feed-in management, on the other hand, responds to the instantaneous changes in the grid voltage and limits P_{dem} accordingly.

The thermal loading of the transformer is a measure for the utilisation of the same and of other assets in the power system. Comparing the transformer temperature after 12:00 (comparing Figures 12 and 13) it can be seen that conventional feed-in management makes much more use of power system assets than conventional feed-in management. While continuous feed-in management keeps the transformer at its target temperature of 50 °C for several hours, in conventional feed-in management it barely reaches up to 45 °C.

The variability of V_C is a measure of the quality of the power fed into the power system. Over the whole day the lowest value of V_C is 1.013 pu. In case of conventional feed-in management it regularly reaches up to 1.082 pu. In contrast to this, there is only one single peak where V_C reaches up to 1.086 pu while it is controlled with continuous feed-in management. At all other times continuous feed-in management limits V_C reliably to 1.073 pu.

4.2. Mechanical Loads in the WT

In power production operation a WT can experience excitation from four external sources: rotation, varying wind, varying terminal voltage, and varying P_{dem}. Controlling P_{dem} with respect to the loading of the power system to which the WT is connected, means decoupling the controls of the WT from the wind that instantaneously prevails at the rotor of the WT. This potentially means stress for the WT [8]. Such stress can be associated with two different categories:

- Varying operating points and the necessity to level out variations by adjusting the pitch angle, potentially even with the maximum pitch rate.
- Exciting resonances.

Vibrations are primarily excited by excitations that have the same frequency as the eigenfrequency of the vibrating WT component. Single excitation events, like a step change in a signal, are less harmful as they usually do not cause vibrations of constant or even increasing magnitude. It has to be noted that such single events might cause extreme loads that are not related to resonances, but such extreme events are not caused by feed-in management operation. Therefore, the persistent excitations to vibrations are assessed as follows. As discussed in Section 2.6 "Wind Model", the wind speed time series is offset with sinusoidal components that are of the same frequencies as the eigenfrequencies of the WT components. Hence, in addition to the stochastic natural wind speed variations, there are also wind speed variations that are directly targeted to excite the 5M to vibrations, see Figure 9. In the scenario simulated here the voltage (V_C) has no significant effect, as it varies in a too narrow band. The other source of excitation is the P_{dem} signal that results from the loading of the transformer. Hence, it is affected by the wind speed at the E30, v_{wind_meas}, which leads to P_{E30}, and together with the load power these add up to P_C. In order to assess the potential to excite vibrations in the 5M, Figure 15 shows the frequency spectra of the different power signals. The frequency spectrum of P_C comprises all relevant frequencies but does not exhibit any particular frequency peaks. The same applies to the P_{dem} signal of conventional feed-in management. The P_{dem} signal of continuous feed-in management comprises distinct frequencies that result from the heating up of the transformer and from the eigenfrequencies of the WT. Looking at Figure 10 it becomes obvious that the dynamics of both, the transformer, as well as the 5M, have a bearing on P_{dem} of continuous feed-in management.

Consequently, these frequencies are reproduced in the power that the 5M feeds into the power system. In contrast to this, in conventional feed-in management the generator power of the 5M only exhibits the eigenfrequencies of the blades in the edgewise direction and the torsional eigenfrequency of the drive train. It barely exhibits the eigenfrequency of the blade in the flapwise direction and it does not exhibit the eigenfrequency of the tower of the 5M.
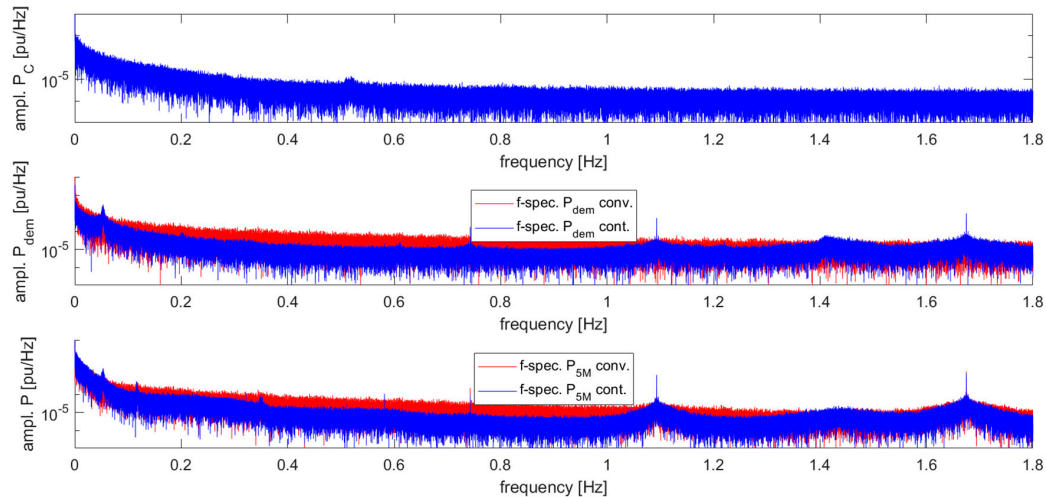
Figure 15. Frequency spectra of power. Top: of P_C; middle: of power setpoint, P_{dem}, from feed-in management; bottom: of P_{5M}.

With these excitations the dynamic behaviour of the WT can be assessed. In the following figures, time traces are limited to the part of the day where feed-in management takes place. The units of the signals shown in some of the following graphs are per unit (pu), which relates to the rotational speed of the rotor. A detailed discussion of the units is omitted here, as this can be found in the documentation of the simulation model [10]. The following figures also show the distribution of the frequencies with which the different values occur in the time traces. (Blue bars are for continuous feed-in management, red bars are for conventional feed-in management and dark red areas show overlap of blue and red bars.)

Figure 16 shows that the pitch angle of the 5M varies in the same range in both cases. There are differences in the frequency distribution for pitch angles above 10 deg, which should not be overrated due to the logarithmic scale.
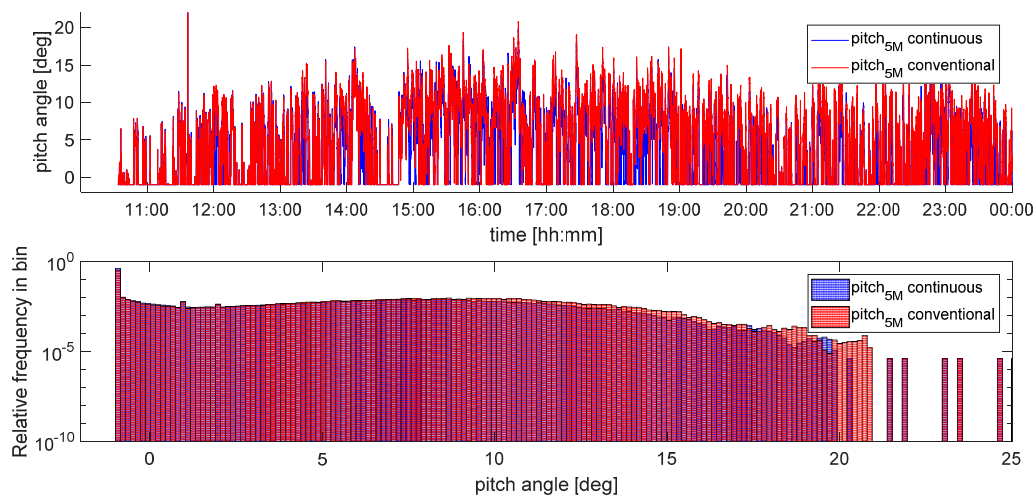
Figure 16. Pitch angle (**top**) and frequency distribution of pitch angles (**bottom**) of 5M.

The pitch rates are also comparable, as can be seen in Figure 17. In both cases they regularly reach -8 deg/s and 8 deg/s, which is the maximum pitch rate of the 5M. Continuous feed-in management causes only somewhat more frequent high pitch rates. (Again, when looking at Figure 17 it has to be kept in mind that the relative frequency of the pitch rates is plotted on a logarithmic scale.) This might appear surprising at first sight, as it could be suspected that maintaining a constant P_{dem} (conventional feed-in management) requires less pitching actions than continuously varying P_{dem} (continuous feed-in management). Comparing Figures 12 and 17 reveals that conventional feed-in management, on average, requires somewhat lower pitch rates. However, a constant P_{dem} still requires drastic pitching actions, as the wind speed still varies. This effect becomes more dominant for higher wind speeds or lower P_{dem} as these two variables have an effect on the pitch sensitivity [8].
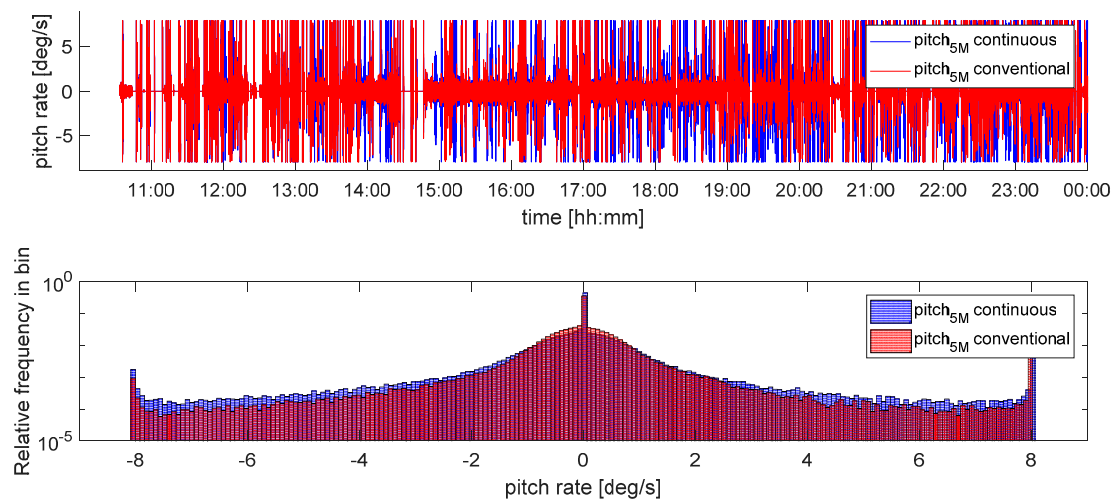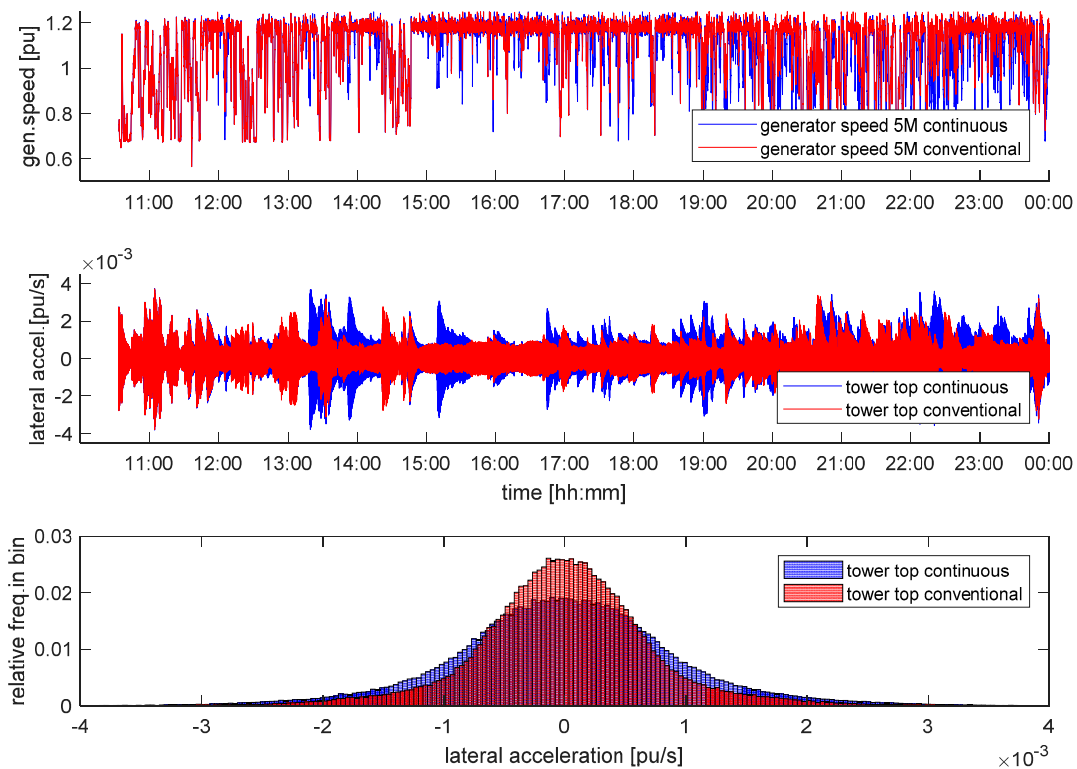

Figure 17. Pitch rate (**top**) and frequency distribution of pitch rate (**bottom**) of 5M.

Another measure for mechanical stress is the acceleration of the tower top, which can occur in the lateral direction (in rotor plane direction) and in the longitudinal direction (in out of rotor plane direction). Excitation in the lateral direction is mainly caused by imbalances in the rotor. To emulate imperfections in manufacturing one of the rotor blades of the 5M is 100 kg heavier than the other two. This imbalance in the rotor leads to lateral excitation, especially when the rotor speed is close to the eigenfrequency of the tower. Looking at Figure 3 makes it obvious that whenever the rotational speed of the rotor is low, the 3p excitation is close to the eigenfrequency of the tower. To illustrate cause and effect of this phenomenon Figure 18 shows the rotational speed, the resulting lateral acceleration of the tower, and the frequency distribution of this acceleration.

Figure 18 reveals that the lateral vibrations of the tower top occur more often in case of continuous feed-in management. This is obvious as in continuous feed-in management the power varies on a regular basis, leading to more variations of the rotor speed.

Tower vibrations in the longitudinal direction are mainly caused by wind speed variations and pitch angle variations. In particular pitch angle variations with high pitch rates have drastic effects on the thrust of the rotor, and hence, excite the tower in the longitudinal direction. While the time traces of the wind speed are comparable for both scenarios, the pitch variations are considerably different, as can be seen in Figures 16 and 17.

Figure 19 shows the tower top acceleration of the 5M in the longitudinal direction. It can be seen that the tower is more strongly excited when P_{dem} requires pitch angle variations with high pitch rates. Consequently, continuous feed-in management causes somewhat more frequent higher accelerations in the longitudinal direction.

Figure 18. Rotational speed of drive train (**top**), lateral acceleration of tower top of the 5M (**middle**) and frequency distribution of lateral acceleration (**bottom**).
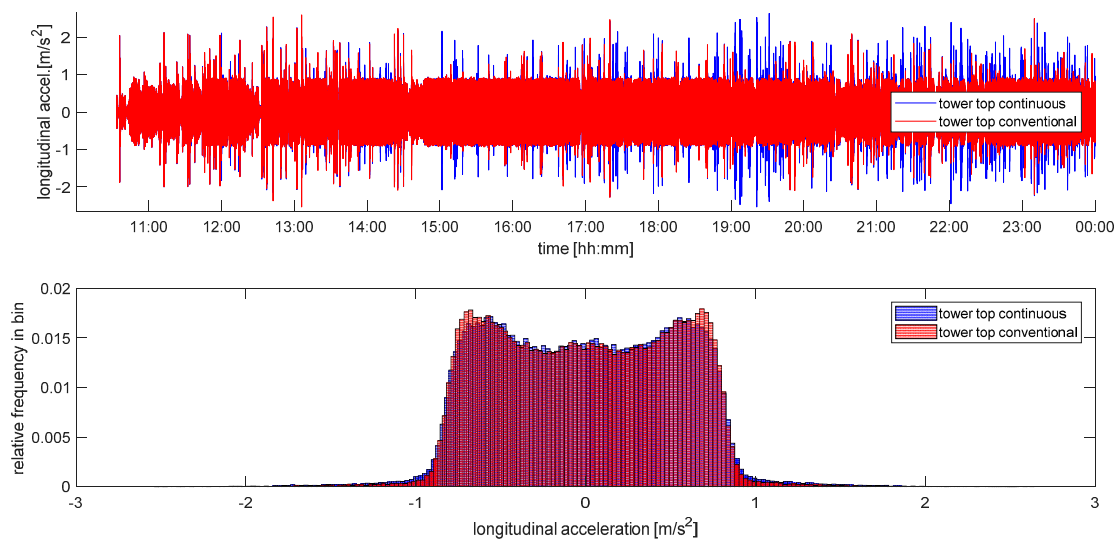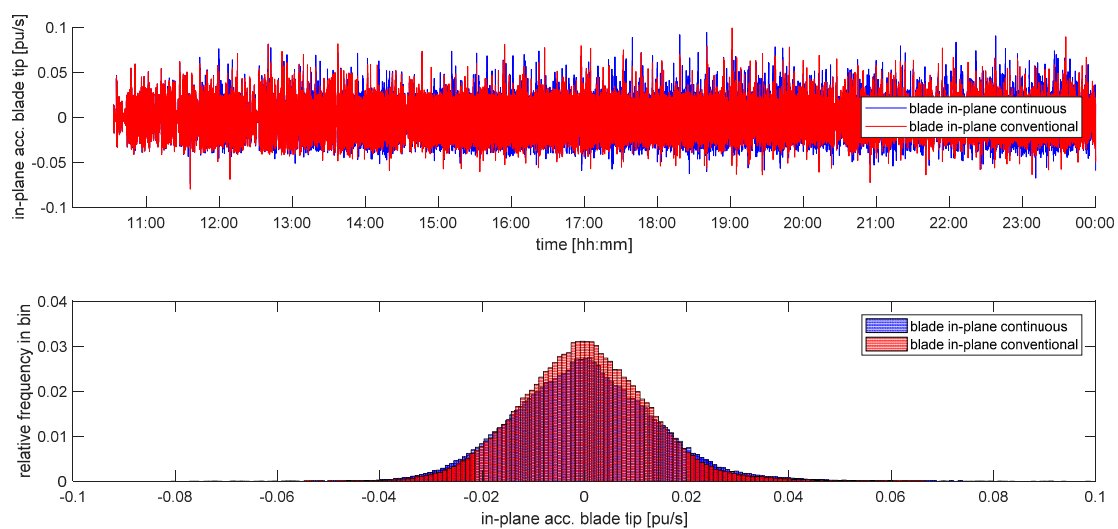

Figure 19. Longitudinal tower top acceleration of the 5M (**top**) and frequency distribution of this acceleration (**bottom**).

In the longitudinal direction a persistent vibration with the eigenfrequency of the tower, f_t, and with a magnitude of about 0.9 m/s^2 is observable almost all the time. There is a constant excitation in the wind, because f_t is contained in the wind speed signal (compare Figure 9). In the lateral acceleration such persistent vibrations are not contained, because the drive train speed, which is the primary cause for lateral tower vibrations, varies all the time. Therefore, excitation in the lateral direction from the imbalance in the rotor happens at different frequencies.

Looking at Figures 18 and 19 it can be seen that conventional feed-in management causes fewer single excitations of the tower. However, the maximum accelerations (height of the peaks in Figures 18 and 19) are identical in both types of feed-in management. The persistent vibrations in the longitudinal direction are also identical. Figure 18 further shows that the variation of the generator speed does not exhibit persistent or even unstable vibrations.

The remaining degrees of freedom of the WT model are the motions of the blade tip with respect to the blade root in the in-plane direction and in the out-of-plane direction. Figure 20 shows the accelerations that the blade tip section of one arbitrary blade of the 5M experiences in the in-plane direction. The acceleration in the in-plane direction exhibits a persistent vibration with a magnitude of about 0.03 pu/s most of time. This acceleration is mainly caused by the rotation of the rotor, i.e., alternating gravitational forces that act on the rotor blade. In addition, also the wind speed variations, which have the same frequency as the blade eigenfrequency in the in-plane direction cause such vibrations. The diagram in Figure 7 reveals that the magnitude of this wind speed component is constantly high when the wind speed is high. Beyond this persistent vibration, variations in in-plane acceleration are caused by varying operating points. Therefore, continuous feed-in management causes somewhat more frequent higher in-plane acceleration than conventional feed-in management. The only rarely occurring high peaks that arise from drastic changes in instantaneous wind speed at the blade, or from drastic changes in operating point are comparable in both scenarios.

Figure 20. In-plane acceleration of blade tip section with respect to blade root section of one arbitrary blade of the 5M (**top**) and frequency distribution of this acceleration (**bottom**).

Figure 21 shows that the acceleration in the out-of-plane direction exhibits a persistent vibration with a magnitude of about 5 m/s^2 most of the time. This acceleration is mainly caused by the variations in thrust forces that result from wind shear and rotation of the rotor. Wind speed variations that are of the same frequency as the out-of-plane blade eigenfrequency also directly cause acceleration out-of-plane. Beyond this persistent vibration, variations in out-of-plane acceleration are to a minor extent caused by varying operating points. Therefore, continuous feed-in management causes somewhat more frequently occurring out-of-plane accelerations of moderate magnitude.
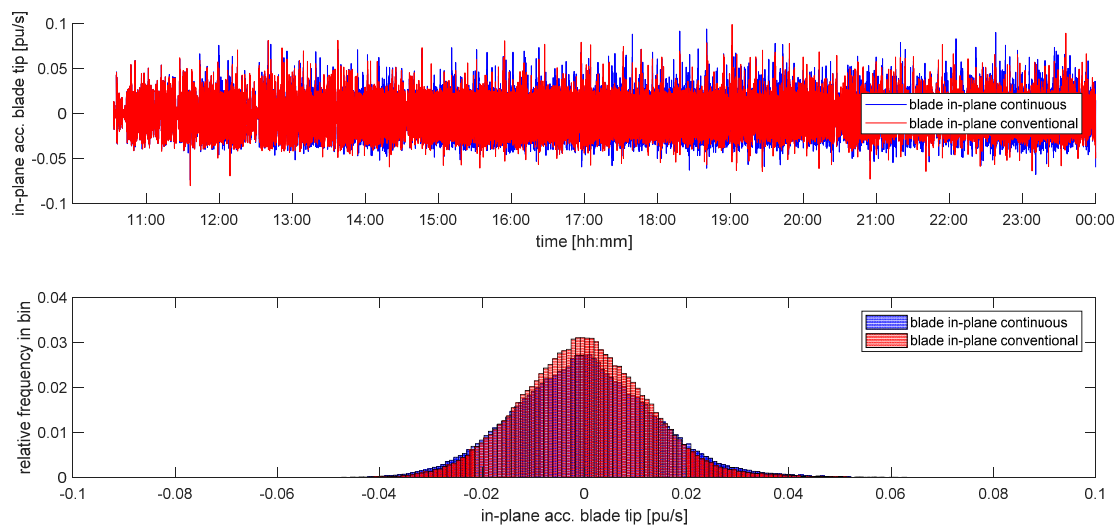
Figure 21. Out-of-plane acceleration of blade tip section with respect to the blade root section of one arbitrary blade of the 5M (**top**) and frequency distribution of this acceleration (**bottom**).

The persistent vibrations are either caused naturally by the rotation of the rotor, or by the deliberately added sinusoidal wind speed components. The sole purpose of these wind speed components is to excite the eigenfrequencies of the WT. Despite these persistent excitations, there are no vibrations with large magnitude that persist for long, or whose magnitude even increases because they are excited by continuous feed-in management. The stochastic nature of the excitations ensure that the WT never dwells long enough in one operating point so that an eigenmode develops vibrations with a critical magnitude [8]. Even if such critical excitation persists, the aerodynamic damping helps to avoid the vibrations becoming unstable.

5. Conclusions

It is a common problem that wind power installations grow faster than the power system, into which these installations feed their power. In order to avoid thermal overloading of the power system and unfavourable voltages, it is common practice for power system operators to restrict the power that WTs may feed into the affected system: known as feed-in management. Currently, it is state of the art that feed-in management is optimised to serve the compromise between control effort and lost electric energy yield. Therefore, the direct connection between the current loading of the power system and the maximum power that WTs are allowed to feed in is lost completely. Consequently, the power system assets are not utilised to their full potential and large amounts of wind energy are wasted.

To avoid these problems continuous feed-in management is assessed in this paper. The idea is that the value, to which WT power is limited, is adjusted continuously. Hence, at any time WTs feed in just as much power as is acceptable for the power system. This leads to the maximum wind energy yield and the maximum utilisation of power system equipment.

The continuous feed-in management applied in this paper is assessed by means of a realistic case study. In this case study the WT that causes the overloading of the power system is first controlled with conventional feed-in management. The result of this simulation is used as reference in order to have a benchmark for assessing the performance of continuous feed-in management, which is simulated in the second step.

From a power system's point of view, continuous feed-in management proves to be superior, both in terms of voltage and in terms of utilisation of the thermal capacity of the considered power system transformer. In addition, the wind energy yield is much larger. In the case considered here continuous feed-in management leads to a wind energy yield that is 13.5% larger compared to conventional feed-in management. It has to be mentioned that the conventional feed-in management simulated here is done

without any precautionary reductions of the power limit as can be observed in reality. Otherwise the difference in energy yield would be even larger.

From a WT's point of view a continuously varying power demand value causes more frequent and more rapidly changing operating points. A measure for this is the variation in the pitch angle and the frequency of occurrence of high pitch rates. However, this increased stress on the WT is not as large as expected, because a constantly reduced power demand (conventional feed-in management) also leads to stress due to the wind speed variations and the operating point dependent pitch sensitivity.

Looking at all degrees of freedom that are represented in the WT model used in this study, allows the mechanical stress to be assessed in terms of accelerations. It can be seen that continuous feed-in management causes somewhat more frequent accelerations. Hence, the fatigue loads are expected to be higher than in the case of conventional feed-in management. The peaks in the acceleration, however, are not larger compared to the peaks resulting from conventional feed-in management. Hence, it can be concluded that continuous feed-in management is an appropriate method for increasing wind energy yield without the need for massive over-dimensioning of the affected power system components.

Author Contributions: Clemens Jauch conceived the concepts presented in this paper. He created the simulation model, conducted the simulations and wrote the paper. Arne Gloe set up the power measurement system at the grid connection point of campus Flensburg. He further contributed to the technical discussions and reviewed the paper. Henning Thiesen contributed to the data acquisition and designed the interface between measurements and simulations. He further contributed to the technical discussions and reviewed the paper. Sebastian Hippel yielded the parameters of the 5M, contributed to the technical discussions and reviewed the paper.

Conflicts of Interest: The authors declare no conflict of interest. The founding sponsors had no role in the design of the study; in the collection, analyses, or interpretation of data; in the writing of the manuscript, and in the decision to publish the results.

Appendix A

Table A1. Parameters of grid connection transformer.

Name	Value	Unit	Description
V_{rated}	24,000	V	rated voltage
u_k	6	%	short circuit voltage
S_{rated}	3150,000	VA	rated apparent power
P_{scl}	27500	W	short circuit power
f_{rated}	50	Hz	rated frequency
m_{TR}	6100	kg	total mass of transformer
m_{oil}	1070	kg	mass of oil in transformer
m_{Al}	1100	kg	mass of aluminium conductor
A_{cool}	111	m^2	cooling surface of transformer
c_{TR}	786	Ws/kg/K	specific heat capacity of transformer
α_{TR}	100	$W/m^2/K$	heat transfer coefficient of cooling air

Table A2. Parameters of WT model.

Name	Value	Unit	Description
f_{bf}	0.7429	Hz	1st eigenfrequency blade bending flapwise
f_{be}	1.0931	Hz	1st eigenfrequency blade bending edgewise
f_t	0.3230	Hz	1st eigenfrequency tower bending
f_{dt}	1.6749	Hz	1st eigenfrequency drive train torsion

Table A3. Lookup table $A(v_{\text{wind\_meas\_filt}})$ in wind model.

Wind Speed (90 m) [m/s]	Magnitude [m/s]
3.19	0.07
4.58	0.02
5.87	0.02
7.65	0.25
9.79	0.35
12.24	0.40
15.37	0.40

Table A4. Parameters of temperature controller and P_{dem} controller.

Temperature Controller	Value	Unit
Proportional gain	0.1	pu/$^\circ$C
Integral gain	0.9	pu/$^\circ$C/s
P_{dem} Controller	**Value**	**Unit**
Proportional gain	3	pu/pu
Integral gain	9	pu/pu/s
V_C [pu]	**$P_{\text{max\_TR\_volt}}$ [pu]**	
0	1	
1.07	1	
1.1	0	

References

1. Federal Ministry for Economic Affairs and Energy, Germany. Act on the Development of Renewable Energy Sources. Available online: http://www.bmwi.de/Redaktion/EN/Downloads/renewable-energy-sources-act-eeg-2014.html (accessed on 22 June 2017).

2. Tenne, T.; Holding, B.V. Operation and Usage—How does Feed-in Management Work? Available online: https://www.tennet.eu/electricity-market/german-market/eeg-kwkg/feed-in-management/operation-and-usage/ (accessed on 22 June 2017).

3. Monitoring Report 2015. Available online: https://www.bundesnetzagentur.de/SharedDocs/Downloads/EN/BNetzA/PressSection/ReportsPublications/2015/Monitoring_Report_2015_Korr.pdf?__blob=publicationFile&v=4 (accessed on 5 May 2017).

4. Monitoring Report 2016. Available online: https://www.bundesnetzagentur.de/SharedDocs/Downloads/DE/Sachgebiete/Energie/Unternehmen_Institutionen/DatenaustauschUndMonitoring/Monitoring/Monitoring2016/MonitoringSummary2016.pdf?__blob=publicationFile&v=2 (accessed on 22 June 2017).

5. Jauch, C. *FH Flensburg Erforscht Dynamische Leistungsbereitstellung Durch WEA*; Ingenieurspiegel: Bingen, Germany, 2013; pp. 20–21. (In German)

6. Wieben, E. Der 5%-Ansatz im Kontext der Netzqualität. In Proceedings of the Energiesymposium Westküste, Heide, Germany, 10 September 2015. (In German)

7. FGW, RWTH Aachen. *Abschlusspräsentation zur Systemstudie zum Einspeisemanagement Erneuerbarer Energien*; Oldenburg, Germany, 9 July 2015. Available online: http://de.slideshare.net/EWE_AG/20150702-abschlussprsentation-systemstudie-einspeisemanagementfinal (accessed on 22 June 2017). (In German)

8. Jauch, C.; Gloe, A. Improved feed-in management with wind turbines. In Proceedings of the 15th Wind Integration Workshop, Vienna, Austria, 15–17 November 2016.

9. Jonkman, J.; Butterfield, S.; Musial, W.; Scott, G. Definition of a 5-MW Reference Wind Turbine for Offshore System Development. Available online: http://pop.h-cdn.co/assets/cm/15/06/54d150362c903_-_38060.pdf (accessed on 22 June 2017).

10. Jauch, C. *First Eigenmode Simulation Model of a Wind Turbine—For Control Algorithm Design, 21 December 2016*; WETI Hochschule: Flensburg, Germany, 2016.

11. Gloe, A.; Jauch, C. *Simulation Model Design and Validation of a Gearless Wind Turbine 23 March 2016*; WETI Fachhochschule: Flensburg, Germany, 2016.

12. Jonkman, J.; Jonkman, B. Fast modularization framework for wind turbine simulation: Full-system linearization. In Proceedings of the Science of Making Torque from Wind (TORQUE 2016), Munich, Germany, 5–7 October 2016.

13. Schaffarczyk, A. *Understanding Wind Power Technology, Theory, Deployment and Optimisation*; Wiley: New York, NY, USA, 2014.

14. Standard Transformatoren ismet GmbH, VS-Schwenningen, Germany. Available online: http://www.ismet. de/de/downloads (accessed on 22 June 2017). (In English)

15. Fischer, R. *Elektrischer Maschinen*, 10th ed.; Carl Hanser Verlag: München, Germany, 2000. (In German)

16. Regionen mit Einspeisemanagement—Abgeschlossene Einsätze des Einspeisemanagement—SH Netz Mittel-und Hochspannung, TenneT Höchstspannung, 2017. Available online: https://www.sh-netz.com/cps/rde/xchg/sh-netz/hs.xsl/3972.htm (accessed on 22 June 2017). (In German)

Publication 7

Simultaneous Inertia Contribution and Optimal Grid Utilization with Wind Turbines

Simultaneous Inertia Contribution and Optimal Grid Utilization with Wind Turbines

Clemens Jauch * and **Arne Gloe**

Wind Energy Technology Institute, Flensburg University of Applied Sciences, 24943 Flensburg, Germany

* Correspondence: clemens.jauch@hs-flensburg.de; Tel.: +49-461-805-1660

Abstract: This paper presents findings of a study on continuous feed-in management and continuous synthetic inertia contribution with wind turbines. A realistic case study, based on real measurements, is outlined. A wind turbine feeds into a weak feeder, such that its power has to be adapted to the permissible loading of this feeder. At the same time the wind turbine is to provide inertia to the grid by applying the previously published variable inertia constant controller. It is discussed that optimal grid utilization and simultaneous inertia contribution are mandatory for the frequency control in power systems that are heavily penetrated with renewable energies. The study shows that continuous feed-in management can be combined well with continuous inertia provision. There are hardly any negative consequences for the wind turbine. The benefits for the grid are convincing, both in terms of increased system utilization and in terms of provided inertia. It is concluded that wind turbines can enhance angular stability in a power system to a larger extent than conventional power plants.

Keywords: feed-in management; frequency domain; inertial energy; inertial response; power control; synthetic inertia; wind turbine

---

1. Introduction

In the transition to renewable energy, wind turbine (WT) generators substitute conventional power plants. Therefore, WTs must no longer merely behave like passive power sources; instead, they have to take over grid stabilizing functionalities that were traditionally carried out by conventional power plants.

The intermittent power infeed of WTs and the dispersed installation of WTs in the grid lead to temporary congestions in the grid and/or costly grid extensions. Germany, particularly the state of Schleswig-Holstein in the very north of Germany, is a prime example for this development [1,2]. In order to minimize the costs for grid extensions the power infeed of WTs should be matched to the maximum permissible power transfer capability of the affected part of the grid [3]. For this purpose, continuous feed-in management (FIM) was proposed in the past [4]. It was shown that continuous FIM allows maximizing the utilization of the grid and, consequently, maximizing the wind energy yield [5]. However, both during conventional FIM (as it is state of the art today [6]) as well as during continuous FIM, the control of a WT is partly decoupled from the wind speed. Hence, the stress on the WT increases.

Another task that WTs have to take over when conventional power plants are replaced is the contribution to grid inertia, which aims at stabilizing the grid frequency. Here, it has to be mentioned that different approaches are conceivable, which can be categorized into fast frequency response and synthetic inertia [7]. In this paper, the provision of synthetic inertia is in the focus for reasons outlined below. Also inertia contribution partly requires decoupling the controls of a WT from the instantaneously prevailing wind. Therefore, the stress on the WT potentially increases even more, depending on the control strategy and the wind condition. Load simulations and field measurements

show that there is no negative effect on the ultimate loads to be expected, but fatigue loads are bound to increase [8,9].

The study on continuous FIM with a fictitious controllable WT (mentioned above) was based on measurements of wind speed, local consumption, and the passive wind power infeed of a real WT without grid support functionalities. Since the grid frequency was also measured, this study was extended to inertia provision with the controllable WT. Hence, the considered WT has to adjust its instantaneous power to not only fit the loading of the affected grid components, but also to the rate of change of frequency (*ROCOF*) in the grid, in order to provide the grid with synthetic inertia.

At first sight, the combination of continuous FIM and continuous provision of synthetic inertia seems random. Comparing the priorities that are set in the context of power system stability, it seems obvious that angular stability comes first and any secondary aspects, such as thermal loading of grid components or overvoltages, are of minor importance [10]. However, in a power system that is heavily penetrated with dispersed renewably energy sources, the traditional rules are no longer applicable. For economic reasons, grid connection of dispersed renewable energy generation develops slower, and often not to the same extent, as the installation of the generators. Consequently, the power infeed of these generators has to be restricted in weather situations that allow the production of large amounts of renewable power [5,11]. The transition to renewable energies is only economically feasible if conventional power plants are replaced; i.e., if they do not have to remain in standby, waiting to step in if renewable energy infeed is insufficient. This means that the availability of renewable power infeed must not be unduly hampered by the transfer capabilities of grid components, as this would interfere with the balance between generation and demand; i.e., continuous FIM is mandatory as it interacts with grid frequency control. At the same time, replacing conventional generation (based on AC connected rotating machines) with frequency converter-based renewable energy generators leads to a decline in inertia in the power system. However, power system inertia is essential for the control of the frequency, i.e., the balance between generation and demand [12,13]. There is no consensus whether frequency converter-based generation should enhance grid frequency control by contributing to the grid inertia continuously, or by responding to predefined frequency events in a predefined manner (fast frequency response). Some scientists advocate fast frequency response and even deem continuous provision of synthetic inertia to be inappropriate [14]. Different grid codes prefer fast frequency response; others demand continuous provision of synthetic inertia by emulating the inertial behavior of synchronous generators [15–18]. In future power systems, where frequency converter-based generation substitutes almost all AC connected rotating machines (i.e., very low natural inertia), continuous provision of synthetic inertia is mandatory. Consequently, the simultaneity of continuous FIM and continuous provision of synthetic inertia is inevitable.

In this study, the assessed WT is enhanced to continuously provide inertia, comparable to a synchronous generation of a conventional power plant. To avoid the risk that the WT disconnects from the grid when during low wind speeds a large negative *ROCOF* requires a large increase in power, the previously proposed variable inertia constant (H_{var}) controller [19] is applied.

In the following sections, first, the case study is outlined. Secondly, the WT simulation model with its different controllers is introduced. A frequency domain analysis compares the response of the WT to the demanded continuous inertia provision and the continuous FIM. It is outlined that the prioritization mentioned above: 1st priority is inertia contribution, 2nd priority is addressing grid congestions (FIM) is implemented in the proposed controllers. Hence, the simultaneous coexistence of synthetic inertia and continuous FIM is facilitated. Finally, simulation results prove that combining continuous synthetic inertia with continuous FIM is no problem for the affected WT and that it is a big gain for the grid.

2. Case Study

The university campus in Flensburg, Germany, is a small power system that comprises consumption, generation, and a connection to the external grid. For the purpose of this study,

the campus grid is assumed to be supplemented by a 5 MW WT and the connection to the external grid is assumed to be made of an oil-immersed transformer whose rating is sufficient only most of the time. Hence, this study case replicates the situation that commonly occurs when wind power grows faster than the power system into which the WTs feed their power. The NREL 5 MW reference turbine is chosen for this extension, and is called 5M in the following, as the details of this WT are well documented and openly accessible [20]. The 5M is represented with a simulation model that exhibits the most dominant vibratory behaviours of a WT: the first eigenmodes of the tower, the drive train, the rotor blades in edgewise direction, and the rotor blades in flapwise direction [21]. This model is chosen because it is easy to implement and use. Also, it can be easily extended with grid models and additional controllers.

Figure 1 shows a sketch of the Flensburg university campus with the supplements necessary for this case study. It can be seen that already, today, the local consumption is partially covered by the power of a WT on campus, which is an Enercon E30, whose power is indicated as P_{E30} in Figure 1. In this case study, the residual load, which either has to be covered by the 5M, or by power import from the external grid, is called P_C (see Figure 1).
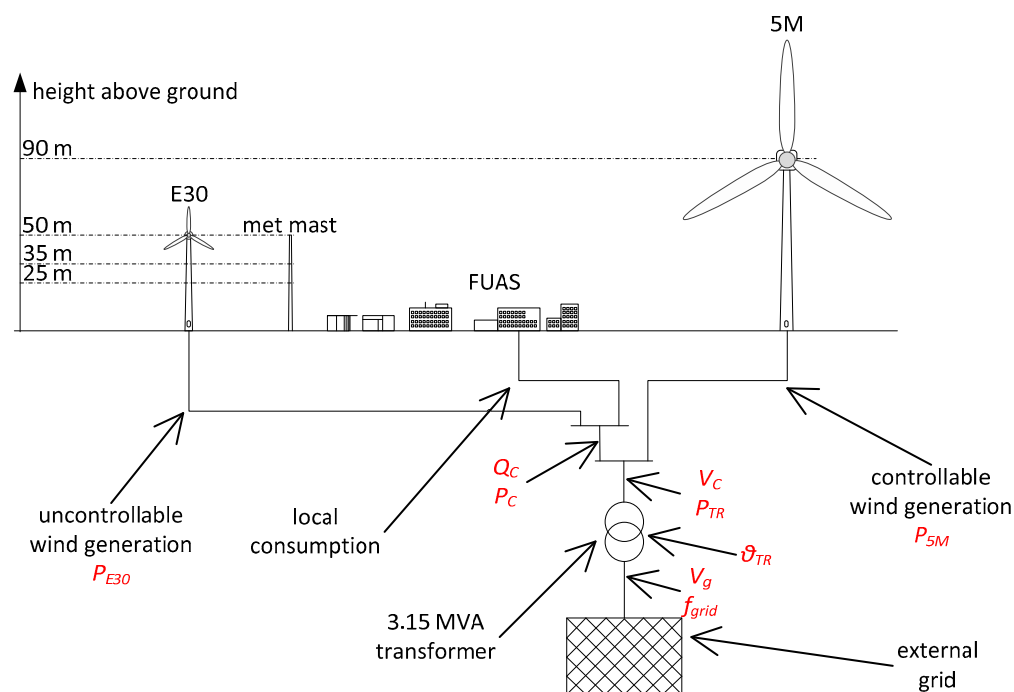
Figure 1. Setup of the case study of Flensburg campus supplemented by a 5 MW WT (5M) with connection to the external grid.

For this study P_C, P_{E30}, wind speed, grid frequency, f_{grid}, and the ambient temperature were measured on 05 April 2017, which was a day with changing and eventually quite good wind conditions and a typical load profile for the campus. The measurements of P_C, P_{E30}, wind speed, and the ambient temperature are already published [5]; hence, they are not reproduced here.

For the assessment of inertia contribution, the measurement of the grid frequency, f_{grid}, is essential [22]. Therefore, Figure 2 shows f_{grid}, the calculated *ROCOF* and the frequency spectrum of f_{grid} and the *ROCOF* as measured on 5 April 2017.
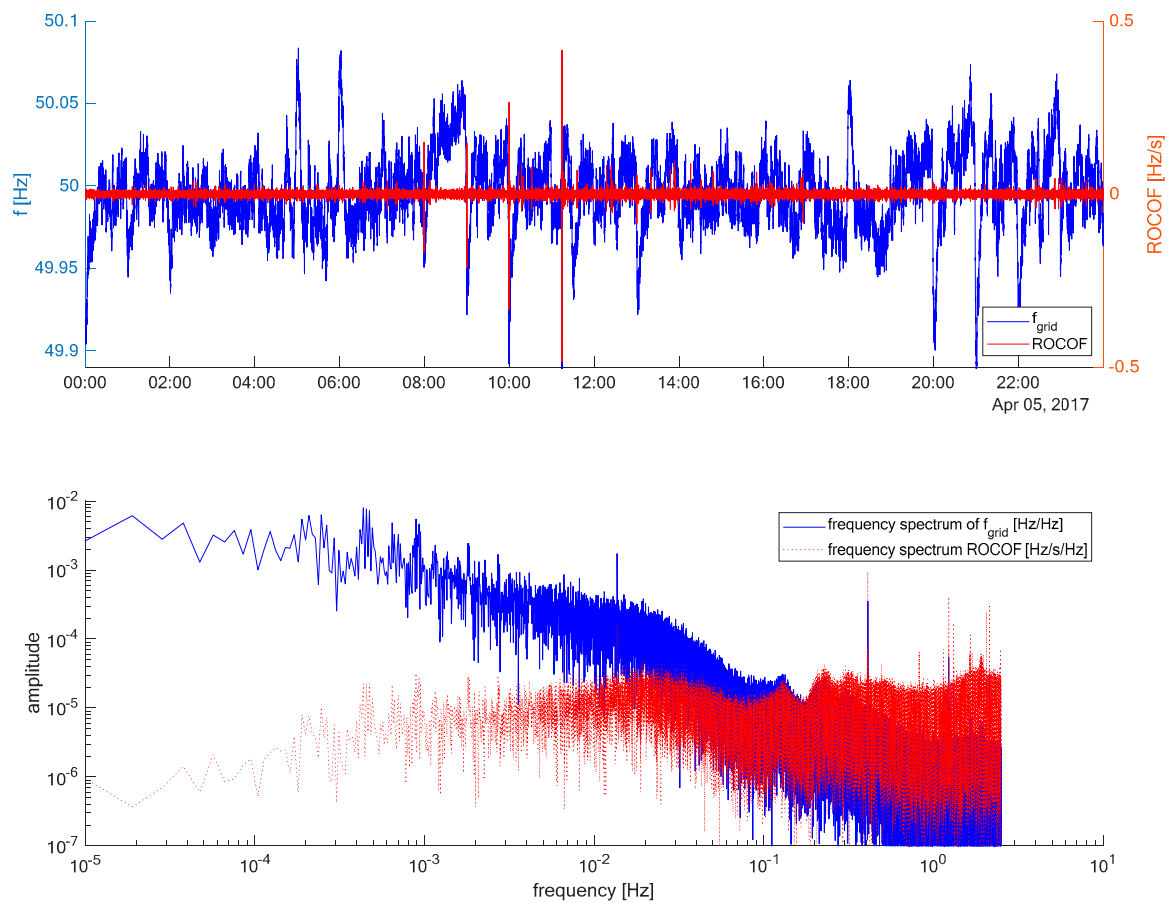
Figure 2. Measured grid frequency and *ROCOF* (top); frequency spectrum of grid frequency (bottom).

Figure 2 reveals that the *ROCOF* the WT has to respond to is very small most of the time, (|*ROCOF*| < 0.02 Hz/s). However, there are some single peaks, the largest even reaches −0.484 Hz/s. These peaks are only a rarely occurring phenomenon. It is not clear where these peaks come from; however, their frequency of occurrence, their durations, and their magnitude suggest that they are not of electromechanical nature. It is rather assumed that distortions in the grid voltage lead to these large *ROCOF*s. Previously conducted research revealed this effect and quantified the number of fake *ROCOF* incidences, i.e., occurrence of large *ROCOF* values that are not of electromechanical nature, but that are caused by electromagnetic effects [23]. Instead of eliminating these fake *ROCOF* values, they are deliberately left in the time series. If a real WT has to perform inertial response it has to measure the voltage to determine the frequency and the *ROCOF* in real-time. In such online computation of the *ROCOF*, a distorted grid voltage will also lead to large values. This is particularly important for the WT, as it can have noticeable effects on the mechanical loads, and hence, on the fatigue of the WT.

3. WT Simulation Model

3.1. Power Controller

The 1st eigenmodes model of a WT represents the generator–converter unit as a first order low pass filter (PT1). This means that the dynamics of the generator, the machine side inverter, the grid side inverter, as well as the capacitor in the DC circuit are modelled as one lumped PT1 element. In the previous study on continuous FIM [5], the time constant of this PT1 filter (T_PT1_geno_substi [21]) was set to 150 ms, which is a reasonable value for normal power control of a WT. In the inertial response study shown here, this time constant has to be reduced to a lower, yet realistic value, to allow more rapid power variations as this is needed for effective inertial response. Hafiz and Abdennour propose

a time constant of 20 ms for a multi-MW generator–converter unit [24]. In a Bachelor thesis composed at WSTECH GmbH, which is a manufacturer for frequency converters, a PT1 response with a time constant of 25 ms was applied for simulating the power response of MW frequency converters [25]. Hence, in this study, T_PT1_geno_substi is set to 25 ms (T_PT1_geno_substi = 0.025 s) as this is more conservative and facilitates running the simulation with a simulation time step of dT = 0.001 s. A smaller simulation time step would lead to computational problems as the scenario to be assessed lasts 24 hours. Hence, the amount of data resulting from such long time series becomes very large and Matlab [26], which is the software with which the simulations are conducted, can no longer handle this amount of data on a normal personal computer.

Figure 3 shows the power control loop with the PI power controller and the PT1 filter that represents the generator–converter unit. The aforementioned reduction of T_PT1_geno_substi causes the open loop power control path to exhibit a higher crossover frequency; compare the green and the dashed blue curve in the bode plot in Figure 4. A higher crossover frequency allows rapid power variations to pass through with less damping, which causes the PI controller to exhibit overshoots. Overshooting of the controller leads to hitting the controller output limitations and triggers the anti-windup facility of the I-part of the PI controller [21]. The anti-windup block is shown in grey in Figure 3 as it is normally not involved in power control operation. Consequently, the gains of the PI controller are tuned to restore the initial crossover frequency of about 12 Hz. This is achieved with the proportional gain K_P_power = 2.1 and the integral gain K_I_power = 12. With these gains, the phase margin increases to about 109 degrees, see Figure 4, which proves stability. However, stability is not the problem to be dealt with here. Instead, a large phase margin is required in order to avoid oscillations and overshoots, which would trigger the anti-windup of the integrator. Although the anti-windup facility prevents numerical instability, excessive triggering of it can lead to numerical oscillations between the upper and the lower controller output limits. Such numerical oscillations lead to wrong results. With these parameter settings, the transfer function of the open power control loop is given in Equation (1).

$$G_{P\_cntrl\_OL}(s) = \frac{P_{gen}(s)}{P_{ref}(s)} = \frac{0.7{\cdot}s + 2.1}{0.008333{\cdot}s^2 + 0.3333{\cdot}s} \tag{1}$$
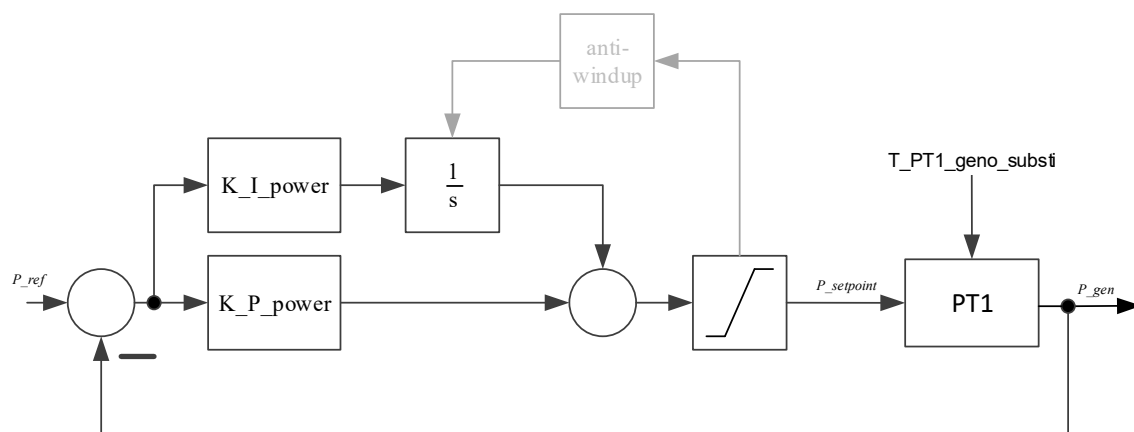

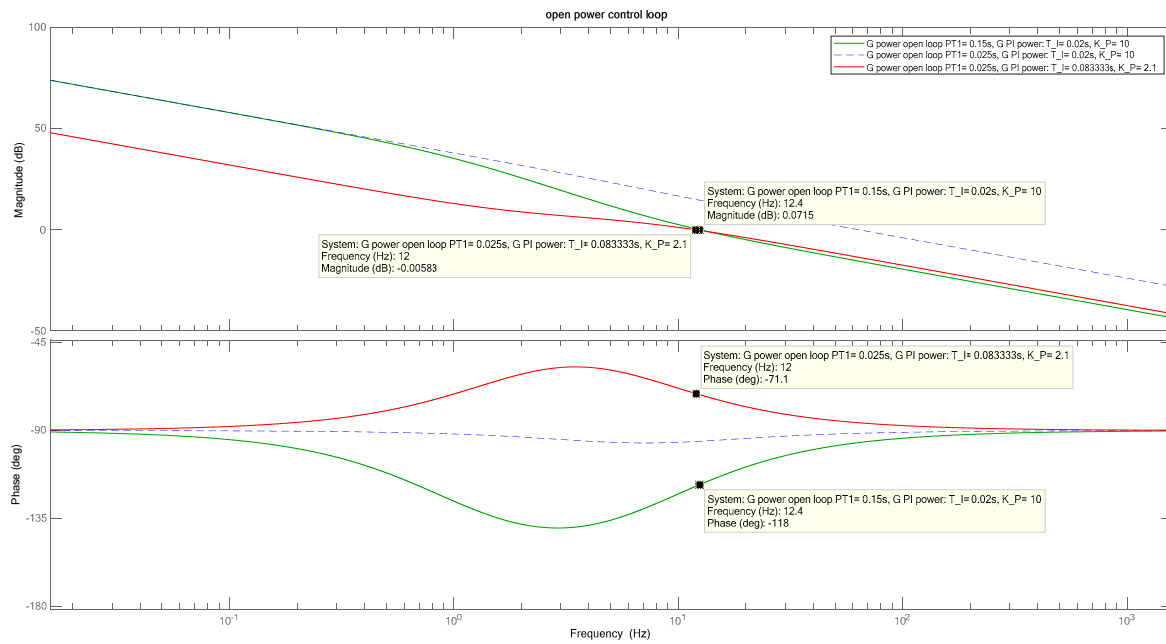**Figure 3.** Close loop power control in the 1st eigenmodes model of a WT.

Figure 4. Bode plots of the open power control loop.

3.2. Continuous Feed-In Management Control

The power generated by the 5M is first and foremost determined by the prevailing wind speed. Whenever the power approaches rated power, the transformer that connects the campus grid with the upstream grid is bound to get overloaded. This overload appears in the shape of overheating of the transformer (ϑ_{TR}) and too high voltage, V_C, in the campus grid (see Figure 1). Consequently, FIM becomes necessary in situations of high wind speeds, and/or very low local consumption in the campus grid. The FIM controller, which is shown in Figure 6 addresses the thermal loading of the transformer as well as V_C [5].

3.3. Continuous Inertial Response Control

The previously proposed variable inertia constant (H_{var}) controller has numerous advantages [19]. The main motivation for this controller is that WTs can continuously contribute to the inertia in the power system, without running the risk that drastic negative *ROCOF*s lead to disconnections of the WT. In principle, a WT with the H_{var} controller behaves like a synchronous generator. However, unlike a synchronous generator, the rotational speed of a WT is not constant. In an AC-connected synchronous generator, the rotor speed varies with f_{grid}. Since in most power systems f_{grid} varies only in a very narrow band, the rotational speed of AC connected synchronous generators can be considered almost constant. In a WT, however, the rotational speed is not determined by f_{grid}, but by the wind speed. Hence, it can vary in a wide range. Therefore, the H_{var} controller varies the inertia constant, which is emulated by the WT, according to the current rotational speed, see Figure 5. At rated speed, the variable inertia constant is equal to the value demanded by the grid operator (H_{dem}).

Equation (2) shows the definition of the inertia constant as known from the literature [10].

$$\text{H} = \frac{E_{kin}}{P_{rated}} = \frac{\frac{1}{2} \cdot J \cdot \omega_{rated}^2}{P_{rated}} \qquad (2)$$

Based on this concept, the H_{var} controller defines an inertia constant for every prevailing rotational speed [9]:

$$H_{var} = \frac{\omega^2 - \omega_{cut-in}^2}{\omega_{rated}^2 - \omega_{cut-in}^2} \cdot H_{dem} \qquad (3)$$

Figure 5 reveals the main advantage of the H$_{var}$ controller: Since the inertia contribution drops to zero when the rotational speed is as low as the cut-in speed, the WT never disconnects from drastic negative *ROCOF*s. At low wind speeds (i.e., also low rotational speed and low power), a single WT provides little inertia. However, this seeming disadvantage is not a problem for the grid: in such a situation, the prevailing load is either supplied by a larger number of WTs (which in total supply sufficient inertia) or by other generators, which can also supply the needed inertia. Equation (2) and Equation (3) reveal that the contributed inertia is scaled with the current speed and therefore also with current power infeed of the WT. Hence, if low wind speed allows one WT to produce only little power, then the overall load in the grid has to be covered by a larger number of WTs. This automatically distributes the generation of H$_{dem}$ over all WTs that are equipped with an H$_{var}$ controller. In total the grid is supplied with the inertia that the grid operator demands.
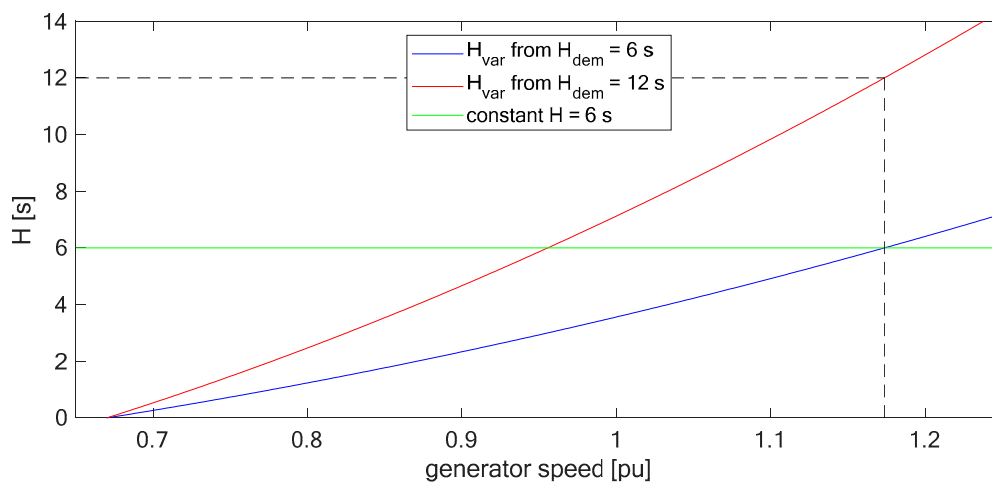
Figure 5. Variable inertia constant, H$_{var}$, for the demanded rated inertia constants H$_{dem}$ = 6 s and H$_{dem}$ = 12 s. Constant inertia constant H = 6 s.

3.4. Combined Control Circuit

Both, the continuous FIM controller and the H$_{var}$ controller interact with the 5M WT via the power setpoint, P_{dem}. Figure 6 illustrates that the continuous FIM controller responds to the transformer temperature, ϑ_{TR}, and the voltage in the campus grid, V_C. The H$_{var}$ controller generates the H_{var} from the demanded inertia constant, H$_{dem}$, and the generator speed. The inertial response power setpoint, P_{SI_varH}, is a result of the *ROCOF*, f_{grid} and the current H_{var}, see Equation (4) [19].

$$P_{SI\_varH} = -2 \cdot H_{var} \cdot P_{rated} \cdot \frac{ROCOF}{f_{grid}} \tag{4}$$

In the version of the 1st eigenmodes model applied here, P_{dem} has no impact on the rotational speed reference of the WT. Hence, even with P_{dem} < 1 pu, the speed of the WT reaches rated speed if the wind speed suffices [21]. This characteristic is beneficial for continuous inertia provision, as it allows the WT to produce H$_{dem}$ for a maximum duration.

FIM and inertial response do not only decouple the controls of a WT from the prevailing wind at the rotor. Since they both act on P_{dem}, they could, potentially, also interfere with each other. However, Figure 6 shows that they are decoupled from each other by the different controllers. Due to the long thermal time constant of the transformer, the temperature controller lets P_{max_TR} respond only very slowly. $P_{max\_TR\_volt}$ has an instantaneous effect on $P_{max\_TR\_lim}$. This variable only serves as setpoint for the P$_{dem}$ controller, which is tuned to fit the vibratory behaviour of the WT. P_{SI_varH}, however, acts instantaneously on P_{dem}. With this configuration, inertia contribution is clearly prioritized over FIM. Even if P_{SI_varH} leads to V_C violating any limits, this can only impact on the power output of

the WT via the dynamics of the P_{dem} controller. This prioritization is justified, as power from inertia contribution oscillates around zero. Hence, it has no lasting impact on the transformer temperature. However, if inertial power is essential for maintaining angular stability, violations of voltage limits are of subordinate importance. This is discussed further in the section on frequency domain analysis.
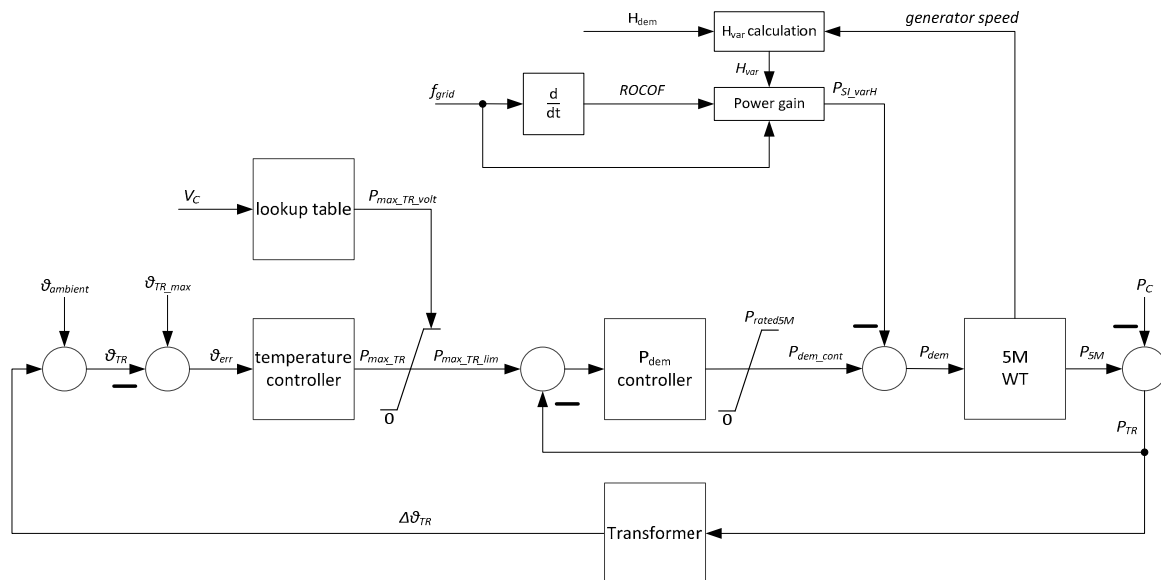
Figure 6. Control circuit for continuous FIM and inertial response with H_{var} controller.

It has to be noted that the H_{var} controller was initially published with a functionality to mitigate potentially harmful excitations on the mechanical structure of the WT [19]. This functionality is deliberately omitted here to be able to assess the maximum inertial response capabilities. At the same time, it is the goal of this paper to reveal the maximum negative impact of inertial response on the WT. Hence, the worst case scenario is considered here.

While in this paper all explanations are given for the case of one WT only, the same result could be realized with an arbitrary number of WTs. As described above, the H_{var} controller inherently distributed the inertial power generation among any participating generators. Even in a wind farm, where wake effects lead to grossly differing operating points of neighbouring WTs, the H_{var} controller assures that the inertia contribution of individual WTs is adapted to their instantaneous capabilities.

The FIM controller, on the other hand, does not take the current operating point of a WT into account. It could be assumed that what is called 5M in Figure 1 is not a single WT, but a wind farm with multiple WTs that interfere with each other via wake. Since all these WTs would contribute to the congestion in the point of common coupling (excessive transformer temperature and too high voltage), they would respond to this congestion equally. This would not be ideal, as the instantaneous power operating points of the individual WTs would differ due to wake and due to the natural wind speed variations in time and space. Also, due to the spatial distribution of the individual WTs in the wind farm, the cable lengths to the point of common coupling would be different. Hence, the voltage drops and the power losses in these cables would be different. Consequently, the task of FIM should be distributed among the different WTs taking the wind direction (wake) and the geometry of the wind farm (beelines and cable lengths) into account. However, the design of such an FIM wind farm controller is beyond the scope of this paper.

4. Frequency Domain Analysis

4.1. Transfer Function of WT

In contrast to assessing the different eigenfrequencies, as they result from the design of the 5M [27], in this section, a frequency domain analysis is presented. This yields the advantage that the frequency response of the entire system becomes obvious. In a complex system, eigenfrequencies of adjacent subsystems can couple and consequently interfere. The controller design described above has an impact on the eigenfrequencies and damping of different subsystems of the WT system. In the power controller section, the assumption is made that the power of the generator, P_{gen}, is independent of the rotational speed. This assumption is only valid in the case of small signal perturbation. Hence, in the following, the response of the rotational speed to power variations is assessed.

For the purpose of frequency domain analysis, the WT system is linearized around the upper part load operating point P = 0.8894 pu and generator speed, *speed_gen* = 1.138 pu, see Figure 7. It has to be noted that Figure 7 shows the power vs. speed characteristic that results from the aerodynamics of the 5M when the 5M is assumed to be equipped with a full scale converter. In contrast to a doubly fed induction generator, a full-scale converter allows the WT to operate in a considerably larger speed band.
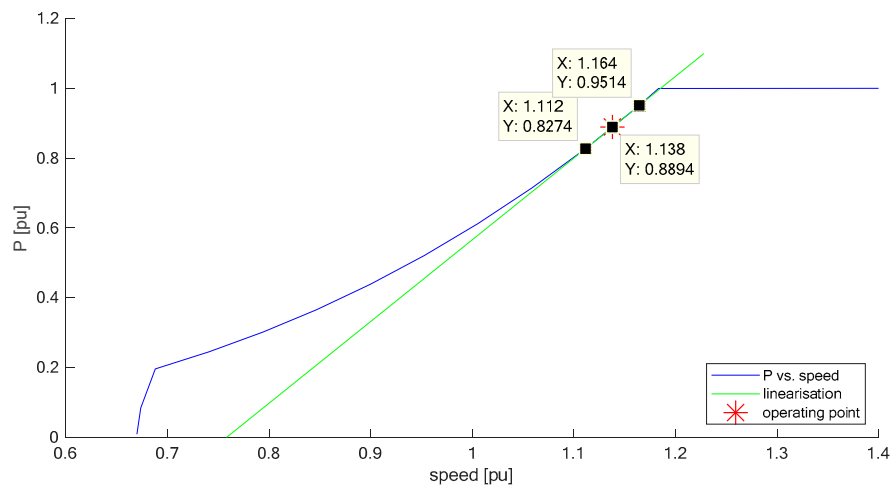
Figure 7. P vs. speed characteristic and linearization around the operating point.

Upper part load is most interesting: In lower part load, the power of a WT is not likely to cause FIM as it is too low for causing the transformer to heat up unhealthily, or for running the voltage into its limit. Also, in lower part load, i.e., low rotational speed, the power resulting from inertial response is small due to the H_{var} controller, see Figure 5. Full load, on the other hand, is also less interesting as this operating point is only seldomly met when the grid connection capabilities demand FIM. In addition, inertial response can draw extra power from the wind when the WT is in full load operation; hence, the impact on the speed is not decisive for the power.

The rotational speed responds whenever there is a mismatch between aerodynamic driving power and electric output power. Such a mismatch has to be catered for by kinetic energy in the rotating masses of the WT. Hence, a transfer function of the WT drive train from electric torque to rotational speed of the generator, *speed_gen*, is required. High frequency variations in the generator torque (*T_elec*) mainly act on the energy storages close to the generator; i.e., the inertia on the high speed shaft, J_hss, the torsional spring that represents the stiffness of the drive train, spring_coeff, and with decreasing effect also the inertia of the hub, J_hub, and the spring that represents the blades in in-plane direction, K_s_blades (Figure 8). Therefore, the aerodynamic operating point is considered constant for the linearization of the operating point.
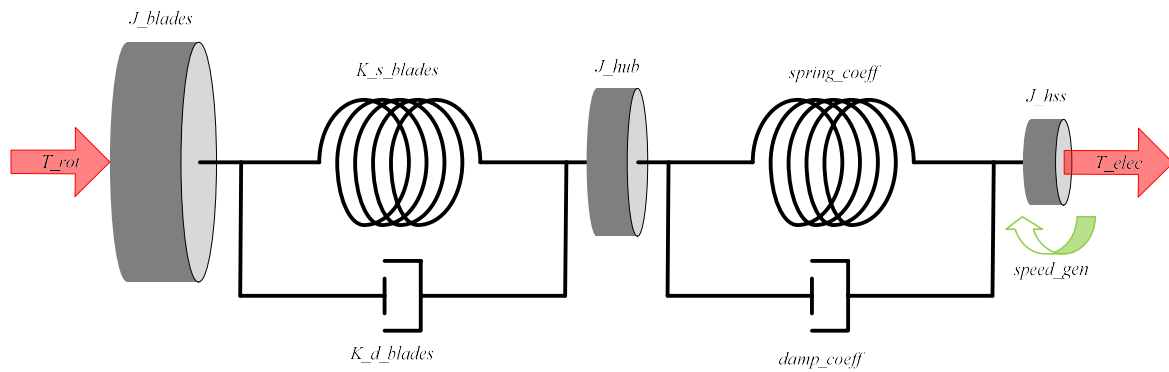
Figure 8. WT drive train model.

In the WT model applied here, the blades are represented as single mass and spring vibrators. However, they behave differently only if they are excited differently [21]. Wind speed and rotor position vary with time. In order to do the transition to the frequency domain, these time-dependent differences are neglected, which allows considering the blades to vibrate synchronously. This simplification leads to the rotational system of the WT as shown in Figure 8.

The variable names and parameter names shown in Figure 8 and in the following equations are identical with those in the documentation of the model [21]. Differing from the model documentation, some new parameters are introduced in Figure 8, which result from the simultaneity of the aforementioned blade motion. These new parameters are introduced in the following equations.

Aggregated blade inertia:

$$J\_blades = \frac{m\_bladetip \cdot 3 \cdot (R\_cntr\_gravi\_bladetip)^2}{J\_base\_lss} \tag{5}$$

Aggregated blade stiffness:

$$K\_s\_blades = \frac{K\_s\_blade\_inplane\_SI \cdot 3}{J\_base\_lss} \tag{6}$$

Aggregated blade damping:

$$K\_d\_blades = \frac{K\_d\_blade\_inplane\_SI \cdot 3}{J\_base\_lss} \tag{7}$$

Inertia aggregated in the rotor hub:

$$J\_hub = \frac{J\_hub\_SI + 3 \cdot J\_bladeroot}{J\_base\_lss} \tag{8}$$

Since part load operation is assumed, the pitch angle is assumed to be constant at approximately 0°. Therefore, the stiffness in-plane (*K_s_blade_inplane_SI*) is the edgewise stiffness and the damping in-plane (*K_d_blade_inplane_SI*) is the edgewise damping of the blades.

Applying free-body diagrams for the inertias shown in Figure 8 allows deriving the transfer function of the drive train from generator torque (*T_elec*) to generator speed (*speed_gen*), where *T_elec* is the input variable and *speed_gen* is the unknown [28]. For this purpose a constant aerodynamic driving torque, $T\_rot = \frac{P}{speed} = 0.7815$ pu is applied according to the previously specified operating point (Figure 7).

The transfer function from torque to speed of the WT is shown in Equation (9).

$$G_{DT}(s) = \frac{speed\_gen(s)}{T\_elec(s)} = \frac{-15.02 \cdot s^5 - 9.405 \cdot s^4 - 2509 \cdot s^3 - 1031 \cdot s^2 + 7.276E(-12) \cdot s}{17.59 \cdot s^6 + 32.77 \cdot s^5 + 4670 \cdot s^4 + 7045 \cdot s^3 + 2.577E5 \cdot s^2 + 1.827E5 \cdot s - 1.456E(-9)} \tag{9}$$

It has to be noted that other dynamics in the WT, i.e., dynamics of the tower and of the blades in out of plane direction, can be neglected. These dynamics have no direct coupling with the rotational speed. There is only an indirect coupling via the perceived wind speed and the aerodynamics of the rotor blades, which has only a small influence on the generator speed, compared to the effects of in-plane vibrations.

The transfer function of the drive train, $G_{DT}(s)$, can be combined with the transfer function of the power control loop to form the transfer function from *P_ref* to *speed_gen*, $G_{WT}(s)$. For this purpose, $G_{P\_cntrl\_OL}(s)$ in Equation (1) has to be turned into the transfer function of the closed power control loop. Linearization around the operating point *speed_gen* = 1.138 pu allows setting up the block diagram of $G_{WT}(s)$, as shown in Figure 9.
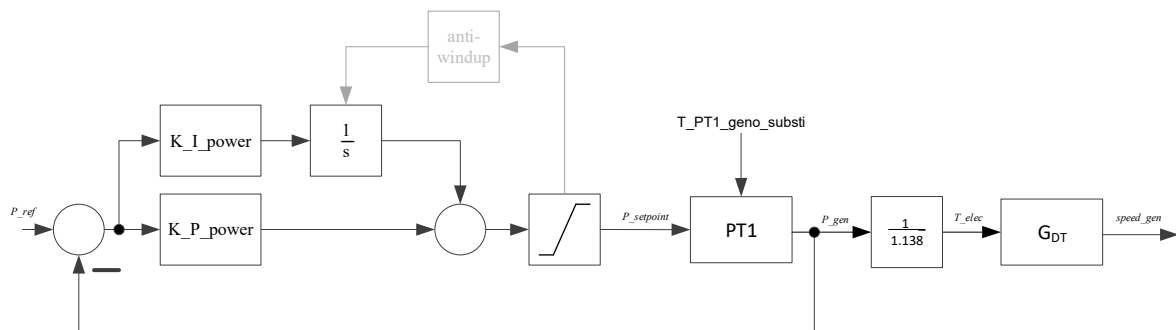

Figure 9. Block diagram of WT system from *P_ref* to *speed_gen*.

The complete transfer function from *P_ref* to *speed_gen* is shown in Equation (10).

$$G_{WT}(s) = \frac{speed\_gen(s)}{P\_ref(s)} =$$
$$\frac{-0.08759 \cdot s^7 - 3.821 \cdot s^6 - 27.5 \cdot s^5 - 641.9 \cdot s^4 - 2015 \cdot s^3 - 721.5 \cdot s^2 + 5.093E(-12) \cdot s}{0.001222 \cdot s^{10} + 0.2026 \cdot s^9 + 7.064 \cdot s^8 + 77.85 \cdot s^7 + 1811 \cdot s^6 + 8767 \cdot s^5 + 1.003E05 \cdot s^4 + 2.465E05 \cdot s^3 + 1.279E05 \cdot s^2 - 1.019E(-9) \cdot s} \tag{10}$$

4.2. Transfer Function of Transformer

The thermal behaviour of the transformer is represented by a PT1 filter with a time constant of 960 s. The power losses that heat up the transformer are nonlinearly depending on the power that is fed through the transformer. Therefore, the transformer is linearized around the operating point 0.1 pu power transfer, as this is a realistic maximum extent of inertial power. Since only the interference between FIM and inertia contribution are assessed, the steady state operating point of the transformer is irrelevant. Further considering the heat dissipation at the surface of the transformer leads to the power that is stored in the transformer in the form of heat [5]. Hence, the transfer function from power transfer in pu to variation in the transformer temperature in °C is given in Equation (11).

$$G_{TR}(s) = \frac{\Delta \vartheta_{TR}(s)}{P_{TR}(s)} = \frac{5.005}{1 + 960 \cdot s} \tag{11}$$

4.3. Transfer Function of P_{dem} Controller

The P_{dem} controller is a PI controller with a proportional gain of three and an integral gain of nine. The P_{dem} controller is the separator between FIM and inertia contribution; i.e., if inertial power leads to instantaneous violation of V_C, the P_{dem} controller prevents this having an instantaneous effect on the combined power setpoint, and hence, also the inertia contribution. Equation (12) shows the transfer function of the P_{dem} controller.

$$G_{PI\_P\_dem}(s) = \frac{\overline{P_{dem\_cont}}(s)}{P_{error}(s)} = \frac{0.3333 \cdot s + 2.1}{0.1111 \cdot s} \tag{12}$$

4.4. Comparison of Frequency Responses

In this section, the frequency responses of the transfer functions derived above are compared with the frequency spectra of the excitations. The excitations for inertia contribution are the *ROCOF*. Continuous FIM has to address the loading of the grid connection transformer; hence, it has to respond to the local active power consumption/production. The voltage in the campus grid, V_C, responds to not only the active power P_C and the power from the 5M, P_{5M}, but mainly to the local reactive power consumption/production, Q_C (see Figure 1). The importance of Q_C is shown by the ratio between reactance and resistance in the grid connection transformer, which is X/R = 3.84 [5].

The analysis conducted here strives to assess the differences and the similarities in the excitations for the 5M when performing continuous FIM and continuous inertia contribution. Normal operation, i.e., with neither of these power system services, was considered previously [5] and is hence out of the scope of this paper. Consequently, Figure 10 shows the bode plots of the WT, $G_{WT}(s)$ (red amplitude response) of the P_{dem} controller, $G_{PI\_P\_dem}(s)$, (green amplitude response) and of the transformer, $G_{TR}(s)$, (blue amplitude response); as well as the frequency spectra of *ROCOF* (green line), P_C (magenta dotted line) and Q_C (cyan dotted line).
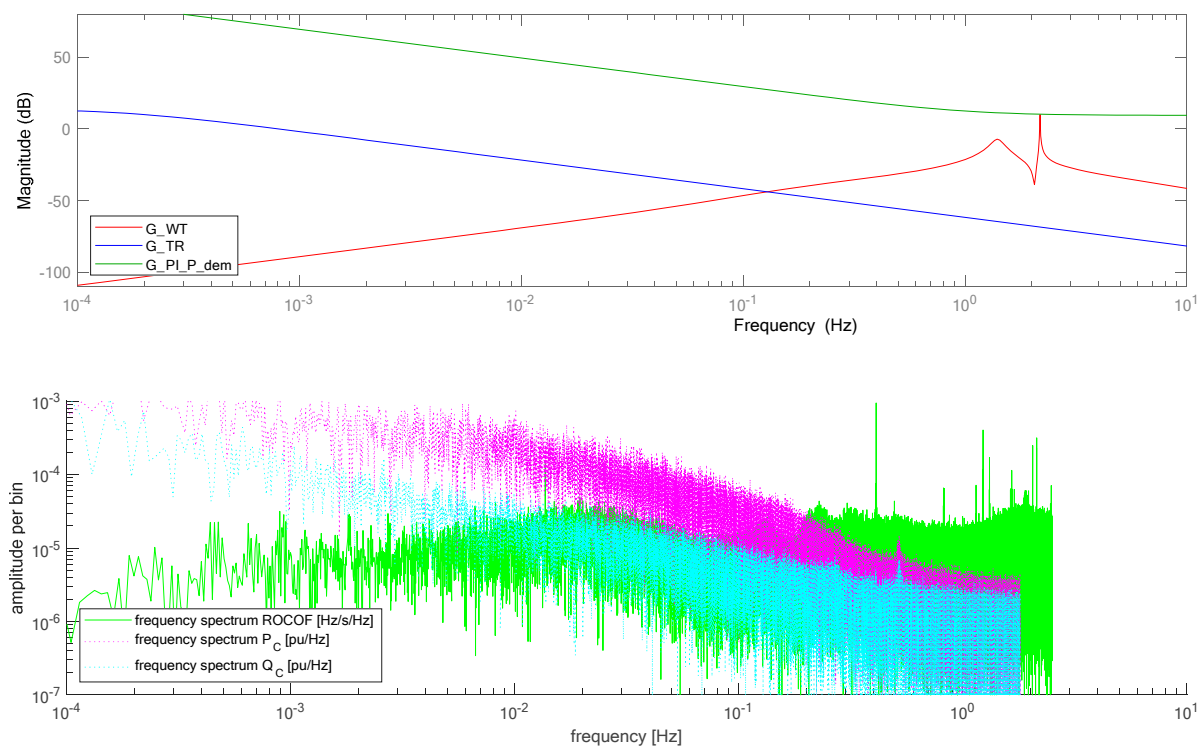
Figure 10. Bode plots of the transfer functions $G_{WT}(s)$, $G_{PI\_P\_dem}(s)$ and $G_{TR}(s)$ (top) in comparison to the frequency spectra of the different excitations: *ROCOF*, P_C and Q_C (bottom).

Figure 10 clearly shows that there is a strong decoupling between the WT and the transformer. The transformer temperature ($G_{TR}(s)$) responds strongly to very low frequencies only. The generator speed of the WT, however, responds to power setpoint (P_{ref}) changes strongest in the range from 1 Hz to 3 Hz ($G_{WT}(s)$).

In the lower diagram of Figure 10 it becomes obvious that there is also a clear decoupling between the excitations of FIM and of inertia contribution. Continuous FIM addresses the transformer temperature (discussed above) and the voltage (V_C). Both active and reactive power variations decline with increasing frequency. Hence, also the extent to which FIM has to respond to V_C declines with increasing frequency. In contrast to this, the magnitude of the *ROCOF* increases with frequency.

Figure 10 also shows that the P_{dem} controller decouples FIM very well from inertial power. Comparing the green lines in Figure 10 reveals that the response to *ROCOF* happens in a frequency range where the P_{dem} controller exhibits very small gain. Hence, if inertial power leads to excessive V_C FIM cannot respond to that, i.e., it cannot dampen the inertial power as the P_{dem} controller prevents this.

Therefore, it can be concluded that FIM takes place at lower frequencies while inertia contribution takes place at higher frequencies. In addition, continuous FIM is most relevant for the transformer temperature, while inertia contribution has the potential to excite the WT. In the following section, this is assessed by means of the study case.

5. Simulations and Discussion of Results

In power systems that are heavily loaded with wind power, it is inherent to FIM that it leads to drastic power reductions in WTs whenever the wind speed is high [5,11]. In addition, it is inherent to the H_{var} controller that it potentially leads to drastic power variations in the affected WT whenever the wind speed is high [19]. Hence, both continuous FIM and inertial response with the H_{var} controller are most dominant in upper part load. The inertial response can potentially worsen the overloading of the grid. Due to the decoupling from the wind both controllers add to the mechanical loads in the WT at the same time.

Figure 11 shows the power, the generator speed, and the pitch angle of the 5M for the whole day of 5 April 2017. It can be seen that the 5M runs in part load most of the time in the first half of the day. Before noon, the wind speed increases and with it also the loading of the grid [5]. Hence, in the second half of the day the 5M runs in rated operation whenever the FIM controller and the H_{var} controller allow it to. Figure 11 shows the simulated scenario for continuous FIM operation with enabled (blue) and disabled (red) continuous inertia contribution. The blue curve is hardly visible, as there is only little effect of inertial response on FIM operation.
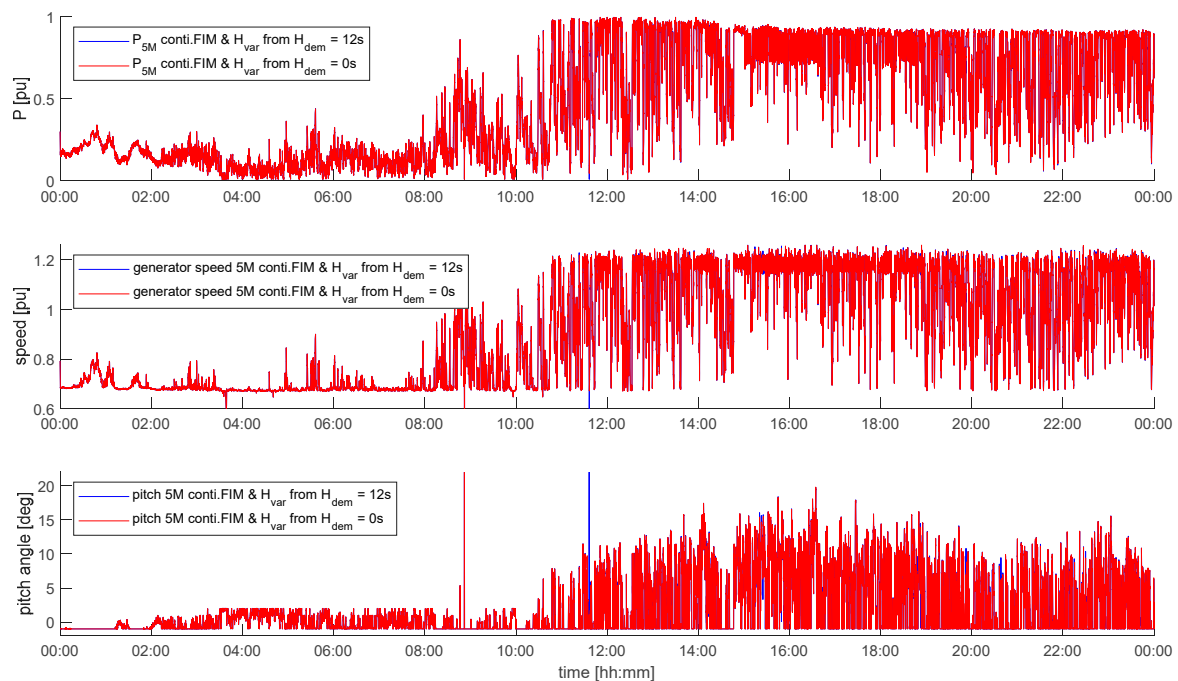
Figure 11. WT power (top) generator speed (middle) and pitch angle (bottom) of 5M for the case of continuous FIM operation (red curves) and for the case of continuous FIM with inertial response (blue curves in the background).

5.1. Effect of Generator–Converter Time Constant on Continuous FIM

As discussed in the WT simulation model section, in a previous study [5], T_PT1_geno_substi of the generator–converter unit was set to 150 ms. For reasons outlined above, it is set to 25 ms here. In order to assess whether the results in the previous paper are comparable to the results in this paper, the effect of the time constant is studied. It can be seen that the results presented previously [5] are hardly affected by this parameter change. The only visible effect is on the acceleration of the generator and of the tower in lateral direction. To illustrate this effect, Figure 12 shows the scenario of continuous FIM operation with T_PT1_geno_substi set to 150 ms [5] and with T_PT1_geno_substi set to 25 ms.
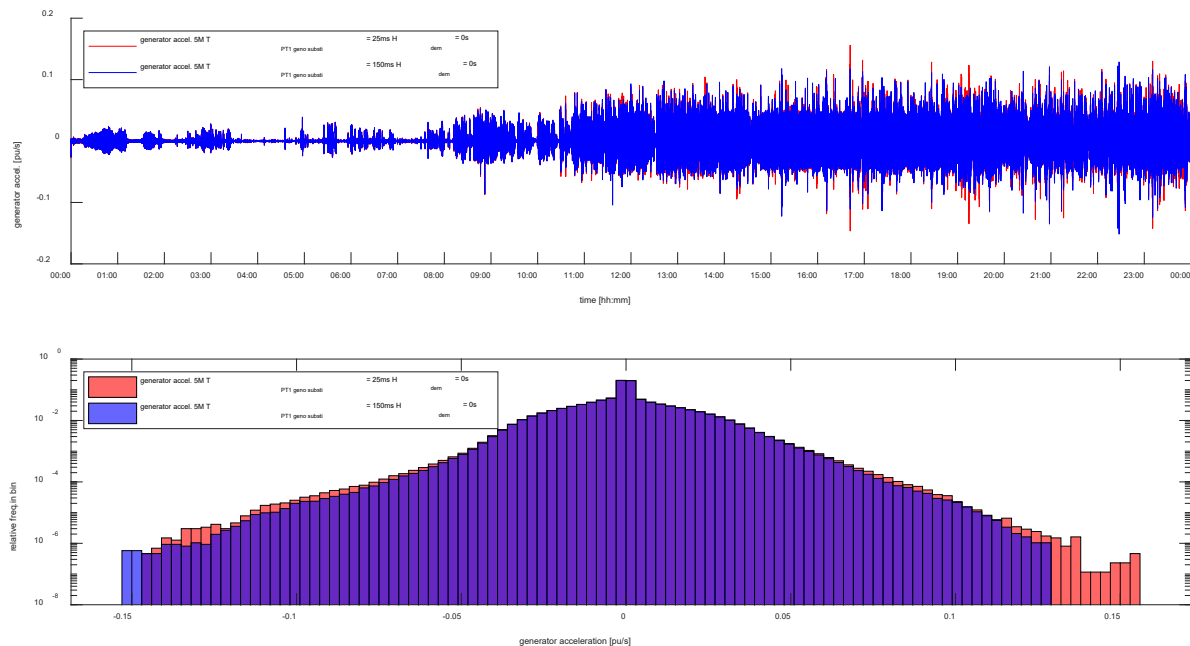
Figure 12. Generator acceleration (top) and frequency distribution of generator acceleration (bottom) of 5M in continuous FIM operation for two different generator-converter time constants.

The comparison shown in Figure 12 is important as in the following study, the effect of continuous inertia provision is compared with the case when the WT only provides continuous FIM. Figure 12 suggests that the reduction in T_PT1_geno_substi (from 150 ms to 25 ms) has drastic consequences; however, due to the logarithmic scale, the relative frequency of occurrence of larger generator accelerations is moderate. It can be noted that with lower time constant, the relative frequency of occurrence is moved in positive direction, i.e., larger positive accelerations are more likely to occur. This phenomenon is caused by the instantaneous limitation of $P_{max\_TR\_lim}$ whenever the voltage is too high ($P_{max\_TR\_volt}$ in Figure 6), which demands a de-loading of the generator by lowering the generator torque.

Figure 13 shows that the reduction in T_PT1_geno_substi has the opposite effect on the lateral tower accelerations. With longer time constant, i.e., slower generator control, the tower is bound to vibrate more often in lateral direction. This phenomenon is due to the fact that lateral vibrations are caused by an imbalance in the rotor in combination with rotor speeds that allow lateral excitation of the tower by this imbalance. There is only an aerodynamic coupling between tower vibrations and the torque at the shaft (via the perceived wind speed). Faster generator control allows more rapid response of the generator by producing a counter torque. Hence, via the slope in the power vs. speed characteristic, the generator can produce more damping torque if its time constant is short.

Difference in acceleration of the other components in the 5M are hardly measurable. Consequently, the results presented previously [5] remain valid. Hence, it is justified that the effect of continuous

inertial response on the WT is assessed against the case of continuous FIM with T_PT1_geno_substi set to 25 ms.
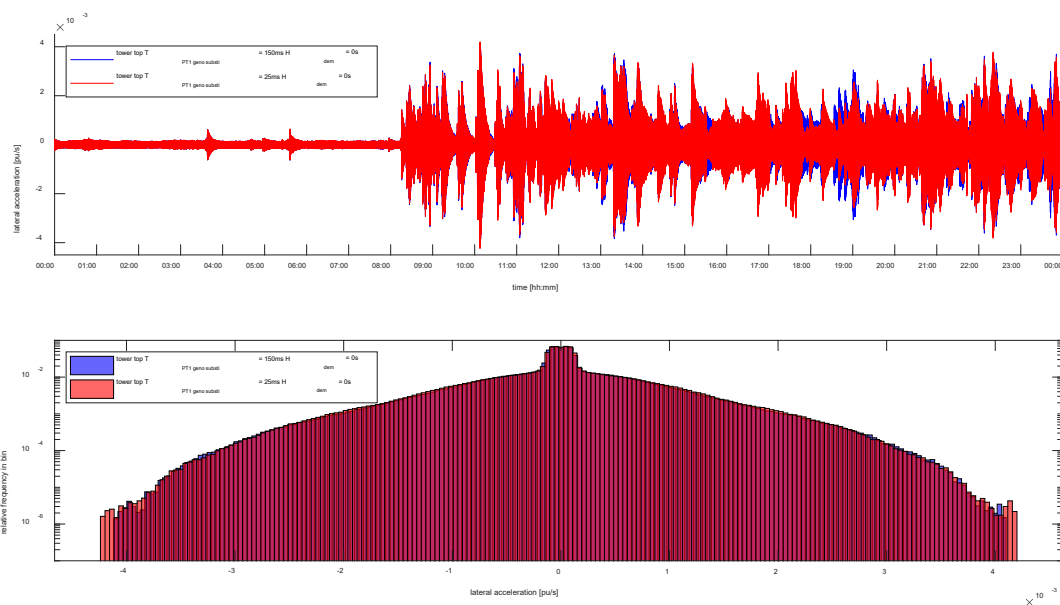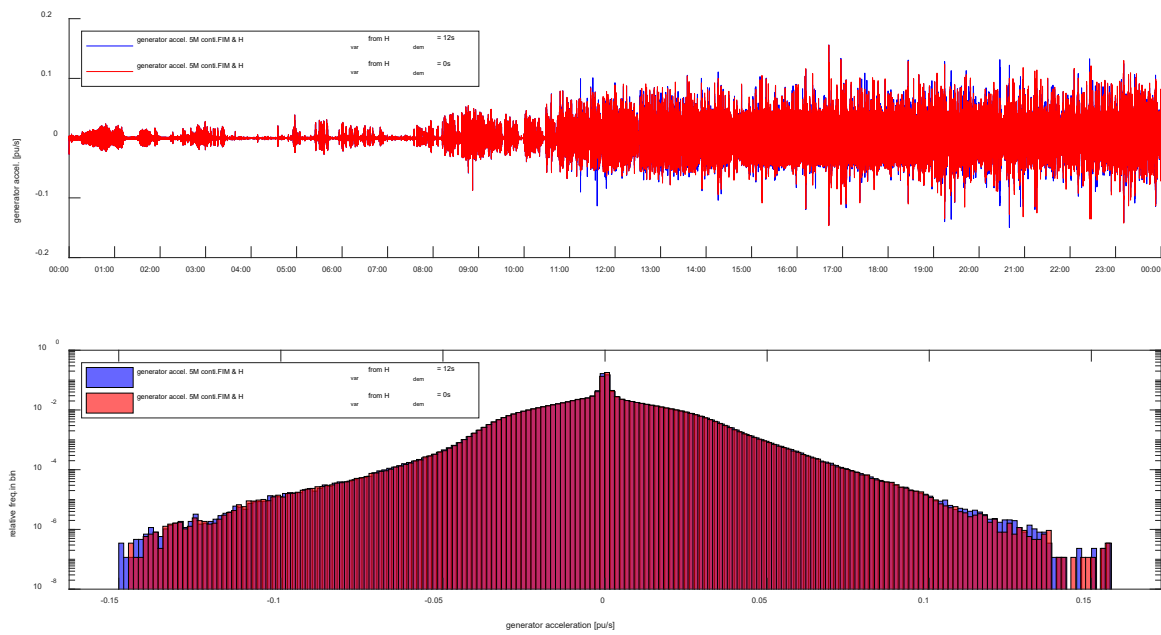

Figure 13. Lateral tower top acceleration (top) and frequency distribution of lateral tower top acceleration (bottom) of 5M in continuous FIM operation for two different generator–converter time constants.

### 5.2. Effect of Variable H Controller on the WT

The effect that continuous FIM has on the WT was assessed in previous publications [5,29]. Therefore, only the additional effect that continuous inertia contribution with the H_{var} controller has on the WT shall be discussed here.

Different H_{dem} values are tested. Generally, the H_{var} controller causes little impact on the WT, which is already visible from the fact that the two curves in Figure 11 hardly differ. Since the continental European grid frequency only rarely exhibits large *ROCOF*s, H_{dem} is set to 12 s to achieve high power setpoint changes due to inertial response. This way, also the circumstances in smaller, i.e., more agile grids can be emulated. The analysis of all WT signals reveals that the acceleration of the generator and of the tower in lateral direction are affected most. Hence, these are the only signals considered here. However, Figures 14 and 15 show that even H_{dem} = 12 s has hardly any effect on the generator acceleration and on the lateral tower acceleration, respectively. It has to be mentioned, that the grid frequency recorded on 5 April 2017 is representative of a normal day in continental Europe. Although it did not contain any extreme events, it is still challenging in terms of inertial response, as the grid frequency appears to vary with extreme *ROCOF*s due to electromagnetic illusions.

These findings confirm the results yielded in a field test and fatigue load analysis conducted earlier. During a research project carried out with the WT manufacturer Suzlon Energy, a small multi-MW WT was equipped with the H_{var} controller where H_{dem} was set to 6 s. The f_{grid} time series were artificially generated to contain severe frequency events. With these time series the performance of the WT and the resulting loads were assessed at different wind speeds. The fatigue load analysis revealed that even with regularly occurring severe events in f_{grid} the H_{var} controller consumes only very little lifetime of the WT [9]. Also, as one consequence of the findings of this project, the demanded inertia constant is set to H_{dem} = 12 s here.

Figure 14. Generator acceleration (top) and frequency distribution of generator acceleration (bottom) of 5M when performing continuous FIM, with and without continuous inertia provision.
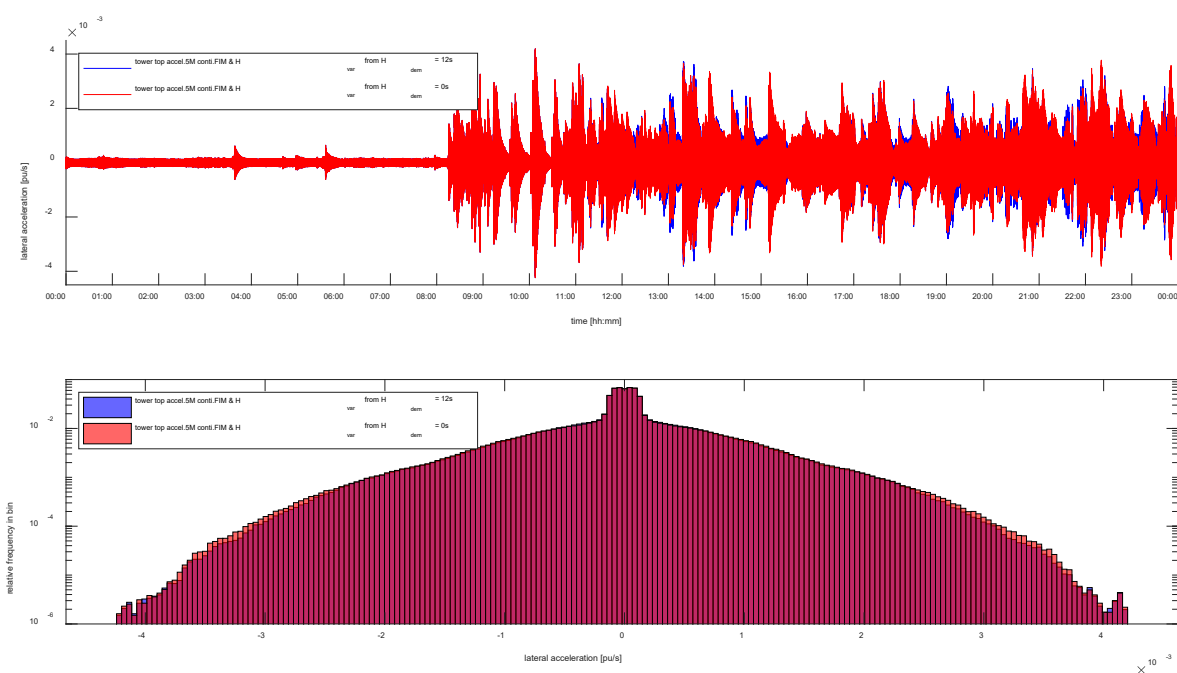
Figure 15. Lateral tower top acceleration (top) and frequency distribution of lateral tower top acceleration (bottom) of 5M when performing continuous FIM, with and without continuous inertia provision.

5.3. Effect of Continuous FIM and Inertia Provision on the Grid

The advantage of continuous FIM on the power infeed of the WT is published already [5]. It has to be added though, that such rapid optimization of the grid utilization is entirely inconceivable with conventional power plants (thermal or hydro) that are based on AC-connected generators. Hence, for their power to be reliably available for maintaining the balance between generation and demand (f_{grid} control), either oversized feeders or conservative power truncation is inevitable.

When a generator provides inertia to the grid, it produces power that is a function of the frequency, $\omega = 2 \cdot \pi \cdot f_{grid}$, and the *ROCOF*, see Equation (13).

$$P_{inertia} = J \cdot \omega \cdot \frac{d\omega}{dt} \tag{13}$$

When a variable speed WT provides inertia to the grid, it is not the inherent inertia, J, which determines $P_{inertia}$. Instead, the frequency converter has to be controlled such that the WT exhibits inertial behaviour, i.e., it produces synthetic inertia. Hence, H_{dem}, or in case the H_{var} controller is applied, H_{var} is decisive for the inertial power, see Equation (14).

$$P_{inertia} = \frac{2 \cdot H_{var} \cdot P_{rated}}{J\omega} \cdot \frac{d\omega}{dt} \tag{14}$$

This power theoretically contributes to the loading of the feeder that connects the WT with the grid. However, Figure 10 reveals that there is virtually no coupling between continuous FIM and inertial response, i.e., $P_{inertia}$. In addition, it has to be pointed out that the mean value of $P_{inertia}$ is zero in normal power system operation (only if there is a persistent deviation of f_{grid} from its rated value the mean value of $P_{inertia} \neq 0$). This is further shown in Figures 16 and 17. Hence, $P_{inertia}$ cannot interfere with the transformer temperature and it can only temporarily interfere with V_C.

The effect of inertia contribution on the grid can be quantified with the inertial energy, $E_{inertia}$. When considering certain durations, such as the 24 h of the 5 April 2017, the energy exchange between grid and WT, which results from inertia contribution, can be derived according to Equation (15).

$$E_{inertia} = \int_{5/4/2017\ 00:00}^{5/4/2017\ 24:00} \left(\sqrt{P_{inertia}(t)^2} \right) dt \tag{15}$$
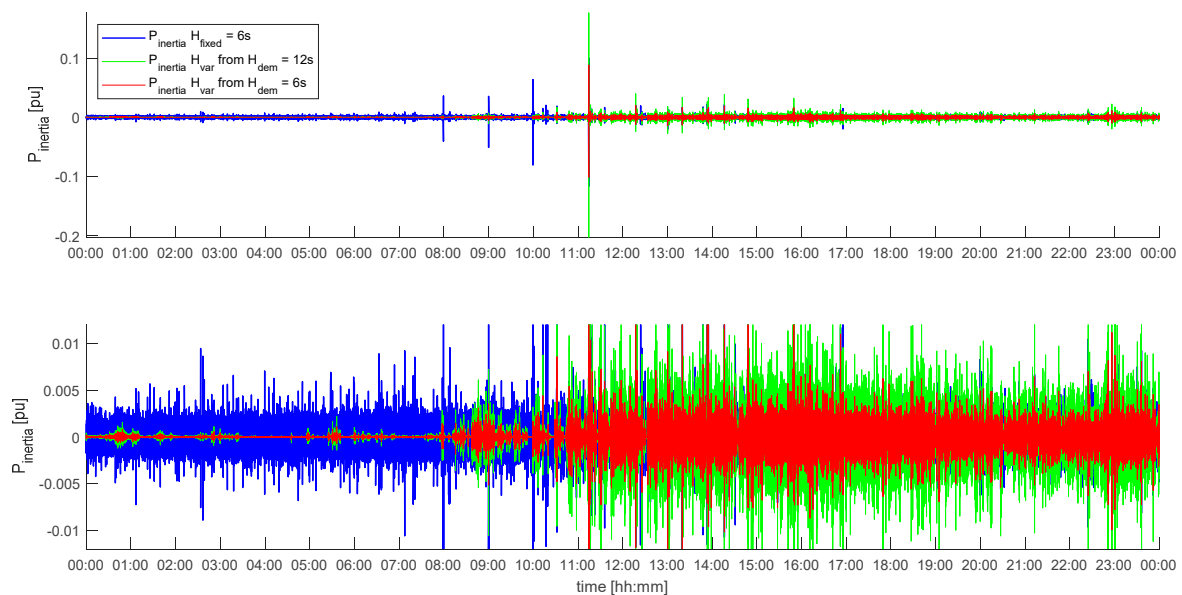
Figure 16. $P_{inertia}$ from an AC connected synchronous generator with H = 6 s (blue), $P_{inertia}$ from the 5M with H_{var} controller and H_{dem} = 6 s (red) and H_{dem} = 12 s (green). The bottom diagram is a zoom-in view of the top diagram.
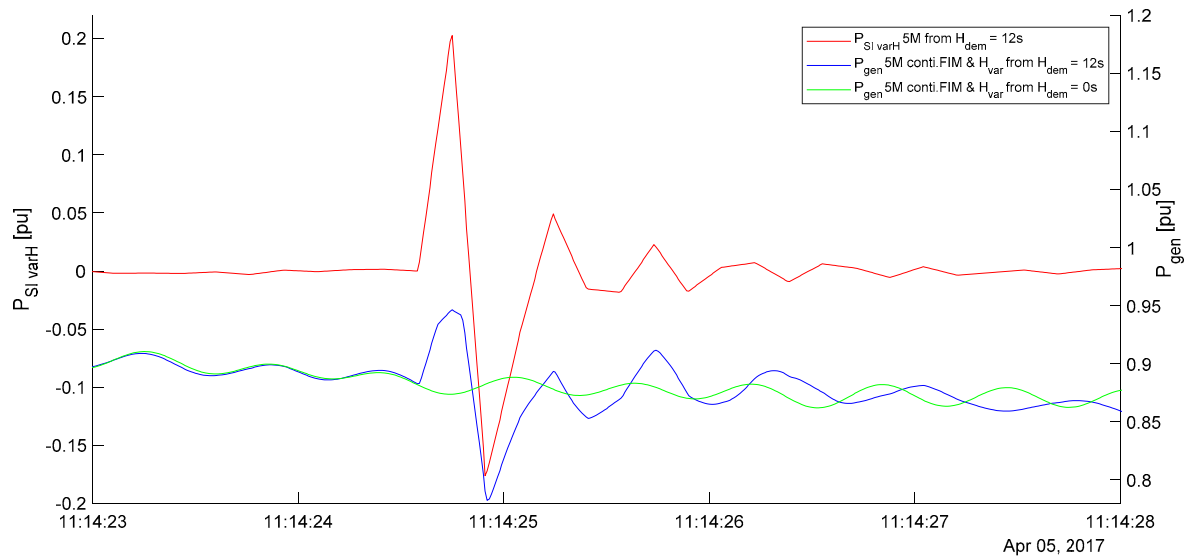
Figure 17. The inertial response power setpoint, P_{SI_var}, (red) and the generator power, P_{gen}, from the 5M. P_{gen} is shown for the case of FIM only (green) and FIM with inertial response (blue).

To assess the ability to contribute to system inertia, H_{dem} of the H_{var} controller in the 5M is set to 6 s and to 12 s. The resulting $P_{inertia}$ are compared with the $P_{inertia}$ of an AC connected synchronous generator with a fixed inertia constant H_{fixed} = 6 s. Figure 16 shows these three different $P_{inertia}$ for the 24 h of 5 April 2017. Comparing Figure 16 with Figure 11 reveals that the inertia contribution of the 5M depends on the prevailing power operating point. Integrating $P_{inertia}$ according to Equation (15) leads to the inertial energies, $E_{inertia}$, which are listed in Table 1. In Table 1 $E_{inertia}$ is not only given for the whole day, but also for the first half and for the second half of the day.

Table 1. $E_{inertia}$ from an AC connected synchronous generator with H = 6 s, $E_{inertia}$ from the 5M with H_{var} controller and H_{dem} = 6 s and H_{dem} = 12 s.

	5 April 2017 00:00–24:00	5 April 2017 00:00–12:00	5 April 2017 12:00–24:00
H_{fixed} = 6 s	88.2029 kWh	41.5384 kWh	46.6645 kWh
H_{var} from H_{dem} = 6 s	33.0589 kWh	4.3307 kWh	28.7283 kWh
H_{var} from H_{dem} = 12 s	66.1327 kWh	8.6603 kWh	57.4724 kWh

In the morning, when the wind speed is low, the inertia contribution is also low. From a grid point of view, this is no problem. In this case, either a larger number of WTs has to cover the consumption in the grid, or other generators have to produce the demanded power and, hence, also the necessary inertia.

In the afternoon, when the wind speed is high, the 5M has to deal with continuous FIM, but the inertia contribution increases nonetheless.

Table 1 shows very clearly that the inertia contribution of the 5M is comparable to that of a synchronous generator. When H_{dem} is set to 12 s, the inertia contribution in the afternoon of 5 April 2017 is even 23% greater than that of the synchronous generator. It has to be kept in mind that in the scenario simulated here, the 5M is burdened with continuous FIM. Hence, it operates only intermittently and only for short durations at rated power and rated speed. Each time the speed drops the inertia contribution drops as well, see Figure 5. Without FIM the inertia contribution could increase even further in the afternoon.

Table 1 further reveals that doubling H_{dem} leads to a doubling of $E_{inertia}$. This proves that inertia contribution has virtually no impact on the rotational speed and on the aerodynamic performance of the WT.

The discussion so far revolves around results that are produced from the power demand necessary for inertial response, i.e., P_{SI_varH} in Figure 6, as it is not possible to extract $P_{inertia}$ from P_{5M}. There are several factors that make such a comparison impossible: $P_{inertia}$ is camouflaged in P_{5M} by the turbulent wind and the motion of the mechanical components of the WT, namely the generator rotor, the blades in-plane and out-of-plane, as well as the motion of the tower in longitudinal and in lateral direction. The power reference for the frequency converter (in the model this variable is called *P_setpoint*, see Figure 3) is derived from the measured rotational speed of the generator. The driving power that is instantaneously available for the WT is determined by the wind speed and the aforementioned motions of mechanical components, as these interfere with the ambient wind speed, leading to a perceived wind speed. Therefore, $P_{inertia}$ can be magnified or weakened in single occasions. Considering longer durations, these effects are assumed to level out. However, very rapid $P_{inertia}$ variations cannot be realized by the generator–converter unit with its time constant (T_PT1_geno_substi = 25 ms). It has to be kept in mind, however, that the response of the AC-connected synchronous generator (in Table 1) is derived with Equation (14). The limited dynamic response of a synchronous generator is not taken into account here either.

Figure 17 shows an exemplified comparison between the power setpoint for inertial response, P_{SI_varH}, and the power that the 5M feeds into the grid, P_{gen}. To show a drastic example Figure 17 shows the response to the peak in *ROCOF* at 11:14 (compare Figure 2), which is assumed to be an electromagnetic illusion. Figure 17 reveals that P_{gen} follows P_{SI_varH} quite well (note that the ranges of the two y-axes in Figure 17 are identical). The difference in magnitude of the excursion in P_{SI_varH} and in P_{gen} is caused by the damping effects of the power controller and the generator–converter unit. Hence, the comparison in Table 1 is deemed valid.

The energy yield of the 5M is virtually not affected by inertial response. During the 24 h of 5 April 2017, the 5M generates 57,097.4 kWh without inertial response and 57,095.5 kWh with the H_{var} controller and H_{dem} = 12 s; both with continuous FIM.

6. Conclusions

This paper presents simulation results of continuous FIM and continuous provision of synthetic inertia with a WT. The case simulated is based on measurements. The conclusion of this study is that WTs can deal with excessively weak grid connections and, at the same time, can contribute to grid inertia continuously. With their rapid power control, WTs can adjust their power infeed to satisfy the needs of limited grid connection points a lot quicker than conventional power plants. By doing so, their power is available reliably with neither undue waste of energy nor overdimensioned grid enhancements. At the same time, they can contribute to grid inertia to a larger extent than conventional power plants. In the study at hand, the inertia constant reaches up to 12 s in rated operation of the WT. This number has to be put into perspective with the inertia constants of conventional power plants. These range from 2 s to 9 s [30], in case of hydro power plants only up to 4 s, and in the case of generators with two pole pairs up to 10 s [10]. Hence, WTs enhance angular stability in a power system to a larger extent than conventional power plants.

While many current grid codes focus on grid frequency support by WTs in prespecified events (fast frequency response), this study shows that it is advantageous when WTs provide inertia to the grid continuously with the H_{var} controller. By doing so, the grid reliably maintains controllability of the frequency. The WTs, on the other hand, suffer neither undue wear, nor noticeable loss of energy yield.

Author Contributions: C.J.: conceptualization, methodology, development of the wind turbine simulation model, conducting the simulation, data analysis, writing—original draft preparation. A.G.: design and programming of variable H controller model, literature review, support in visualization of time traces, discussions and comments, writing—review and editing.

Conflicts of Interest: The authors declare no conflict of interest.

References

1. Bundesnetzagentur, *Pressemitteilung: Bundesnetzagentur Veröffentlicht Zahlen zu Redispatch und Einspeisemanagement für 2017*. 2018. Available online: https://www.bundesnetzagentur.de/SharedDocs/Downloads/DE/Allgemeines/Presse/Pressemitteilungen/2018/20180618_NetzSystemSicherheit.pdf?__blob=publicationFile&v=2 (accessed on 1 May 2019).

2. Ministerium für Energiewende, Landwirtschaft, Umwelt, Natur und Digitalisierung (MELUND) Schleswig-Holstein, *Kurzbericht zum Engpassmanagement in Schleswig-Holstein*. 2018. Available online: https://www.schleswig-holstein.de/DE/Fachinhalte/E/erneuerbareenergien/Bericht_Einspeisemanagement.pdf;jsessionid=CAD6BCDD96E9F0CFFB6472B2DA2B6E5F?__blob=publicationFile&v=1 (accessed on 1 May 2019).

3. Larscheid, P.; Maercks, M.; Dierkes, S.; Moser, A.; Patzack, S.; Vennegeerts, H.; Rolink, J.; Wieben, E. Increasing the Hosting Capacity of RES in Distribution Grids by Active Power Control. In Proceedings of the International ETG Congress, Bonn, Germany, 17–18 November 2015; Available online: https://ieeexplore.ieee.org/stamp/stamp.jsp?tp=&arnumber=7388485&tag=1 (accessed on 1 May 2019).

4. Jauch, C. FH Flensburg erforscht dynamische Leistungsbereitstellung durch WEA. *Ingenieurspiegel* **2013**, *4*, 20–21.

5. Jauch, C.; Gloe, A.; Hippel, S.; Thiesen, H. Increased Wind Energy Yield and Grid Utilisation with Continuous Feed-In Management. *Energies* **2017**, *10*, 870. [CrossRef]

6. Jauch, C.; Gloe, A. Improved feed-in management with wind turbines. In Proceedings of the 15th Wind Integration Workshop, Vienna, Austria, 15–17 November 2016; Available online: https://www.researchgate.net/publication/311485049_Improved_Feed-in_Management_with_Wind_Turbines (accessed on 31 May 2019).

7. Eriksson, R.; Modig, N.; Elkington, K. Synthetic inertia versus fast frequency response: A definition. *IET Renew. Power Gener.* **2018**, *12*, 507–514. [CrossRef]

8. Fleming, P.A.; Aho, J.; Buckspan, A.; Ela, E.; Zhang, Y.; Gevorgian, V.; Scholbrock, A.; Pao, L.; Damiani, R. Effects of power reserve control on wind turbine structural loading. *Wind Energy* **2015**, *19*, 453–469. [CrossRef]

9. Gloe, A.; Jauch, C.; Thiesen, H.; Viebeg, J. Inertial Response Controller Design for a Variable Speed Wind Turbine. *WETI Flensbg. Univ. Appl. Sci.* **2018**. [CrossRef]

10. Kundur, P. *Power System Stability and Control*; McGraw-Hill: New York, NY, USA, 1994.

11. Bird, L.; Lew, D.; Milligan, M.; Carlini, E.M.; Estanqueiro, A.; Flynn, D.; Gomez-Lazaro, E.; Holttinen, H.; Menemenlis, N.; Orths, A.; et al. Wind and solar energy curtailment: A review of international experience. *Renew. Sustain. Energy Rev.* **2016**, *65*, 577–586. [CrossRef]

12. Ulbig, A.; Borsche, T.S.; Andersson, G. Impact of low rotational inertia on power system stability and operation. In Proceedings of the 19thWorld Congress of the International Federation of Automatic Control (IFAC 2014), Capetown, South Africa, 24–29 August 2014; Available online: https://reader.elsevier.com/reader/sd/pii/S1474667016427618?token=1130DA98E61ECBD9185907D2DE5A4F90E659BFC754B1D06E7CABAF20EF66856E7A2E7072C5268A2049CBF7AD6D84C5A0 (accessed on 3 May 2019).

13. Tielens, P.; Hertem, D.V. The relevance of inertia in power systems. *Renew. Sustain. Energy Rev.* **2016**, *55*, 999–1009. Available online: http://www.sciencedirect.com/science/article/pii/S136403211501268X (accessed on 3 May 2019).

14. Gonzalez-Longatt, F.M. Activation schemes of synthetic inertia controller on full converter wind turbine (type4). In Proceedings of the IEEE Power and Energy Society General Meeting, Denver, CO, USA, 26–30 July 2015; Available online: https://ieeexplore.ieee.org/stamp/stamp.jsp?tp=&arnumber=7286430 (accessed on 2 May 2019).

15. EirGrid; Soni, *All Island TSO Facilitation of Renewables Studies*. 2010. Available online: http://www.eirgridgroup. com/site-files/library/EirGrid/Facilitation-of-Renewables-Report.pdf (accessed on 2 May 2019).

16. Hydro Québec TransÉnergie. Technical Requirements for the Connection of Generation Facilities to the Hydro-Québec Transmission System. Supplementary Requirements for Wind Generation. 2005. Available online: http://www.hydroquebec.com/transenergie/fr/commerce/pdf/eolienne_transport_en.pdf (accessed on 2 May 2019).

17. Red Electrica. Technical Requirement for Wind Power and Photovoltaic Installations and Any Generating Facilities Whose Technology Does Not Consist on a Synchronous Generator Directly Connected to the Grid. Available online: http://joaocarvalhosa.weebly.com/uploads/6/6/1/5/6615139/espanha.pdff (accessed on 3 May 2019).

18. Salehi Dobakhshari, A.; Azizi, S.; Ranjbar, A.M. Control of Microgrids: Aspects and Prospects. In Proceedings of the IEEE International Conference on Networking, Sensing and Control, Delft, The Netherlands, 11–13 April 2011; Available online: https://ieeexplore.ieee.org/stamp/stamp.jsp?tp=&arnumber=5874892 (accessed on 2 May 2019).

19. Gloe, A.; Jauch, C.; Craciun, B.; Winkelmann, J. Continuous provision of synthetic inertia with wind turbines: Implications for the wind turbine and for the grid. *IET Renew. Power Gener.* **2019**, *13*, 668–675. [CrossRef]

20. Jonkman, J.; Butterfield, S.; Musial, W.; Scott, G. Definition of a 5-MW Reference Wind Turbine for Offshore System Development. Available online: http://pop.h-cdn.co/assets/cm/15/06/54d150362c903_-_38060.pdf (accessed on 3 May 2019).

21. Jauch, C. First Eigenmode Simulation Model of a Wind Turbine—for Control Algorithm Design. *WETI Flensbg. Univ. Appl. Sci.* **2016**. Available online: https://www.researchgate.net/publication/312935476_ First_Eigenmode_Simulation_Model_of_a_Wind_Turbine_-_for_Control_Algorithm_Design (accessed on 3 May 2019). [CrossRef]

22. Gloe, A.; Thiesen, H.; Jauch, C. Grid frequency analysis for assessing the stress on wind turbines. In Proceedings of the 15th Wind Integration Workshop, Vienna, Austria, 15–17 November 2016; Available online: https://www.researchgate.net/publication/311485049_Improved_Feed-in_Management_with_Wind_ Turbines (accessed on 3 May 2019).

23. Thiesen, H.; Jauch, C. Identifying electromagnetic illusions in grid frequency measurements for synthetic inertia provision. In Proceedings of the IEEE CPE-POWERENG 2019, 13th International Conference on Compatibility, Power Electronics and Power Engineering, Sonderborg, Denmark, 23–25 April 2019.

24. Hafiz, F.; Abdennour, A. An adaptive neuro-fuzzy inertia controller for variable-speed wind turbines. *Renew. Energy* **2016**, *92*, 136–146. [CrossRef]

25. Andresen, M. Simulation eines Einspeisereglers für Erzeugungsanlagen. Bachelor's Thesis, WSTECH GmbH, Flensburg, Germany, 2 January 2019.

26. MATLAB Version: 9.4.0.813654 (R2018a). Available online: http://uk.mathworks.com/products/matlab/ (accessed on 2 May 2019).

27. Jonkman, J.M.; Jonkman, B.J. FAST modularization framework for wind turbine simulation: Full-system linearization. In Proceedings of the Conference: Science of Making Torque from Wind (TORQUE 2016), Munich, Germany, 5–7 October 2016; Available online: https://www.nrel.gov/docs/fy17osti/67015.pdf (accessed on 3 May 2019).

28. Nise, N.S. *Control Systems Engineering*, 3rd ed.; John Wiley & Sons: Hoboken, NJ, USA, 2000; ISSN/ISBN 0-471-36601-3.

29. Jauch, C.; Gloe, A. Flexible Wind Power Control for Optimal Power System Utilisation. In Proceedings of the WindAc Africa 2017, Cape Town, South Africa, 14–15 November 2017; Available online: https://www.researchgate.net/publication/321212504_Flexible_Wind_Power_Control_For_Optimal_ Power_System_Utilisation (accessed on 3 May 2019).

30. Stevenson, W.; Grainger, J. *Power System Analysis*; McGraw-Hill: New York, NY, USA, 1994.